SURFACE TO SUBSURFACE RESERVOIR/ AQUIFER CHARACTERIZATION AND FACIES ANALYSIS OF THE JURASSIC NAVAJO SANDSTONE, CENTRAL UTAH

Thomas C. Chidsey, Jr., Thomas H. Morris, Stephanie M. Carney,
Ashley D. Hansen, John H. McBride, and Craig D. Morgan

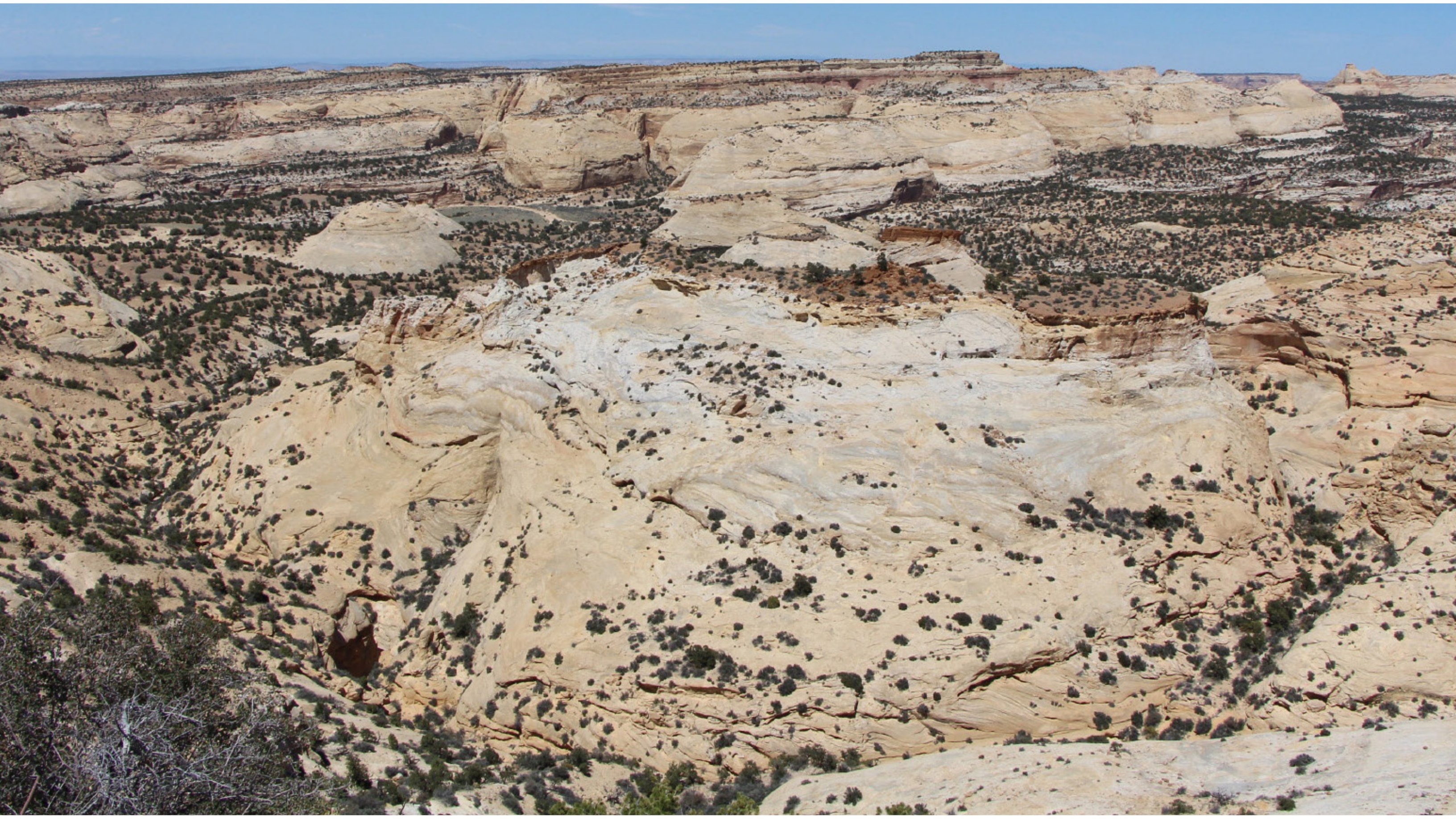

SPECIAL STUDY 167
UTAH GEOLOGICAL SURVEY
UTAH DEPARTMENT OF NATURAL RESOURCES
2020

Blank pages are intentional for printing purposes.

SURFACE TO SUBSURFACE RESERVOIR/ AQUIFER CHARACTERIZATION AND FACIES ANALYSIS OF THE JURASSIC NAVAJO SANDSTONE, CENTRAL UTAH

by Thomas C. Chidsey, Jr.[1], Thomas H. Morris[2], Stephanie M. Carney[1], Ashley D. Hansen[3], John H. McBride[2], and Craig D. Morgan (retired)[1]

[1]Utah Geological Survey, Salt Lake City, Utah
[2]Brigham Young University Department of Geological Sciences, Provo, Utah
[3]Petroleum Systems International, LLC, Salt Lake City, Utah

Cover photo: *Classic rounded cliffs, domes, and knobs of the eolian Lower Jurassic Navajo Sandstone, Glen Canyon Group; view into Eagle Canyon on the western flank of the San Rafael Swell north of Interstate 70. Photograph by Michael B. Chidsey, Sqwak Productions Inc.*

Suggested citation:

Chidsey, T.C., Jr., Morris, T.H., Carney, S.M, Hansen, A.D., McBride, J.H., and Morgan, C.D., 2020, Surface to subsurface reservoir/aquifer characterization and facies analysis of the Jurassic Navajo Sandstone, central Utah: Utah Geological Survey Special Study 167, 102 p., 3 appendices, 1 plate, https://doi.org/10.34191/ss-167.

SPECIAL STUDY 167
UTAH GEOLOGICAL SURVEY
UTAH DEPARTMENT OF NATURAL RESOURCES
2020

STATE OF UTAH
Gary R. Herbert, Governor

DEPARTMENT OF NATURAL RESOURCES
Brian C. Steed, Executive Director

UTAH GEOLOGICAL SURVEY
R. William Keach II, Director

PUBLICATIONS
contact
Natural Resources Map & Bookstore
1594 W. North Temple
Salt Lake City, UT 84116
telephone: 801-537-3320
toll-free: 1-888-UTAH MAP
website: utahmapstore.com
email: geostore@utah.gov

UTAH GEOLOGICAL SURVEY
contact
1594 W. North Temple, Suite 3110
Salt Lake City, UT 84116
telephone: 801-537-3300
website: geology.utah.gov

CONTENTS

FIGURES

TABLE

PLATE

ABSTRACT

The Early Jurassic Navajo Sandstone represents a large erg system that covered much of Utah. It serves as a reservoir both for hydrocarbons (oil and gas) and carbon dioxide (CO_2), an aquifer for disposal of produced water from coalbed methane fields, a potential storage unit for CO_2 captured from coal-fired power plants in the region, and in much of southern Utah the Navajo is the major aquifer for culinary water. Spectacular outcrops of the Navajo in the San Rafael Swell of east-central Utah and cores from Covenant oil field in the central Utah thrust belt, display the eolian facies characteristics, geometry, distribution, and nature of boundaries contributing to the overall heterogeneity of reservoir rocks and aquifers. This study focuses on the reservoir and aquifer characteristics of the Navajo Sandstone, from the surface to the subsurface, to expand the understanding of its ancient erg system.

We chose the Devils Canyon–Eagle Canyon area on the western flank of the San Rafael Swell for outcrop analogs because of their proximity to Covenant field to the west as well as to coal-fired power plants, Navajo produced-water disposal wells, and a CO_2-productive Navajo field, all to the north. Petrographic description, provenance determination, porosity and permeability analyses, and gamma-ray scintillometer measurements were completed along correlated composite measured sections of the Navajo Sandstone. The outcrop results were compared to those obtained from cores in Covenant field.

The Navajo Sandstone is famous for massive cross-stratified sandstone beds representing ancient dunes and is the dominant eolian deposit vertically and laterally in the stratigraphic section. The Navajo Sandstone is divided into eight facies in the study area: three dune facies – Large Trough Cross-stratified (LTC), Small Trough Cross-stratified (STC), and Reworked Eolian (RWE); and five interdune facies – Wavy Algal Mat (WAM), Sandy Algal Mat (SAM), Poorly Developed Interdune (PDI), Evolving Interdune (EID), and Ephemeral Fluvial Channel (EFC). The lateral extent of each interdune facies varies greatly, ranging from a few tens of meters to kilometers and accounts for less than 10% of the section. However, these deposits create baffles and barriers to fluid flow, partitioning the Navajo reservoirs or aquifers. This type of compartmentalization impacts drilling and completion strategies within the Navajo.

The 2004 discovery of Covenant oil field in the central Utah thrust belt, or “Hingeline” as it is often called, proved that this region contains the right components for large accumulations of oil. The field has produced more than 28 million barrels of oil from the Navajo Sandstone and overlying Middle Jurassic Temple Cap Formation. The Covenant core shows both dune and interdune facies in the Navajo Sandstone. All dune facies described in outcrop are present (LTC, STC, and RWE), whereas only two interdune facies are recognized (WAM and SAM). Porosity and permeability in dune facies range from 12% to 15%, and up to 156 millidarcies (mD), respectively. Within the interdune facies, porosity ranges from 5.8% to 9.4% and permeability is less than 1 mD. Thus, as seen in outcrop, the Navajo reservoir in Covenant field contains heterogeneity that is important to recognize for field development and production.

The world-class outcrops of the Navajo Sandstone in the San Rafael Swell demonstrate the complex nature of dune and interdune facies. The detailed descriptions of these facies and those identified in Covenant field cores provide a template for exploring and developing new oil fields, disposing of produced water, and targeting zones to store CO_2, in the Navajo and other formations elsewhere in Utah and worldwide that were deposited in eolian environments.

CHAPTER 1:
INTRODUCTION

by

Thomas C. Chidsey, Jr., and Thomas H. Morris

Access road to Devils Canyon is on the bench just above the prominent red, slope-forming mudstone unit in middle of photograph. The access road at this location is essentially at the transitional contact between the fluvial-dominated Kayenta Formation below the eolian-dominated Navajo Sandstone above.

CHAPTER 1:
INTRODUCTION

PURPOSE

The Navajo Sandstone represents a large erg system that covered much of Utah during the Early Jurassic (figure 1.1). Covenant and Providence oil fields were discovered within the central Utah thrust belt in 2004 and 2008, respectively, and both produce from the Navajo Sandstone (figures 1.2 and 1.3). They proved the viability of the Navajo as a subsurface reservoir. The Navajo also serves as a (1) natural gas (both hydrocarbon [mostly methane] and carbon dioxide [CO_2]) reservoir (Morgan, 2007), (2) produced-water disposal aquifer for coalbed methane (CBM) fields along the northwestern flank of the San Rafael Swell as well as Covenant field to the west (Montgomery Watson, 1997; Freethey and Stolp, 2010; Morgan and Kirby, 2017; Tabet, 2017), (3) potential storage unit for CO_2 that could be captured from coal-fired power plants in the region including the nearby Hunter and Huntington plants (Allis and others, 2003, 2005; White and others, 2003, 2004, 2005; Parry and others, 2007; Steele and others, 2018) (figure 1.2), and (4) aquifer for culinary water supplies in much of southern Utah.

Utah is unique in that representative outcrop analogs are present in or near each major oil and gas play and in significant aquifers. Production-scale analogs provide an excellent exposure, often in three dimensions, of facies characteristics, geometry, distribution, and nature of boundaries contributing to the overall heterogeneity of reservoir rocks and aquifers. An outcrop-analog model, combined with the details of internal facies characteristics, can be used as a "template" for evaluating data from conventional core, geophysical and petrophysical logs, and seismic surveys. When combined with subsurface geological and production data, the analog model will improve development drilling and production strategies, reservoir-simulation and groundwater models, reserve and water volume calculations, potential CO_2 or produced water storage capacity, and design and implementation of secondary/tertiary oil recovery programs and other best practices used in the oil and gas fields of Utah.

The determination that the two-part "upper and lower Navajo" reservoir of Covenant field is actually two different formations—the Navajo Sandstone and the Middle Jurassic Temple Cap Formation (deposited in a marine to marginal marine intertonguing eolian environment) (Sprinkel and others, 2009, 2011a; Doelling and others, 2013; Chidsey and others, 2014; Chidsey and Sprinkel, 2016)—suggests there are still things to learn about these Jurassic erg systems. With numerous reservoir baffles and barriers affecting communication between reservoir/aquifer flow units, the Covenant and Providence fields have also demonstrated the need to further understand the characteristics of the Navajo, particularly the effects of depositional facies on developing these partitions and baffles. Partitioning elsewhere within the Navajo has been recognized regionally in both the subsurface and in outcrop (Dalrymple and Morris, 2007; Hansen, 2007; Martin and others, 2007; McLelland and others, 2007; Sorber and others, 2007; Sprinkel and others, 2011a; Allen and others, 2013; Steele and others, 2018). The productive facies of the Temple Cap Formation (White Throne Member) have a limited distribution however, whereas the Navajo is regionally extensive.

Chidsey and others (2007) summarized core analyses from Covenant field. Their work, portions of which are incorporated herein, has improved our understanding of characteristics of the Covenant reservoir, yet by its nature, the data set is limited in view. For example, which "interdune" units (if any) are laterally extensive and consistently impermeable to partition the reservoir over its geographic extent? Which units could potentially serve as baffles to flow units? Finally, within the scale of a core, are there sedimentary structures and/or petrophysical characteristics that could help us differentiate baffles from barriers?

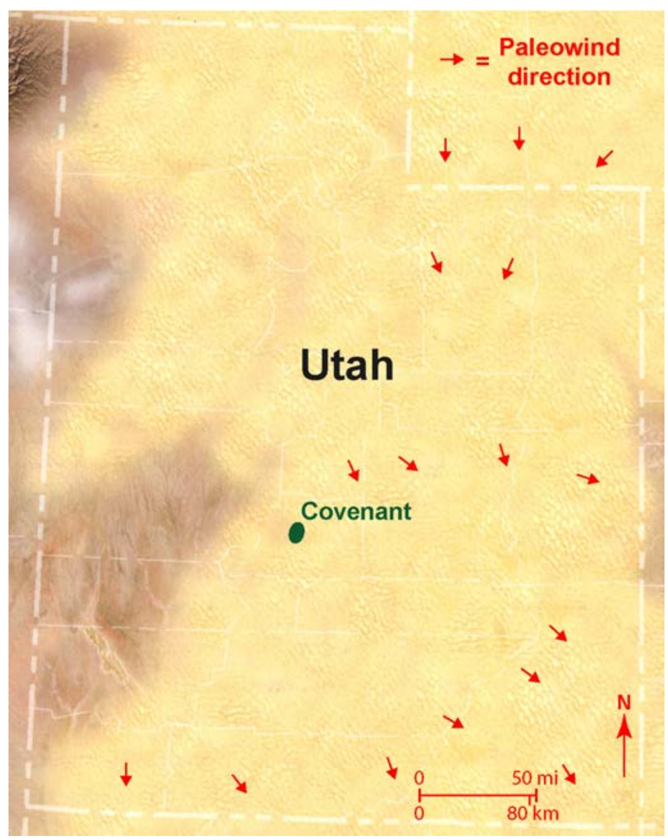

Figure 1.1. Paleogeographic map of Utah during deposition of the Early Jurassic (190 Ma) Navajo Sandstone and showing present-day Covenant oil field. Modified from Blakey and Ranney (2008).

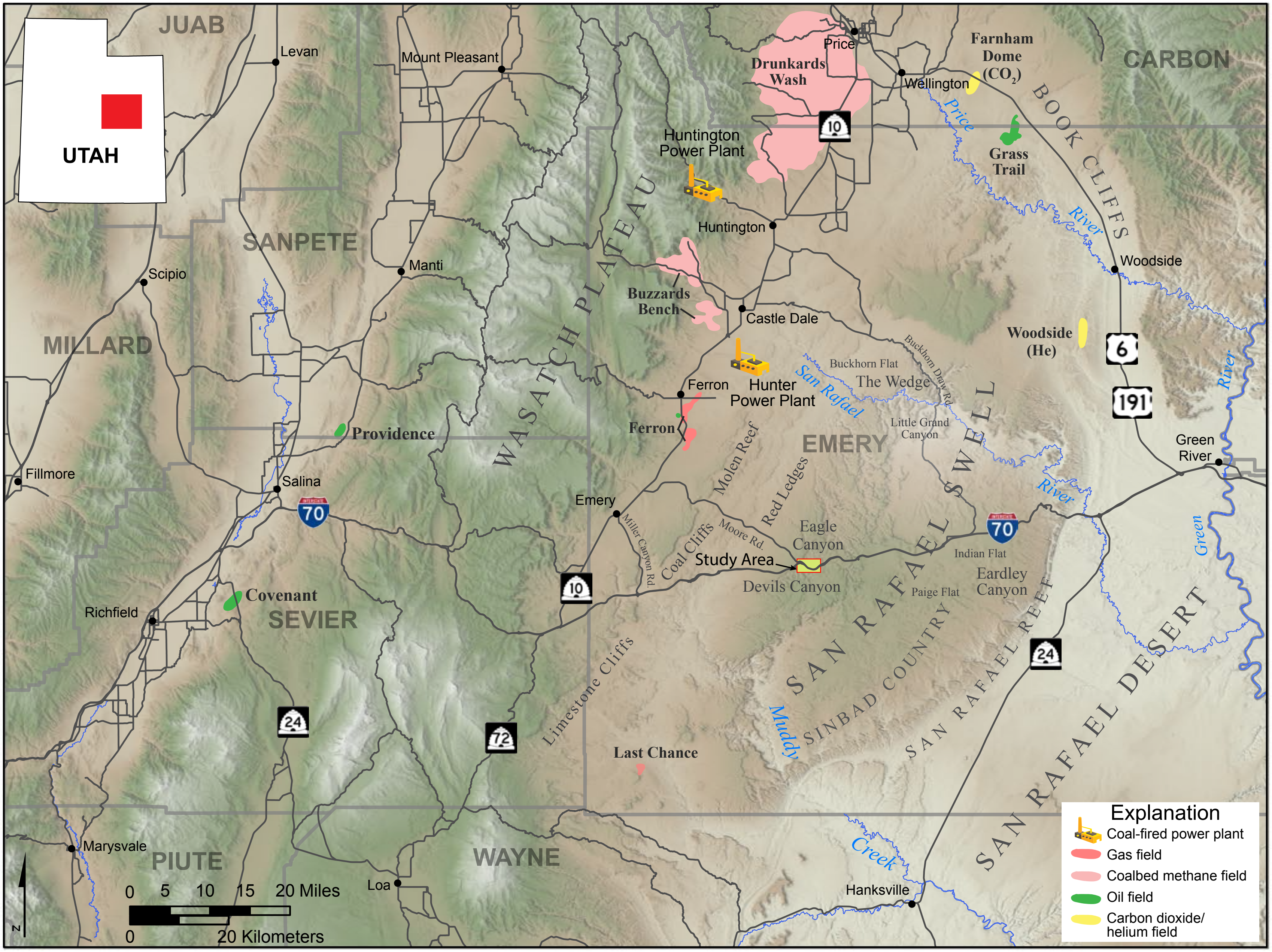

Figure 1.2. The San Rafael Swell and central Utah thrust belt, and the general location of the study area, oil and gas fields, the Hunter and Huntington coal-fired power plants, as well as major physiographic features, surrounding towns, and highways.

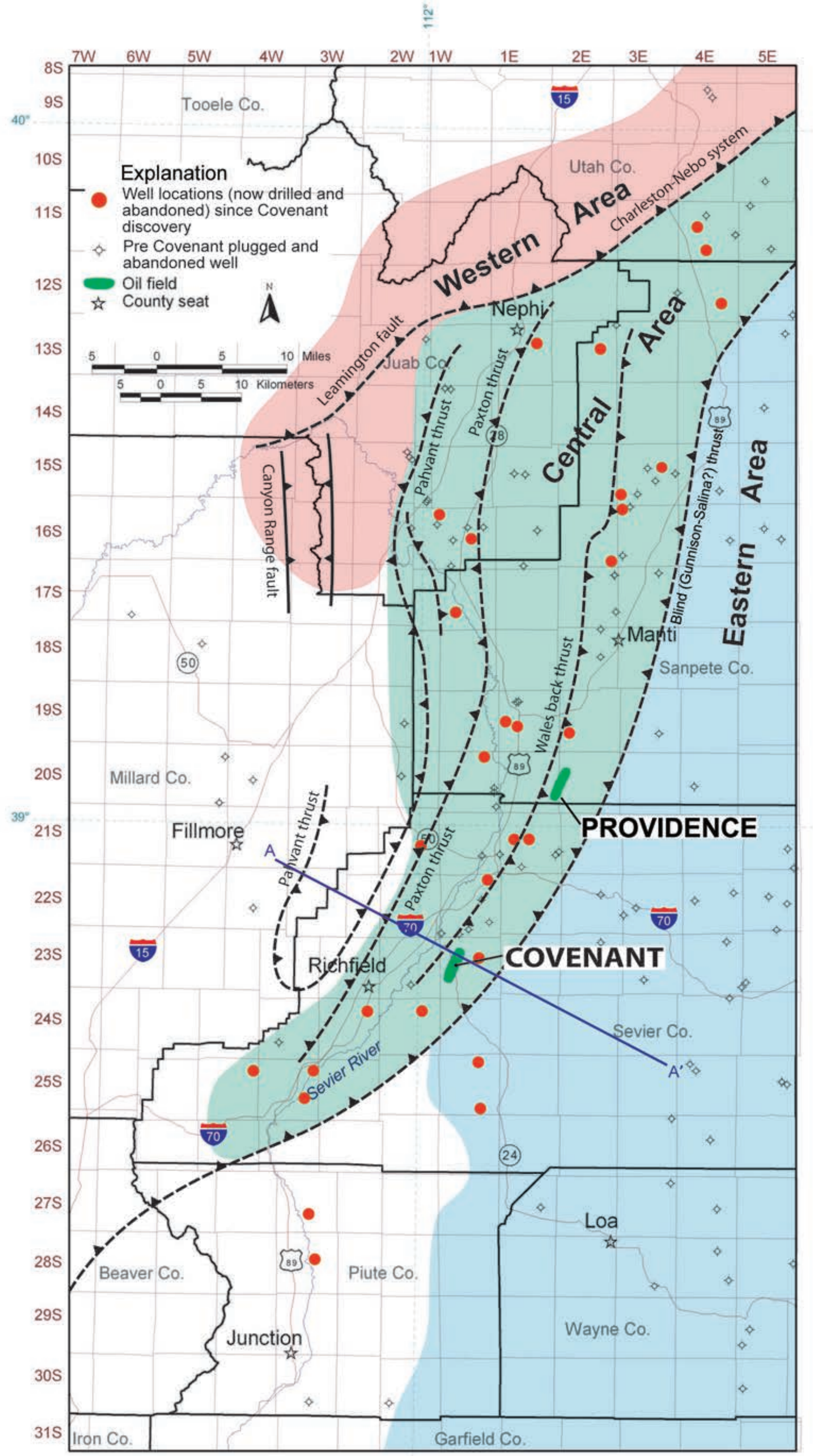

Figure 1.3. Selected thrust systems and oil field and well locations in the eastern, central, and western area of the central Utah thrust belt. Cross section A–A' shown on figure 1.7. After Chidsey and Sprinkel (2016).

A broader view of the Navajo Sandstone that addresses these questions is presented in this report. Our research incorporates sedimentologic, stratigraphic, and petrophysical studies to interpret lithofacies and the type of reservoir each would make in the subsurface (flow unit, baffle, or barrier). These studies were completed in two outcrop locations in an attempt to compare and better understand the Navajo reservoir characteristics of Covenant field and other potential oil discoveries, water-disposal aquifers, units for carbon capture and storage (CCS) in central Utah, or culinary water aquifers. We also investigated the variability of dune and interdune facies. This included both the lateral extent of different interdune facies as well as a wide variety of petrophysical characteristics between (and sometimes within) each interdune and dune facies. Whereas these interdune facies make up a relatively small amount of the total volume of the Navajo (less than 10%), they have a profound effect on the characteristics of the rock as a reservoir unit.

For ease of reading and reference, we have divided this report into chapters. This first chapter is an introduction to the Navajo Sandstone and the methods applied to our outcrop studies. Chapters 2 and 3 include all the research completed at each outcrop location—Devils Canyon and Eagle Canyon, respectively (figure 1.2). Chapter 4 includes analysis completed on core from Covenant field. Chapter 5 summarizes a high-resolution, shallow seismic experiment conducted in the Justensen Flats area in the Devils Canyon location. Chapter 6 summarizes the important findings and comparisons of our multidisciplinary research.

This report will aid the geoscientist and engineer in more accurately interpreting reservoir or aquifer flow units, baffles, and barriers within the Navajo and analogous depositional systems. With this enhanced knowledge, strategies for completion, development, production, enhanced oil recovery, produced-water disposal, culinary water management, and CCS should improve. We anticipate this work, which focuses on reservoir and aquifer characterization, will add to the already impressive amount of research completed on the Navajo Sandstone and benefit all those involved in understanding ancient erg systems.

REGIONAL OVERVIEW

San Rafael Swell

The San Rafael Swell is a broad, asymmetric, north-south- to southwest-northeast-trending anticlinal structure, about 120 kilometers (~75 mi) long and 56 kilometers (~35 mi) wide, that formed in response to compressional forces of the Laramide orogeny between latest Cretaceous time (about 70 million years ago [Ma]) and the Eocene (about 40 Ma) (Hintze and Kowallis, 2009) (figures 1.4 and 1.5). Uplift and erosion have made it a showcase of Colorado Plateau geology with a colorful array of sedimentary rocks over 2100 meters (>7000 ft) thick, ranging in age from Permian to Cretaceous (figure 1.6 represents those on the western flank of the Swell where the outcrop study sites are located), exposed in spectacular cliffs along cuestas, mesas, and deep canyons, especially in the Lower Jurassic Navajo Sandstone.

The sedimentary formations and their many members exposed in the San Rafael Swell were deposited in a wide range of environments including floodplain, stream, deltaic, swamp, tidal flat, shallow and restricted marine, and eolian—the focus of this study, i.e., the Navajo Sandstone (figure 1.6). Several major unconformities represent significant periods of erosion or non-deposition (Pipiringos and O'Sullivan, 1978), and the overlying J-1 unconformity is of primary importance in evaluating the Navajo (figure 1.6). Pliocene-age igneous rocks are present in the form of dikes, conduits, and sills intruded into exposed Triassic to Cretaceous sedimentary strata (figure 1.4).

The rocks in the San Rafael Swell have been folded, faulted, jointed, fractured, and uplifted. The backlimb beds of the study area dip approximately 8° to the northwest. Small to large subsidiary anticlines and synclines are found north to south along the San Rafael Swell. The major uplift and deformation of the San Rafael Swell was likely controlled by a large, blind (buried), basement-involved, high-angle reverse fault (hanging wall on the western side) bounding the eastern flank of the structure (figure 1.5). Three sets of high-angle normal faults are mapped at the surface, striking (1) northwest-southeast, (2) east-west, and (3) north-south to northeast-southwest (figure 1.4). Two styles of reverse faulting are identified in the San Rafael Swell: (1) west-directed, blind reverse faults on the eastern flank, and (2) east-directed, ramp-style thrusting. Sandstone beds in the Navajo and other thick formations in the San Rafael Swell are quartz rich and brittle, and when folded or bent, produce prominent joints and fractures.

The Colorado Plateau began to rise in late Cenozoic time during the Miocene Epoch (Hunt, 1956; Lucchitta, 1979; Hintze and Kowallis, 2009). This regional uplift changed the landscape from one of deposition to one of massive erosion by running water, mass wasting, and wind. Burial history models estimate the removal of 2400 meters (8000 ft) of sedimentary rock in the San Rafael Swell area (Nuccio and Condon, 1996; Nuccio and Roberts, 2003; Williams and others, 2007). The Green and Colorado Rivers probably came into existence synchronously with the uplift of the Colorado Plateau. As the plateau rose, the major rivers and their tributaries rapidly cut into the strata. The incision rate near the center of the Colorado Plateau (Lees Ferry, Arizona) is calculated at about 35 centimeters per thousand years (~14 in./k.y.) (Pederson and others, 2013). This incision produced the countless canyons in the San Rafael Swell and throughout the plateau. Most of the eroded material from the Colorado Plateau has been carried to the sea by the Colorado River system.

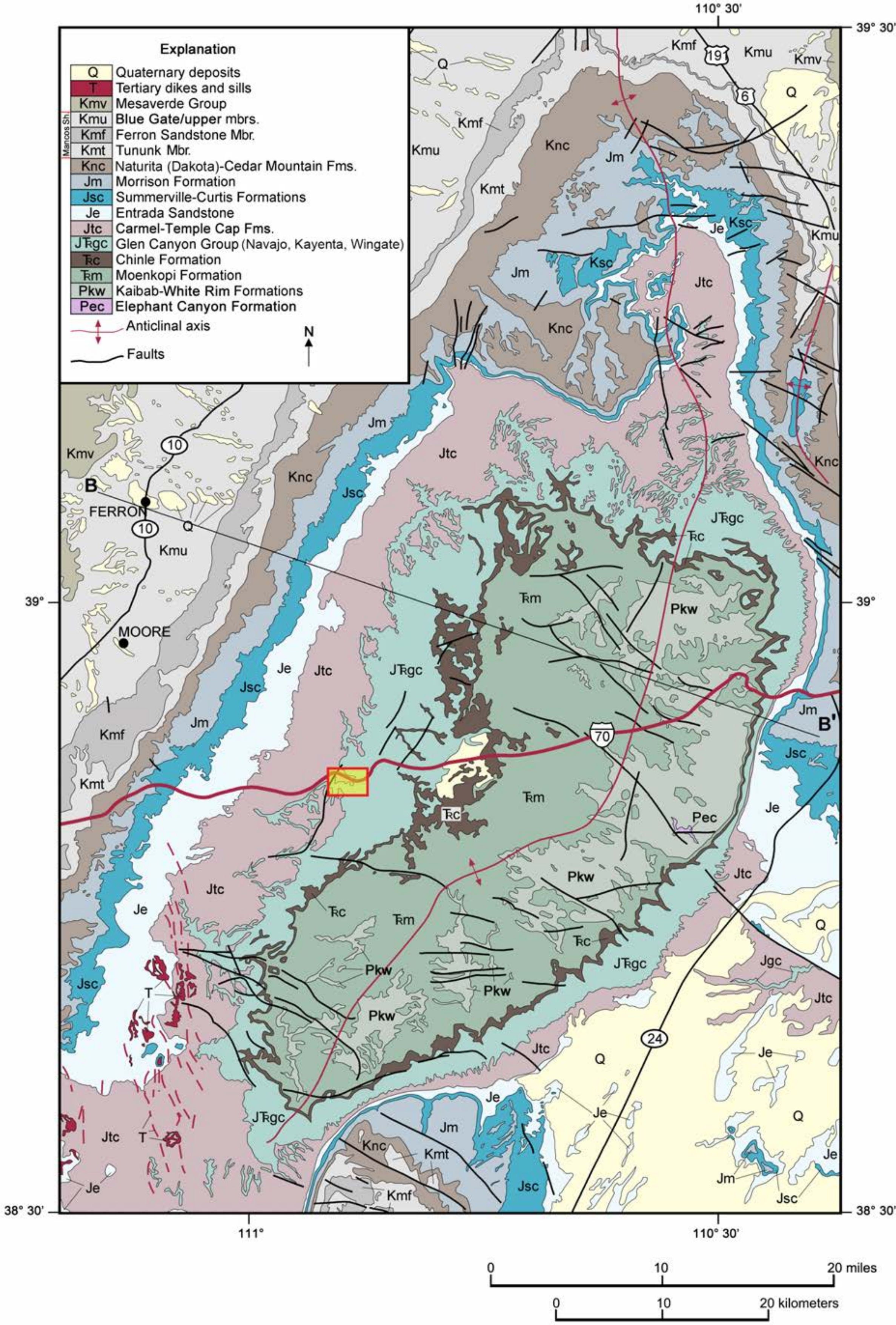

Figure 1.4. *Generalized geologic map of the San Rafael Swell and location of the study area (yellow box) within the Jurassic-Triassic Glen Canyon Group, which includes the Navajo Sandstone. Cross section B–B' shown on figure 1.5. After Doelling and Hylland (2002).*

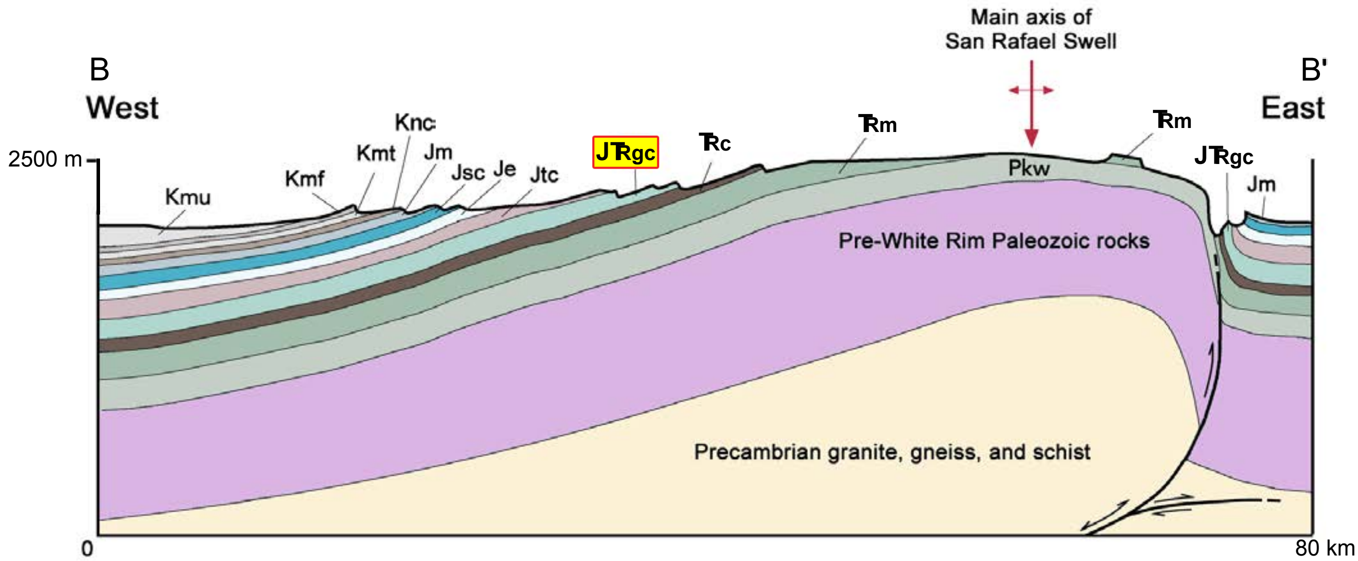

Figure 1.5. *Diagrammatic cross section across the middle of the San Rafael Swell. The cross section is not drawn to scale, but the vertical dimension is exaggerated about eight times relative to the horizontal; the horizontal length of the cross section covers about 80 kilometers (50 mi). Approximate location of the study area (yellow box) within the Jurassic-Triassic Glen Canyon Group indicated. Symbols and colors of geologic formations correspond to those shown on figure 1.4; location of cross section B–B' also shown on figure 1.4. After Doelling and Hylland (2002).*

Oil and gas (including CBM, CO_2, and helium), coal, industrial minerals (gypsum, bentonite clay, and humate), and uranium are found within the San Rafael Swell (Chidsey, 2013). The Navajo Sandstone serves as a produced water-disposal aquifer or reservoir for several of the gas fields found along the flanks of the Swell. Drunkards Wash CBM field, located on the northwestern flank near the town of Price (figure 1.2), was discovered in 1992 and is the third-largest gas field in Utah, having produced about 1.1 trillion cubic feet of gas along with 272 million barrels of water (BW) as of August 1, 2020 (Utah Division of Oil, Gas and Mining, 2020). Thermogenic and secondary biogenic gas are both sourced and produced from coalbeds of the Upper Cretaceous Ferron Sandstone Member of the Mancos Shale (figure 1.5) (Tabet and Burns, 1996). Helper and Buzzards Bench CBM fields located north and south of Drunkards Wash, respectively, have combined to produce over 386 billion cubic feet of gas (BCFG) and 205 million BW as of August 1, 2020 (Utah Division of Oil, Gas and Mining, 2020), also from the Ferron. The produced water from these three major gas fields is disposed into the Navajo Sandstone via 22 injection wells (Tabet, 2017; Utah Division of Oil, Gas and Mining records). Farnham Dome field, located on the north-plunging nose of the San Rafael Swell (figure 1.2), was discovered in 1924 and has produced more than 2 BCFG of 99% CO_2 from the Navajo (used in the past to make dry ice and in hydraulic fracturing operations in the Uinta Basin) (Moore and Sigler, 1987; Morgan, 2007). The trap for the field is a broad, elongate, south-north to southwest-northeast-trending anticline defined by surface mapping, drilling, and seismic data (Peterson, 1961; Morgan and Chidsey, 1991; Colson, 1993; Morgan, 2007). The CO_2 was likely generated from the thermal decomposition of Paleozoic carbonates deep in the Uinta Basin to the north and migrated up the stratigraphic section into the Navajo in the Farnham Dome structure (Morgan, 2007); CO_2 is present in other reservoirs in some fields in the region including Woodside Dome along the eastern flank of the San Rafael Swell (figure 1.2).

Central Utah Thrust Belt – Hingeline

The central Utah thrust belt is part of the Sevier (Cordilleran) thrust belt that trends through the entire state, also referred to by many geologists as “the Utah Hingeline.” It is loosely defined as the part of the thrust belt south of the Uinta Mountains of northeastern Utah, trending through central Utah to the Marysvale–Wah Wah volcanic complex of south-central Utah; the volcanic rocks shown on figure 1.7 represent the northern extent of the complex. Throughout this area’s geologic history, the Hingeline marks a pronounced boundary between different geologic terranes and processes. From Late Proterozoic to Triassic time, it marked the boundary between a very thick succession of sediments deposited in western Utah and a much thinner succession deposited in eastern Utah. During Cretaceous and early Tertiary time, the Hingeline coincided with and influenced thrusts at the eastern edge of the Sevier orogenic belt. Today in central Utah it marks the general boundary between the Basin and Range and Colorado Plateau physiographic provinces.

In reality, the Hingeline is an area rather than a line, and includes geologic features common to both the Basin and Range and Colorado Plateau physiographic provinces: Sevier orogenic thrust faults, basement-cored Late Cretaceous–Oligocene Laramide uplifts (plateaus and the Wasatch monocline), and Miocene to Holocene normal faults. Paleozoic rocks

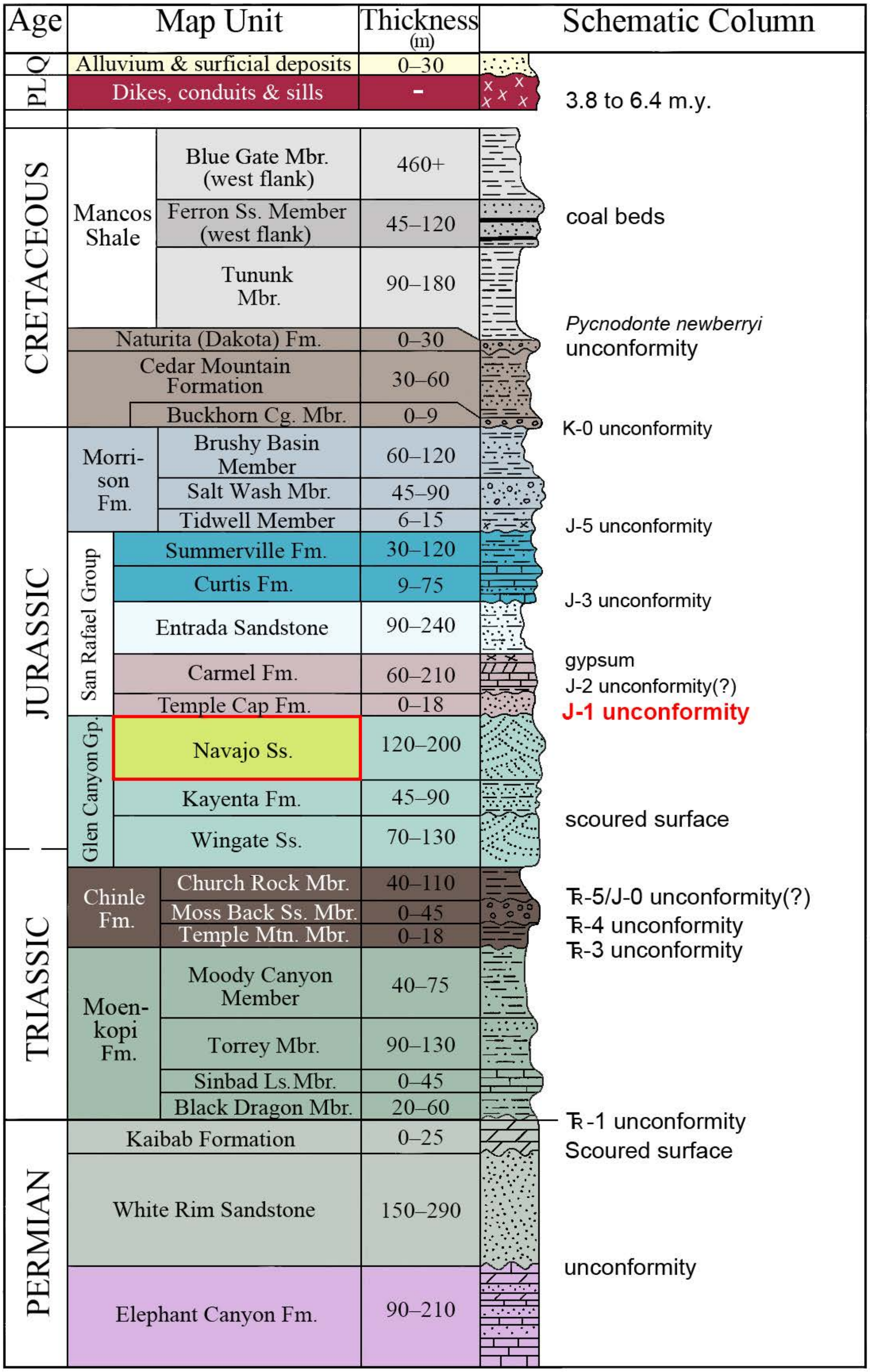

Figure 1.6. *Stratigraphic column of exposed rocks along the western flank of the San Rafael Swell, including age, thickness, lithology, and weathering profile. Modified from Hintze and Kowallis (2009).*

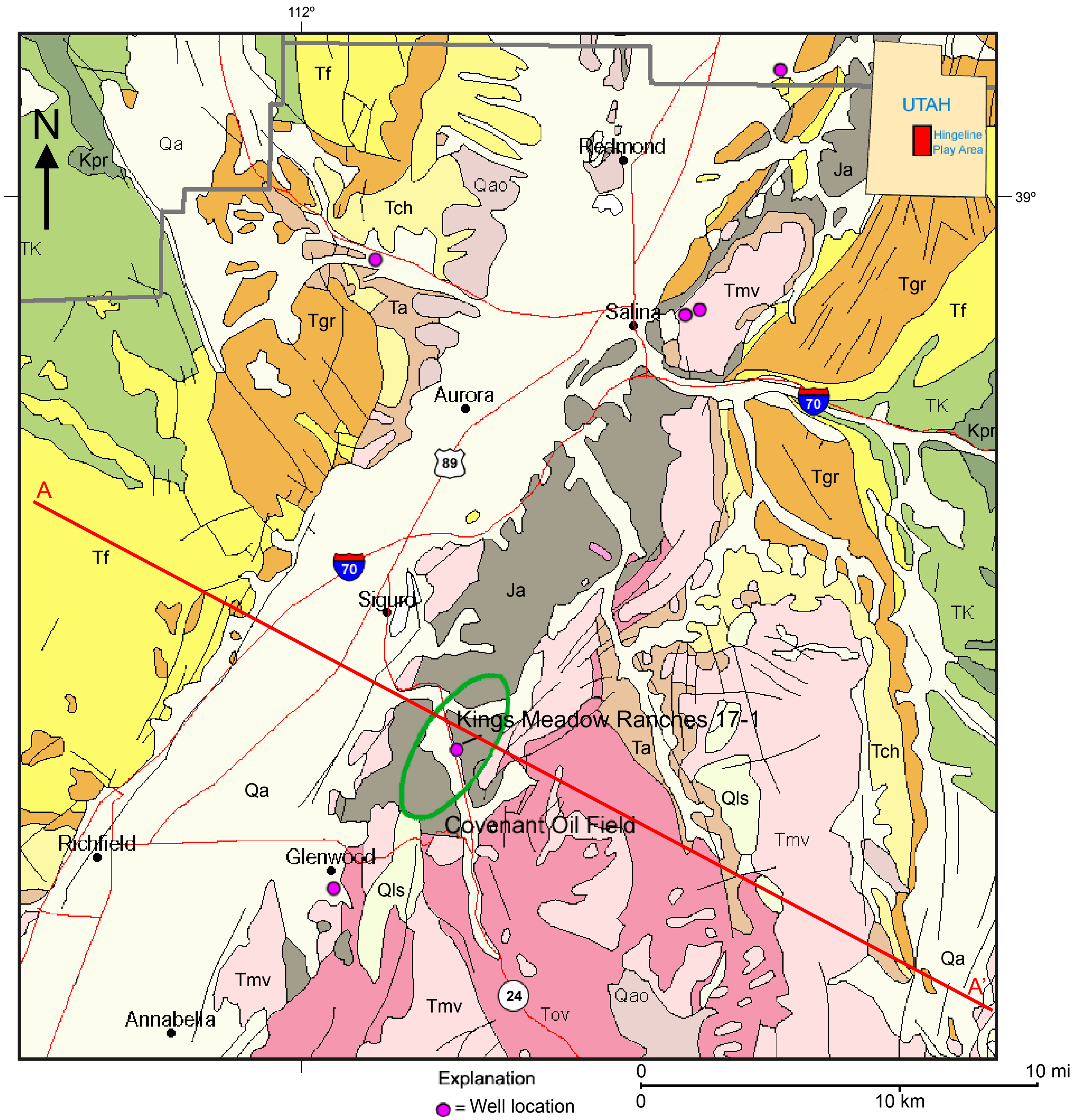

Qa - Quaternary alluvium and colluvium
Qao - Quaternary older alluvial deposits
Qls - Quaternary landslide deposits
Tmv - Tertiary (Miocene) volcanic rocks undivided
Tov - Tertiary (Oligocene) volcanic rocks undivided
Ta - Tertiary (Eocene) Aurora Formation
Tch - Tertiary (Eocene) Crazy Hollow Formation
Tgr - Tertiary (Eocene) Green River Formation
Tf - Tertiary (Paleocene) Flagstaff Limestone
Tk - Tertiary (Paleocene)-Cretaceous North Horn Formation
Kpr - Cretaceous Price River Formation
Ja - Jurassic Arapien & Twist Gulch Formations

Figure 1.7. *Generalized geologic map of the Covenant oil field area (green circle), Sevier County, central Utah. Cross section A–A', which extends beyond the edges of this figure, is shown on figure 1.8. Modified from Hintze and others (2000).*

thicken westward across the Hingeline area from thin cratonic deposits, whereas the Upper Cretaceous section includes thick synorogenic deposits reflecting proximity of the Sevier orogenic belt to the west. Several depositional environments during the Mississippian through Permian produced organic-rich deposits capable of generating hydrocarbons.

An extensional fault system, including the high-angle, basement-involved "Ephraim fault," was located in central Utah during the Middle Jurassic (Moulton, 1976; Schelling and others, 2007). In central Utah, large-scale thrust sheets were emplaced during latest Jurassic through early Tertiary time by compression of the actively evolving foreland basin (DeCelles and Coogan, 2006; Schelling and others, 2007). The youngest evidence of thrust faulting is about 40 Ma in central Utah (Lawton, 1985; DeCelles and others, 1995; Lawton and others, 1997; Willis, 1999; Constenius and others, 2003; DeCelles, 2004; DeCelles and Coogan, 2006). The thrust belt is more than 160 kilometers (100 mi) wide.

Major thrust faults in central Utah (from west to east) include the Canyon Range, Nebo, Pahvant (Royse, 1993), Paxton, Aurora, and Gunnison-Salina (Villien and Kligfield, 1986; Schelling and others, 2007) (figures 1.3, 1.8, and 1.9). These thrust faults represent detached, thin-skinned, compressional styles of deformation, with eastward combined movement of greater than 140 kilometers (90 mi) (DeCelles and Coogan, 2006). Easternmost thrust systems moved less than western thrust systems and are generally younger; the Canyon Range thrust was emplaced during latest Jurassic–Early Cretaceous time, the Pahvant thrust was emplaced in Albian time, the Paxton thrust was emplaced in Santonian time, and the Gunnison-Salina thrust was active from late Campanian through early Paleocene time (DeCelles and Coogan, 2006). The Ephraim fault and other Middle Jurassic faults may have also experienced Laramide-age (Campanian through Eocene) movement.

Surface traces of the thrust faults generally trend in a north-northeastern direction. Some of the thrust faults do not extend to the surface, and the term "blind" thrust is applied to buried faults like the Gunnison-Salina thrust. The Pahvant, Paxton, Aurora, and Gunnison-Salina thrust systems contain Lower Cambrian through Cretaceous strata (figures 1.8 and 1.9). Jurassic shale, mudstone, and evaporite beds in the Arapien Formation serve as the main glide planes along the hanging-wall flats of these thrust systems. The leading edges of the thrust faults are listric in form and structurally complex. They include numerous thrust splays, back thrusts, duplex systems (particularly in the younger eastern thrusts), fault-propagation folds (fault-bend folds), and ramp anticlines.

Central Utah thrust plates, like the Canyon Range thrust plate, are as much as 12,000 meters (36,000 ft) thick (DeCelles and Coogan, 2006), although younger eastern plates tend to be thinner. The eastern plates also deformed into smaller-amplitude fault-propagation folds and ramp anticlines than did western plates (Willis, 1999). Middle Jurassic extensional faults, such as the Ephraim and similar faults in the region, determined the position of these ramp anticlines and associated duplexes along thrust systems by acting as buttresses to plate movement (Schelling and others, 2007).

Listric normal faults formed during the Neogene by movement along many pre-existing thrust ramps, splays, and associated back thrusts. Other normal faults related to Basin

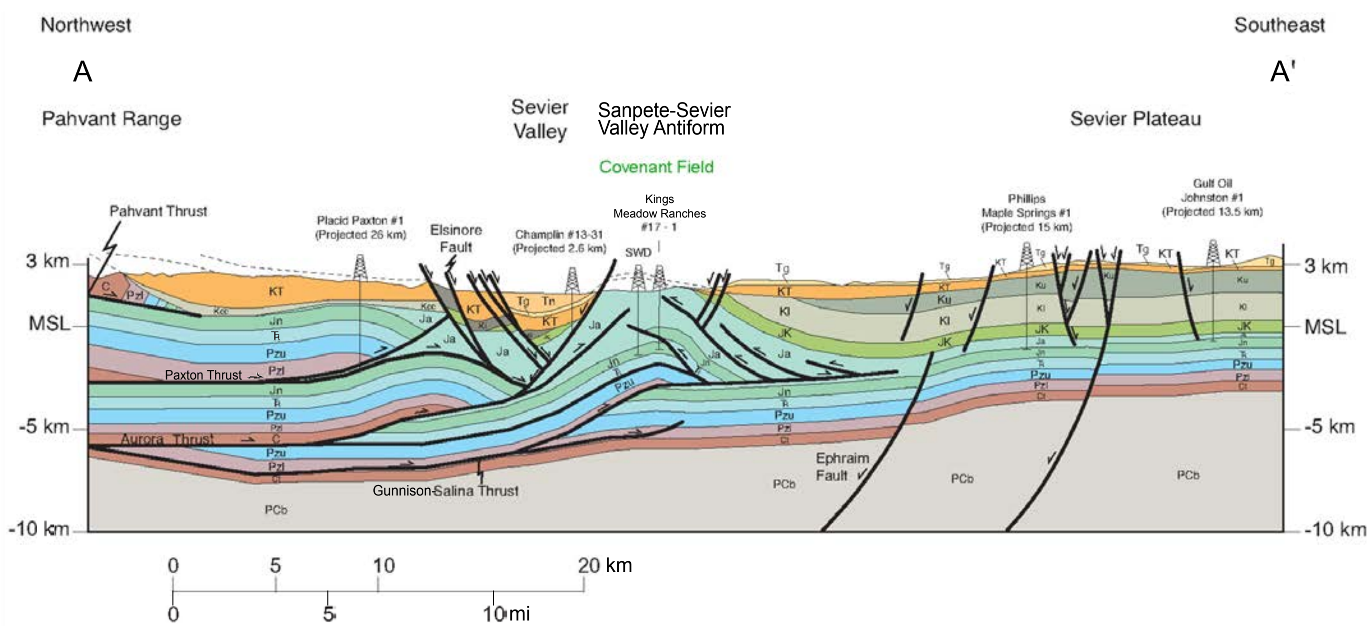

Figure 1.8. Balanced structural cross section through the central Utah thrust belt from the Pahvant Range through Covenant oil field to the Sevier Plateau. Stratigraphic labels are shown on figure 1.9; location of cross section A–A' shown on figures 1.3, 1.7, 4.1, and 4.3. Modified from Schelling and others (2007).

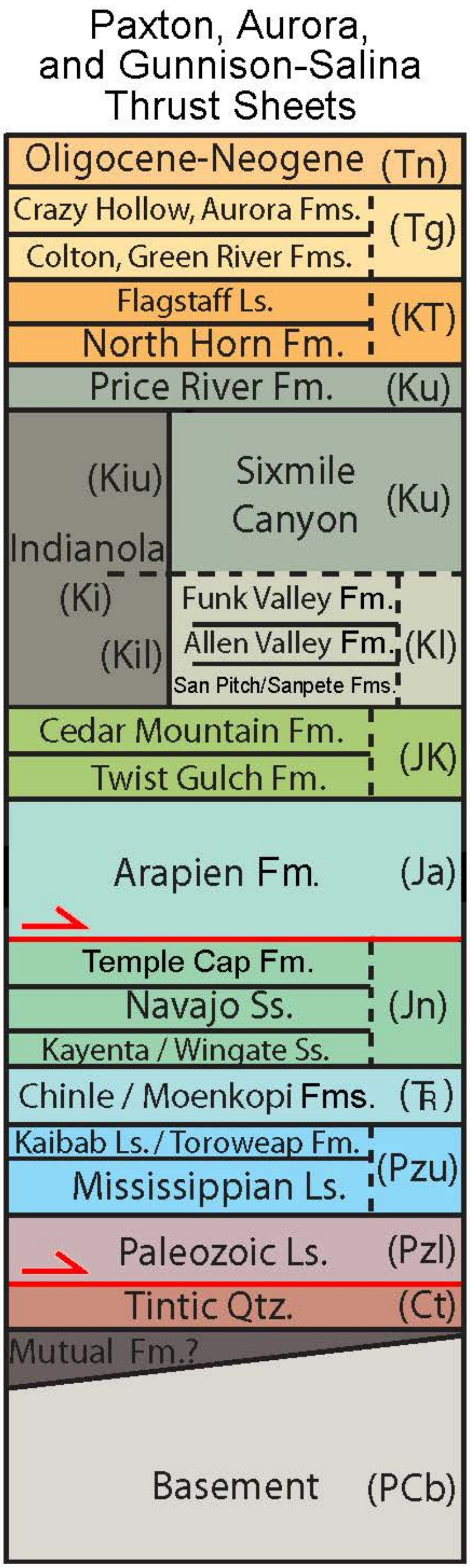

Figure 1.9. *Tectono-stratigraphic column for the Paxton, Aurora, and Gunnison-Salina thrust sheets. Stratigraphic labels used on structural cross section A–A' (figure 1.8) are included; arrows indicate significant detachments within or at the base of the thrust sheets. Modified from Schelling and others (2007).*

and Range extension dissected thrust plates into additional, compartmentalized blocks (Schelling and others, 2007). Some local ductile deformation of Arapien evaporites further complicated the structural picture of the region (Witkind, 1982). Potential hydrocarbon traps form on discrete, seismically defined, subsidiary closures on major ramp anticlines and fault-propagation/fault-bend folds.

The rocks exposed in the Covenant field area include the Middle Jurassic Arapien and Twist Gulch Formations, which are unconformably overlain by Cretaceous and Tertiary strata (figures 1.7 and 1.10). Oligocene and Miocene volcanic rocks also cover much of the area. Small normal faults generally trend north-south or northeast-southwest parallel to the west-northwest-dipping Wasatch monocline, particularly in the Eocene Green River Formation (figure 1.7).

The Jurassic Navajo Sandstone

General Description

The Early Jurassic (Pliensbachian/Toarcian) Navajo Sandstone represents a large erg system that covered much of Utah and Arizona and extending into Wyoming and Nevada (figure 1.1), where it is called the Nugget and Aztec Sandstones, respectively (Kiersch, 1950; Hintze and Kowallis, 2009). This sandstone was deposited approximately 200 Ma when the western United States had an arid climate at about 5° to 20° north latitude (Kocurek and Dott, 1983; Allen and others, 2000; Loope and others, 2001). Desert and erg systems were intermittent in this area from the late Paleozoic through the Jurassic. The Navajo/Nugget erg covered approximately 350,000 square kilometers (~140,000 mi^2) (Beitler and others, 2005) and began in latest Triassic time lasting approximately 20 million years (Hintze and Kowallis, 2009). The Navajo Sandstone is noted for its picturesque rounded outcrop exposures, its white to reddish-orange color, and its broad, sweeping high-angle, trough cross-stratification (figure 1.11). The Navajo produces some of the great vistas on the Colorado Plateau and is one of the most studied sedimentary formations on the plateau.

Chemical analysis of zircons within the Navajo Sandstone suggests a sand source as distal as the Appalachian Mountains in the eastern part of the continent. Sand was likely carried north, around the Ancestral Rockies by rivers and then blown south into the erg system (Dickinson and Gehrels, 2003, 2010; Rahl and others, 2003). Some of the sand may have been supplied to the erg from beach sediments in the northwest which were replenished by longshore drift from the epicontinental sea. For example, the marine Sunrise Formation in western Nevada is associated with Navajo deposits to the northwest of our study area (Doe and Dott, 1980; Kocurek and Dott, 1983).

The eolian deposits in the Navajo Sandstone include dunes, interdunes, and sand sheets. Navajo dunes were often large (widths up to 670 meters [2200 ft]) transverse barchanoid

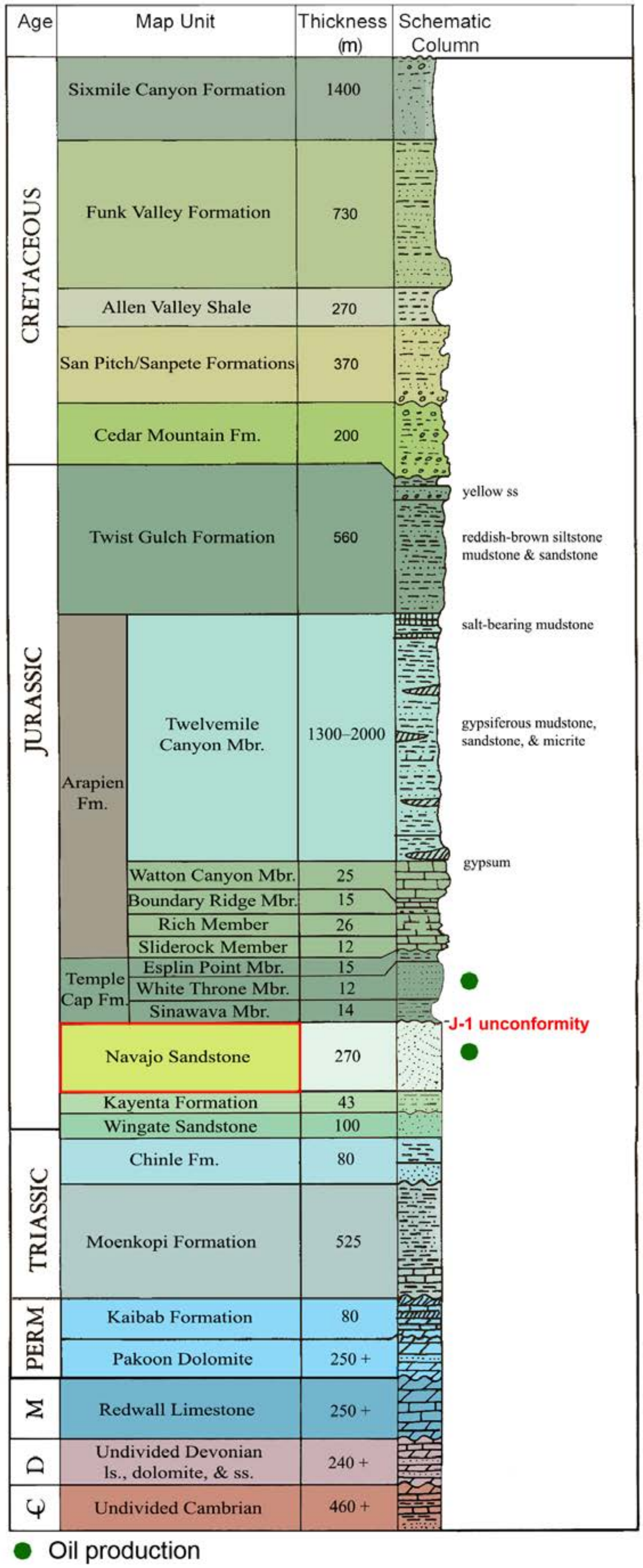

Figure 1.10. *Stratigraphic column of rocks exposed and in the subsurface of the central Utah thrust belt in the Covenant field area, including age, thickness, lithology, and weathering profile. Modified from Hintze and Kowallis (2009).*

ridges as suggested by large-scale cross-stratification that indicated paleowind directions were dominantly from the north and northwest (figures 1.1 and 1.11) (Picard, 1975; Peterson, 1988; Kocurek and Dott, 1983; Fryberger, 1990; Hartwick, 2010). Interdunes consisted of playas and oases. A high water table produced oases; deposition occurred when springs and lakes existed for relatively long periods of time. The high water table also resulted in early soft-sediment deformation in overlying dune sands (Sanderson, 1974; Doe and Dott, 1980). Some Navajo interdunes were erosional (deflation) areas associated with running water, such as a wadi (desert wash). Sand sheets, represented by low-relief, poorly drained, vegetated or gravel pavement deposits, were also common (Lindquist, 1988). These areas acted as sand transport surfaces.

Outcrops of the Navajo Sandstone display classic eolian bedforms (Ahlbrandt and Frybreger, 1982) such as tabular planar, wedge planar, and large-scale trough cross-strata (figure 1.11), which may occur in sets up to 8 meters (25 ft) thick. Dips of cross-beds between set boundaries vary as much as 40° from the nearly horizontal structural attitude of the formation. Dune sand-flow toes often form tangential contacts of cross-beds with the lower bounding surfaces (Ahlbrandt and Fryberger, 1982). Dune facies from the brink to the toe of the dune slipface consist of (1) thin, reverse graded, tabular, pinstriped grainfall laminae, (2) thick, subgraded avalanche laminae, and (3) thin, tightly packed, reworked ripple strata at the dune toe (Lindquist, 1983). Wind ripples or high-index ripples are occasionally preserved on topset deposits.

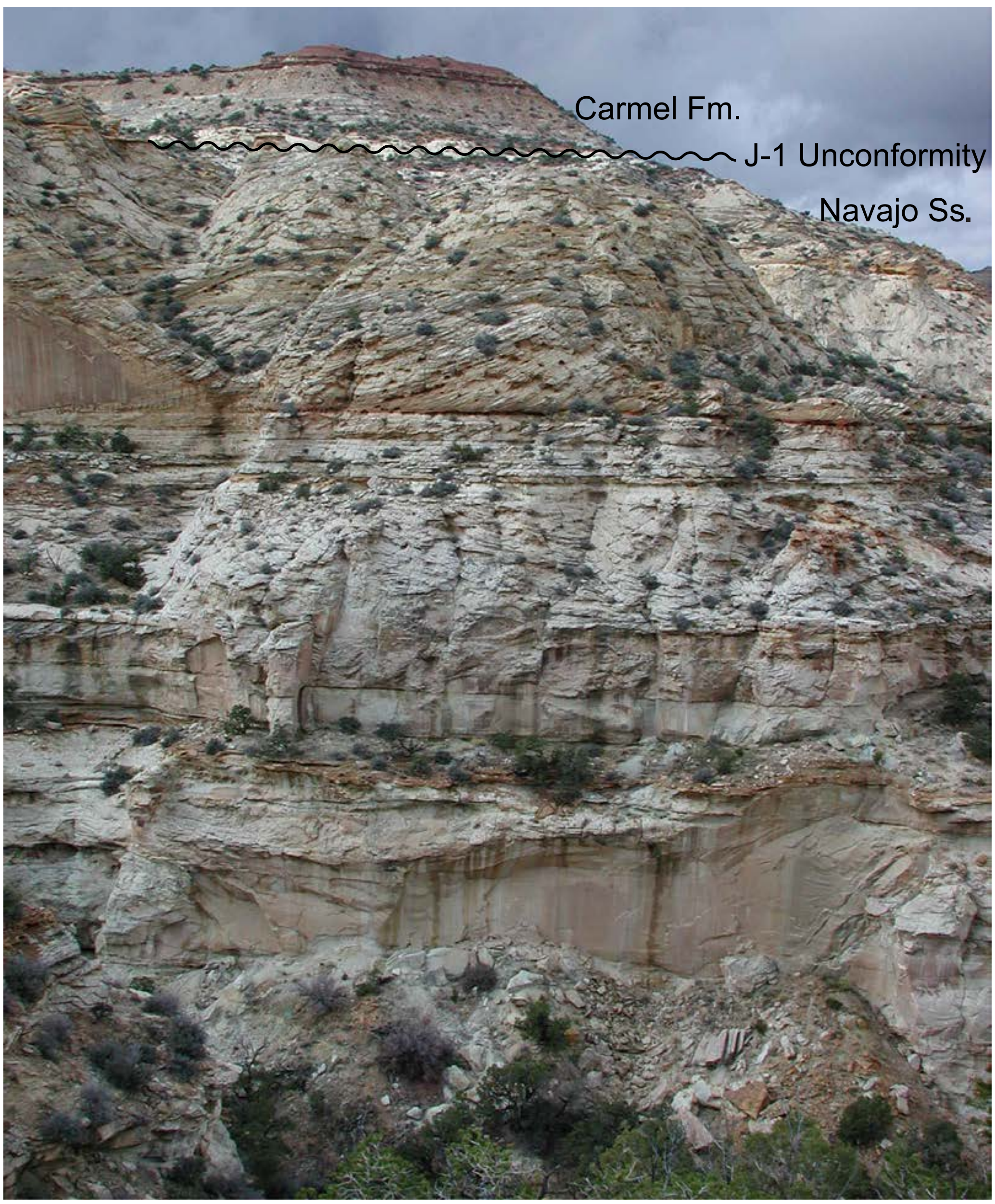

Figure 1.11. *Northwest view from Eagle Canyon of a nearly complete Navajo Sandstone section, displaying numerous dune and interdune facies, capped by the Carmel Formation.*

The Navajo Sandstone in our study area is composed of dominantly subfeldspathic quartz arenites. Grains are dominantly fine to medium in size, moderate to well rounded, frosted, and moderate to well sorted. Several interdune facies display variations in these textures and one facies is dominated by carbonates. Reported porosity within the Navajo has ranged from 0% to 30% depending on cementation, compaction, and mechanical deformation (Sanderson, 1974; Kocurek and Hunter, 1986; Eichhubl and others, 2004; Allen and others, 2013).

The Navajo-Nugget Sandstone as a Subsurface Reservoir or Aquifer

Jurassic-Triassic Nugget Sandstone reservoir, Utah-Wyoming salient of the thrust belt: The Navajo Sandstone produces oil at Covenant and Providence fields in the central Utah thrust belt (figure 1.2); Covenant field is discussed in detail in Chapter 4. The stratigraphically equivalent Jurassic-Triassic Nugget Sandstone is the most prolific oil, condensate, and gas play to the north in the Utah-Wyoming salient of the thrust belt (figure 1.12). The Nugget has produced nearly 300 million barrels of oil (BO) since the first field, Pineview in Summit County, Utah, was discovered in 1975. Thirteen Nugget fields currently exist: eight entirely in Wyoming, four entirely in Utah, and one (Anschutz Ranch East) in both Utah and Wyoming. The Nugget is typically 340 meters (1100 ft) thick in the play area (Hintze and Kowallis, 2009). Nugget net-pay thickness is variable, ranging from 7 to 300 meters (22–900 ft).

The Nugget Sandstone consists of lower, middle, and upper zones based on core and geophysical log analysis (figure 1.13) (Lindquist, 1988). Each zone has a subtle but distinct characteristic geophysical log response. The lower Nugget zone is composed of a basal, thin-bedded unit characterized by horizontal stratification and ripple marks, and an overlying section dominated by climbing ripple laminae and small-scale cross-beds (Picard, 1975; Lindquist, 1988). The middle and upper zones consist of a cyclic dune/interdune sequence (the principal petroleum-bearing section) characterized by cross-stratification. The middle zone is dominated by large-scale, planar or wedge-planar cross-stratification (up to 35°) (Conner and Covlin, 1977), whereas the upper zone is dominated by wind ripples and small-scale cross-stratification.

The Nugget Sandstone has heterogeneous reservoir properties because of (1) cyclic dune/interdune facies with better porosity and permeability that developed in certain dune morphologies, (2) diagenetic effects, and (3) fracturing. The typical Nugget sandstone has an average porosity of 11%. The Nugget reservoirs exhibit significant secondary porosity in the form of fracturing. Permeabilities in the Nugget range from 1 mD to more than 200 mD. The best permeability within Nugget dune deposits is along bounding surfaces (bedding planes); preferred directions are along the dip and strike of the individual slipfaces (cross-stratification) (Lindquist, 1983). Porosity and permeability are greatest in thickly laminated avalanche deposits (Hunter, 1977; Schenk, 1981).

Navajo-Nugget aquifer characteristics for produced-water disposal, eastern and east-central Utah: As mentioned above, the Navajo Sandstone serves as a produced-water disposal aquifer for the CBM fields along the flank of the San Rafael Swell (Drunkards Wash, Buzzards Bench, and Helper) near Price and Covenant oil field in the central Utah thrust belt (figure 1.2), as well as a potential water disposal unit for fields in the Uinta Basin to the north and east (in the northernmost part of the basin it is called the Nugget Sandstone) (Sprinkel, 2006, 2007; Sprinkel and others, 2011b; Morgan and Kirby, 2017). Currently only very minor Navajo oil and gas production occurs in the southern Uinta Basin and abandoned CO_2 production at Farnham Dome field on the north-plunging nose of the Swell, as described previously. The Nugget in most wells in the Uinta Basin and to the west and southwest has a maximum thickness of 250 to 350 meters (800–1200 ft), thinning to less than 120 meters (<400 ft) to the east (figure 1.14); this thickness represents the Jurassic-Triassic Glen Canyon Group (figure 1.6) and the Navajo-Nugget accounts for a significant part of that thickness (Morgan and Kirby, 2017). In southern Utah, the Navajo is a major aquifer for culinary water and ranges in thickness from 90 to 700 m (300–2300 ft), averaging about 425 m (~1400 ft).

Very few cores have been taken from the Navajo-Nugget Sandstone in the Uinta Basin. As a result, little is known about the spatial distribution of the porosity to permeability relationship in the reservoir. Based on porosity determined from density or sonic well logs, sandstone with 6% or more effective porosity ranges from 4 to 390 meters (14–1280 ft) thick (figure 1.15), with an average thickness of 206 meters (675 ft). In the deeper parts of the Uinta Basin, compaction and secondary diagenesis has greatly reduced the reservoir quality (Morgan and Kirby, 2017). The hydraulic conductivity of the Navajo aquifer south of the Uinta Basin is 0.03 to 3 meters (0.1–10.0 ft) per day (Freethey and Cordy, 1991).

The Navajo Sandstone aquifer in east-central Utah was investigated by Freethey and Stolp (2010). They described groundwater flow and solute transport between the San Rafael Swell recharge area and the San Rafael and Green River discharge areas. The Uinta Basin has little or negligible groundwater flow in the Navajo. Freethey and Stolp (2010) also found that total dissolved solids concentrations in the Navajo (Glen Canyon) aquifer increase from about 3000 milligrams per liter (mg/L) to greater than 10,000 mg/L in less than 8 kilometers (<5 mi) as depth of burial increases by about 460 meters (~1500 ft). Freethey and Cordy (1991) reported that Mesozoic aquifers, including the Navajo, in the upper Colorado River basin generally have sodium chloride water in the deep basins in excess of 35,000 mg/L and calcium bicarbonate water in shallow basins less than 2000 mg/L. Both waters have minor concentrations of iron and manganese.

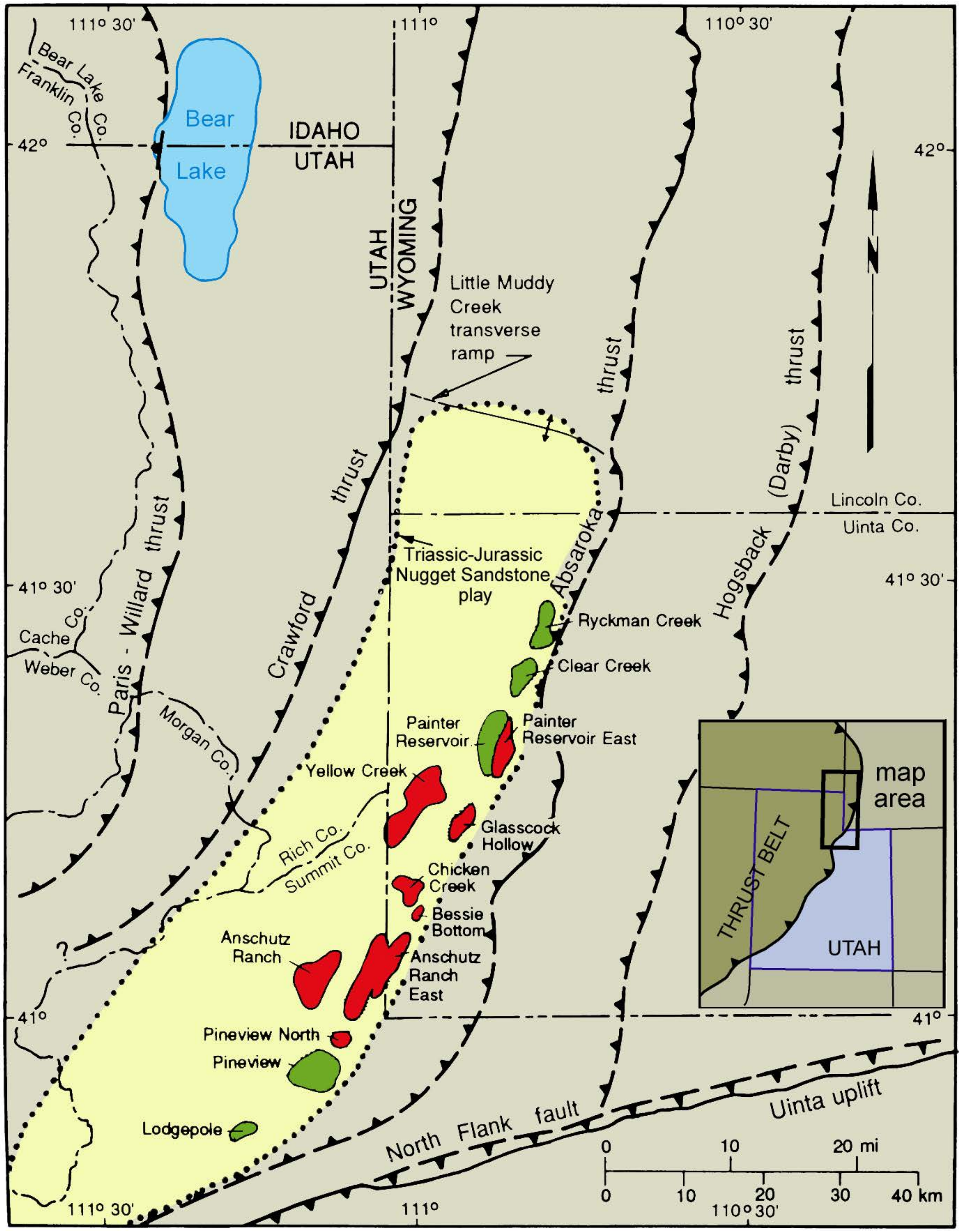

Figure 1.12. Location of reservoirs that produce oil (green) and gas and condensate (red) from the Jurassic-Triassic Nugget Sandstone, Utah and Wyoming; major thrust faults are dashed where approximate (teeth indicate hanging wall). The Nugget Sandstone thrust belt play area is dotted. Modified from Chidsey (1993).

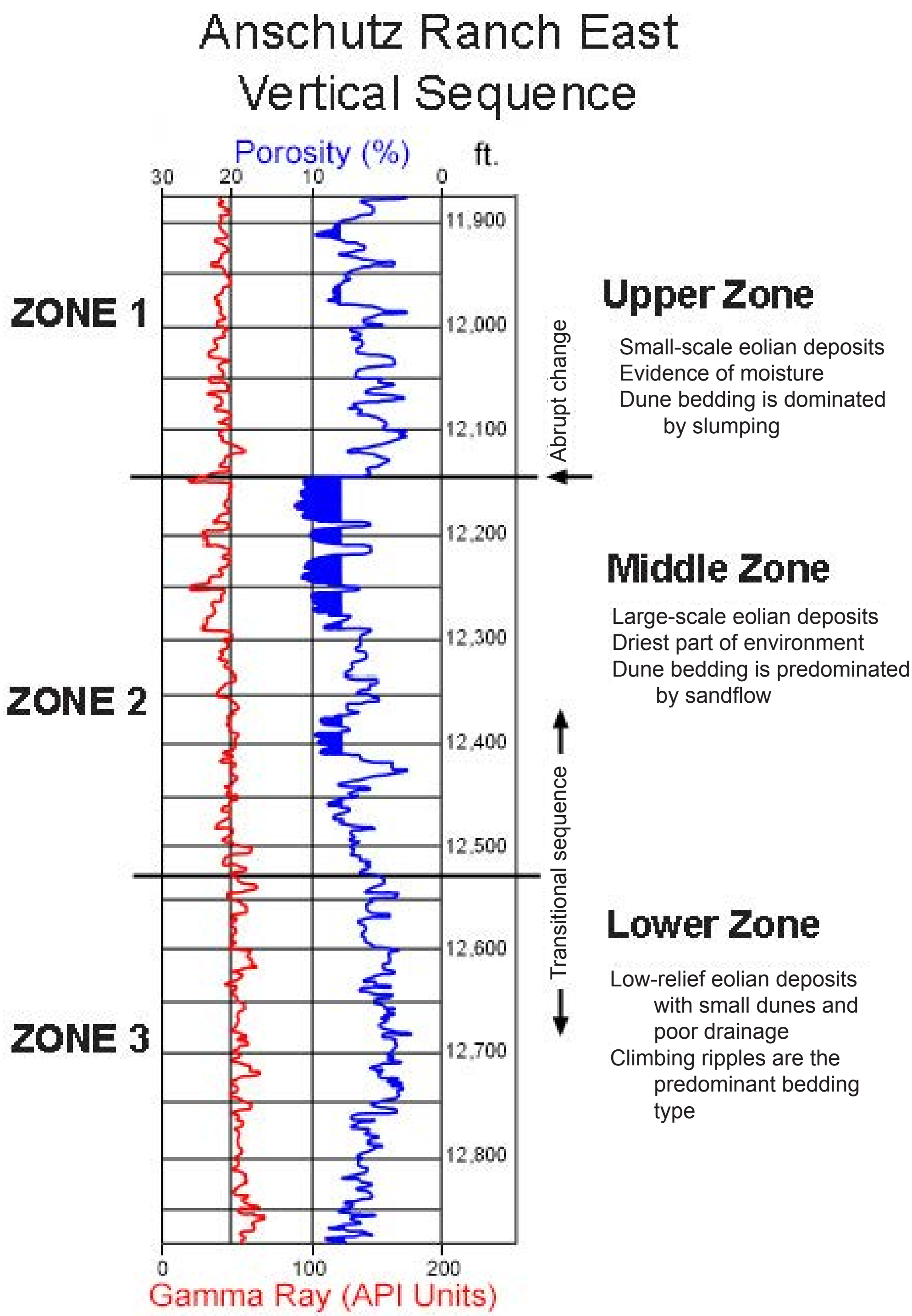

Figure 1.13. *Reservoir quality of the Nugget Sandstone based on porosity and gamma-ray characteristics, ARE No. W29-12 well (section 29, T. 4 N., R. 8 E., Salt Lake Base Line & Meridian), Anschutz Ranch East field, Summit County, Utah. Modified from Lindquist (1988), White and others (1990), and Keele and Evans (2008).*

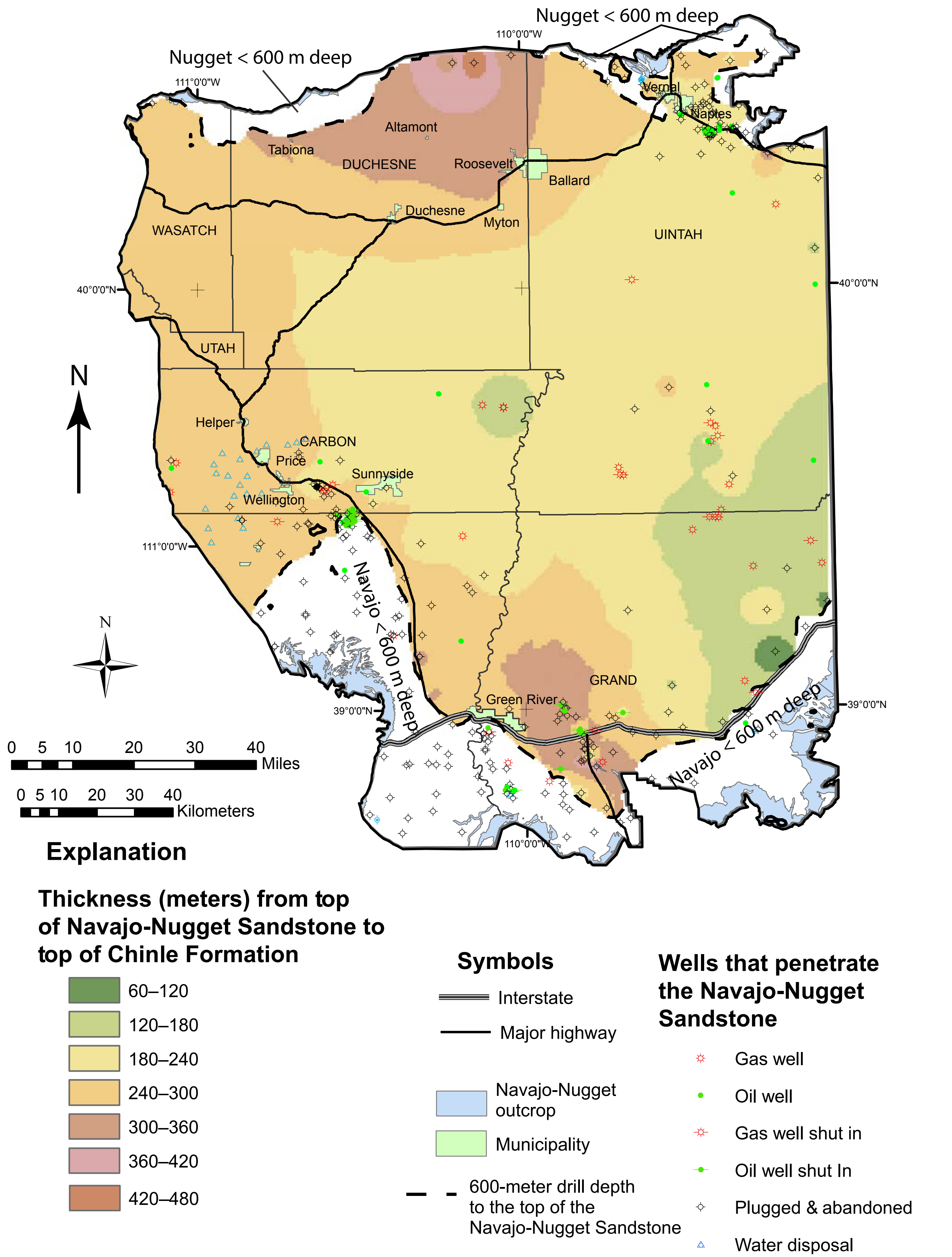

Figure 1.14. *Thickness from the top of the Navajo-Nugget Sandstone to the top of the Upper Triassic Chinle Formation (figure 1.6) for areas where the Navajo-Nugget is greater than 600 meters (>2000 ft) deep. After Morgan and Kirby (2017).*

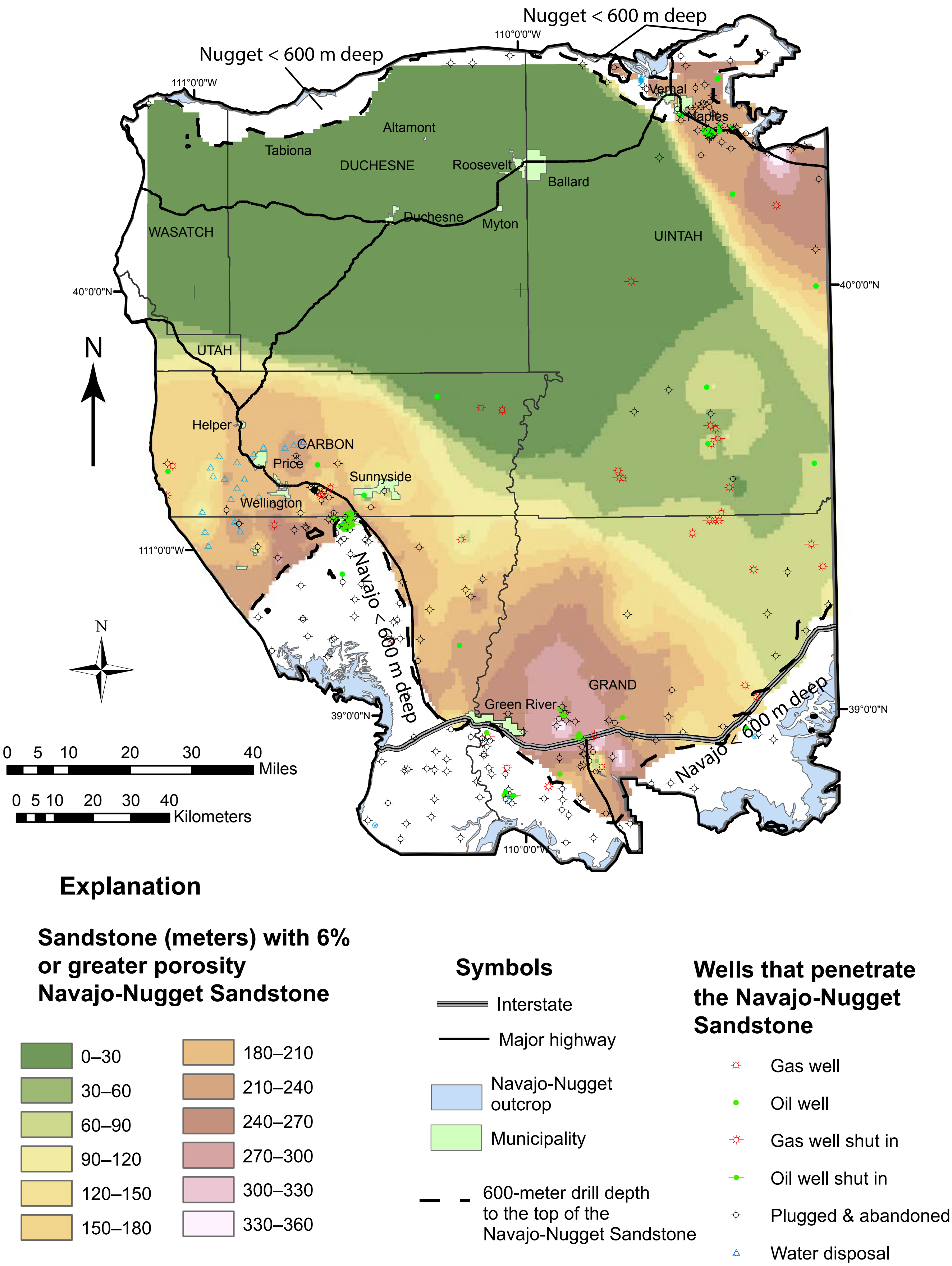

Figure 1.15. *Thickness of sandstone in the Navajo-Nugget aquifer with ≥6% porosity. Porosity determined from density and sonic well logs for areas where the Navajo-Nugget is deeper than 600 meters (>2000 ft) of depth. After Morgan and Kirby (2017).*

STUDY SITES

We chose the Devils Canyon and Eagle Canyon area, located adjacent to Interstate 70 (I-70) on the western flank of the San Rafael Swell, Emery County, east-central Utah, as outcrop analogs for Covenant field because this area is one of two locations where Navajo outcrops are nearest the field, coal-fired power plants, and Navajo produced-water disposal wells for CBM fields (figures 1.2 and 1.4). In this region a complete section of the Navajo Sandstone is exposed. The outcrop study area is approximately 60 kilometers (~45 mi) east of the oil field. Another potential outcrop area for field study is located north of Covenant field, near the town of Nephi, Utah, but there the Navajo is highly deformed and faulted. In the Devils and Eagle Canyons area, the Navajo is less structurally deformed, exposures are vertically complete and laterally extensive, and a variety of interdune facies can be observed. These outcrop parameters allowed us to more fully evaluate potential subsurface reservoir characteristics and better predict reservoir performance.

Two composite sections were measured from outcrop. The Devils Canyon composite section was located south of I-70; the Eagle Canyon composite section was located north of I-70. The lower parts of these composite sections are separated by a distance of 1.1 kilometers (0.7 mi), whereas the upper parts are separated by 1.8 kilometers (1.1 mi). In addition, a two-dimensional (2D), shallow P-wave seismic survey was conducted south of I-70 at the Moore Road exit along Justensen Flats in the Devils Canyon area.

Covenant field is located about 3 kilometers (~2 mi) southeast of the small town of Sigurd in Sevier County, Utah, along U.S. Highway 24 (figure 1.2). The field is about 50 kilometers (~30 mi) west of the San Rafael Swell where the Navajo Sandstone dips into the subsurface and is incorporated into the central Utah thrust belt. The central Utah thrust belt is divided into western, central, and eastern areas based on regional Jurassic stratigraphy (Chidsey and Sprinkel, 2016). Prior to the Covenant field discovery, fewer than 120 wells had been drilled in the region. About 30 exploratory wells have been drilled since 2004 (figure 1.3), all were plugged and abandoned.

OUTCROP METHODOLOGY

Measured Sections – Facies Analysis

The two composite stratigraphic sections of the Navajo Sandstone were measured within the study sites in an effort to describe the dune and interdune facies, document the lateral extent of each facies, and to collect samples for petrophysical measurement and petrologic interpretation. Ultimately, our goal was to understand reservoir/aquifer characteristics of each facies.

The description of the stratigraphic sections included identifying meso- and macro-scale primary and secondary sedimentary structures, grain size, grain and cement composition, rounding and sorting of grains, degree and types of bedding, color, and thickness of the units. We also described the algal development in interdune facies. The color of each unit is described by using the Geological Society of America rock color chart, which is based on the Munsell color system. Photographs and photomosaics were also taken of the entire measured sections. These data were the primary source from which we interpreted facies. Several of the facies were given genetically interpreted names. We decided to use interpretive facies names in addition to the descriptive names because overlap exists between facies relative to sedimentary features.

The lateral extent of each facies is a critical aspect of reservoir characterization. Outcrop locations were selected in part because the lateral extent of each facies was readily observable in the area. The thickness and the estimated range of the lateral extent of each facies were recorded which helped in interpreting depositional conditions.

The Kayenta-Navajo contact is transitional and its position has been placed at different stratigraphic levels in the canyon. Sanderson (1974) placed the contact just above the first significant amount of silt and clay (interpreted to be Kayenta Sandstone) in the section. In that model, the basal part of the Navajo Sandstone is finer grained than the majority of the unit. In defining the base of the Navajo Sandstone in our sections, we followed the model of Sorber and others (2007) and Doelling and Kuehne (2007), who defined a basal Navajo unit and placed the Navajo-Kayenta contact at the first very thick bedded, high-angle, trough cross-stratified sandstone that is fine to medium sand-sized and moderately well to well sorted. This basal stratigraphic unit was interpreted to have been clearly deposited under eolian conditions. In reality, the Kayenta-Navajo contact will be an inconsistent boundary over a broad area. The top of the section was interpreted to be at the contact of flat-lying, heterolithic beds of the Middle Jurassic Carmel Formation. We did not interpret the existence of any Middle Jurassic Temple Cap Formation between the Navajo and the Carmel within our particular composite sections. However, the Temple Cap does exist (6.4 meters [21 ft]) on the western flank of the San Rafael Swell immediately west of our study area based on regional correlations, facies interpretation, and the recognition of the J-1 unconformity (unpublished measured section by D.A. Sprinkel and H.H. Doelling, Utah Geological Survey, 1998). The Navajo Sandstone is separated from the overlying Temple Cap Formation by the J-1 unconformity (Pipiringos and O'Sullivan, 1978).

Gamma-Ray Scintillometer

A surface gamma-ray profile was taken, using a hand-held scintillometer, as a supplement to both of the measured composite stratigraphic sections. Measurements were taken at

0.5-meter (1.6-ft) intervals along the lower and middle sections and 1.0-meter (3.2-ft) intervals along the upper section. The scintillometer used by the Utah Geological Survey (UGS) at the Eagle Canyon site detects total gamma radiation (in parts per million [ppm]) emitted by naturally occurring radioactive elements in the rocks (appendix A). After properly stabilizing the instrument, a sampling time of one minute was used for each measurement. The scintillometer also measured potassium (K in weight %), thorium (Th in ppm), and uranium (U in ppm) radiation and generated spectral gamma-ray curves (appendix A). The scintillometer used by Brigham Young University (BYU) in the Devils Canyon site produced gamma-ray data in API units.

The surface gamma-ray profiles proved to be a useful complement to the measured composite stratigraphic sections and provided correlation tools to any downhole logs for wells drilled in the region. Generally, gamma radiation responses correspond to overall lithological patterns. Typically, sandstone and limestone intervals exhibit low responses whereas mudrock intervals respond variably, depending mainly on calcium carbonate content.

Sampling – Porosity, Permeability, and Petrology

Dune and interdune facies were sampled for petrophysical measurement (porosity and permeability) and/or petrographic classification and petrologic interpretation. Whenever possible, samples were collected away from obvious fracture systems and highly weathered surfaces for each unit. Some of the units were too friable to collect samples large enough for core plug analysis. During sample collection, care was taken to eliminate induced fractures. Samples were plugged in the laboratory.

Core plugs were cut from each sample taken from the field, with the exception of some of the eolian deposits, which turned out to be too friable to cut plugs. Where possible, plugs were cut in both the horizontal and vertical directions on all samples. Approximately 60 core-plug samples were collected from the Devils Canyon section although only 51 could be analyzed due to the highly friable nature of some samples. Thirty-three samples were collected from the Eagle Canyon composite section; 26 core plugs were analyzed. Helium porosity and nitrogen permeability were measured at the BYU Department of Geological Sciences lab using a TerraTek 8400 Dual Porosimeter/Permeameter™. Standard core plugs provided by TerraTek – A Schlumberger Company were used to calibrate each core plug run.

Thin sections from 30 stratigraphic units of the Devils Canyon section were cut directly from the core plugs for point count analysis and petrographic classification. Petrographic analysis was performed on 15 outcrop samples from the Eagle Canyon section. A 300-point count was performed on each thin section, using Van Der Plas and Tobi's (1965) methods to determine the confidence interval. Thin section analysis with a standard petrographic microscope included study of grain type, grain texture, cementation, alteration/replacement and diagenetic history, and provenance of each sample. Petrophysical observations and interpretations were also recorded. Each sample was then given a clastic sedimentary rock classification based on Dott's (1964) Quartz, Feldspar, Lithics (QFL) ternary diagram, modified by Milliken and others (2002) and Boggs (2006).

Core-plug porosities were compared to porosities determined from point counts. In every case the point counted porosities were lower than the core-plug porosities. This is due to "edge effects" in the point counts and the microporosity in the matrix and clay. Therefore, core-plug measurements are considered more accurate (within ±3% of porosity and within 10% of the permeability measurement).

Seismic Survey

A two-dimensional (2D), shallow P-wave seismic survey (consisting of three profiles) was conducted northwest and southeast of I-70 near the Moore Road exit west of Eagle Canyon and along Justensen Flats, respectively (figure 1.2). The high-resolution reflection survey was conducted with a 45-kilogram (100-lb) accelerated elastic weight dropper mounted to an all-terrain vehicle. Impacts from the weight dropper were recorded on a 72-channel seismograph. A common depth point (CDP) roll-along survey was used with a CDP interval of about 1.5 meters (~5.0 ft) and 48 active channels at a time using single 28-hertz (Hz) geophones. The nominal fold of cover was 24.

CHAPTER 2:
GEOLOGY OF THE DEVILS CANYON/ JUSTENSEN FLATS AREA

by

Thomas H. Morris and Ashley D. Hansen

Northeast view across Devils Canyon to Justensen Flats. The lower half of the photograph represents the lower one-third of the Devils Canyon composite section. This lower section displays numerous interdune facies.

CHAPTER 2:
GEOLOGY OF THE DEVILS CANYON/JUSTENSEN FLATS AREA

INTRODUCTION

A complete section of Navajo Sandstone is exposed in the Justensen Flats area where outcrops are excellent and accessibility is relatively easy (figures 1.2 and 2.1). As such, the UGS has funded several studies in this area—Dalrymple and Morris (2007) and Hansen (2007), both part of the initial work on this project and presented herein, and Allen and others (2013). Additional work was conducted in Justensen Flats by the University of Utah as part of a CCS project completed in 2018 (Steele and others, 2018) involving the Hunter and Huntington coal-fired power plants to the north (figure 1.2) and the potential for the Navajo as a CO_2 storage aquifer.

The composite section of the Navajo Sandstone was measured in the Devils Canyon/Justensen Flats area (figure 2.2; also see figure 3.14 in Chapter 3, Dalrymple and Morris [2007], and Hansen [2007]). The lower part of the section was measured northeast of the entrance to Devils Canyon, just north of the road traversing Justensen Flats where there is a knob of Navajo Sandstone capped with a brown bed. The eastern side of this knob drops into a ravine. The units in this section are labeled JFCG (Justensen Flats Campground) and begin with JFCG 1 as the basal unit of the Navajo through JFCG 19 (figures 2.2 and 2.3). The upper two-thirds of the Navajo Sandstone was measured farther into Devils Canyon, on a prominent Carmel-capped butte (figure 2.4). The butte is south of the Devils Canyon streambed just as the canyon opens into a wider valley and the streambed turns south. The units here are labeled DCB (Devils Canyon Butte). These units start with DCB 1 and continue upward to DCB 6 (figure 2.4), which is the uppermost unit in the Navajo. Two units (DCB 1 and JFCG 16) were correlated as each was a very well cemented unit that appears to be continuous throughout the region and their presence is probably the reason Justensen Flats formed. These two units had similar porosities, permeabilities, facies, and petrologic features.

FACIES

The Navajo Sandstone is divided into eight facies in the Devils Canyon/Justensen Flats area. Five facies are interpreted to have been deposited in interdune environments but together these facies account for less than 10% of the section. Three of the facies were deposited by dunes and together they account for more than 90% of the section. Most samples from both dune and interdune facies are quartz-rich feldspathic arenites; however, one dune-dominated unit was a quartz arenite, two interdune units were classified as feldspathic wackes, and a third as a mudstone (figure 2.5).

Each facies is described in detail below, followed by our interpretation of depositional environment and reservoir character. Table 2.1 summarizes many of the characteristics of these facies.

Interdune Facies

The first five facies represent interdune deposits. Three of these facies names are interpretive in nature rather than purely descriptive. We chose to do this because overlap exists between facies relative to sedimentary structures and lateral extent, which were the primary features used to interpret facies. Interdune faces include Wavy Algal Mat (WAM), Sandy Algal Mat (SAM), Poorly Developed Interdune (PDI), Evolving Interdune (EID), and Ephemeral Fluvial Channel (EFC).

Wavy Algal Mat (WAM)

Outcrop characteristics: The WAM facies is characterized by millimeter- to centimeter-scale wavy lamination (figure 2.6A). Desiccation features such as mud cracks, busted crust, and disrupted bedding are visible in the WAM facies in several locations in the Devils Canyon/Justensen Flats area, as well as throughout the Navajo Sandstone (Winkler and others, 1991). The WAM facies is calcite-rich and reacts strongly to a 10% hydrochloric (HCl) acid solution. It is finer grained than the dune facies. The WAM facies is the most resistant facies in the Navajo section and forms laterally extensive surfaces such as Justensen Flats (visible over more than 1 square kilometer [>0.4 mi^2]). Stratigraphic units DCB 1 and JFCG 16, both interpreted to represent the WAM facies, were correlated between the upper and lower measured sections. The color ranges from pale-reddish-brown (10 R 6/6) to moderate reddish-brown (10 R 4/6).

Petrology: Lithologic classification of the WAM facies varies from a feldspathic arenite to a feldspathic wacke, and one sample (JFCG 16) plots as a mudstone due to its interpreted abundance of original matrix (figures 2.6B, 2.6C, and 2.6D). Another sample (DCB 1) is dominated by replacive calcite cement (76%) and could be considered a diagenetic or crystalline limestone. The provenance is continental block, craton interior (Dickinson and Suczek, 1979; Dickinson and others, 1983; Dickinson and Gehrels, 2003). Samples are dominated by monocrystalline and undulose quartz, potassium feldspar, and calcite cement with a significant number of oxides (figure 2.6D). The calcite appears as rhombs growing into pore space where porosity is present. Detrital grains are smaller than typical eolian grains of the Navajo Sandstone and they are usually angular. Together, these observations suggest that calcite

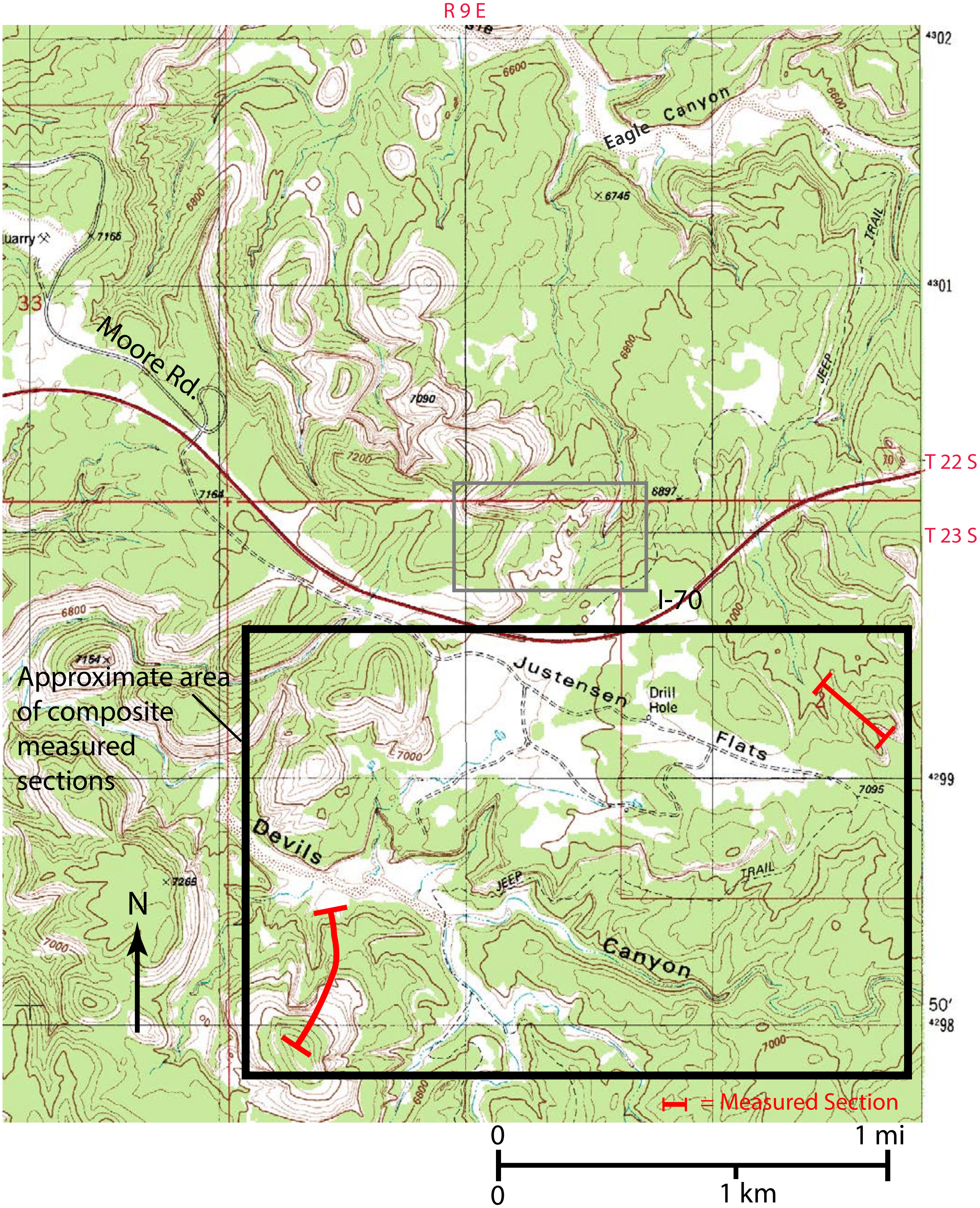

Figure 2.1. Location of Devils Canyon/Justensen Flats study area (black rectangle) in the northeastern corner of U.S. Geological Survey Copper Globe 7.5' quadrangle (contour interval = 40 ft); Eagle Canyon study area shown in the light gray rectangle to the north. Composite measured section shown on figure 2.2 and described in detail by Hansen (2007).

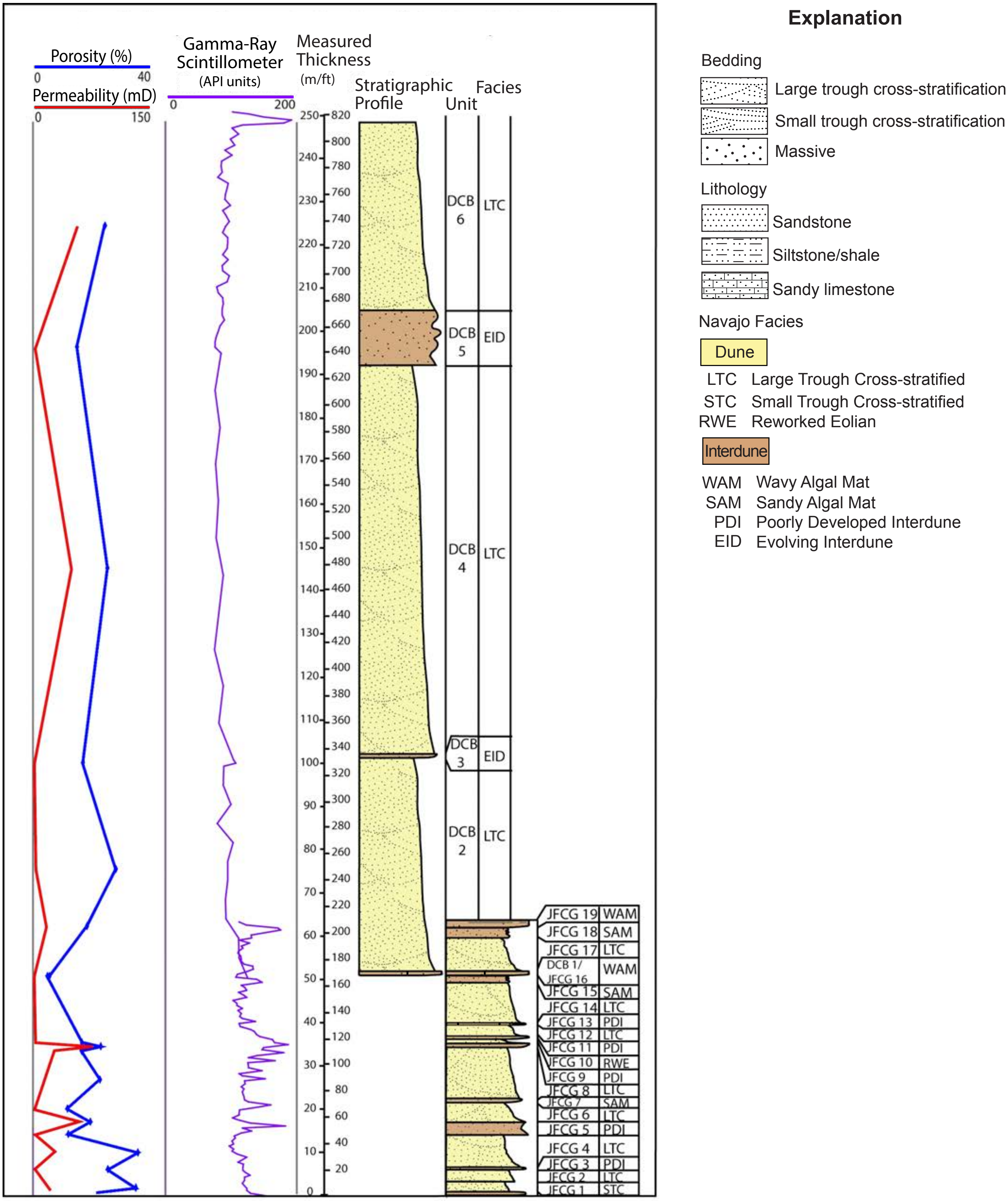

Figure 2.2. *Stratigraphic column of composite measured section of the Navajo Sandstone at Justensen Flats and Devils Canyon. The lower 60 meters (200 ft) was measured on the eastern side of Justensen Flats adjacent to a campground (JFCG). The upper 200 meters (600 ft) was measured on the southern side of Devils Canyon (DCB). See figure 2.1 for locations of measured sections. Gamma-ray scintillometer measurements shown on the left were taken along the measured section and samples were collected from most units for porosity and permeability analysis. See table 2.1 for explanation of facies. After Hansen (2007).*

Figure 2.3. *Photograph of the lower part of the composite section located in the northeastern part of the Justensen Flats area; view is to the west. Stratigraphic units of the Justensen Flats Campground section are annotated and keyed to the composite stratigraphic column on figure 2.2. Note the white circle that highlights a person for scale.*

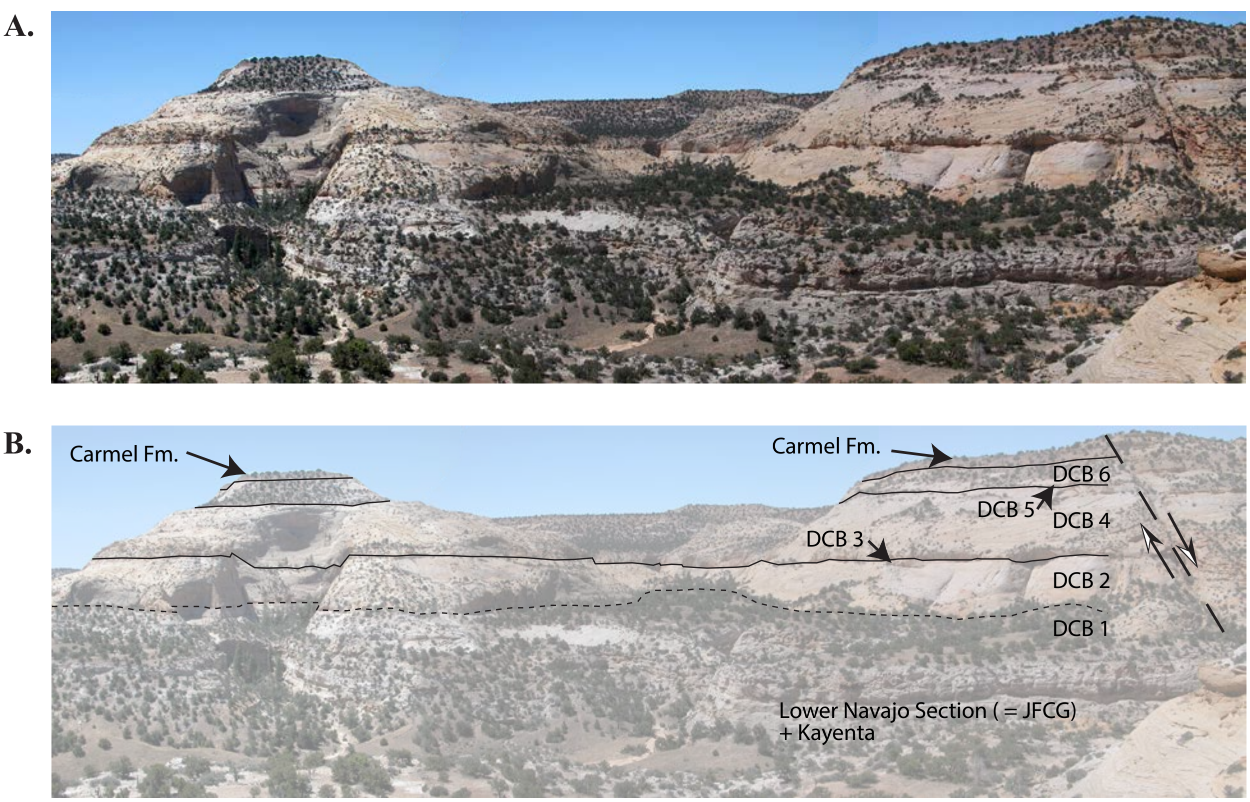

Figure 2.4. *Unannotated **A.** and annotated **B.** photomosaics of the upper part of the composite section located adjacent to Devils Canyon; view is to the south. Stratigraphic units of the Devils Canyon Butte section are annotated and keyed to the composite stratigraphic column on figure 2.2, and described in detail by Hansen (2007).*

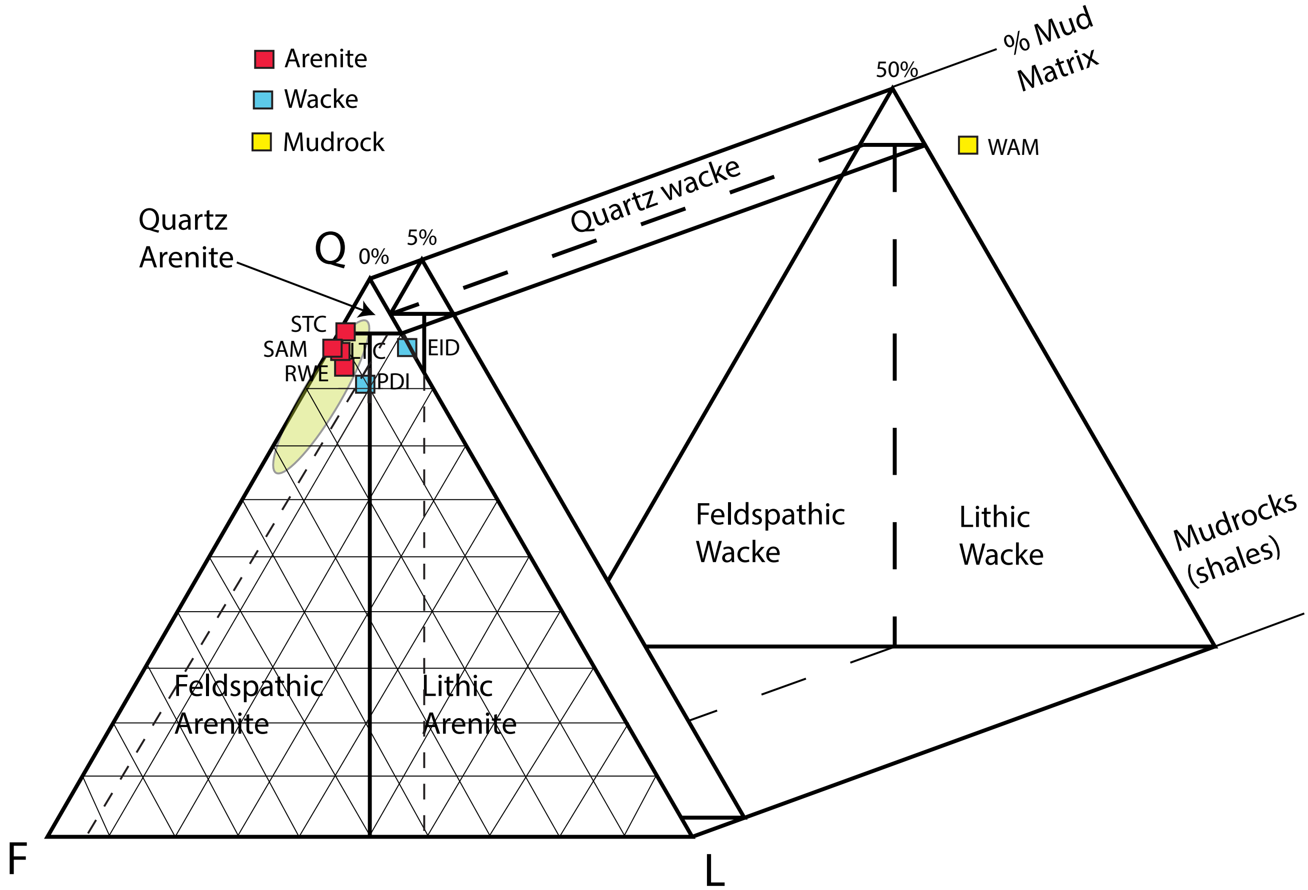

Figure 2.5. *Petrographic plot of point-counted Navajo Sandstone samples indicates that the majority are either quartz arenites or quartz-rich feldspathic arenites (pale-yellow). Seven individual samples from different facies are also illustrated (see text for discussion and table 2.1 for explanation of facies). Modified from Boggs (2006).*

is replacing the detrital silicate grains and that diagenesis is a dominant process (Picard, 1977). In sample JFCG 19, grain contacts are primarily "floating" in matrix with minor point contacts. Likely many grains have been fully replaced.

Porosity/permeability: The WAM facies has porosities from 5% to 11%. Permeabilities range from 0.06 to 0.5 millidarcies (mD); one of the five total samples measured 39 mD and was not counted in the average permeability. The average permeability of the remaining four samples was 0.3 mD. The WAM facies has the lowest porosity and permeability of any facies in the Navajo Sandstone due in part to the abundant replacive calcite cement and matrix.

Interpretation: The WAM facies was deposited as a laterally extensive (greater than 1 kilometer [>0.6 mi]) algal mat during a period of non- or very slow deposition (low energy activity) of the erg. Dunes were likely few and far between. The WAM facies fits many of the criteria of a supersurface including apparent near cessation of dune deposition for a time and significant lateral extent (Kocurek, 1988; Chan and others, 1992; Dalrymple and Morris, 2007; Parrish and others, 2017). The climate during WAM deposition was wetter than during normal dune deposition, creating an argillaceous sabkha (Fryberger and others, 1983). Because of this, the water table sat at or near the surface allowing a stromatolitic algal mat to form (Picard, 1977; Eisenberg, 2003). In some places, standing water existed and there was little sand supply during this time. Because the algal mat was so extensive, this could not be a simple interdune surface between dune sets or draas. The extremely low porosity and permeability combined with the lateral extent could make this unit a barrier to fluid flow of crude oil, natural gas, injected produced water, or stored CO_2 from coal-fired power plants.

Sandy Algal Mat (SAM)

Outcrop characteristics: The SAM facies contains thin planar laminae and wavy lamination that looks similar to ripple lamination. However, we do not believe it is ripple lamination because no foresets were observed. The bedding can be described as centimeter-scale laminations that enclose millimeter-scale wavy lamination (figure 2.7A). The sandstone is well sorted and very fine grained. The SAM facies is generally 1 to 2 meters (3–6 ft) thick. It is laterally extensive when compared to other interdune facies, visibly extending more than 1000 meters (>3000 ft). Because outcrops are usually recessive, it is hard to observe the total extent of this

Table 2.1. *Summary of characteristics of Navajo Sandstone facies in the Devils Canyon area. After Hansen (2007).*

	Facies[1]	Observable Reservoir/Aquifer Characteristics	Units[2]	Thickness (m)	Lateral Extent (m)	Relative Time of Formation	Affect on Fluid Flow
				1 2 3 4 5	0 10 100 1000 10,000		
Interdune	WAM	Stromatolitic wavy laminae (1 to 5 mm [0.025–0.063 in.]); desiccation features including mud cracks, busted crusts, disrupted bedding; absence of fossils; calcite cement; avg. of 8% porosity and 0.27 mD permeability; very laterally extensive.	JFCG 16, 19			Long	Barrier
Interdune	SAM	Thin planar laminae (appear similar to ripples); well sorted, very fine grained; recessive; avg. of 19% porosity and 15.0 mD permeability.	JFCG 7, 15, 18			Long to intermediate	Baffle
Interdune	PDI	Massive to thin planar beds; lacks any indication of algal influence; subrounded and well sorted, fine grained; cementation varies; limited lateral extent; avg. of 20% porosity and 5.6 mD (wide range) permeability.	JFCG 3, 5, 9, 11, 13			Very short	Baffle (only locally effective)
Interdune	EID	Undulating contacts; thickness up to 15 m (49 ft) locally, but more often 1 to 2 m (3–6 ft); massive to planar (10 to 40 mm [0.4–1.6 in.]) bedding; minor calcite cement; avg. of 20% porosity and viable permeability, variable.	DCB 3, 5			Short to intermediate	Baffle
Interdune	EFC	Lensoidal shape; interbeds of planar (15 to 45 cm [6–18 in.]) and low-angle trough cross-stratification (15 to 60 cm [6–24 in.]); may contain soft-sediment deformation; sparse-intermediate degree of bioturbation; associated laterally with large-scale convolute bedding.	Various Devils Canyon localities			Short to intermediate	Baffle
Dune	LTC	Large trough cross-stratification (15 m [49 ft]); thick bedded; moderately recessive; subangular to subrounded, well sorted; fine to medium grained; avg. of 27% porosity and 122 mD permeability.	JFCG 2, 4, 6, 8, 12, 14, 17 DCB 2, 4, 6	Up to 90 m		Long	Reservoir/aquifer
Dune	STC	Small trough cross-stratification (1 m [3 ft]); very recessive; subrounded to subangular, well sorted; gradational upper contacts; occurs mostly in the lower Navajo; avg. of 40% porosity and 26 mD permeability.	JFCG 1			Intermediate	Reservoir/aquifer
Dune	RWE	Massive and contorted bedding; recessive; rounded to subrounded, moderately sorted; fine grained; avg. of 23% porosity and 70 mD permeability.	JFCG 10			Intermediate	Reservoir/aquifer

[1]Facies: WAM= Wavy Algal Mat; SAM=Sandy Algal Mat; PDI= Poorly Developed Interdune; EID= Evolving Interdune; EFC= Ephemeral Fluvial Channel; LTC= Large Trough Cross-stratified; STC= Small Trough Cross-stratified; RWE= Reworked Eolian. [2]Refer to figure 2.2 for location of units in the measured Navajo section; JFCG = Justesen Flats campground; DCB = Devil's Canyon Butte.

A.

B.

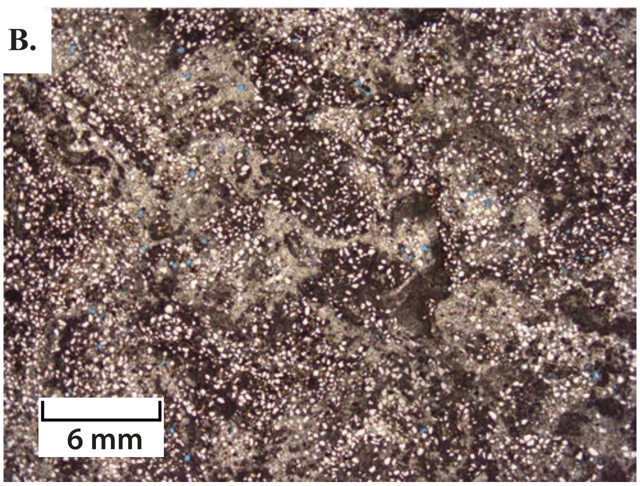

C.

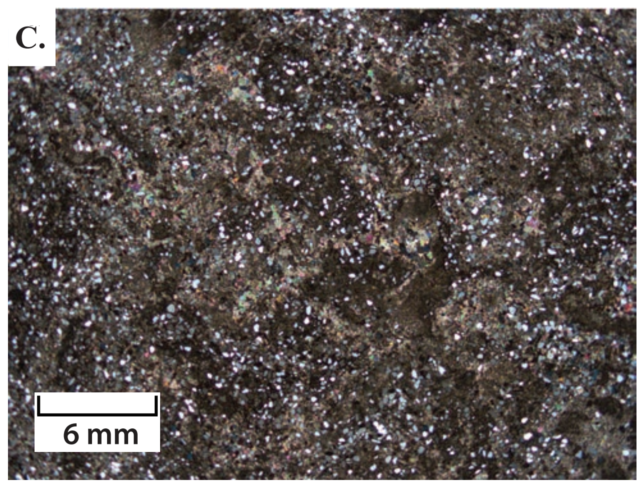

D.

Mineral	Count	Percent	Error (+/-)	Normalized
Mono qtz	38	12.66	3.5	
undulose	14	4.66	1.6	
Poly qtz	7	2.33	1	
Micro qtz	0	0	0	
Total Quartz	59	19.65		0.88
K spar	8	2.66	1	
Plag	0	0	0	
Total Feldspar	8	2.66		0.12
Lithics	0	0	0	0
Clay	0	0	0	
Matrix	173	57.66	5.6	
Porosity	2	0.66	<1	
Oxides	11	3.66	1.5	
Calcite	46	15.33	4.1	
Heavies	1	0.33	<1	
Total	300	99.95		1
Grain Size	Silt-fine-grained sand			
Roundness	Subrounded			
Sorting	Moderately sorted			

Figure 2.6. *Lithologic and petrologic analysis of the Wavy Algal Mat (WAM) facies.* ***A.*** *Outcrop view of wavy and crinkled laminae of the JFCG 16 unit interpreted to be the WAM facies.* ***B.*** *Photomicrograph displaying abundant matrix under plane-polarized light.* ***C.*** *Same image as B under cross-polarized light.* ***D.*** *300-point count analysis indicates that this rock would be considered a mudstone given its abundant matrix.*

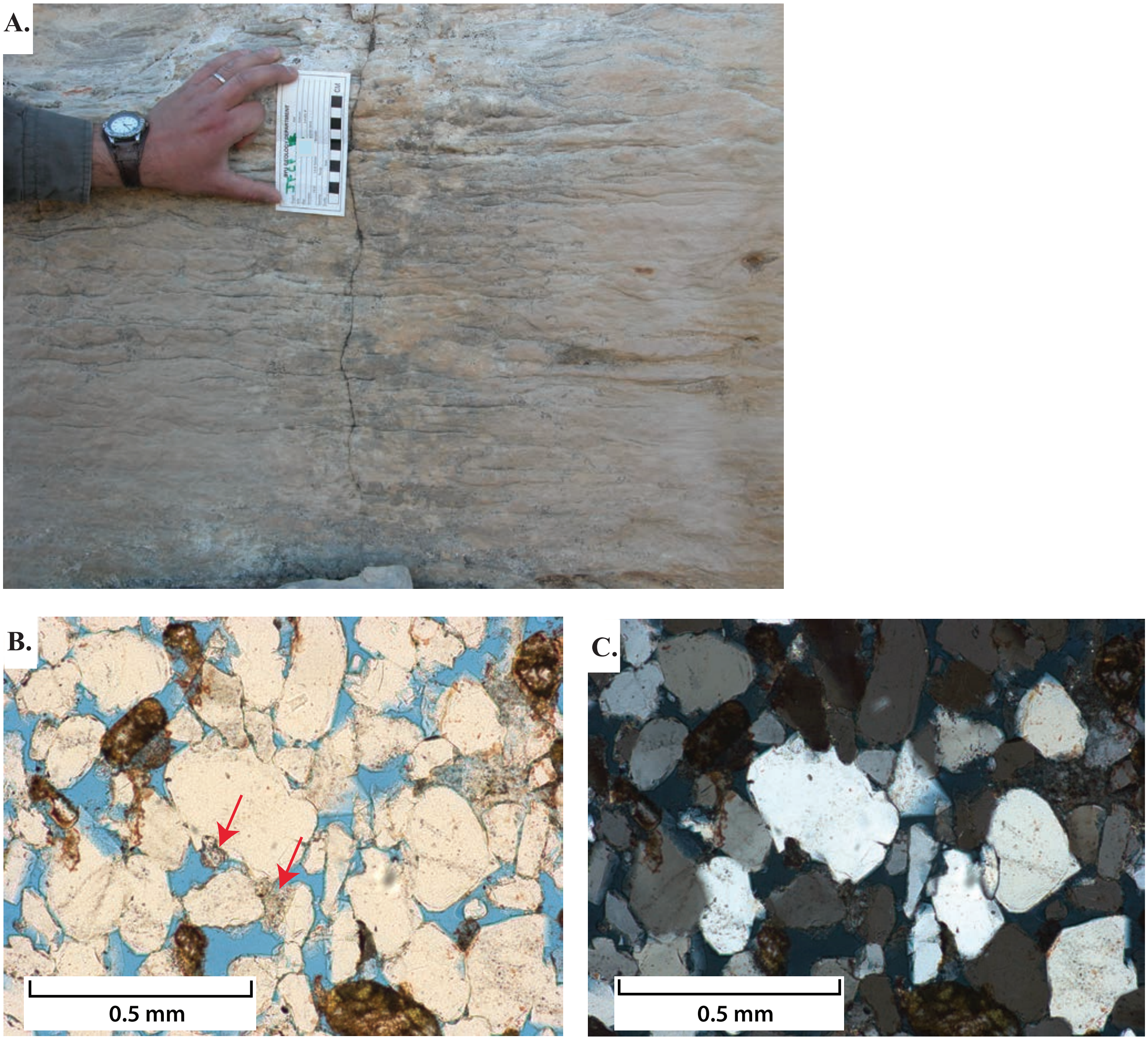

D.

Mineral	Count	Percent	Error (+/-)	Normalized
Mono qtz	90	30	5.4	
undulose	38	12.66	3.5	
Poly qtz	8	2.66	1	
Micro qtz	0	0	0	
Total Quartz	136	45.32		0.87761425
K spar	11	3.66	1.5	
Plag	8	2.66	1	
Total Feldspar	19	6.32		0.12238575
Lithics	0	0	0	0
Clay	1	0.33	<1	
Matrix	8	2.66	1	
Porosity	8	2.66	1	
Oxides	25	8.33	3.2	
Calcite	103	34.33	5.5	
Heavies	0	0	0	
Total	300	99.95		1
Grain size	Very fine-medium sand			
Roundness	Subrounded to well rounded			
Sorting	Moderately poorly sorted			

Figure 2.7. *Lithologic and petrologic analysis of the Sandy Algal Mat (SAM) facies.* ***A.*** *Outcrop view of crinkly to planer laminae interpreted to be the SAM facies.* ***B.*** *Photomicrograph displaying abundant quartz overgrowths (red arrows) under plane-polarized light.* ***C.*** *Same image as B under cross-polarized light.* ***D.*** *300-point count analysis indicates that this rock is a quartz-rich feldspathic arenite.*

facies. The SAM facies usually occurs just below the WAM facies. The color ranges from dark yellowish-orange (10 YR 6/6) to very pale-orange (10 YR 8/2) to pale yellowish-orange (10 YR 8/6).

Petrology: The SAM facies plots as a feldspathic arenite based on point count analysis of thin sections (figures 2.7B, 2.7C, and 2.7D). The provenance is continental block, craton interior (Dickinson and Suczek, 1979; Dickinson and others, 1983; Dickinson and Gehrels, 2003). The SAM facies appears transitional from the Large Trough Cross-stratified (LTC) facies below to the WAM facies above. It is sandier, with sorting, roundness, and grain size similar to the LTC near the base of the facies. The SAM facies has similar sedimentary structures to the WAM facies and near the top of the facies has similar sorting, roundness, and grain size to the WAM facies. Cements can be dominated by calcite and oxides such as JFCG 7 (8% oxides, 34% calcite) or be dominated by quartz overgrowths (<1% oxides, 2% calcite) (figure 2.7D). Cementation varies vertically (within 1 meter [3 ft]). All of the samples are dominated by monocrystalline and undulose quartz, with some (~4%) potassium feldspar.

Porosity/permeability: The porosity ranges from 13% to 25% and varies with cement type. The permeability also varies with cementation from less than 1 mD to 29 mD (two samples). Calcite cement reduces the porosity and permeability.

Interpretation: The SAM facies is interpreted as a transitional facies between the drier time of normal dune deposition (below) and wetter periods when the WAM facies was deposited (above). During this time an algal mat covered the area. Unlike the WAM facies, this algal mat incorporated significant quantities of sand. The wavy lamination is a result of the algal mat sedimentation. As the water table continued to rise and eolian sand supply decreased, the algal mat transitioned into the WAM facies. Clemmensen and others' (1989) "variously stratified sandstone," interpreted to be a transitional facies between normal dune deposits and sabkha deposits, contains wavy/crinkly lamination and horizontal lamination similar to our SAM facies. JFCG 7 does not have the WAM facies overlying it, presumably because the climate dried out before it could fully develop.

Poorly Developed Interdune (PDI)

Outcrop characteristics: Sedimentary structures vary from one PDI unit to the next, depending on the conditions of deposition. Two units in the PDI facies exhibit massive bedding with some faint areas of centimeter-scale planar lamination (JFCG 9, JFCG 11) (figure 2.8A). Other units such as JFCG 5 are dominated by obvious planar lamination. Desiccation features were also visible (JFCG 3) but there is little to indicate algal influence. Winkler and others (1991) observed similar features in Navajo Sandstone interdune deposits. The PDI facies is not laterally extensive (usually less than 500 meters [<1500 ft]), and JFCG 11 pinches out about 10 meters (~30 ft) to the north of the measured section. The thickness varies as well, but the PDI facies is usually 1 meter (3 ft) thick or less. The color ranges from dark yellowish-orange (10 YR 6/6) to moderate yellowish-brown (10 YR 5/4).

Petrology: The PDI facies plots as a feldspathic arenite based on point count analysis of thin sections (figures 2.8B, 2.8C, and 2.8D). Like the rest of the Navajo Sandstone, the provenance is continental block, craton interior to transitional (Dickinson and Suczek, 1979; Dickinson and others, 1983; Dickinson and Gehrels, 2003). Grains are dominantly monocrystaline (27% of rock) and undulose quartz (11%) with some potassium feldspar (8%) (figure 2.8D). The most distinguishing feature in most units of this facies is the pervasive calcite and oxide cements (figure 2.8B). The type and amount of cement varies from predominantly oxide (up to 24% of total rock volume) to predominantly calcite cement (up to 23% of total rock volume). The abundance of oxide cement in the PDI facies explains the darker (red to brown) color when compared to the Large Trough Cross-stratified (LTC) facies (see below).

Porosity/permeability: The porosity of the PDI facies ranges from 12% to 27% (eight samples). The permeability ranges from 1 to 27 mD with most samples (seven) below 5 mD.

Interpretation: The PDI facies is present only in the lower 50 meters (150 ft) of the Navajo Sandstone. Five PDI units are in this lower part of the section. They intermittently divide the larger eolian sections (LTC, Reworked Eolian [RWE]). The PDI facies developed when the water table was at or near the surface and was rapidly fluctuating (Picard, 1977). However, the PDI facies does not represent large-scale cessation in eolian deposition. The lateral extent of the PDI facies is small (less than 500 meters [<1500 ft]), suggesting that these interdune facies were surrounded by eolian dunes. Apparently, the PDI facies did not migrate to any significant extent with dune migration. As the dunes migrated, they covered the interdune deposits before there was enough time to develop an algal mat environment. Thus, we see only planar to massive bedding in PDI facies as opposed to the WAM and SAM facies where algal mats had time to more fully develop. The variation in cementation accounts for the variance in porosity. Often these layers have more oxide cement than the LTC facies (see below). Due to the limited lateral extent of these deposits (less than 500 meters [<1500 ft]), the PDI facies is not likely an effective barrier. It may serve as a baffle within a larger flow unit.

Evolving Interdune (EID)

Outcrop characteristics: The sedimentary features of the EID facies vary based on location. Within about 10 meters (~30 ft) of the measured section, DCB 5 displayed massive bedding, planar lamination, and millimeter-scale wavy lami-

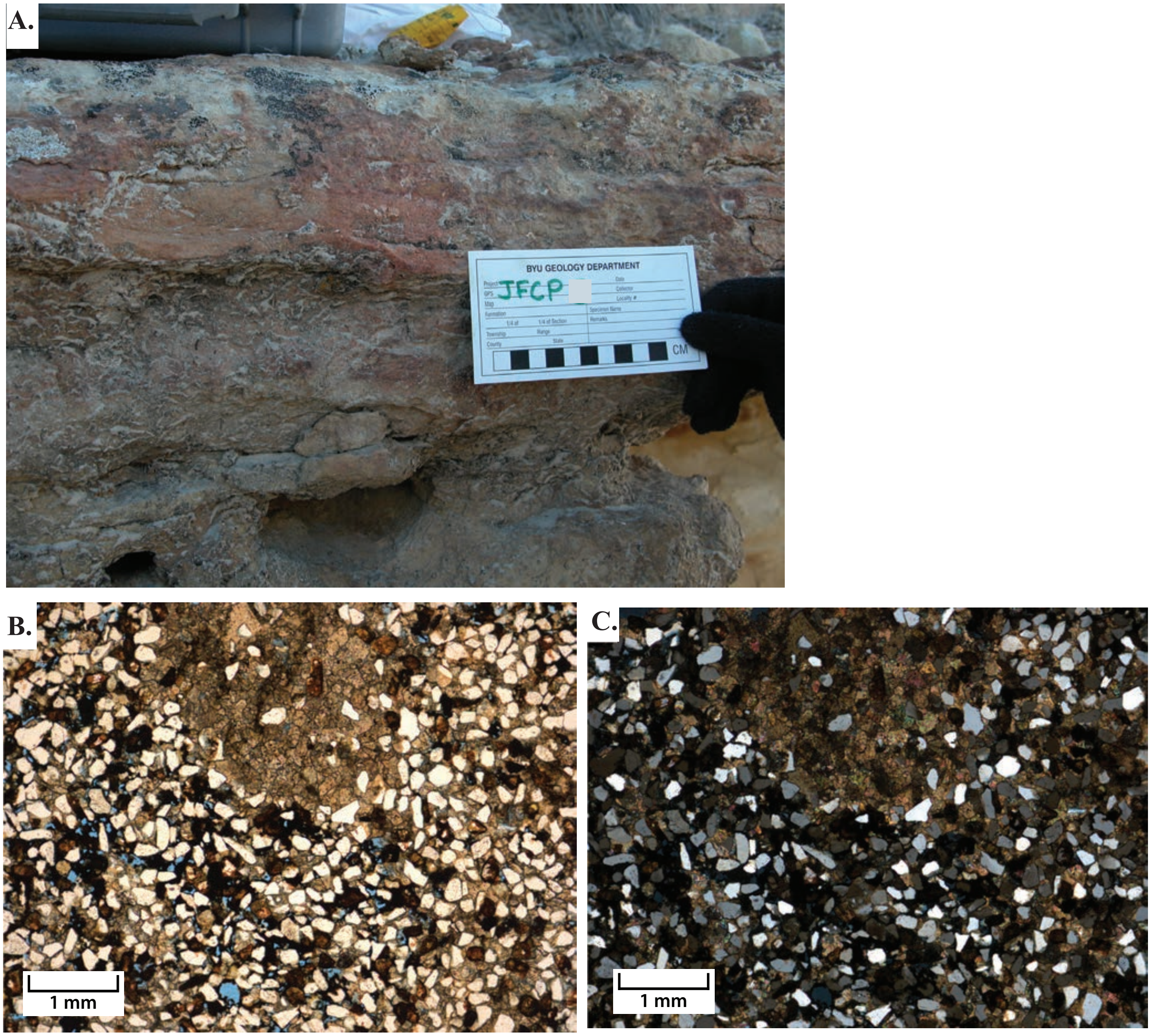

D.

Mineral	Count	Percent	Error (+/-)	Normalized
Mono qtz	80	26.67	5	
undulose	33	11	3.5	
Poly qtz	9	3	1.5	
Micro qtz	0	0	0	
Total Quartz	122	40.67		0.792208
K spar	23	7.67	2.5	
Plag	5	1.67	1	
Total Feldspar	28	9.33		0.181818
Lithics	4	1.33	1	0.025974
Clay	0	0	<1	
Matrix	25	8.33	3	
Porosity	30	10	3.5	
Oxides	19	6.33	2.7	
Calcite	71	23.67	4.7	
Olivine	1	0.33	1	
Total	300	100		1
Grain size	Fine sand			
Roundness	Rounded			
Sorting	Moderately well sorted			

*Figure 2.8. Lithologic and petrologic analysis of the Poorly Developed Interdune (PDI) facies. **A.** Outcrop view of the PDI facies displaying centimeter-scale planer beds to massive beds. **B.** Photomicrograph displaying abundant calcite cement and oxides under plane-polarized light. **C.** Same image as B under cross-polarized light. **D.** 300-point count analysis indicates that this rock is a feldspathic arenite.*

nation. DCB 3 had some of the same structures including planar lamination and millimeter-scale wavy lamination. The thickness of the EID facies is variable. For example, in the measured section, DCB 5 was 15 meters (45 ft) thick. However, the unit appears to thin laterally to less than 5 meters (<15 ft) within 50 meters (150 ft) of offset to the north and west. The EID facies undulates laterally (figure 2.9A). The color ranges from dark yellowish-orange (10 YR 6/6) to dark reddish-brown (10 R 3/4).

Petrology: The EID facies plots as a feldspathic arenite based on point count analysis of thin sections (figures 2.9B, 2.9C, and 2.9D). The provenance is continental block, craton interior (Dickinson and Suczek, 1979; Dickinson and others, 1983; Dickinson and Gehrels, 2003). Like other facies in the Navajo Sandstone, grains are dominated by monocrystalline quartz (33%) and most feldspars were potassium feldspar (6% of total) (figure 2.9D). The EID facies displays abundant calcite cement (4% to 23%) and oxides (8%) (figure 2.9D). The calcite usually forms rhombs with surrounding oxides. The abundant oxides create the brown-red color of the facies. The amount of cement varies laterally and appears to mimic the pattern of changing sedimentary structures.

Porosity/permeability: The porosity of the EID facies is approximately 15% to 17%, with some units (two samples) up to 28% porosity (a total of six samples). The permeability is approximately 1 mD with some areas (two samples) as high as 74 mD.

Interpretation: In the upper 200 meters (600 ft) of the measured section, the Navajo Sandstone is dominated by the LTC facies. Very few interdunes exist within this part of the section. We interpret these relatively rare interdune deposits as belonging to the EID facies. These interdune deposits also represent an intersection of the water table and ground surface. However, as the extensive dune system migrated, it buried the interdune before thick algal deposits could develop. Therefore, the EID facies represents a transition between the short-lived PDI facies and the longer-lived WAM facies, but in a setting where interdunal areas were more extensive. In this scenario, the interdune migrated with the dunes (Kocurek, 1988; Mountney, 2006). As the edge of the interdune was buried by one dune set, the opposing edge was extended by deflation and scour to the water table. Deposits of the EID facies are laterally extensive (greater than 1 kilometer [>0.6 mi]), but because of their changing characteristics they are not considered barriers to flow.

Ephemeral Fluvial Channel (EFC)

Outcrop characteristics: The EFC facies is lensoidal, not laterally extensive (less than 100 meters [<300 ft]), and up to 5 meters (15 ft) thick in the two places we observed it in the Navajo Sandstone (figure 2.10). Sedimentary structures within the lenses include planar bedding, low-angle trough cross-stratification, soft-sediment deformation, and sparse to intermediate levels of bioturbation. Near one lens is a large, macro-scale, soft-sediment deformation feature in the LTC facies lateral to the EFC facies. The EFC facies is not seen in our measured section and thin sections and core plugs were not collected. The EFC facies was not physically crossed in the line of section, but it was apparent in outcrops near (approximately 500 meters [~1500 ft]) the line of our lower (JFCG) section and observed adjacent to the upper section as well.

Interpretation: The lensoid-shaped EFC facies is interpreted as an ephemeral fluvial channel or wadi. At times water flowed in the interdune areas, creating EFC deposits. Flow must have varied resulting in planar and low-angle trough cross-stratification, as well as allowing for bioturbation at times. Similar facies are found in the Upper Triassic-Lower Jurassic Wingate Sandstone (Kiersch, 1950; Picard, 1977; Clemmensen and others, 1989). Because the EFC facies is so limited in lateral extent (less than 100 meters [<300 ft]), it probably acts as a baffle to flow within a reservoir.

Dune Facies

There are three dune facies in the Navajo Sandstone in the Devils Canyon/Justensen Flats area: Large Trough Cross-stratified (LTC), Small Trough Cross-stratified (STC), and the Reworked Eolian (RWE) facies. These three facies represent the main body of the Navajo reservoir.

Large Trough Cross-Stratified (LTC)

Outcrop characteristics: The LTC facies is dominated by high-angle large trough cross-stratified bedding (figure 2.11A). In some places the individual sets are up to 15 meters (45 ft) thick. However, in other places the beds are contorted to massive, which has been observed in other locations within the Navajo Sandstone erg system (Netoff, 2002). The LTC facies is up to 90 meters (270 ft) thick and is also laterally extensive (traced in outcrop for 10 kilometers [>6 mi]). Stratigraphic units in the LTC facies can be observed throughout the study area (at least 5 kilometers [3 mi] in length). The contacts above and below the LTC facies vary from sharp to gradual, and contain many undulating contacts. The color ranges over a large distance (100s of meters) from grayish-orange (10 YR 7/4) to very pale-orange (10 YR 8/2) to moderate yellowish-brown (10 YR 5/4) to pale yellowish-brown (10 YR 6/2).

Petrology: The LTC facies plots as a feldspathic arenite based on point count analysis of thin sections (figures 2.11B, 2.11C, and 2.11D). The provenance is continental block, craton interior (Dickinson and Suczek, 1979; Dickinson and others, 1983; Dickinson and Gehrels, 2003). Overall quartz dominates the LTC facies (63%) with about 60% of the quartz being monocrystalline (figure 2.11D). There are some plagioclase feldspars (2%) but most are potassium feldspar (6%)

A.

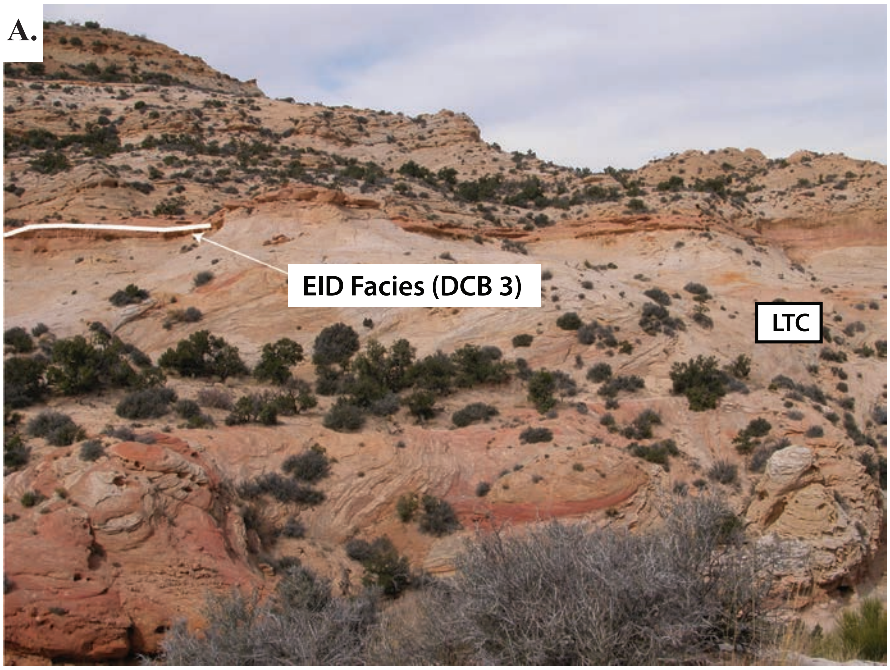

B.

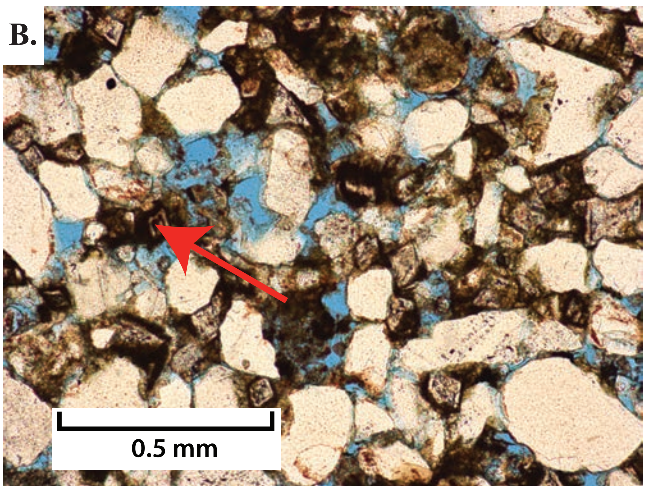

C.

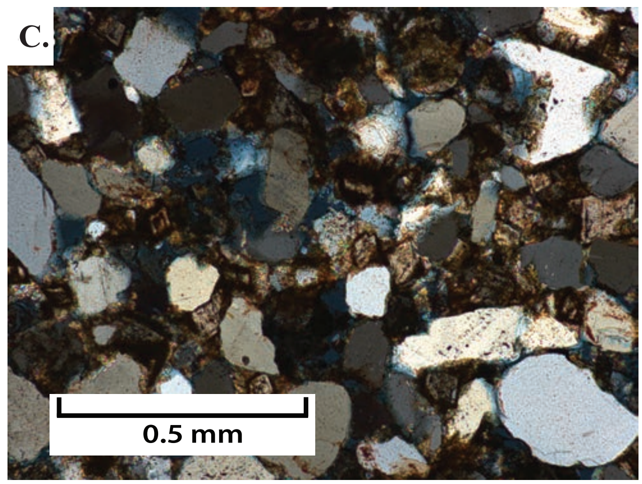

D.

Mineral	Count	Percent	Error (+/-)	Normalized
Mono qtz	99	33	5.4	
undulose	31	10.33	3.5	
Poly qtz	9	3	1.5	
Micro qtz	0	0	0	
Total Quartz	139	46.33		0.879747
K spar	17	5.67	3	
Plag	2	0.67	1	
Total Feldspar	19	6.33	<1	0.120253
Lithics	0	0	0	0
Clay	0	0	<1	
Matrix	22	7.33	3	
Porosity	24	8	3.1	
Oxides	25	8.33	3.1	
Calcite	71	23.67	4.8	
Silica cement	0	0	0	
Total	300	100		1
Grain size	Upper very fine-lower coarse			
Roundness	Subrounded to well rounded			
Sorting	Poorly sorted			

Figure 2.9. *Lithologic and petrologic analysis of the Evolving Interdune (EID) facies.* ***A.*** *Outcrop view of the EID facies which is variable in thickness, undulatory, and laterally extensive.* ***B.*** *Photomicrograph displaying calcite cement and oxides (red arrow), under plane-polarized light, which provide the reddish color in outcrop.* ***C.*** *Same image as B under cross-polarized light.* ***D.*** *300-point count analysis indicates that this rock is a quartz-rich feldspathic arenite.*

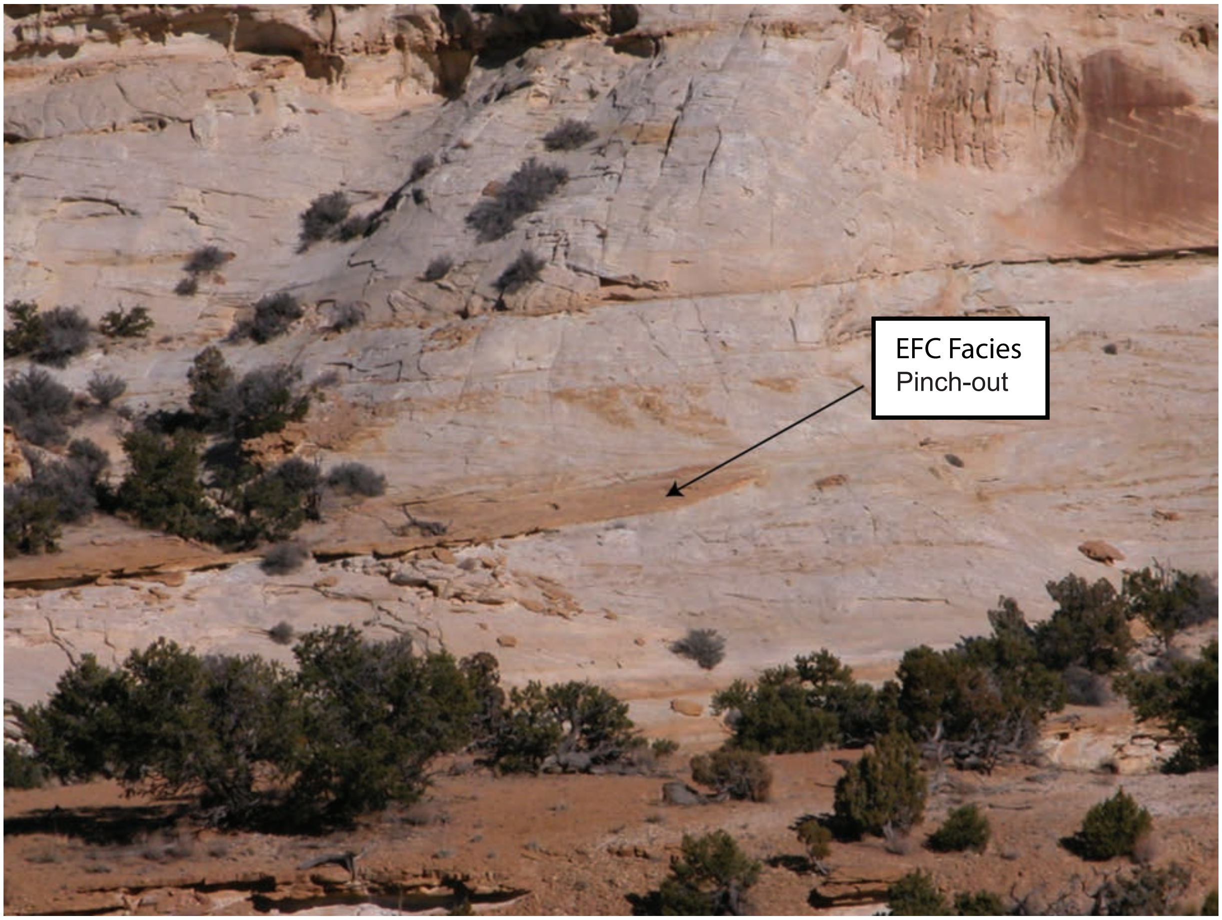

Figure 2.10. *Outcrop view of the pinch-out of the Ephemeral Fluvial Channel (EFC) facies located less than 100 meters (<300 ft) from the JFCG section. The EFC facies contains planar beds, moderate bioturbation, and can be associated with soft-sediment-deformed beds. Tree in the lower left is about 3 meters (9 ft) tall.*

(figure 2.11D). Generally, the LTC facies has very limited cement (less than 1% of total composition), which explains its sloping topographic expression (figure 2.11A). The cement that is present varies from quartz overgrowths to clay and calcite rims on some grains. Many of the samples did not have any visible lamination. Others displayed bimodal lamination. The LTC facies is moderately well sorted to well sorted. Picard (1977) found a similar facies that was also well sorted. This LTC facies had fewer altered grains than the rest of the Navajo Sandstone.

Porosity/permeability: The porosity ranges from 21% to 37%, with most (10 samples) around 27% porosity. The permeability ranges from 8 to 709 mD (16 samples). The average permeability is 122 mD. The LTC facies is the most porous and permeable facies in the Navajo Sandstone.

Interpretation: The LTC facies comprises approximately 90% of the Navajo Sandstone. It represents large-scale eolian dune deposits typical of an erg system. In the upper Navajo section, while interdunes were present, they were not common and/or not well preserved (in the Devils Canyon area). We interpret this to be due to deflation once the water table fell. The LTC facies represents the main reservoir of the Navajo. Its high porosity and permeability, large lateral extent, and lack of flow barriers provide a huge volume to store hydrocarbons, produced water, or CO_2.

Small Trough Cross-Stratified (STC)

Outcrop characteristics: The STC facies displays relatively small trough cross-stratified bed sets (figure 2.12A). Individual sets are not greater than 1 meter (>3 ft) thick (as opposed to the 1- to 15-meter-thick [3–45 ft] sets of the LTC). Most sets are low angle. The STC facies is thin (2.3 meters [7 ft]) and occurs rarely, appearing in only the first unit of the Navajo Sandstone. The STC facies is more friable than the LTC facies.

Petrology: The STC facies plots as a feldspathic arenite based on point count analysis of thin sections (figures 2.12B, 2.12C, and 2.12D). The provenance is continental block, craton interior (Dickinson and Suczek, 1979; Dickinson and others, 1983; Dickinson and Gehrels, 2003). Forty percent of the total composition is monocrystalline quartz with almost equal amounts of plagioclase (3%) and potassium feldspar (2%) (figure 2.12D). Clay rims and bridges

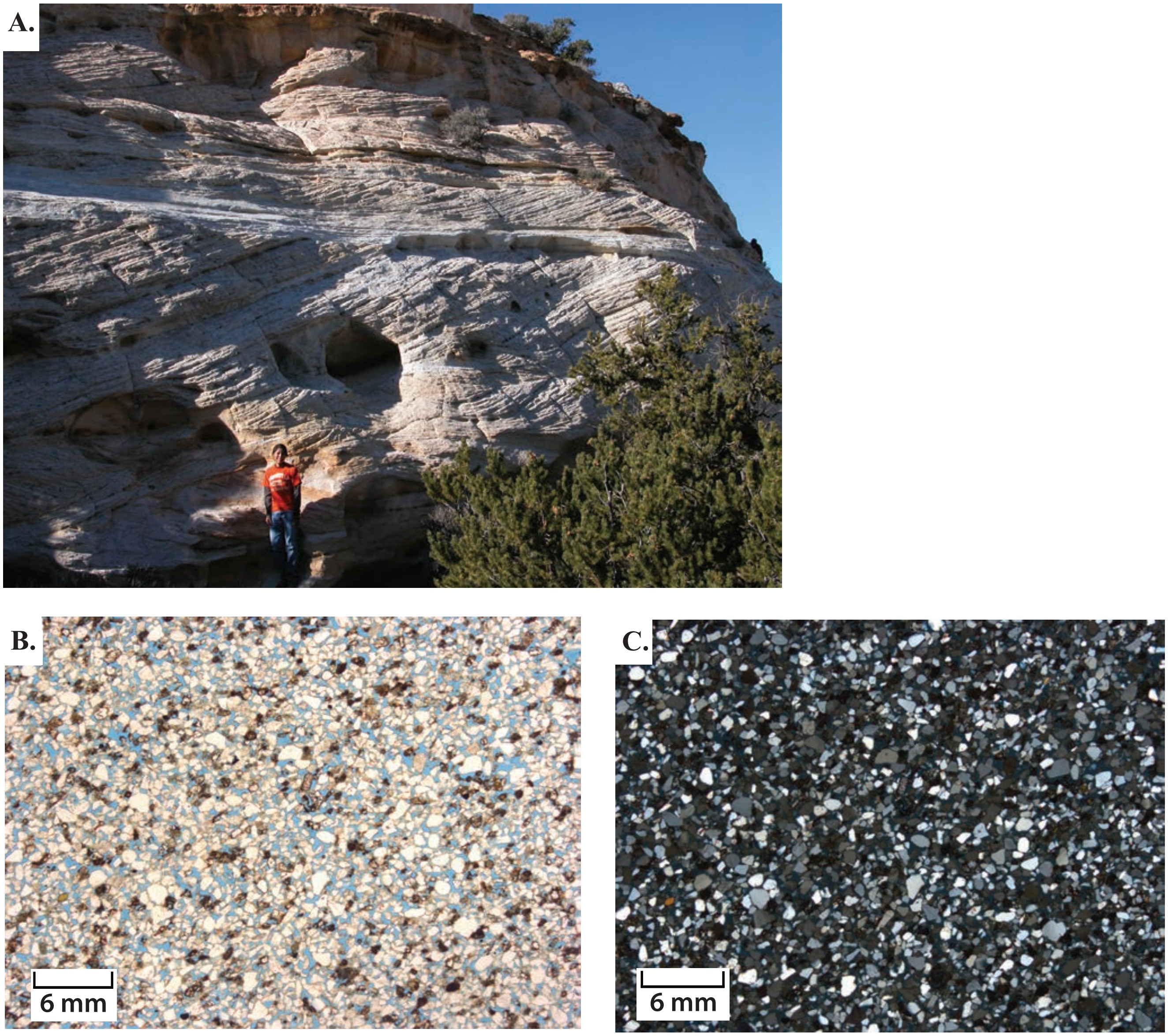

D.

Mineral	Count	Percent	Error (+/-)	Normalized
Mono qtz	118	39.33	5.6	
undulose	56	18.67	4.5	
Poly qtz	13	4.33	2	
Micro qtz	1	0.33	1	
Total Quartz	188	62.67		0.874419
K spar	17	5.67	2.5	
Plag	7	2.33	1	
Total Feldspar	24	8	<1	0.111628
Lithics	3	1	1	0.013953
Clay	0	0	<1	
Matrix	3	1	1	
Porosity	80	26.67	5	
Oxides	0	0	0	
Calcite	2	0.67	1	
Silica cement	0	0	0	
Total	300	100		1
Grain size	Medium			
Roundness	Subrounded			
Sorting	Moderately sorted			

Figure 2.11. *Lithologic and petrologic analysis of the Large Trough Cross-stratified (LTC) facies.* ***A.*** *Outcrop view of approximately 5-meter-high (~15 ft) large trough cross-stratified dune deposits of the LTC facies.* ***B.*** *Photomicrograph under plane-polarized light displaying abundant porosity (blue).* ***C.*** *Same image as B under crossed-polarized light.* ***D.*** *300-point count analysis indicates that this rock is a quartz-rich feldspathic arenite.*

A.

B.

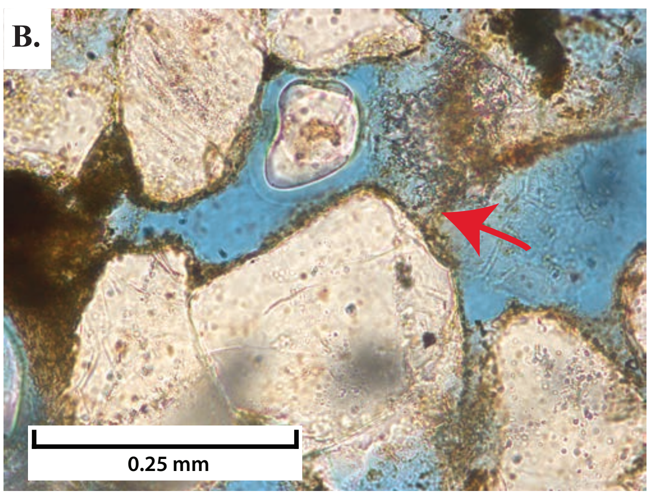

C.

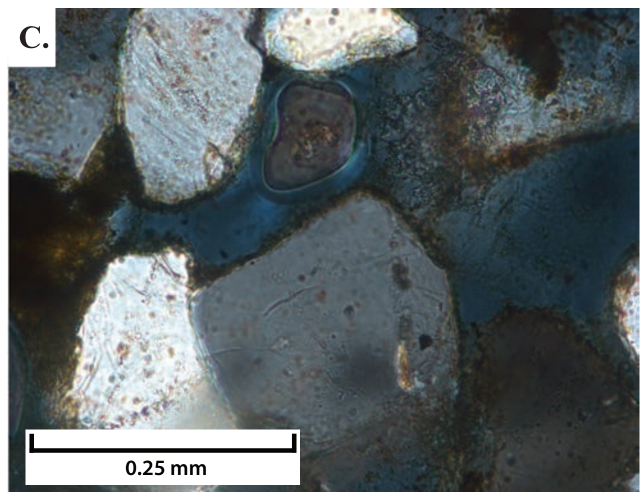

D.

Mineral	Count	Percent	Error (+/-)	Normalized
Mono qtz	121	40.33	5.6	
undulose	48	16	4.3	
Poly qtz	18	6	2.5	
Micro qtz	0	0	0	
Total Quartz	187	62.33		0.908336
K spar	7	2.33	1	
Plag	11	3.66	1.5	
Total Feldspar	18	5.99	0	0.087292
Lithics	1	0.3	1	0.004372
Clay	25	8.33	3	
Matrix	9	3	1.5	
Porosity	56	18.66	4.5	
Oxides	3	1	1	
Calcite	1	0.33	1	
Heavies	0	0	0	
Total	300	99.94		1
Grain size	Lower medium			
Roundness	Rounded			
Sorting	Moderately well sorted			

Figure 2.12. *Lithologic and petrologic analysis of the Small Trough Cross-stratified (STC) facies.* ***A.*** *Outcrop view of STC facies near the contact with the Kayenta Formation (not shown) at the base of the Navajo Sandstone.* ***B.*** *Photomicrograph displaying oxide-rich clay rims and bridges (red arrow) around and between grains under plane-polarized light. These bridges likely reduce permeability in this very porous facies.* ***C.*** *Same image as B under cross-polarized light.* ***D.*** *300-point count analysis indicates that this rock is a quartz arenite.*

appear to be the only effective cement (figure 2.12B). This observation is also true in the stratigraphically equivalent Lower Jurassic Aztec Sandstone in southern Nevada (Eichhubl and others, 2004). The STC facies is moderately to poorly sorted which is not typical of the rest of the Navajo Sandstone that we measured.

Porosity/permeability: The unusually high porosity of the STC facies (almost 40%) is due to sparse cement (based on two samples), possibly the result of dissolution. The permeability is comparable to the LTC facies. The relatively low permeability (26 mD) compared to the high porosity in the STC facies is due to clay-coated grains and associated clay bridges within pore throats (figure 2.12B).

Interpretation: The STC facies appears only once in the measured section. It is the basal unit of the Navajo Sandstone, therefore the STC facies may represent the developing dune field or erg-margin of the Navajo erg system. The first dunes that began to blow over Kayenta fluvial deposits were relatively small (1 meter [3 ft] trough cross-stratified bedding) when compared to the later erg. Due to the high porosity and acceptable permeability, the STC facies can be considered a reservoir facies. However, because it is present only at the base of the Navajo and it is thin, the STC facies is a relatively minor reservoir.

Reworked Eolian (RWE)

Outcrop characteristics: The RWE facies contains massive to contorted bedding. Where we measured unit JFCG 10, it was massively bedded and recessive; however, laterally, some wavy/contorted bedding can be observed (figure 2.13A). The unit is only about 1 meter (~3 ft) thick and does not appear to be laterally extensive (less than 50 meters [<150 ft]). The RWE facies is not common in the Navajo Sandstone. The color is light greenish-gray (5 GY 8/1).

Petrology: The RWE facies plots as a feldspathic arenite based on point count analysis of thin sections (figures 2.13B, 2.13C, and 2.13D). The provenance is continental block, craton interior (Dickinson and Suczek, 1979; Dickinson and others, 1983; Dickinson and Gehrels, 2003). Petrologically, the RWE facies looks very similar to the LTC facies, in that it has very little calcite or oxide cement and contains the same amount of total quartz (64%) (figures 2.12D and 2.13D). There are approximately equal amounts of plagioclase (5%) and potassium feldspar (4%) (figure 2.13D). The main form of cement in the RWE facies is thin quartz overgrowths. The similarity to the LTC facies suggests that the two facies are related.

Porosity/permeability: The porosity of the RWE facies is approximately 23%, slightly lower than that of the average porosity of the LTC facies. The permeability of the RWE facies is approximately 70 mD (two samples).

Interpretation: The RWE facies is interpreted as water-reworked LTC facies, primarily by variations in natural hydraulic processes such as rainfall (i.e., non-channelized and not by debris flow). This reworking destroyed the primary bedding in many places, thereby preserving only massive bedding. In other places the bedding is still visible but contorted. Another possibility for this environment is water-saturated dunes that slumped and deformed until bedding was obliterated (Sanderson, 1974; Loope and others, 2001). The porosity and permeability of the RWE facies make it a potential reservoir, but its rarity in the section and limited lateral extent make it a minor reservoir at best.

Porosity and Permeability of Facies: Discussion

Core plug porosity and permeability can be cross-plotted to illustrate the separation of individual facies as well as to demonstrate the broader differences between dune facies and interdune facies (figure 2.14). A general principle of sedimentology states that eolian facies are typically more porous and permeable than are interdune facies because of the wind's ability to sort grains. The facies interpretations presented in this report concur with this general principle. Those facies most influenced by wind, including the LTC, STC, and RWE facies, are significantly more porous and permeable than the interdune facies.

Interdune areas are intermittently wetted allowing for the potential for algal growth. Both the wetted surface and the algal filaments aid in trapping clay and silt-size particles with blowing sand. Thus, these deposits are less sorted than the eolian-dominated dune facies. The size and mineralogical make-up of the clay and silt-size particles may also make the resulting deposit more susceptible to diagenesis. As a result of both sorting and diagenesis, the interdune facies display lower porosity and permeability relative to the dune facies. There is much overlap between porosity and permeability values between the EID, SAM, and PDI facies. This may be related to the time and specific sedimentological conditions that each developed under. These facies, however, may be differentiated by several other characteristics (see table 2.1).

A very significant observation is that the WAM facies, having the largest lateral extent of the interdune facies, consistently has the lowest porosity and permeability of any Navajo Sandstone facies in the study area. The relatively low porosity and very low permeability combined with the relatively large lateral extent of this facies suggests that it could potentially act as a fluid flow barrier in the subsurface (figure 2.15).

DEPOSITIONAL HISTORY

The depositional history of the Navajo Sandstone in the vicinity of Devils Canyon can be reconstructed by the stacking pattern of facies developed in the composite section (Dalrym-

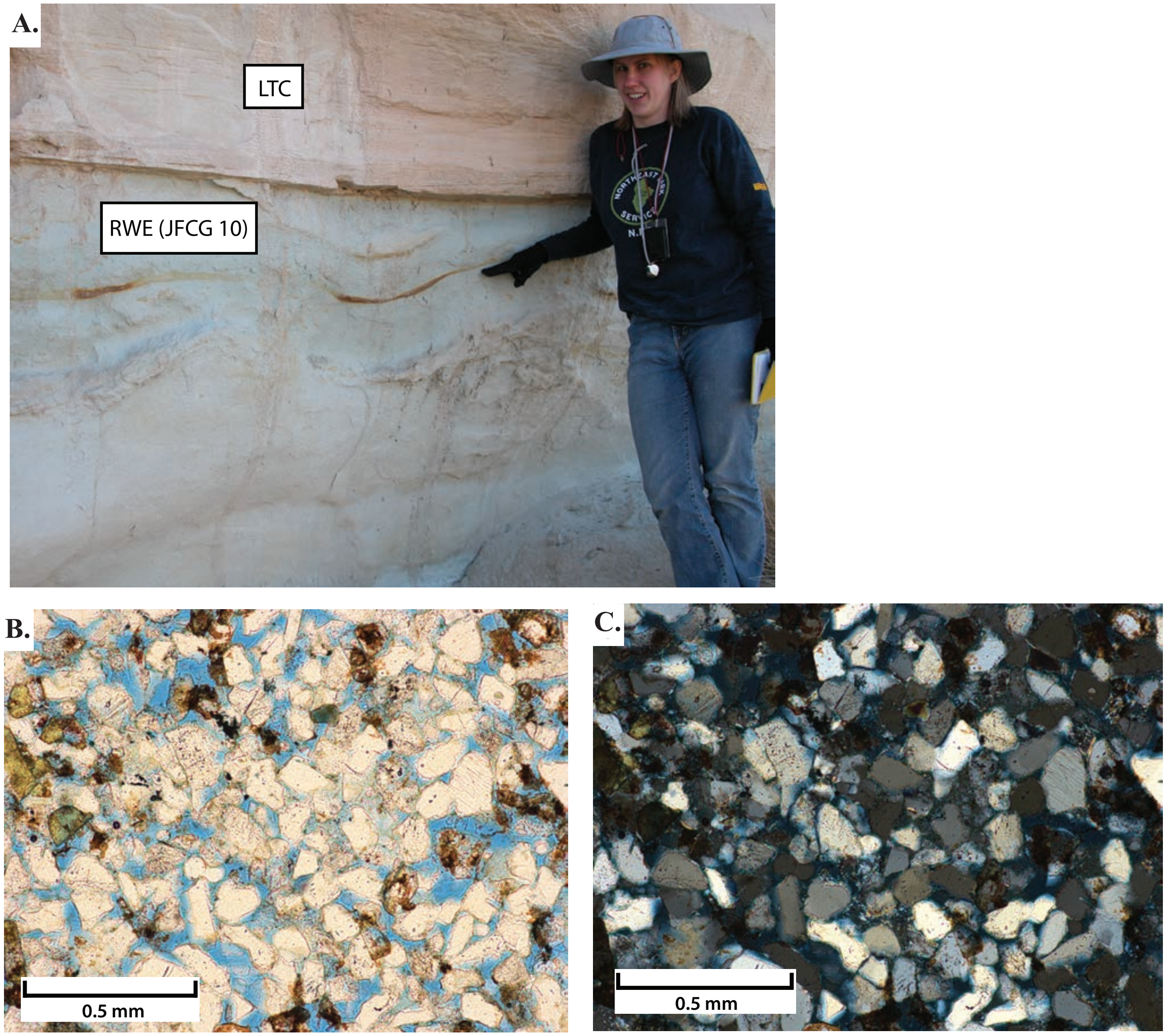

D.

Mineral	Count	Percent	Error (+/-)	Normalized
Mono qtz	81	27	5.2	
undulose	82	27.33	5.2	
Poly qtz	29	9.66	3.4	
Micro qtz	0	0	0	
Total Quartz	192	63.99		0.85342758
K spar	13	4.33	1.6	
Plag	15	5	2.4	
Total Feldspar	28	9.33		0.12443318
Lithics	5	1.66	<1	0.02213924
Clay	16	5.33	2.4	
Matrix	7	2.33	1	
Porosity	43	14.33	4	
Oxides	5	1.66	<1	
Calcite	3	1	<1	
Heavies	1	0.33	<1	
Total	300	99.96		1
Grain size	Fine-medium			
Roundness	Subrounded			
Sorting	Moderately well sorted			

Figure 2.13. *Lithologic and petrologic analysis of the Reworked Eolian (RWE) facies.* ***A.*** *Outcrop view of the RWE facies, which displays soft-sediment deformation and massive bedding. Note overlying Large Trough Cross-stratified (LTC) facies.* ***B.*** *Photomicrograph displaying high (>20%) porosity (blue) under plane-polarized light. Porosity is underestimated (due to edge effects) relative to core plug porosity.* ***C.*** *Same image as B under cross-polarized light.* ***D.*** *300-point count analysis indicates that this rock is a quartz-rich feldspathic arenite.*

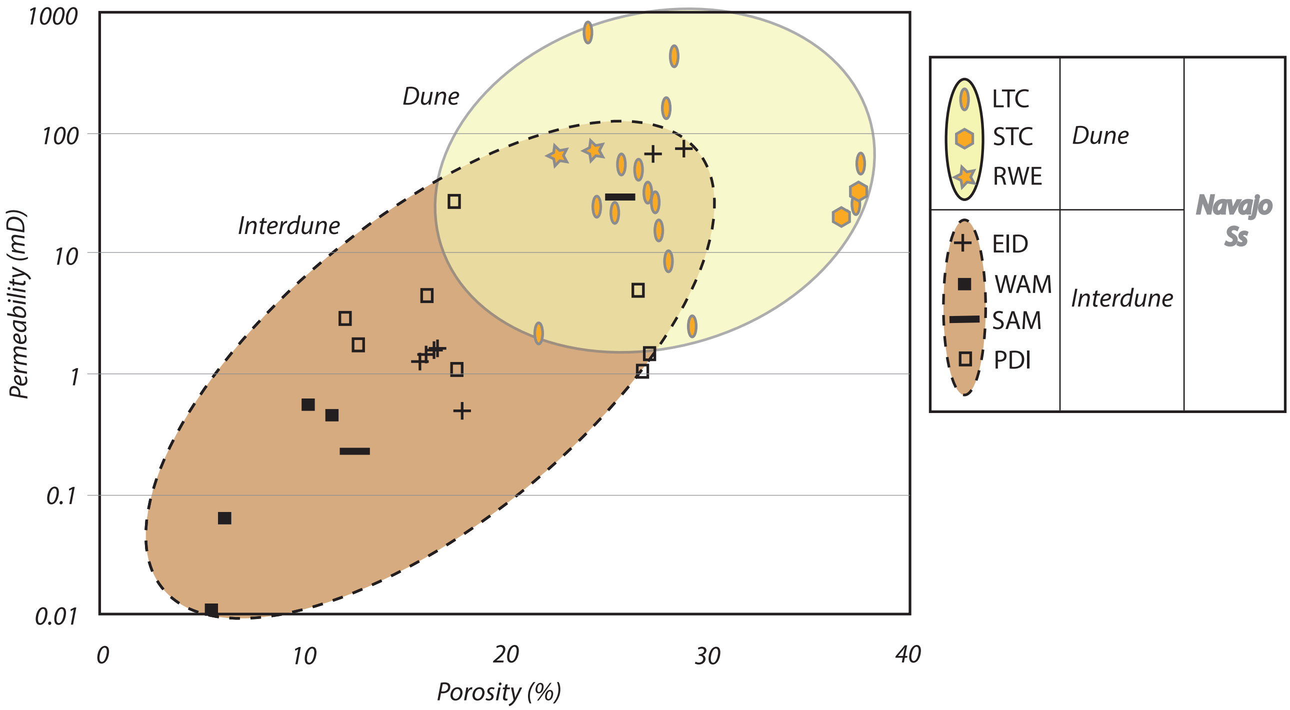

Figure 2.14. *Porosity versus permeability plot of 40 Navajo samples collected from the Devils Canyon study area. Each plug is identified by facies. The Ephemeral Fluvial Channel (EFC) facies was not found in the immediate line of section and was not sampled. Note the broader pattern of high porosity (>20%) and permeability for the dune facies (data points within yellow oval). Of particular note is the very low porosity and permeability of the Wavy Algal Mat (WAM) interdune facies, which is laterally extensive in the study area. The WAM facies could act as a barrier to fluid flow within a subsurface hydrocarbon/CO_2 reservoir, produced water disposal aquifer, or potential storage unit for captured CO_2. Facies are as follows: LTC = Large Trough Cross-stratified; STC = Small Trough Cross-stratified; RWE = Reworked Eolian; EID = Evolving Interdune; WAM = Wavy Algal Mat; SAM = Sandy Algal Mat; PDI = Poorly Developed Interdune.*

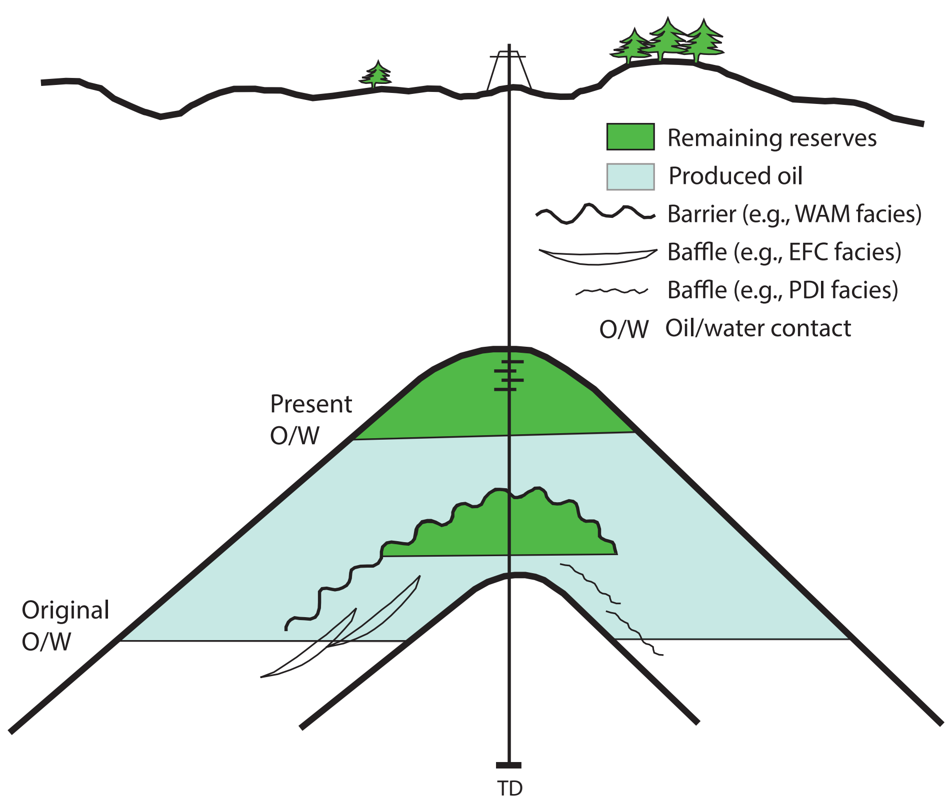

Figure 2.15. *Diagram depicting one possible production concern when barriers and baffles exist within the larger reservoir rock. In this depiction, the lateral extent of the impermeable facies (e.g., WAM) is large enough to produce closure over a tight fold.*

ple and Morris, 2007). It appears that after fluvial-dominated processes of the Kayenta Formation ceased, relatively closely spaced small dunes (STC facies) were deposited in the area. Thin interdune deposits (PDI, EFC, and RWE facies) were common. These deposits were on the order of only a few tens of meters to 200 meters (>30–600 ft) in lateral extent. This early transition from fluvial to small, closely spaced dunes may reflect the migration of the erg system into the study area and/or climate change. Eventually more widely spaced, larger dunes entered the area. On at least two occasions these broad interdune areas were wet enough for meter-thick accumulations of algal mats (WAM facies). The SAM facies, which precedes the WAM facies stratigraphically, could represent the dune-interdune edge wherein sand was more available to be deposited. This stratigraphic relationship indicates that either the dune-interdune system was migrating or that for some interval of time the wet interdune area was expanding (groundwater table was rising) in the area.

As time progressed, the system became more dry and larger dune sets dominated the landscape. Thick successions of high-angle, trough cross-sets accumulated in the area with little interruption (LTC facies). On at least two occasions a laterally extensive, variably thick interdune facies developed (EID facies). The EID facies likely developed from a combination of a short-lived rise in the groundwater table and relatively fast dune migration. It is also possible that these deposits represent extensive interdune surfaces between large parts of the erg proper. After an estimated several million years of Navajo Sandstone deposition, a shallow seaway entered the area and deposited marine rocks of the Middle Jurassic Carmel Formation.

As suggested earlier, petrologic work indicates that Navajo sediment was derived from erosion and transport of Appalachian bedrock (figure 2.16) (Dickinson and others, 1983; Dickinson and Gehrels, 2003; Rahl and others, 2003). The denudation of the Appalachians moved sediment to the northwest by alluvial and fluvial processes. The sand was then transported south into the Navajo depositional basin by wind and possibly longshore processes (Doe and Dott, 1980; Kocurek and Dott, 1983).

The richness of the quartz percentage of most samples and the multiple quartz overgrowths observed on some grains argues that the individual grains of the Navajo Sandstone have evolved through time and that the grains have gone through the rock cycle numerous times. We interpret the tectonic provenance of the Navajo to be within the Craton Interior and Transitional Continental provenances, similar to Dickinson and others (1983).

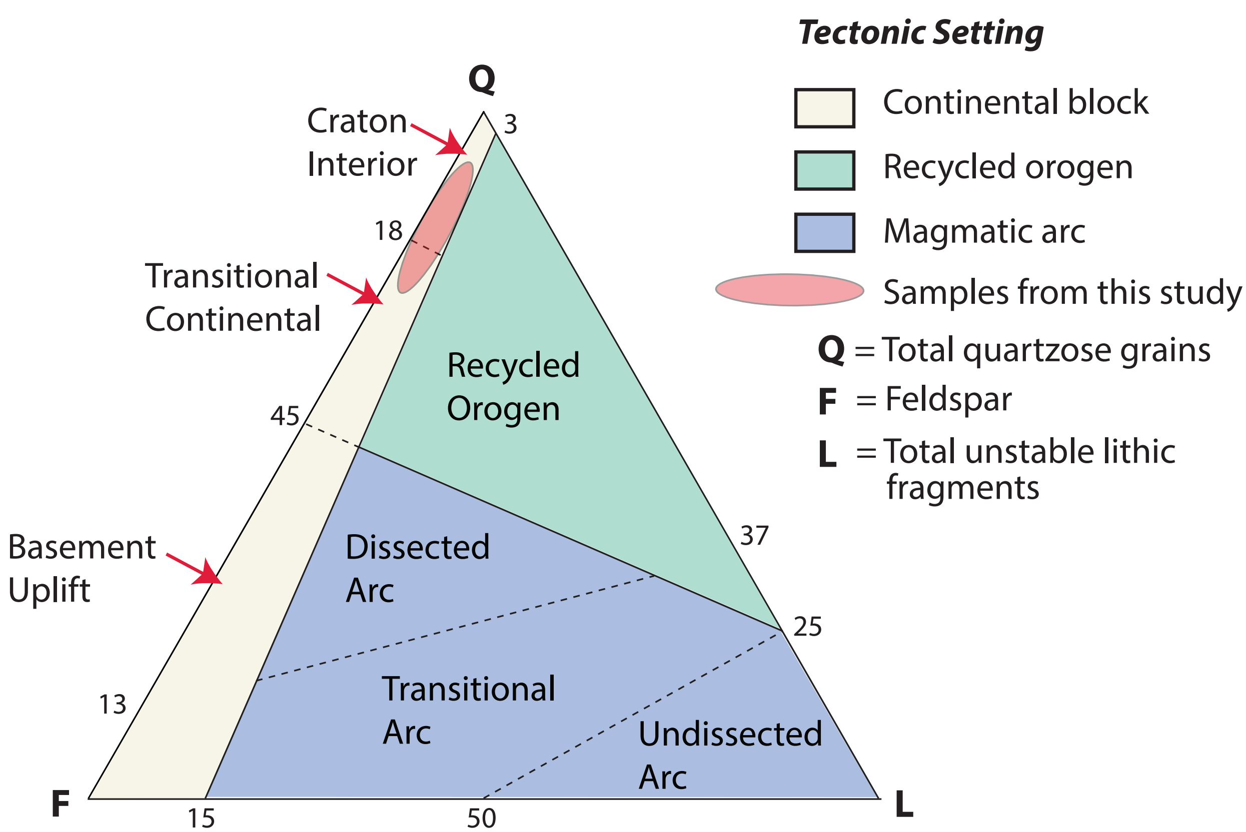

Figure 2.16. *Tectonic provenance plot of Navajo Sandstone samples from the study area indicate that the sand grains were derived from craton interior and transitional continental areas. Modified from Dickinson and others (1983).*

CHAPTER 3:
GEOLOGY OF THE EAGLE CANYON AREA

by

Stephanie M. Carney, Thomas C. Chidsey, Jr., and Craig D. Morgan

Northwest view from Eagle Canyon of the Navajo Sandstone section, displaying classic dune and interdune facies.

CHAPTER 3:
GEOLOGY OF THE EAGLE CANYON AREA

INTRODUCTION

The Eagle Canyon study area is located north of I-70 (figure 3.1), less than 1.6 kilometers (<1.0 mi) north of the Devils Canyon/Justensen Flats study area (Chapter 2). The methods used to obtain data from this measured section are similar to those used at the Devils Canyon/Justensen Flats section and the same suite of analyses on outcrop samples was done to correlate both measured sections.

Due to outcrop access, the Eagle Canyon measured section is a composite of three correlated sections totaling 194 meters (637 ft) (figure 3.2). The lower section is 10 meters (33 ft) thick, the middle section is 47 meters (154 ft) thick, and the upper section is 137 meters (450 ft) thick. All sections are located in a small gully that drains into Eagle Canyon and originates about 458 meters (~1500 ft) north of I-70 (figure 3.1). The trend of the gully follows that of a fault that strikes roughly N. 40° E. and dips steeply (>45°) to the west. Offset along the fault was not measured but is likely less than 10 meters (<33 ft). The section was measured west of this small fault and fault-influenced areas were avoided when collecting samples for analyses. The base of the Navajo Sandstone was not found in the Eagle Canyon section, and therefore an incomplete section was measured. However, Sanderson (1974) reported measuring a complete section nearby. We were unable to find the exact location of the Kayenta-Navajo contact cited in Sanderson's paper.

The units in our measured section are labeled ECT (Eagle Canyon tributary) 1 through 18 and consist of either dune or interdune erg sediments of the Navajo. Each unit was assigned to one of eight facies described and interpreted in Chapter 2.

DESCRIPTION OF THE EAGLE CANYON UNITS OF THE NAVAJO SANDSTONE

The following is a description of the outcrop characteristics observed in each unit at the Eagle Canyon measured section. For units where samples were taken, porosity, permeability, and thin-section analyses are also described. All sandstones in the measured section are classified as sub-feldspathic quartz arenites according to the Miliken and others (2002) and Boggs (2006) QFL ternary diagram (figure 2.5). Each of the units at Eagle Canyon was assigned to one of the eight facies described and interpreted for the Navajo section in the Devils Canyon/Justensen Flats area (table 2.1).

Eagle Canyon Tributary Unit 1 (ECT1)

Unit ECT1 is a 1.5-meter-thick (4.9 ft), fine-grained, massive sandstone with some thin beds near the base. The unit has a weathered, recessive profile and is very pale-orange (10Y/R 8/2). Grains appear subrounded and moderately sorted in hand sample and are cemented with silica. The unit can be traced laterally for several tens of meters to the north and south. Samples for thin section and porosity/permeability analyses were not collected due to the highly friable nature of this unit. Based on outcrop characteristics and limited lateral extent, this unit was assigned to the PDI facies and would likely be a baffle to fluid flow in a reservoir or aquifer.

Eagle Canyon Tributary Unit 2 (ECT2)

Unit ECT2 is a thin bedded (0.08 meter [0.3 ft] thick), fine-grained sandstone. It is relatively resistant in outcrop and creates a small ledge in profile. The unit is brownish (10YR 5/4) and appears similar to the "brown beds" (interdunes) of Dalyrmple and Morris (2007) and Hansen (2007). Grains appear subrounded to rounded and moderately to poorly sorted in hand sample and are cemented with silica. This unit extends several tens of meters to the north and south before pinching out. As with ECT1, samples for thin section and porosity/permeability analyses were not collected. Based on outcrop characteristics and hand sample analysis, this unit was also assigned to the PDI facies and would be a baffle to fluid flow in a reservoir or aquifer.

Eagle Canyon Tributary Unit 3 (ECT3)

Unit ECT3 is a 4.8-meter-thick (15.8 ft), massive bedded, fine-grained sandstone. The unit has a recessive weathering profile, is light gray to very light gray (N8), and has small sets (less than 1 meter [<3 ft] high) of trough cross-beds (figure 3.3). In hand sample, grains are subrounded to rounded, well sorted, and silica cemented. The unit can be traced laterally for tens of meters to the north and south. Again, like the lower two units, samples for thin section and porosity/permeability analysis were not collected from this unit due to its friable nature. Based on the outcrop characteristics, this unit was assigned to the STC facies and could serve as a reservoir or aquifer.

Eagle Canyon Tributary Unit 4 (ECT4)

Unit ECT4 is a 0.3-meter-thick (0.9 ft), calcite cemented, fine-grained sandstone. This unit creates a small, resistant ledge in outcrop and is brown (10YR 6/6) (figure 3.4A). No sedimentary structures are visible in outcrop. Unit ECT4 thins and dies

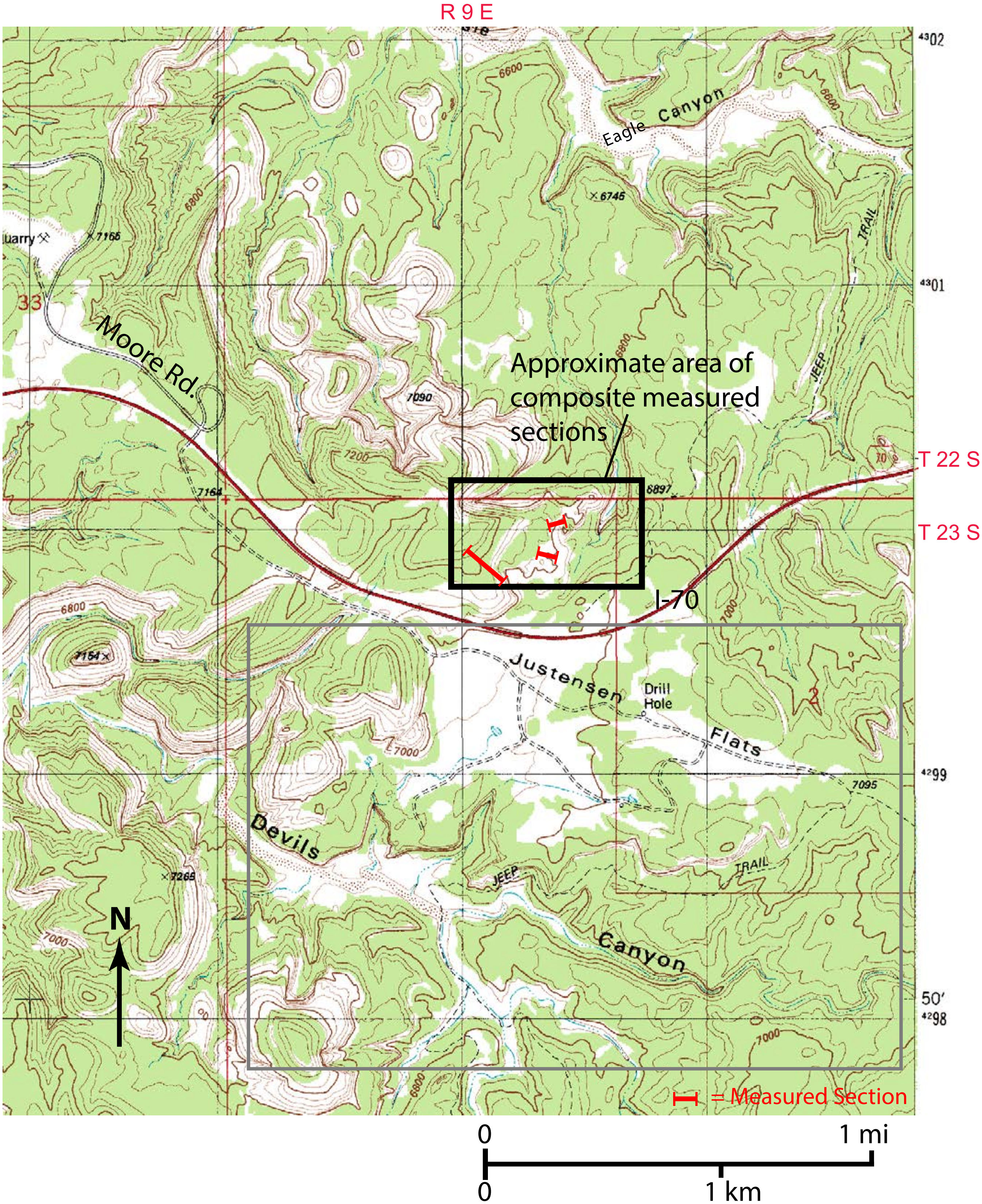

Figure 3.1. Location of Eagle Canyon study area (black rectangle) in the northeastern corner of U.S. Geological Survey Copper Globe 7.5' quadrangle (contour interval = 40 ft); Devils Canyon/Justensen Flats study area shown in the light gray rectangle to the south. Composite measured section shown on figure 3.2 and described in text.

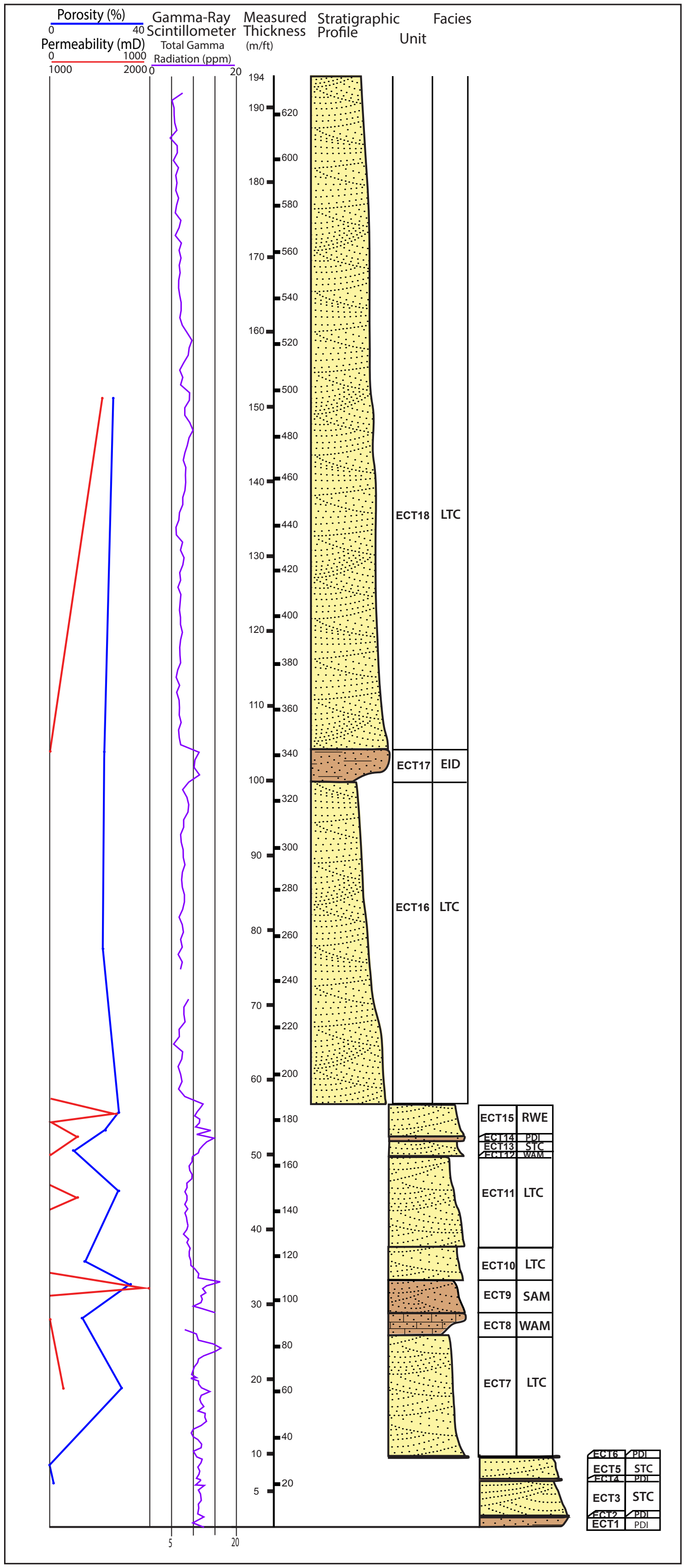

Figure 3.2. *Stratigraphic column of composite measured section of the Navajo Sandstone at Eagle Canyon. Gamma-ray scintillometer measurements shown on the left were taken along the measured section and samples were collected from most units for porosity and permeability analysis. See table 2.1 and figure 2.2 for explanation of facies, lithology, etc.*

Figure 3.3. *Small trough cross-stratification in unit ECT3. This unit is assigned to the STC facies. Rock hammer for scale.*

out to the north but is continuous to the south for several tens of meters. Petrographic analysis shows a composition of 36% quartz, 8% feldspar, 51% calcite cement, and porosity of 2% (figures 3.4B and 3.4C). Grains in thin section appear poorly sorted and are subangular to subrounded (figure 3.4B). No core plug analysis was done for this sample. Based on outcrop and petrographic characteristics, as well as limited lateral extent, ECT4 is assigned to the PDI facies and would be a baffle to fluid flow in a reservoir or aquifer.

Eagle Canyon Tributary Unit 5 (ECT5)

Unit ECT5 is a 2.8-meter-thick (9.2 ft), massive, fine-grained sandstone. The unit has a recessive weathering profile and is yellowish-gray (5Y 8/1). Sedimentary structures present are thin sets of cross-stratified bedding, less than 1 meter (<3 ft). In hand sample the grains are moderately sorted and rounded to subrounded. This unit can be traced laterally for several tens of meters to the south and north. Unfortunately sampling of this unit was not possible and therefore no petrographic or porosity/permeability data were obtained. Based on outcrop characteristics such as the small sets of cross-stratification, this unit was assigned to the STC facies and could serve as a reservoir or aquifer.

Eagle Canyon Tributary Unit 6 (ECT6)

Unit ECT6 is a very thin (20 centimeters [8 in.]), medium- to fine-grained sandstone with calcite cement. It is more resistant than either bed above and below and is medium (5YR 5/6) to light brown (5YR 4/4). The unit can be traced laterally for several tens of meters and varies in thickness along strike. Grains are well rounded to subangular and bimodal in thin section. Calcite cement is mostly poikilotopic (figure 3.5A) and composes 50% of the sample. Thirty-six percent of the sample is quartz, 9% is feldspar, and the sample has less than 2% porosity (figure 3.5B). Core plug analysis was not performed for this unit. Based on limited lateral extent and the high percentage of calcite cement, this unit was assigned to the PDI facies and would likely be a baffle to fluid flow.

Eagle Canyon Tributary Unit 7 (ECT7)

Unit ECT7 is a 16.2-meter-thick (53 ft), fine-grained, silica-cemented sandstone. This unit has a recessive weathering profile and ranges in color from yellowish-gray (5Y 8/1) to grayish-orange (10YR 7/4). Sedimentary structures include trough cross-stratification with sets less than 1 meter (<3 ft) high. In thin section, the sample is mostly fine grained with a few sparse

A.

B.

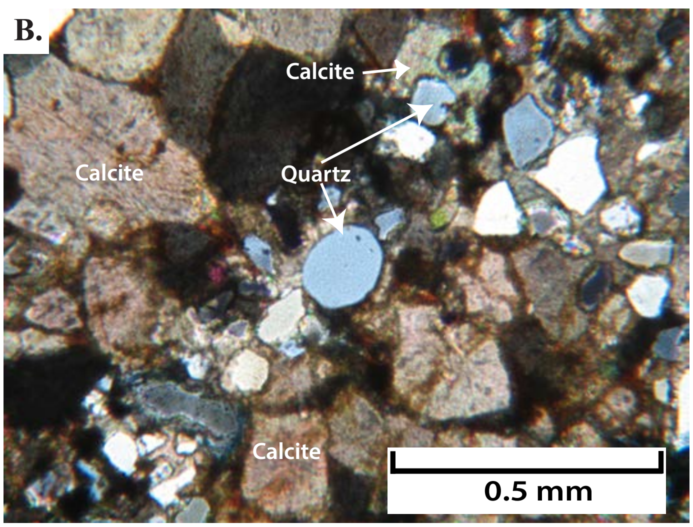

C.

Mineral	Count	Percent	Normalized
Mono qtz	67	22.3	
Undulating qtz	38	12.6	
Poly qtz	4	1.3	
Total Quartz	109	36.3	0.825758
K spar	19	6.3	
Plag	4	1.3	
Total Feldspar	23	7.7	0.174242
Porosity	6	2	
Calcite cement	153	51	
Matrix	0	0	
Lithics	1	0.3	
Fe-clay cement	8	2.6	
Heavy mins	0	0	
Total	300	100	1
Grain size	Medium lower to very fine upper		
Roundness	Subangular to subrounded		
Sorting	Poor		

Figure 3.4. *Lithologic and petrographic analysis of unit ECT4.* ***A.*** *Unit ECT4 in outcrop is a very thin, resistant brown bed and is assigned to the PDI facies.* ***B.*** *Photomicrograph displaying prolific calcite cement encompassing quartz grains, under cross-polarized light.* ***C.*** *300-point count analysis indicates that this rock is a feldspathic arenite.*

medium-sized grains. The grains are poorly sorted and well to subrounded. Thin section composition is 76% quartz and 11% feldspar with 10% calcite cement and very little silica cement (2%). Core plug analysis was performed on two samples from this unit. The average porosity is 25% and average permeability is 75 mD. This unit was assigned to the LTC facies and could serve as an excellent reservoir or aquifer.

Eagle Canyon Tributary Unit 8 (ECT8)

Unit ECT8 is a 3-meter-thick (9.8 ft), thin-bedded, fine-grained sandstone. It is dark brown (10YR 6/6) and resistant to weathering. The unit has wavy laminations (figure 3.6) and pervasive calcite cement. The unit can be traced laterally for hundreds of meters. Grains are poorly sorted and angular to subrounded. Petrographic analysis shows that the unit is 52% quartz, 8% feldspar, and has only 4% porosity (figure 3.7). Microsparite calcite is the dominant cement with minor grain-to-grain silica cementation (figures 3.7B and 3.7C). Core plug analysis for this unit yielded an average porosity of 13% and an average permeability of 4.5 mD. Based on great lateral extent (less than 0.8 kilometers [<0.5 mi]) and low porosity and permeability, this unit was assigned to the WAM facies and would be a barrier to fluid flow in a reservoir or aquifer.

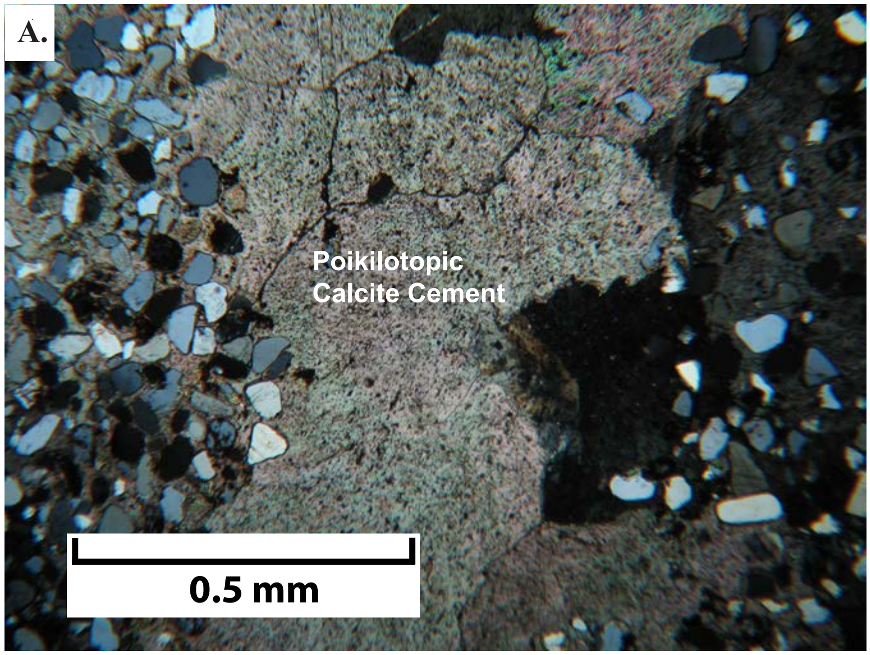

B.

Mineral	Count	Percent	Normalized
Mono qtz	69	23	
Undulating qtz	36	12	
Poly qtz	3	1	
Total Quartz	108	36	0.800000
K spar	19	6.3	
Plag	8	2.7	
Total Feldspar	27	9	0.200000
Porosity	4	1.3	
Calcite cement	152	50.7	
Matrix	0	0	
Lithics	0	0	
Heavy cement	9	3	
Total	300	100	1
Grain size	Medium lower to very fine lower		
Roundness	Subangular to well rounded		
Sorting	Poor		

Figure 3.5. *Lithologic and petrographic analysis of unit ECT6.* ***A.*** *Photomicrograph displaying pervasive poikilotopic calcite cement, under cross-polarized light.* ***B.*** *300-point count analysis indicates that this rock is a quartz-rich feldspathic arenite. Unit ECT6 is assigned to the PDI facies.*

Eagle Canyon Tributary Unit 9 (ECT9)

Unit ECT9 is a 4.5-meter-thick (14.8 ft), yellowish-gray (5Y 7/2), fine-grained sandstone with a ledge-like weathering profile. Grains are rounded and moderately to poorly sorted and are poorly cemented with silica and, to a lesser extent, calcite. Sedimentary structures include a small set, less than 20 centimeters (<8 in.), of trough cross-strata near the base of the unit (figure 3.8A) and planar bedding near the top of the unit. The unit also exhibits thin, planar laminae (figure 3.8B). It has a lateral extent of tens of meters. Petrographic analysis shows that the unit is 70% quartz, 8% feldspar, and has 19% porosity (figures 3.8C and 3.8D). Cementation accounts for 3% of the thin section and consists of minor grain-to-grain silica cementation and patchy poikilotropic calcite cement. Core plug analysis yielded an average permeability of 1976 mD and an average porosity of 31%. Based on the sedimentary structures and petrography, this unit was assigned to the SAM facies. However, its petrophysical properties indicate that the unit would act as a reservoir or aquifer in this area.

Eagle Canyon Tributary Unit 10 (ECT10)

Unit ECT10 is a 4.3-meter-thick (14 ft), fine-grained, friable sandstone cemented loosely with silica. It is very pale-orange (10YR 8/2), has a cliffy weathering profile, and has large sets of trough cross-stratified beds, greater than 1 meter

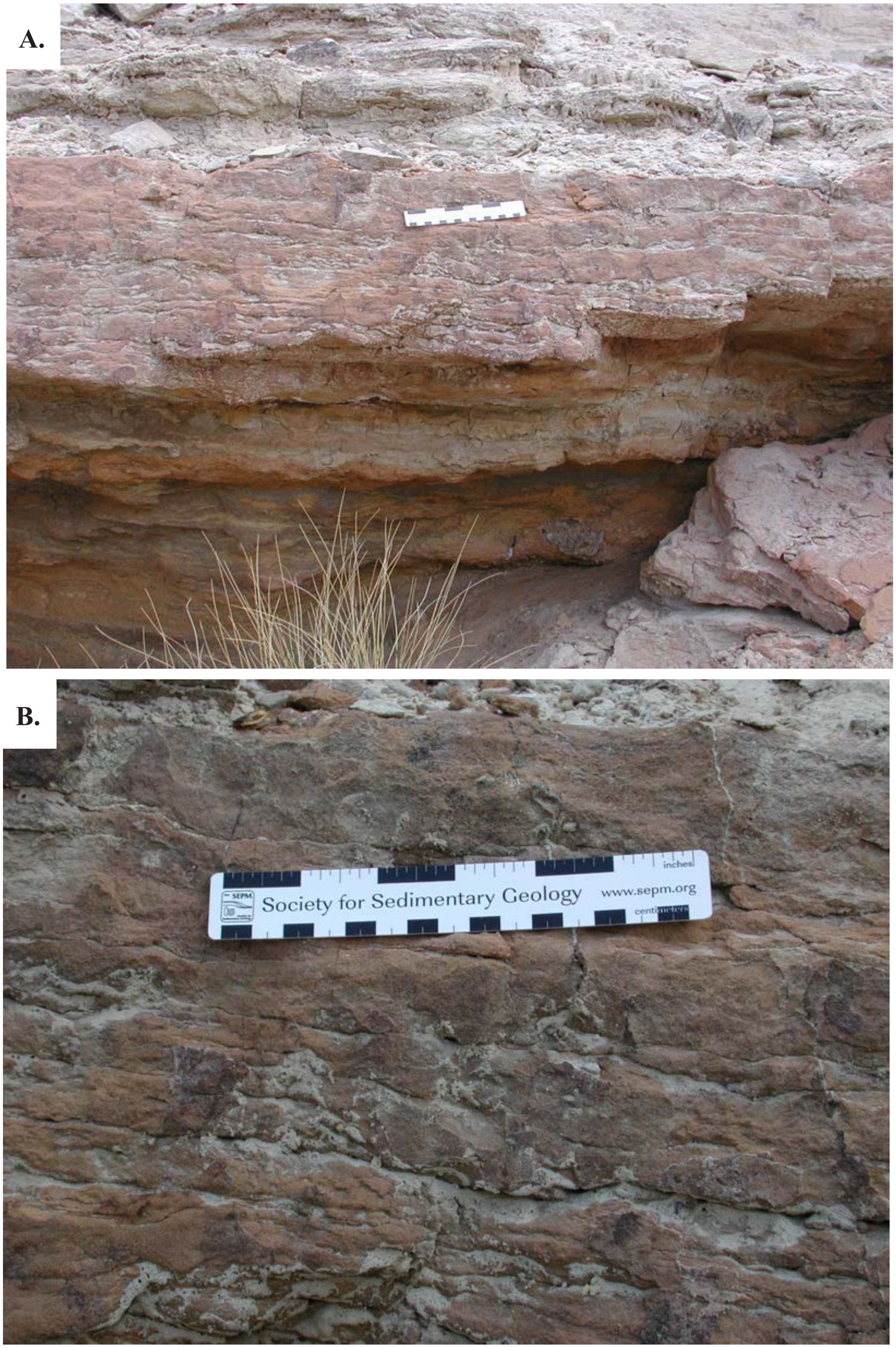

Figure 3.6. *Unit ECT8 in outcrop.* ***A.*** *This unit represents the WAM facies; note the wavy lamination.* ***B.*** *Close-up of laminations.*

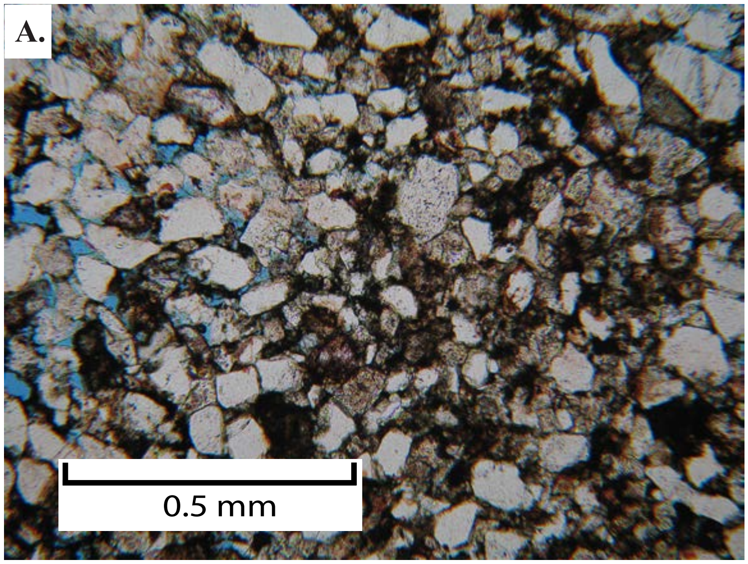

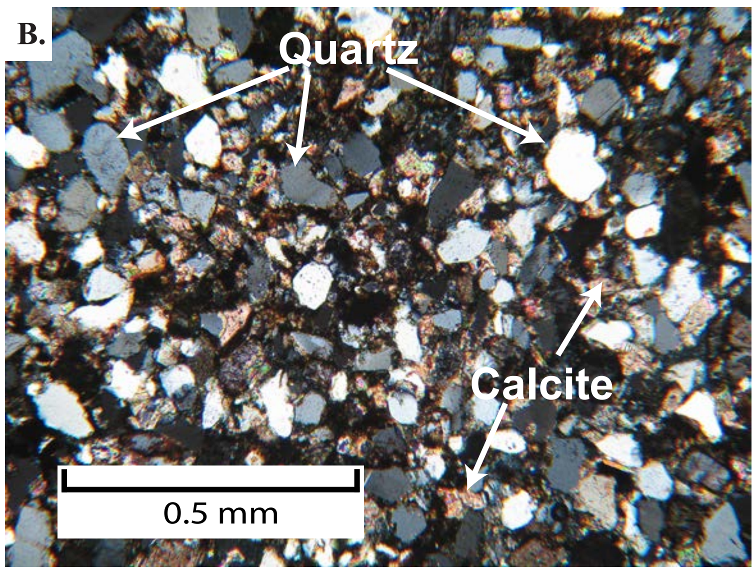

C.

Mineral	Count	Percent	Normalized
Mono qtz	87	29	
Undulating qtz	67	22.3	
Poly qtz	2	0.7	
Total Quartz	156	52	0.871508
K spar	14	4.7	
Plag	9	3	
Total Feldspar	23	7.7	0.128492
Porosity	11	3.7	
Calcite cement	99	33	
Matrix	0	0	
Lithics	0	0	
Heavy cement	11	3.7	
Total	300	100.1	1
Grain size	Very fine upper		
Roundness	Subrounded to angular		
Sorting	Poor to moderate		

Figure 3.7. *Lithologic and petrographic analysis of unit ECT8.* ***A.*** *Photomicrograph displaying the lack of porosity due to pervasive calcite cement, under plane-polarized light.* ***B.*** *Photomicrograph under cross-polarized light showing quartz grains and calcite cement.* ***C.*** *300-point count analysis indicates that this unit is a quartz-rich feldspathic arenite.*

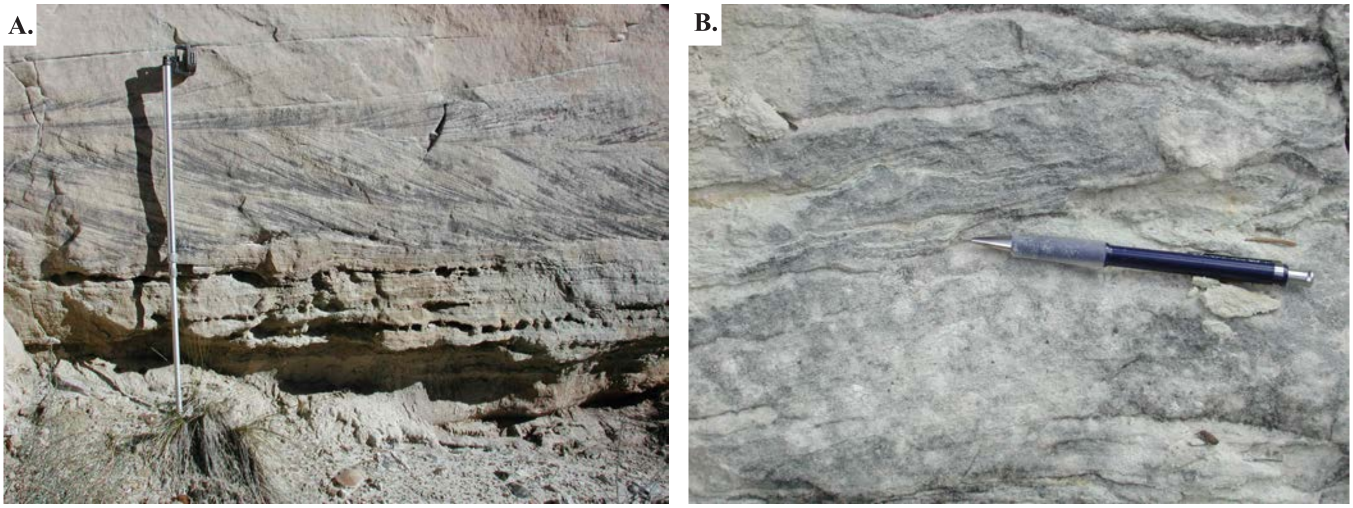

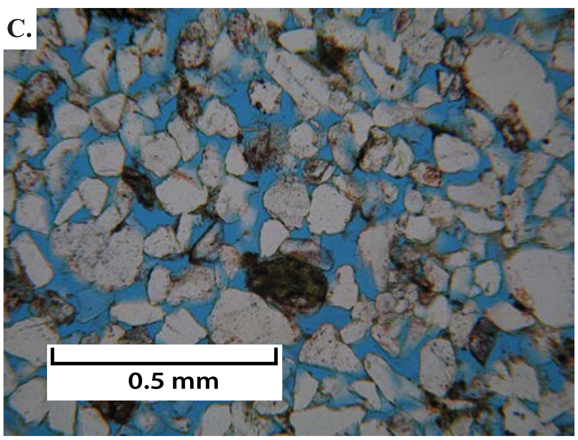

D.

Mineral	Count	Percent	Normalized
Mono qtz	136	45	
Undulating qtz	74	24.5	
Poly qtz	2	0.7	
Total Quartz	212	70.2	0.898305
K spar	10	3.3	
Plag	14	4.6	
Total Feldspar	24	7.9	0.101695
Porosity	56	18.5	
Calcite cement	8	2.7	
Matrix	0	0	
Lithics	0	0	
Heavy mins	2	0.7	
Total	302	100	1
Grain size	Very fine lower to fine lower		
Roundness	Subrounded to rounded		
Sorting	Moderate		

Figure 3.8. *Lithologic and petrographic analysis of unit ECT9.* ***A.*** *In outcrop, the base of Unit ECT9 consists of small trough cross-stratified beds.* ***B.*** *Planar laminae in the SAM facies.* ***C.*** *Photomicrograph displaying abundant quartz grains and high porosity (blue), under plane-polarized light.* ***D.*** *300-point count analysis indicates that this rock is a quartz-rich feldspathic arenite.*

(>3 ft). Grains are moderately sorted and subrounded to angular. The unit can be traced laterally for several tens of meters to the north and south. Petrographic analysis shows that the unit is 74% quartz, 11% feldspar, and has 14% porosity with very little cement (0.3%) (figure 3.9). Cement consists of minor grain-to-grain silica cementation and very sparse calcite. Core plug analysis was not performed for this unit. Based on outcrop and petrographic characteristics, this unit was assigned to the LTC facies and could serve as a reservoir or aquifer.

Eagle Canyon Tributary Unit 11 (ECT11)

Unit ECT11 is a 12.3-meter-thick (40.4 ft), massive bedded, fine-grained sandstone. Outcrop samples range in color from very pale-orange (10YR 8/2) to gray-orange (10YR 7/4) and have moderately to well sorted, subangular to rounded grains. This unit crops out as steep, but recessive slopes. Large trough cross-stratified structures greater than 1 meter (>3 ft) are present and the unit can be traced laterally for several tens of meters. A sample in thin section is 67% quartz, 11% feldspar, and has 21% porosity with very minor calcite cement (1%). Core plug analysis yielded an average permeability of 1237 mD and 27% porosity. This unit was assigned to the LTC facies based on the sedimentary structures and high average porosity and permeability. It could serve as an excellent reservoir or aquifer.

Eagle Canyon Tributary Unit 12 (ECT12)

Unit ECT12 is a very thin (0.3-meter-thick [1 ft]) brown bed. It crops out as a very hard, wavy bedded, dark brown (10YR 8/6) resistant unit that is well cemented with calcite and has a lateral extent on the order of tens of meters. Grains are poorly sorted, angular to subangular, and are medium to fine grained. Petrographic analysis shows that the sample is 45% calcite cement, 48% quartz, 5.6% feldspar, and has 1% porosity. Core plug analysis yielded an average porosity of 2% and permeability of 2.6 mD. Based on outcrop characteristics and low porosity and permeability, this unit was assigned to the WAM facies and would be a barrier to fluid flow in a reservoir or aquifer.

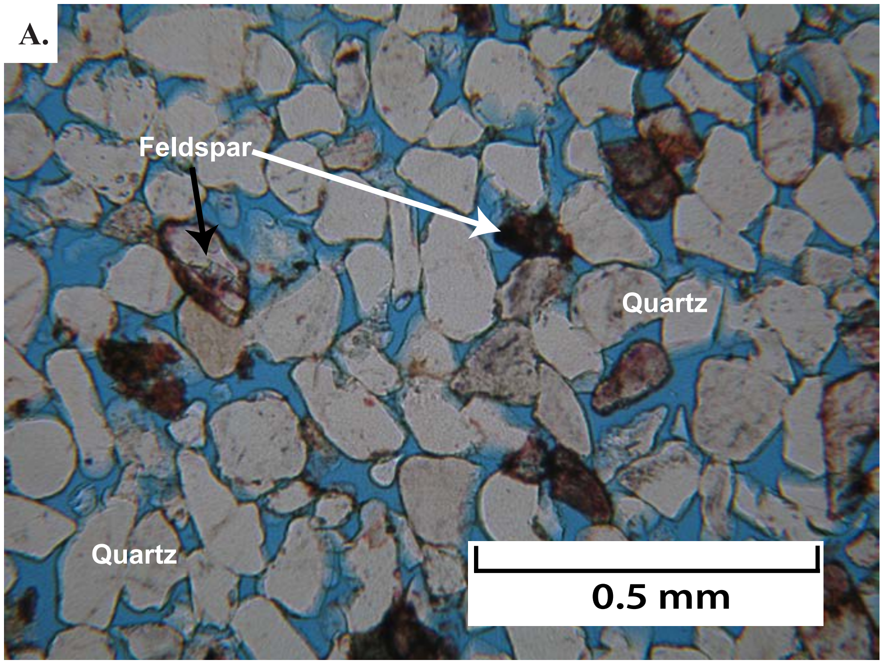

B.

Mineral	Count	Percent	Normalized
Mono qtz	158	52.7	
Undulating qtz	61	20.3	
Poly qtz	3	1	
Total Quartz	222	74	0.867188
K spar	10	3.3	
Plag	24	8	
Total Feldspar	34	11.3	0.132812
Porosity	43	14.3	
Calcite cement	1	0.3	
Matrix	0	0	
Lithics	0	0	
Heavy mins	0	0	
Total	300	100	1
Grain size	Fine upper, some very fine lower		
Roundness	Subrounded to rounded		
Sorting	Moderate to well		

Figure 3.9. *Lithologic and petrographic analysis of unit ECT10.* ***A.*** *Photomicrograph displaying abundant porosity between quartz and feldspar grains, under plane-polarized light.* ***B.*** *300-point count indicates that this rock is a quartz-rich feldspathic arenite.*

Eagle Canyon Tributary Unit 13 (ECT13)

Unit ECT13 is a 1.9-meter-thick (6.2 ft), fine-grained sandstone with small sets of trough cross-stratified beds. This sandstone consists of moderately to well sorted, subangular to subrounded grains loosely held together with silica cement. It is very pale-orange (10YR 8/2) and has iron staining and concretions that occur immediately above the contact with unit ECT12 (figure 3.10). Obtaining a sample of this unit was difficult due to its friable nature and recessive weathering profile, and therefore, petrographic, permeability, and porosity analyses were not performed. Based on outcrop characteristics, ECT13 was assigned to the STC facies and could potentially serve as a reservoir or aquifer.

Eagle Canyon Tributary Unit 14 (ECT14)

Unit ECT14 is another thin (0.5-meter-thick [1.6 ft]), fine-grained sandstone with thin, tabular beds that extend laterally for tens of meters. It is medium (5YR 5/6) to light brown (5YR 4/4). Petrographic analysis shows that the unit is moderately to well sorted with subangular to rounded grains and is composed of 64% quartz and 9% feldspar, with 11% porosity and 16% cement. The cement occurs mostly as large patches of calcite, with some minor silica and clay. Core plug analysis shows that the average porosity is 21% and permeability is 242 mD. This unit was assigned to the PDI facies based on outcrop and petrographic characteristics and limited lateral extent. It would only be a small, ineffective local reservoir or aquifer.

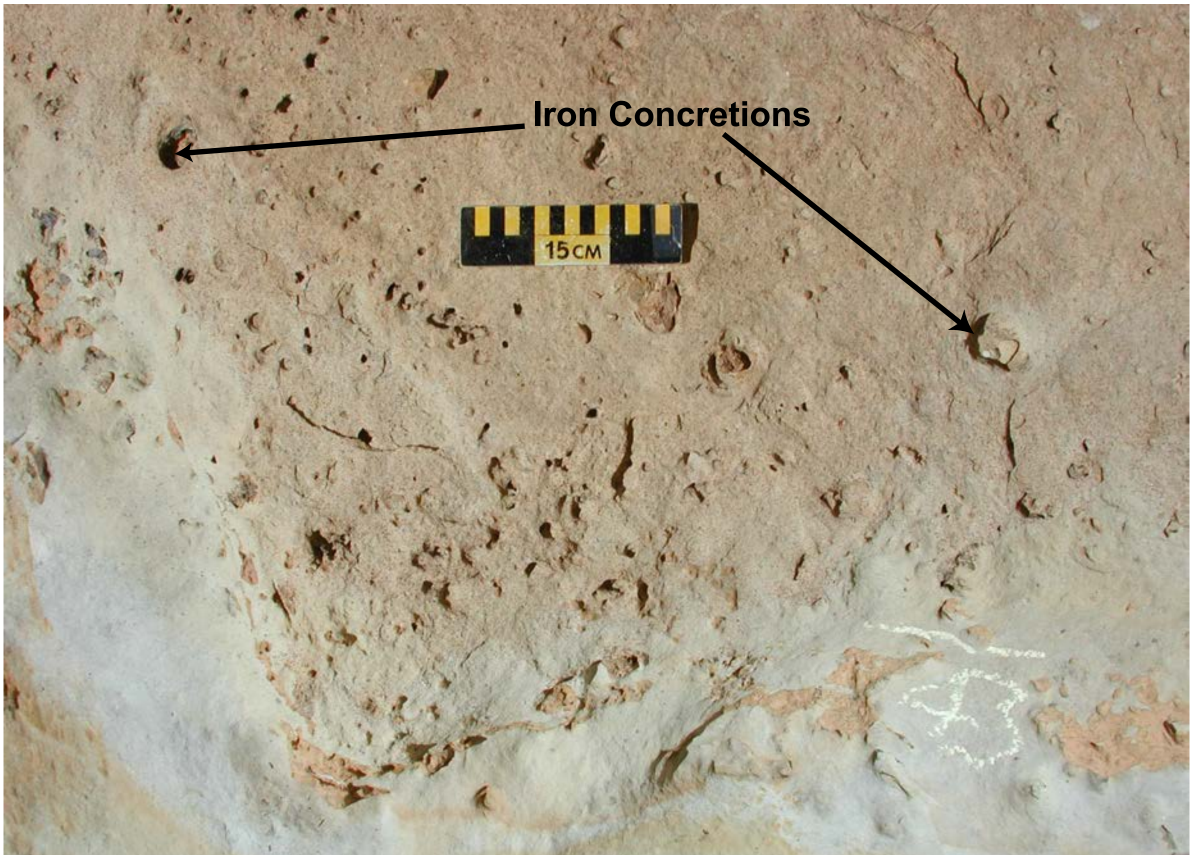

Figure 3.10. *Iron concretions in unit ECT13.*

Eagle Canyon Tributary Unit 15 (ECT15)

Unit ECT15 is a 4.3-meter-thick (14.1 ft), fine-grained sandstone. It has a ledgy to cliff-forming weathering profile, is moderate pink-orange (5YR 8/4) to grayish-orange (10YR 7/4), and exhibits thin to medium bedded lenticular channels (figure 3.11A). Grains are subangular to subrounded and moderate to well sorted (figures 3.11B, 3.11C, and 3.11D). This unit can be traced laterally for several tens of meters to the south and north. In thin section, the sample is 71% quartz, 6% feldspar, and 3% poikilotopic calcite cement with minor silica cement, and 19% porosity (figure 3.11D). Core plug analysis indicated 27% average porosity and 1370 mD average permeability for the unit. This unit was assigned to the RWE dune facies and would serve as a thin, but good reservoir or aquifer.

Eagle Canyon Tributary Unit 16 (ECT16)

Unit ECT16 is a 43.2-meter-thick (141.7 ft), fine-grained sandstone with massive bedding and large trough cross-stratified sedimentary structures. Grains are well sorted and rounded to subangular. The unit has a recessive weathering profile and is yellowish-gray (5Y 8/1). It extends laterally for several tens to hundreds of meters. Petrographic analysis shows that a sample of this unit is 73% quartz, 5% feldspar, and 2% cement. Grain-to-grain silica cement is dominant with rare patches of calcite. Porosity from petrographic analysis is 20%. Core plug analysis was not done on this unit. Based on outcrop and thin-section characteristics, this unit was assigned to the LTC facies and could serve as a good reservoir or aquifer.

Eagle Canyon Tributary Unit 17 (ECT17)

Unit ECT17 is a 4.3-meter-thick (14.1 ft), very fine grained sandstone with massive bedding and possible planar lamination and ripples. The unit has a resistant, ledge-forming profile and is moderate pink-orange (5YR 8/4) (figure 3.12A). It extends for tens of meters to the north but pinches out within 10 meters (30 ft) to the south. In thin section, grains are very fine, subrounded to subangular, and well to moderately sorted, and are composed of 48% quartz and 2% feldspar. Poikilotopic and minor microsparite calcite cement makes up 44% of the sample (figures 3.12B and 3.12C). Core plug analysis yielded an average value of 22% porosity and 10 mD permeability. Based on low permeability and sedimentary structures, this unit was assigned to the EID facies and would serve as a baffle to fluid flow.

Eagle Canyon Tributary Unit 18 (ECT18)

Unit ECT18 is a 90-meter-thick (295 ft), fine-grained sandstone with large trough cross-stratified sedimentary structures (figure 3.13A). It is yellowish-gray (5Y 8/1) and has a reces-

A.

B.

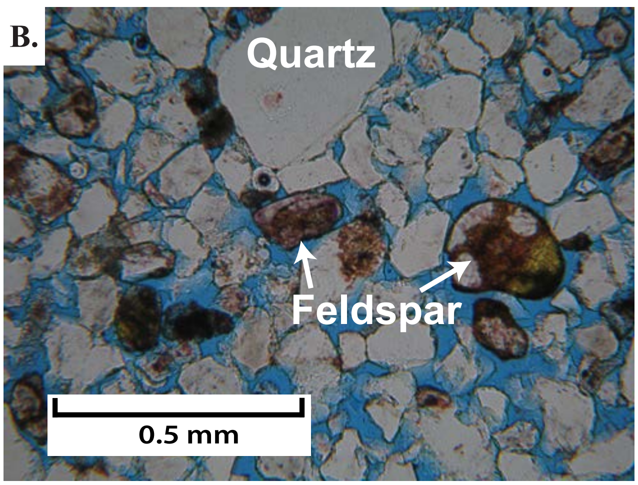

C.

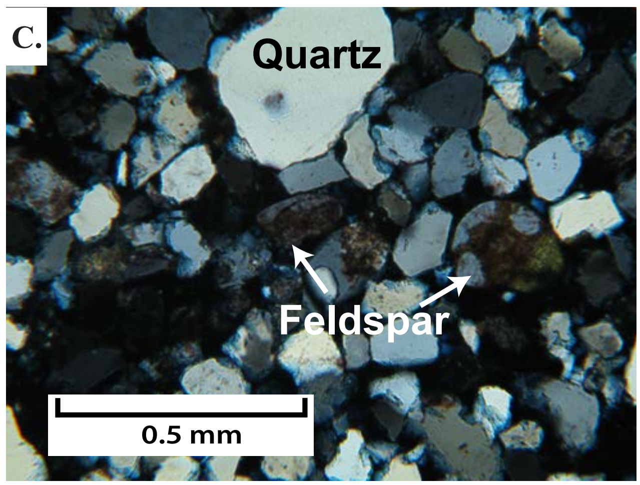

D.

Mineral	Count	Percent	Normalized
Mono qtz	174	57.6	
Undulating qtz	43	14.2	
Poly qtz	0	0	
Total Quartz	217	72.3	0.923405
K spar	11	3.6	
Plag	7	2.3	
Total Feldspar	18	6	0.076595
Porosity	56	18.5	
Calcite cement	9	3	
Matrix	0	0	
Lithics	0	0	
Heavy mins	2	0.7	
Total	300	100	1
Grain size	Very fine lower to fine lower		
Roundness	Subangular to subrounded		
Sorting	Moderate		

Figure 3.11. *Lithologic and petrographic analysis of unit ECT15.* ***A.*** *Outcrop of unit ECT15 displaying lenticular channels.* ***B.*** *Photomicrograph displaying abundant porosity (blue) between subrounded to subangular quartz grains, under plane-polarized light.* ***C.*** *Same image as B under cross-polarized light.* ***D.*** *300-point count analysis indicates that this unit is a quartz-rich feldspathic arenite.*

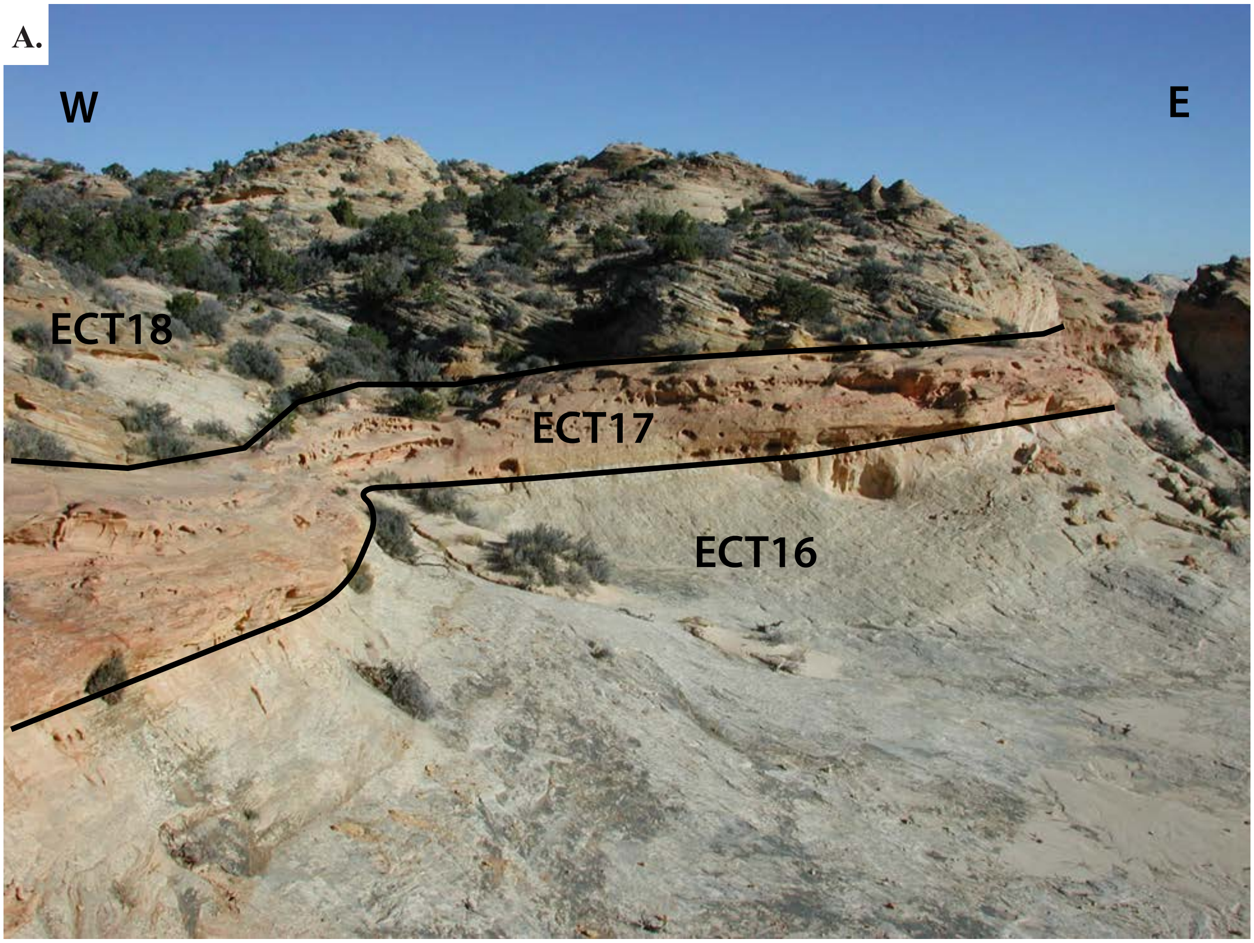

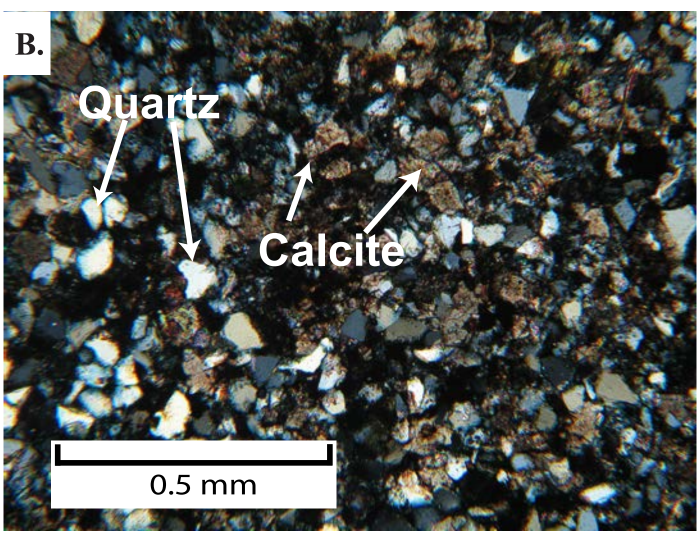

C.

Mineral	Count	Percent	Normalized
Mono qtz	112	37.3	
Undulating qtz	33	11	
Poly qtz	0	0	
Total Quartz	145	48.33	0.953947
K spar	7	2.3	
Plag	0	0	
Total Feldspar	7	2.33	0.043053
Porosity	14	4.7	
Calcite cement	132	44	
Matrix	0	0	
Lithics	0	0	
Fe-oxide/Hem. Cement	2	0.7	
Total	300	100	1
Grain size	Very fine lower to fine lower		
Roundness	Subrounded to rounded		
Sorting	Moderate to well		

Figure 3.12. *Lithologic and petrographic analysis of unit ECT17.* ***A.*** *Outcrops of unit ECT17 have a more resistant weathering profile compared to Unit ECT16.* ***B.*** *Photomicrograph displaying quartz grains in abundant calcite cement, under cross-polarized light.* ***C.*** *300-point count analysis indicates that this is a feldspathic arenite.*

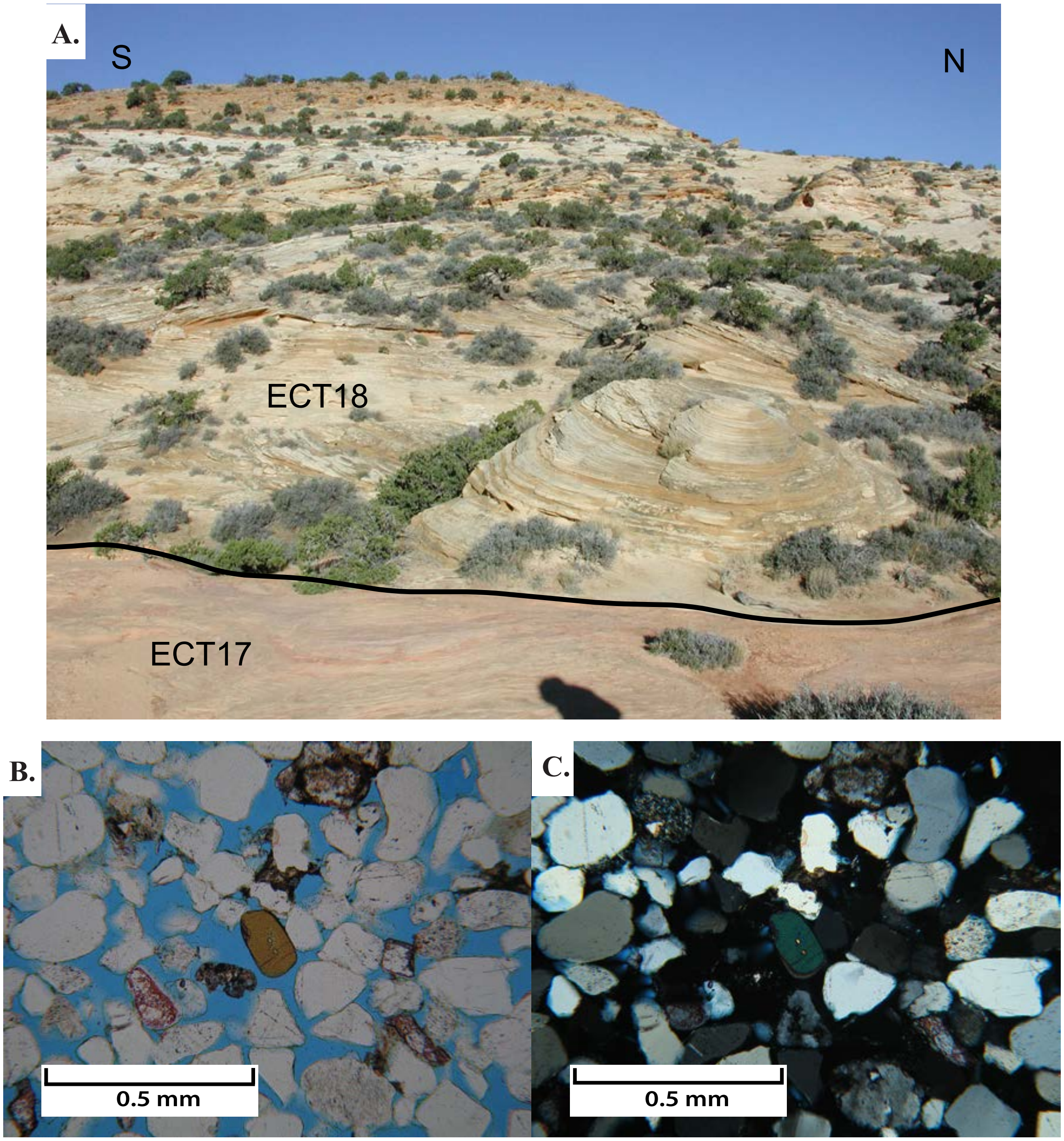

D.

Mineral	Count	Percent	Normalized
Mono qtz	147	49	
Undulating qtz	49	16.33	
Poly qtz	0	0	
Total Quartz	196	65.33	0.951456
K spar	6	2	
Plag	4	1.33	
Total Feldspar	10	3.33	0.048544
Porosity	87	29	
Calcite cement	7	2.33	
Matrix	0	0	
Lithics	0	0	
Fe-oxide/Hem. Cement	0	0	
Total	300	99.9	1
Grain size	Very fine lower to very fine upper		
Roundness	Subrounded to rounded		
Sorting	Moderate to well		

Figure 3.13. *Lithologic and petrographic analysis of unit ECT18.* ***A.*** *Outcrop view, to the west, of unit ECT18 showing large trough cross-stratification.* ***B.*** *Photomicrograph from the lower part of unit ECT18 displaying excellent intergranular porosity, under plane-polarized light.* ***C.*** *Same image as B under cross-polarized light showing amphibole surrounded by mostly quartz grains and very few feldspar grains.* ***D.*** *300-point count analysis indicates that this is a quartz arenite.*

sive weathering profile. This unit can be traced laterally for hundreds of meters to the north and south. Samples from the lower, middle, and upper parts of the unit were taken (three total) for thin-section and core plug analysis. In thin section, the grains are well sorted to bimodal, rounded, and fine sand-sized. Composition is on average 65% quartz and 3% feldspar (figures 3.13B, 3.13C, and 3.13D). Cement abundance varies from 2% to 14% in the lower and upper parts of the unit, respectively. Cements are composed of clay and to a lesser extent calcite. Core plug analysis resulted in an average porosity of 26% and average permeability of 591 mD. Based on sedimentary structures and high porosity and permeability values, this unit was assigned to the LTC facies and would serve as an excellent reservoir or aquifer.

RESULTS AND DISCUSSION

Correlation with the Devils Canyon Section

As mentioned in the introduction, the measured section at Eagle Canyon is a composite of three sections measuring 194 meters (637 ft) total. The lower and middle sections were correlated by laterally tracing unit ECT6 between the two sections. Similarly, the middle and upper sections were correlated by laterally tracing unit ECT15 between the two sections.

The Eagle Canyon measured section was tied to the Devils Canyon/Justensen Flats section by correlating unit ECT8 with unit DCB1/JFCG16 (figure 3.14). These units are composed of the WAM facies and can be traced laterally for more than 1 kilometer (1.6 mi). These correlative units are topographically expressed as the surface of Justensen Flats located between the two measured sections (figure 3.1). Most other units are not as laterally extensive as ECT8 and therefore could not be correlated to the section at Devils Canyon. The notable exception is unit ECT18, which is the LCT facies at the top of the composite section. This unit likely correlates with unit DCB6 as both are LTC facies and are at the top of each measured section; they are separated from the next LTC facies below by the EID facies. The two EID facies, ECT17 and DBC5, however, cannot be correlated because ECT17 pinches out to the south.

Porosity and Permeability of Facies

Twenty-six core plugs were taken from 14 outcrop samples for porosity and permeability analysis in both the horizontal and vertical direction. Of the 14 outcrop samples, results from one sample were excluded due to either not enough core-plug length or mislabeling of the sample. Plotting averaged porosity versus permeability shows three distinct groups (figure 3.15): (1) low porosity/permeability representing interdune facies (excluding SAM), (2) high porosity/permeability representing dune facies, and (3) high porosity/permeability representing interdune facies (SAM).

The gamma-ray scintillometer survey produced a result fairly correlative with porosity changes along the section, particularly between 100 and 105 meters (328–345 ft) at unit ECT17 (figure 3.2). Here a marked increase in radioactive isotopes occurs in the scintillometer analyses (appendix A), which corresponds to the low porosity interdune facies of unit ECT17. The measurement interval was not high enough resolution to capture changes in porosity between thinner interdune facies and thicker dune facies in the lower half of the measured section (figure 3.2). In analyzing the Navajo Sandstone in the subsurface for reservoir or aquifer quality, it may prove difficult to identify thin (less than 0.5 meter [<1.6 ft]) interdune beds based on gamma-ray curves alone. The interdune beds that create baffles and barriers to fluid flow within the Navajo could potentially be overlooked.

Depositional Environments

Seven of the eight facies identified and described in the Devils Canyon/Justensen Flats area were recognized in the Eagle Canyon section (figure 3.14). As in the Devils Canyon/Justensen Flats area, these facies were identified based on sedimentary/diagenetic features observed in outcrop as well as petrology and porosity/permeability analyses. Three dune facies and four interdune facies were found. The EFC interdune described in Devils Canyon/Justensen Flats is absent in the Eagle Canyon section. The number of units representing interdune facies is less in the Eagle Canyon area than in the Devils Canyon/Justensen Flats area: eight versus eleven (figure 3.14).

The interdune facies are stacked into sets in the lower part of the Eagle Canyon section whereas they tend to be separated from one another in the Devils Canyon/Justensen Flats area. However, dunes were small and closely spaced as in the Devils Canyon/Justensen Flats area. The lateral discontinuity of most facies is likely the result of a dynamic erg system with rapidly moving dune/interdune environments and is similar to that found in the Devils Canyon/Justensen Flats area. Assuming a relatively uniform water table in the region, constantly shifting dunes produce different interdune deposits, both laterally and vertically, over short distances and may account for changes observed between the two areas. The laterally extensive nature and nearly consistent thickness of the ECT8 interdune (SAM) facies indicates that the erg system was relatively stable during its formation.

A thicker succession of high-angle, trough cross-stratified beds (LTC) also occurs in the upper two-thirds of the Eagle Canyon section. This succession contains one interdune facies (EID), which has limited extent in comparison to the Devils Canyon/Justensen Flats area where there are two laterally extensive interdune facies (also EID) in the roughly equivalent part of the Navajo Sandstone.

Subtle changes in wind and sand availability could account for some of the differences observed between the Eagle Can-

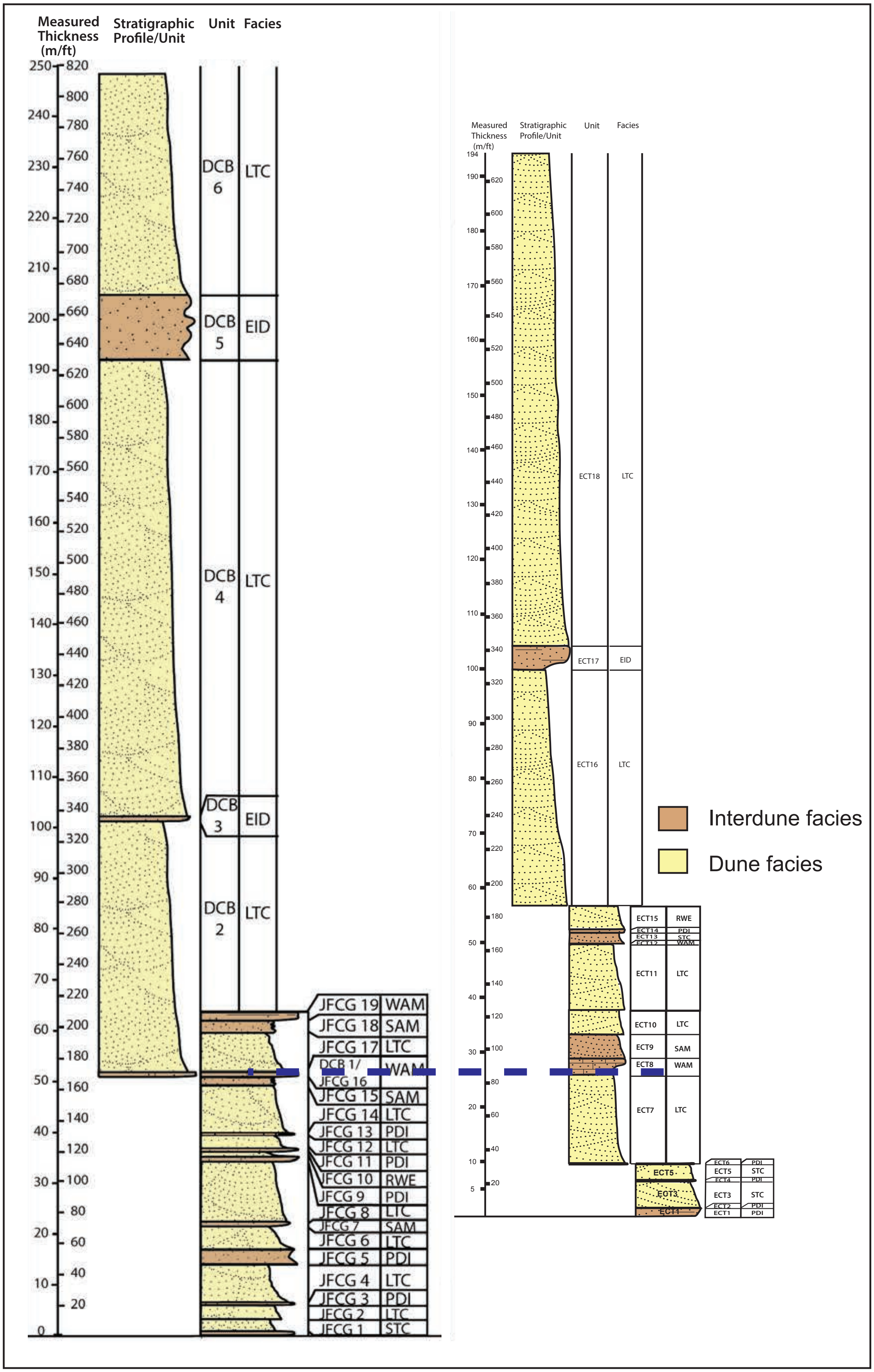

Figure 3.14. *Measured section at Devils Canyon/Justensen Flats (left) tied to the section at Eagle Canyon (right) by correlating units DCB1/ JFCG16 and ECT8. See table 2.1 and figure 2.2 for explanation of facies, lithology, etc.*

yon and Devils Canyon/Justensen Flats areas. A possible cause may be variation in the size of individual dunes from area to area. For example, a large dune in one area may deflect the wind and volume of available sand to another even if the distance between the two is minimal. In addition, perhaps in the Eagle Canyon area, the rise in the groundwater table may have been even more short lived and the dune migration faster than in the Devils Canyon/Justensen Flats area.

Finally, dune types themselves likely varied within the relatively small Eagle Canyon and Devils Canyon/Justensen Flats areas as can be observed in modern analogs. Little Sahara is a large sand dune field in the central part of western Utah (figure 3.16). Here, several types of active dunes are recognized: low parabolic dunes with trailing arms, crescent-shaped barchan dunes, and transverse dunes (Hamblin, 2004). The sizes of the dunes and especially the interdune areas vary widely. Some older dunes have been stabilized by vegetation.

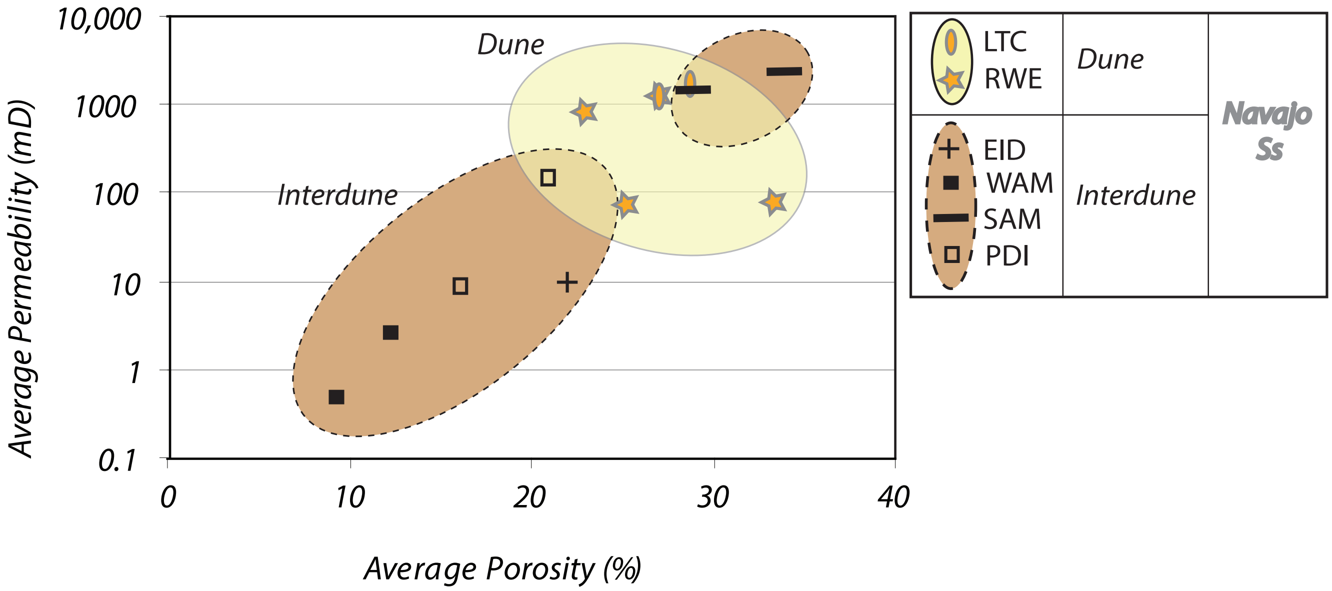

Figure 3.15. *Average porosity versus average permeability plot of 13 core-plug samples collected from the Navajo Sandstone along the Eagle Canyon measured section. Facies are as follows: LTC = Large Trough Cross-stratified; RWE = Reworked Eolian; EID = Evolving Interdune; WAM = Wavy Algal Mat; SAM = Sandy Algal Mat; PDI = Poorly Developed Interdune.*

Figure 3.16. *Little Sahara sand dune field, western Utah (from Hamblin, 2004).*

CHAPTER 4:
COVENANT OIL FIELD CORES

by

Thomas C. Chidsey, Jr., and Thomas H. Morris

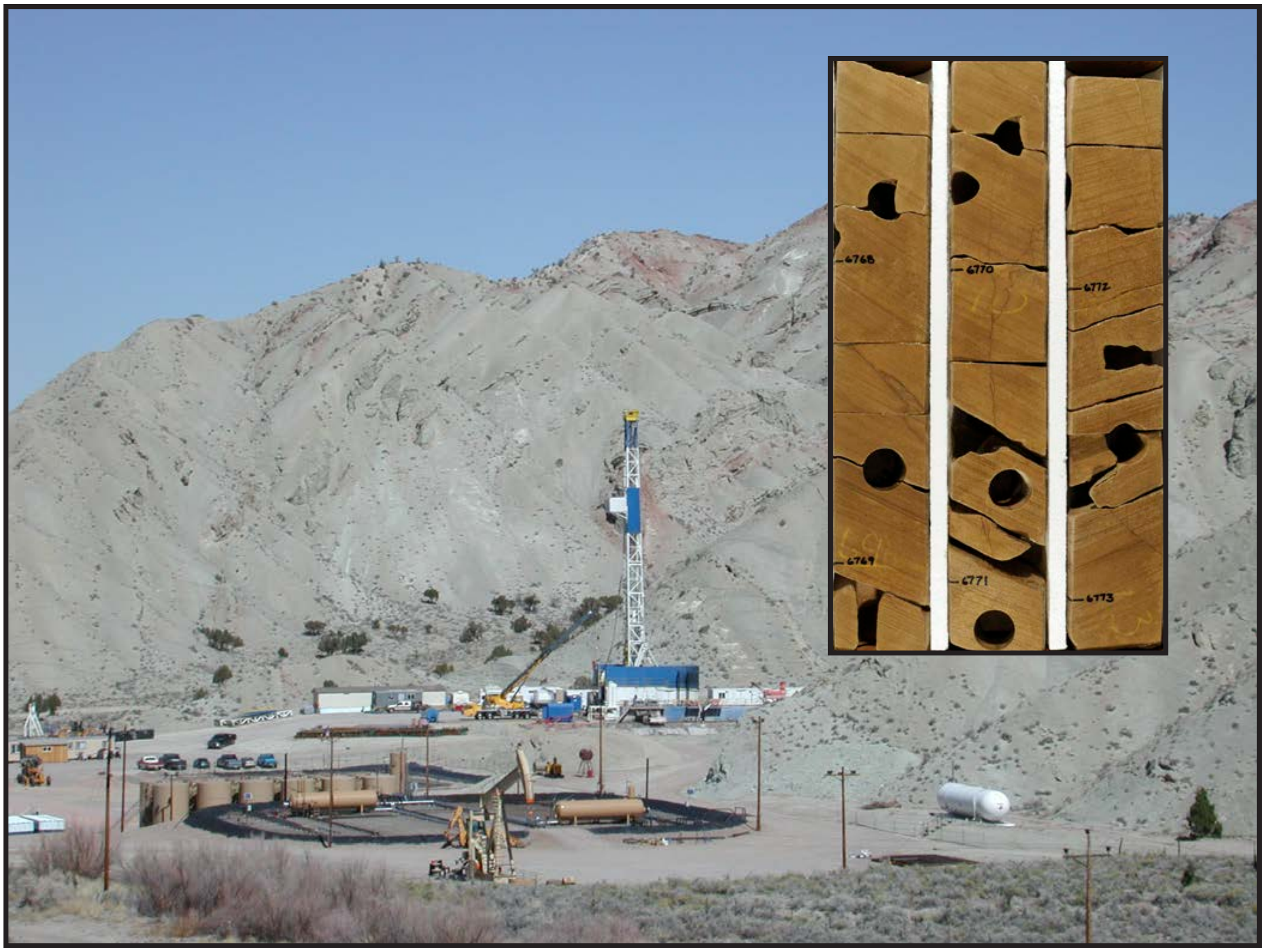

Covenant oil field, Sevier County, in the central Utah thrust belt; inset shows a typical section of cores from the eolian Lower Jurassic Navajo Sandstone reservoir.

CHAPTER 4:
COVENANT OIL FIELD CORES

INTRODUCTION

The 2004 discovery of Covenant oil field in the central Utah thrust belt, or "Hingeline," proved that this region contains the right components (trap, reservoir, seal, source, and migration history) for large accumulations of oil (figures 1.1 and 4.1). More than 100 wells had been drilled in the region with no success until the Wolverine Gas & Oil Corporation's Kings Meadow Ranches No. 17-1 well (SE1/NW1/4 section 17, T. 23 S. R. 1 W., Salt Lake Base Line & Meridian [SLBL&M], Sevier County). The well initially tested over 700 barrels of oil per day (BOPD) from the Lower Jurassic Navajo Sandstone and what was later determined to be Middle Jurassic Temple Cap Formation (Sprinkel and others, 2009, 2011a, 2011b; Chidsey and others, 2014; Chidsey and Sprinkel, 2016). Covenant has produced more than 28 million BO as of August 1, 2020 (Utah Division of Oil, Gas and Mining, 2020).

Early efforts in the central Utah thrust belt tested anticlines identified from surface mapping and seismic reflection data but failed to find commercial hydrocarbon deposits although companies confirmed the area was similar in structural style, reservoir types, and timing to the productive thrust belt to the north. The lack of Cretaceous hydrocarbon source beds below the thrust structures seemingly was to blame for the early exploration failures. Everything changed with the Covenant discovery which set off a frenzy of leasing, seismic acquisition, and exploratory drilling. However, the search for another Covenant field in the central Utah thrust belt has been elusive; one small field, Providence (figure 4.1), about 24 kilometers (~15 mi) northeast in Sanpete County, was discovered in 2008 (Chidsey and others, 2011).

The Jurassic Navajo Sandstone/Temple Cap Formation Hingeline play, as defined by Chidsey and others (2007) and Chidsey and Sprinkel (2016), extends 320 kilometers (200 mi) south-southwest starting 30 kilometers (20 mi) northeast of Provo, Utah, and extending to southwestern Sevier County; it narrows from 40 kilometers (25 mi) wide in the north to zero in the south (figure 4.1). The play lies due south of the Utah-Wyoming-Idaho salient of the thrust belt and straddles the boundary between the eastern Basin and Range (eastern Millard, Juab, and Utah Counties) and High Plateaus (central Sevier and Sanpete Counties) physiographic provinces. The Jurassic Navajo Sandstone/Temple Cap Formation Hingeline play area represents the maximum extent of petroleum potential in the geographical area as defined by the two producing reservoirs, limited well data, potential hydrocarbon sources and migration history, and regional structural interpretations.

Cores from the Navajo reservoir of Covenant field display many of the same eolian facies described in the outcrops of the San Rafael Swell to the east (see Chapters 2 and 3, figure 4.1), as well as fracturing and minor faults which in combination create reservoir heterogeneity. Cores from Covenant field are stored at the UGS's Utah Core Research Center (UCRC) in Salt Lake City. They represent the only publicly available Navajo Sandstone cores in the central Utah thrust belt region (the UCRC also has Nugget Sandstone cores from fields in the northern Utah and southwestern Wyoming salient of the thrust belt). These cores provide a wealth of petrophysical and petrographic information, which serves to compliment data obtained from outcrops to create models for subsurface hydrocarbon and CO_2 reservoirs, water disposal aquifers, and potential CCS from coal-fired power plants in the region.

FIELD OVERVIEW

Stratigraphy and Thickness

The Navajo Sandstone is 190 to 590 meters (610–1620 ft) thick (Hintze and Kowallis, 2009) in the central Utah thrust belt area. The depth to the Navajo in Covenant field is 1860 meters (6090 ft). The Navajo Sandstone is separated from the overlying Temple Cap Formation by the J-1 unconformity (Pipiringos and O'Sullivan, 1978), discussed in more detail later. The Navajo has a subtle but distinct characteristic geophysical log response (figure 4.2); the overlying Sinawava Member of the Temple Cap has a high gamma-ray profile recognized on other logs regionally. The Navajo Sandstone is underlain by the Lower Jurassic Kayenta Formation.

Structure and Trapping Mechanisms

Covenant field is located along the eastern flank of the Sanpete-Sevier Valley regional anticline on the Gunnison-Salina thrust plate (figure 4.1). The Covenant field trap is an elongate, symmetric, northeast-trending fault-propagation/fault-bend anticline (figures 4.3 and 4.4) that has nearly 270 meters (800 ft) of structural closure and a 150-meter (450 ft) oil column (Strickland and others, 2005; Chidsey and others, 2007). The Navajo/Temple Cap oil-filled reservoir covers about 3.9 square kilometers (~1.5 mi^2 [960 ac]). The structure formed above a series of splay thrusts in a passive roof duplex along the Gunnison-Salina thrust and west of a frontal triangle zone within the Arapien Formation (figure 4.4). The Navajo, Temple Cap, and Arapien Formations are repeated due to an east-dipping, blind back-thrust detachment within the structure (figure 4.4).

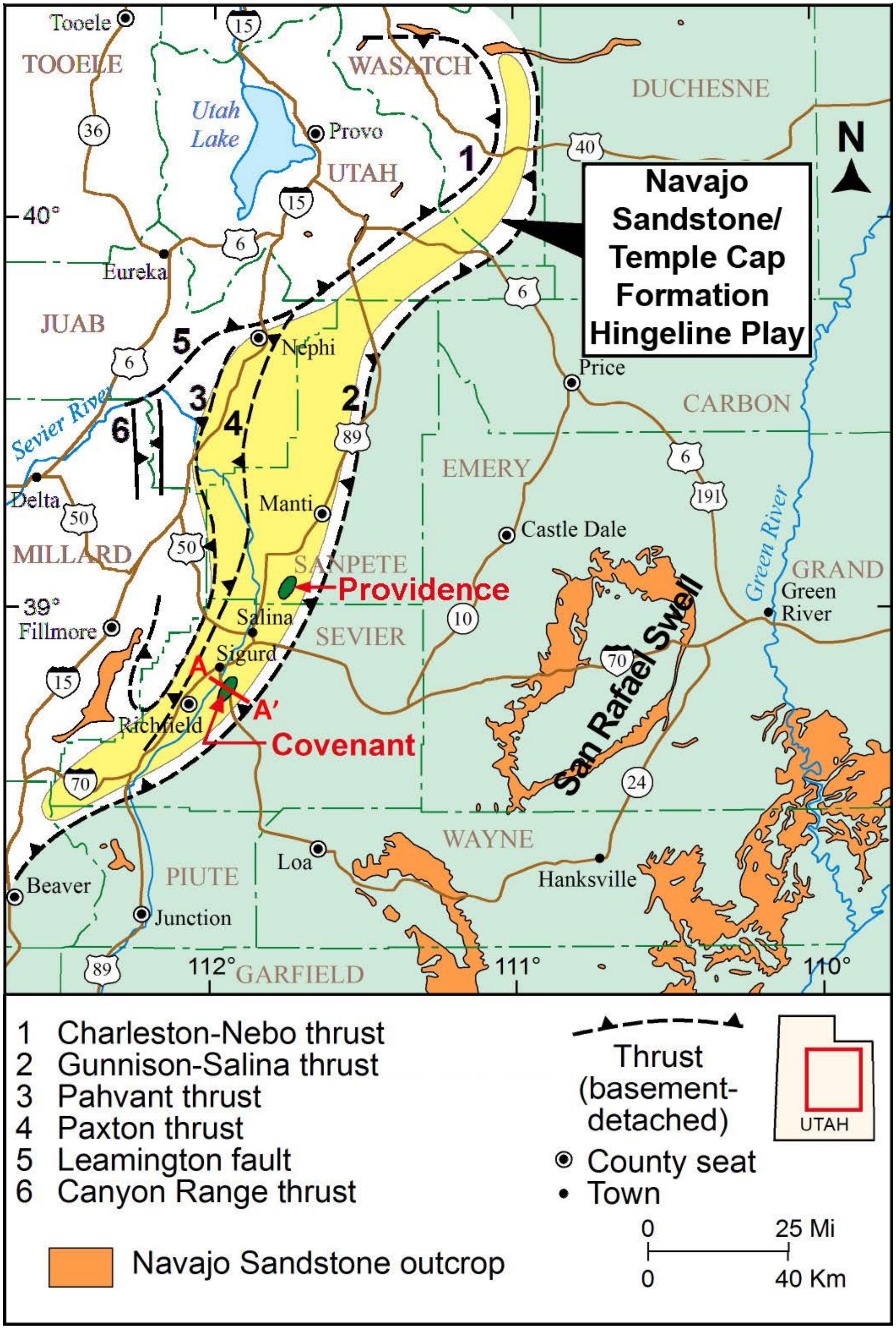

Figure 4.1. Location of Covenant and Providence oil fields, uplifts, and selected thrust systems in the central Utah thrust belt province (often referred to as the "Hingeline"), and Navajo Sandstone outcrops in the region. Numbers and sawteeth are on the hanging wall of the corresponding thrust system. The yellow-colored area shows present and potential extent of the Jurassic Navajo Sandstone/Temple Cap Formation play area. Modified from Hintze (1980) and Sprinkel and Chidsey (1993). Cross section A–A' shown on figure 4.4.

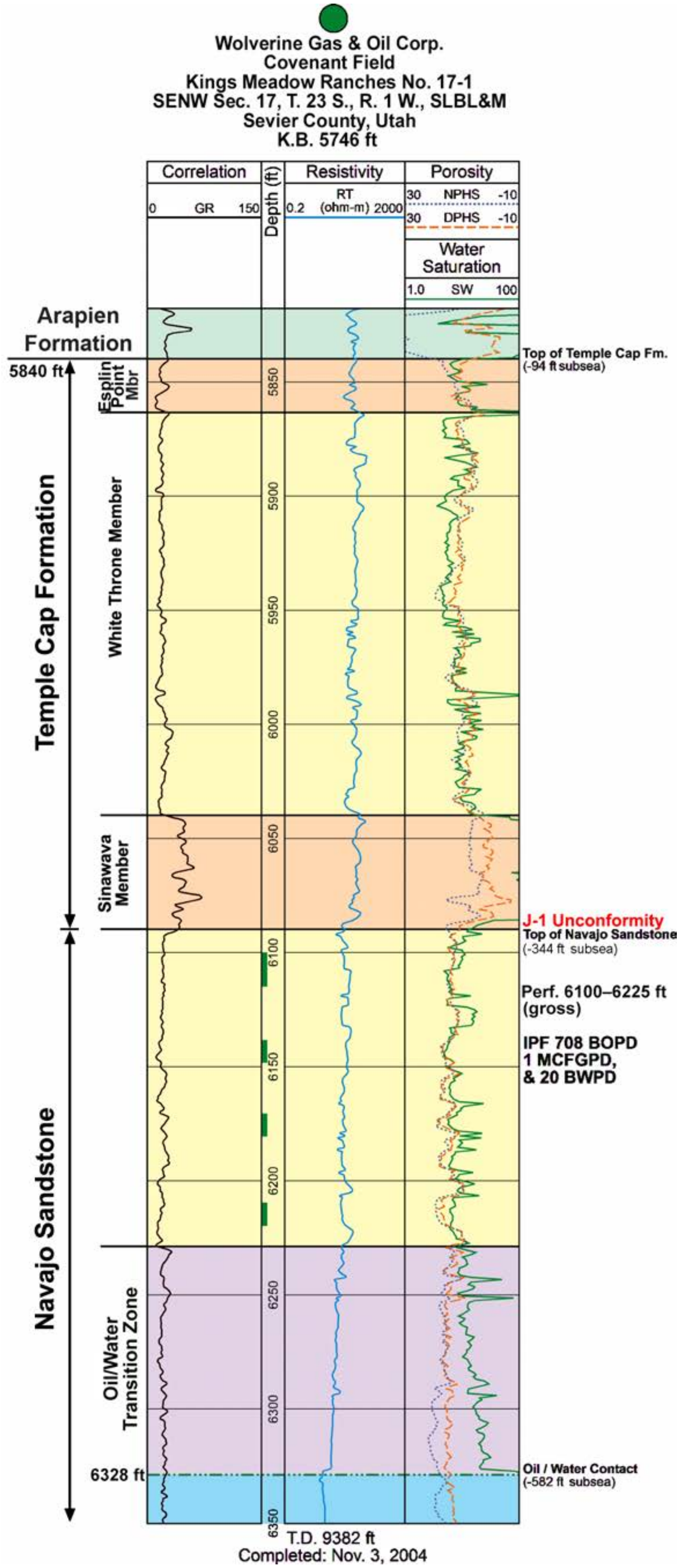

Figure 4.2. *Typical combined gamma-ray, resistivity, and neutron-density log of the Navajo Sandstone and Temple Cap Formation from the Kings Meadow Ranches No. 17-1 discovery well of Covenant field, Sevier County, Utah. The thin, vertical green bars between depths of 1860 and 1897 meters (6100 and 6225 ft) indicate producing (perforated) intervals.*

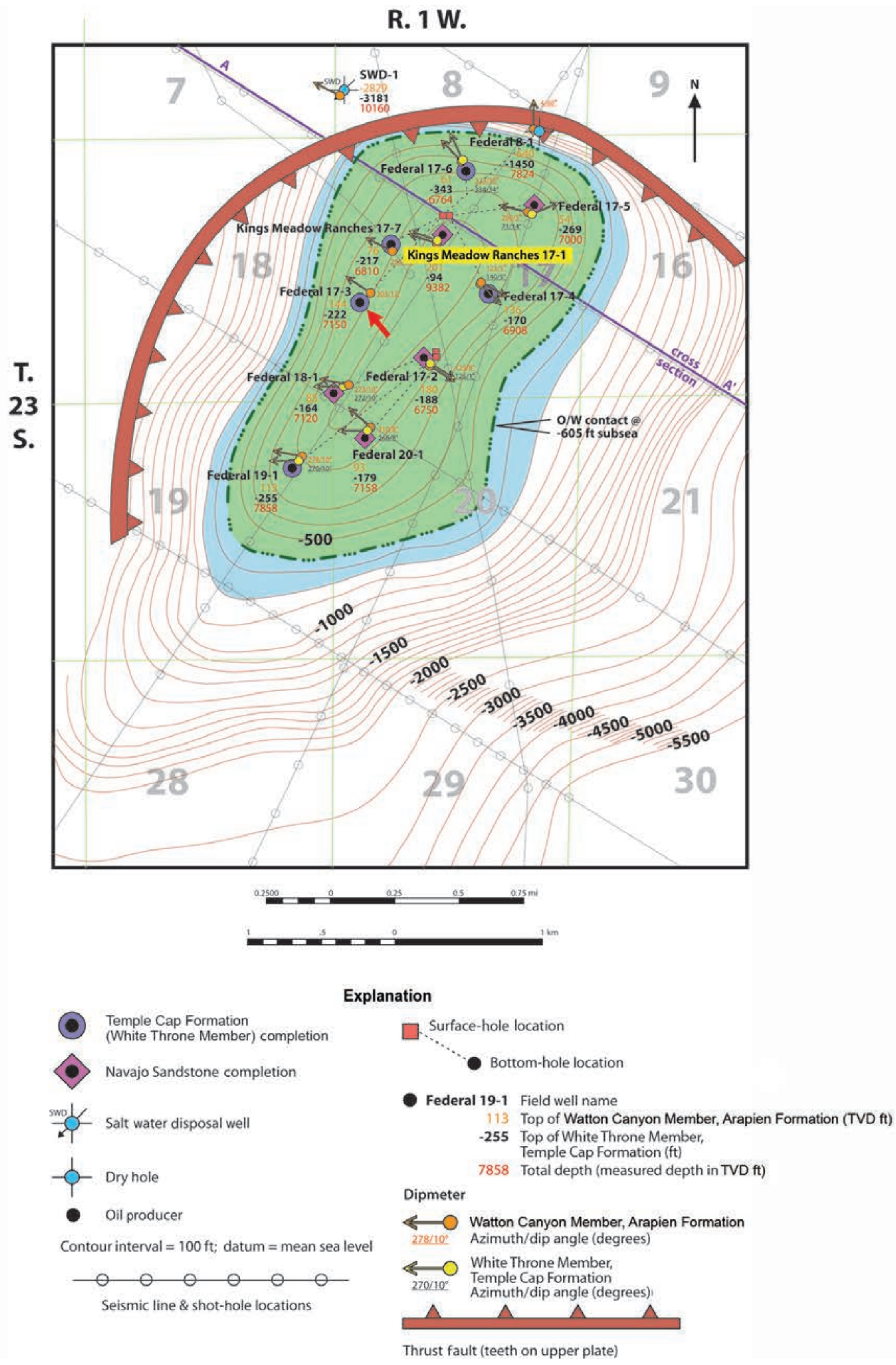

Figure 4.3. *Structure contour map of the top of the White Throne Member of the Temple Cap Formation, Covenant field, based on subsurface well control and seismic data. Original map courtesy of Wolverine Gas & Oil Corporation; after Chidsey and others (2007). Tops corrected to true vertical depths (TVD). Note the locations of the Kings Meadow Ranches No. 17-1 discovery well and the Federal No. 17-3 well (red arrow) that supplied the Navajo core described later in the text and on figure 4.6 and plate 1. Contour interval = 100 feet (30 m), datum = mean sea level. Cross section A–A', which extends beyond the edges of this figure, is shown on figure 4.4.*

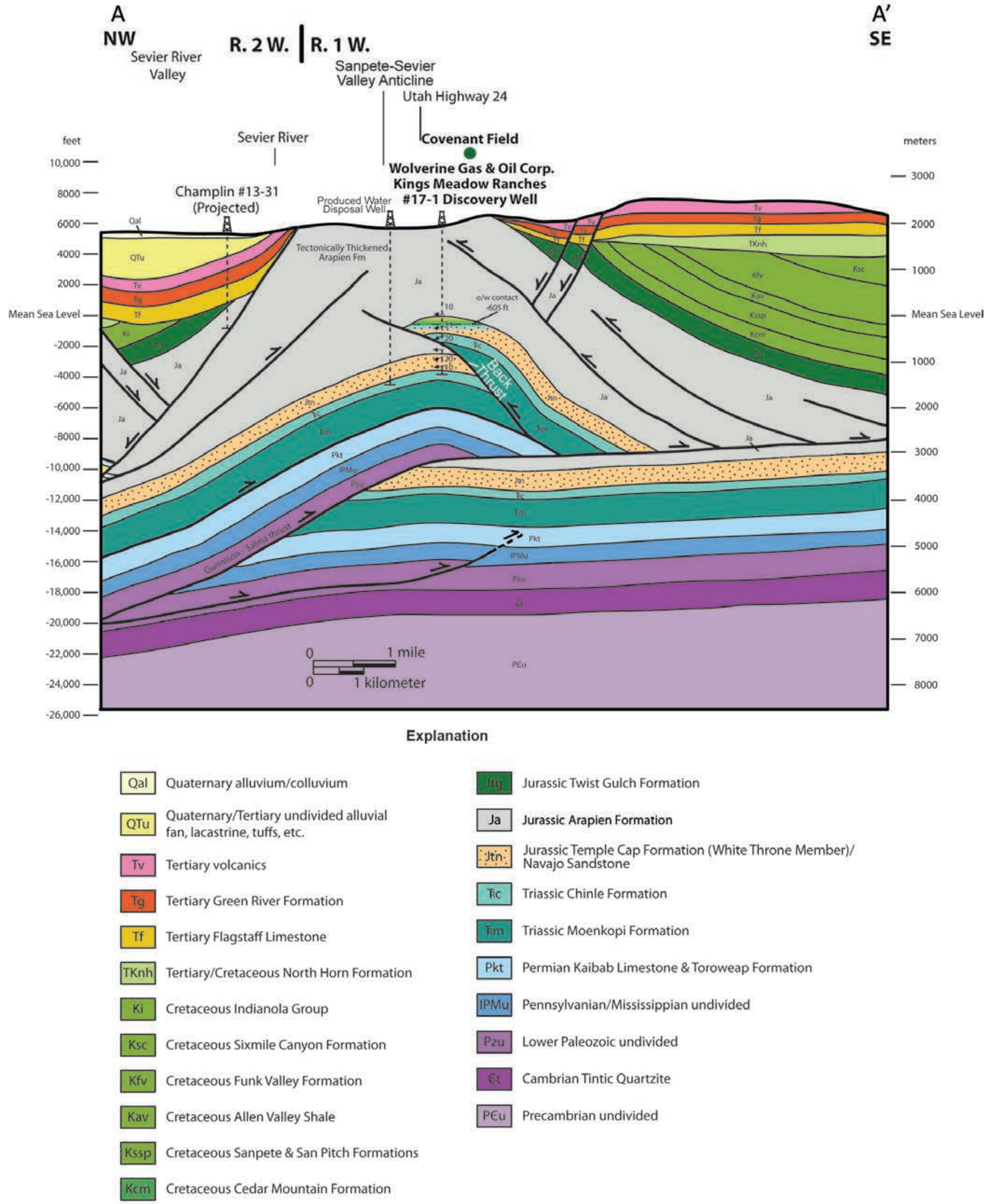

Figure 4.4. *Northwest-southeast structural cross section through Covenant field. Original cross section courtesy of Wolverine Gas & Oil Corporation; modified from Schelling and others (2007) and Chidsey and others (2007). Note small back thrust through the anticline that results in a repeated Navajo Sandstone/Temple Cap Formation section; only the upper section is productive. The produced water is injected into the Navajo Sandstone through a disposal well off structure to the west of the field. Line of cross section A–A' shown on figures 4.1 and 4.3.*

This back thrust forms a hanging-wall cutoff along the western flank and north-plunging nose of the fold. A similar back thrust is mapped on the surface along much of the Sanpete-Sevier Valley anticline to the north.

The principal regional seal for the Navajo and White Throne producing zones in the Covenant trap consists of salt, gypsum, mudstone, and shale in the overlying Middle Jurassic Arapien Formation (figures 4.2 and 4.4). Mudstone and low-permeability siltstone intervals within the Sinawava Member of the Temple Cap Formation are the principal seals for the Navajo Sandstone at Covenant (figure 4.2). Hanging-wall/footwall cutoffs along splay and back-thrust faults may also act as seals within the field (figures 4.3 and 4.4). Interdunal and other low-permeability facies in the Navajo, and possible unrecognized splay and back-thrust faults, may act as local seals, barriers, or baffles to fluid flow.

Hydrocarbon Source

The Covenant oil was derived from marine source beds based on analysis of stable carbon-13 isotopes of saturated versus aromatic hydrocarbons by Wavrek and others (2005, 2007). The geochemistry of the Covenant oil is similar to well-documented Mississippian and Permian oils in the intermountain region (Chidsey and others 2007). Several source rock candidates are present in the region: the Mississippian Delle Phosphatic Member of the Deseret Limestone and equivalent formations (Sandberg and Gutschick, 1984), the Mississippian Chainman Shale (Poole and Claypool, 1984; Sandberg and Gutschick, 1984; Wavrek and others, 2005, 2007), and the Mississippian-Pennsylvanian Manning Canyon Shale (Swetland and others, 1978; Poole and Claypool, 1984; Chidsey and others, 2007; Chidsey and Sprinkel, 2016). Total organic carbon for some units within these rocks is as high as 15%.

The Covenant oil likely migrated primarily along fault planes or through porous Paleozoic and Mesozoic carrier beds from a local Carboniferous source within the central Utah thrust belt (see Wavrek and others, 2005, 2007; Chidsey and others, 2007; Chidsey and Sprinkel, 2016). Source beds were buried deep enough to generate hydrocarbons on the western parts of the hanging walls of the Gunnison-Salina thrust (figures 4.1 and 4.4) or the Aurora-Valley Mountain thrust of Schelling and others (2007). In addition, where the Mississippian section lies just below the basal décollement in the footwall of these thrust plates, loading could have also generated hydrocarbons.

The initial oil trap for Covenant field formed over 100 Ma during the Late Cretaceous Sevier orogeny. Primary migration occurred 90 to 100 Ma into this paleotrap. However, later back thrusting around 70 to 80 Ma reconfigured the trap and, in the process, remigration stripped the original gas-saturated oil of volatiles (Wavrek and others, 2010; Chidsey and others, 2019), thus accounting for the lack of gas in the field.

Reservoir Properties

The Navajo Sandstone at Covenant field has heterogeneous reservoir properties because of (1) the variations in porosity and permeability between dune and interdune facies, (2) diagenetic effects, and (3) extensive fracturing. Most of these same characteristics can be observed in outcrops in the San Rafael Swell (chapters 2 and 3) and elsewhere in southern Utah. They can cause possible barriers or baffles to fluid flow, both vertically and horizontally, within the Navajo reservoir at Covenant and can affect production rates, petroleum movement pathways, and future pressure maintenance programs.

The average porosity for the Navajo Sandstone at Covenant field is 12%; the average grain density is 2.651 g/cm^3 based on core plug analysis (Strickland and others, 2005; Chidsey and others, 2007). Sandstone exhibits significant secondary porosity in the field from natural fracturing. Permeabilities in the Navajo from the core data are upwards of 100 mD but range from less than 0.1 to over several intervals over 150 mD. Diagenetic effects and fracturing have both reduced and enhanced the reservoir permeability of the Navajo.

Navajo Sandstone/White Throne Member gross pay thickness at Covenant field is 148 meters (487 ft) and net pay thickness is 129 meters (424 ft), a net-to-gross ratio of 0.87 (Strickland and others, 2005). The initial reservoir pressures averaged about 18,134 kilopascals (2630 psi). The reservoir drive mechanism is a strong active water drive. Geophysical well logs show a transition zone in terms of water saturation above a very sharp oil/water contact within the Navajo (figures 4.2 and 4.5A).

Production and Reserves

Covenant field produces oil and water (now about 83% water) and essentially no gas. Cumulative production as of August 1, 2020, was 28,017,489 BO and 47,792,219 BW (Utah Division of Oil, Gas and Mining, 2020). The oil is a dark brown, low-volatile crude. The API gravity of the oil is 40.5°; the specific gravity is 0.8280 at 16°C (60°F). The viscosity of the crude oil is 4.0 centistokes at 25°C (77°F) and the pour point is -16.5°C (2.2°F). The average weight percent sulfur of produced oil is 0.48; nitrogen content is 474 parts per million (Chidsey and Sprinkel, 2016; Chidsey, 2018).

Currently (2020), daily oil production averages more than 2850 BO and about 13,760 BW. The field currently has 34 producing wells (about equally divided between the Navajo and White Throne reservoirs) and two dry holes, drilled from three pads. Original oil in place (OOIP) reserves are estimated at 100 million barrels (Chidsey and others, 2007). A 40% to 50% recovery of the OOIP may be achieved with efficient operations and completion techniques (Strickland and others, 2005). Produced water is injected back into the Navajo Sandstone off structure through a disposal well west of the field (figure 4.4).

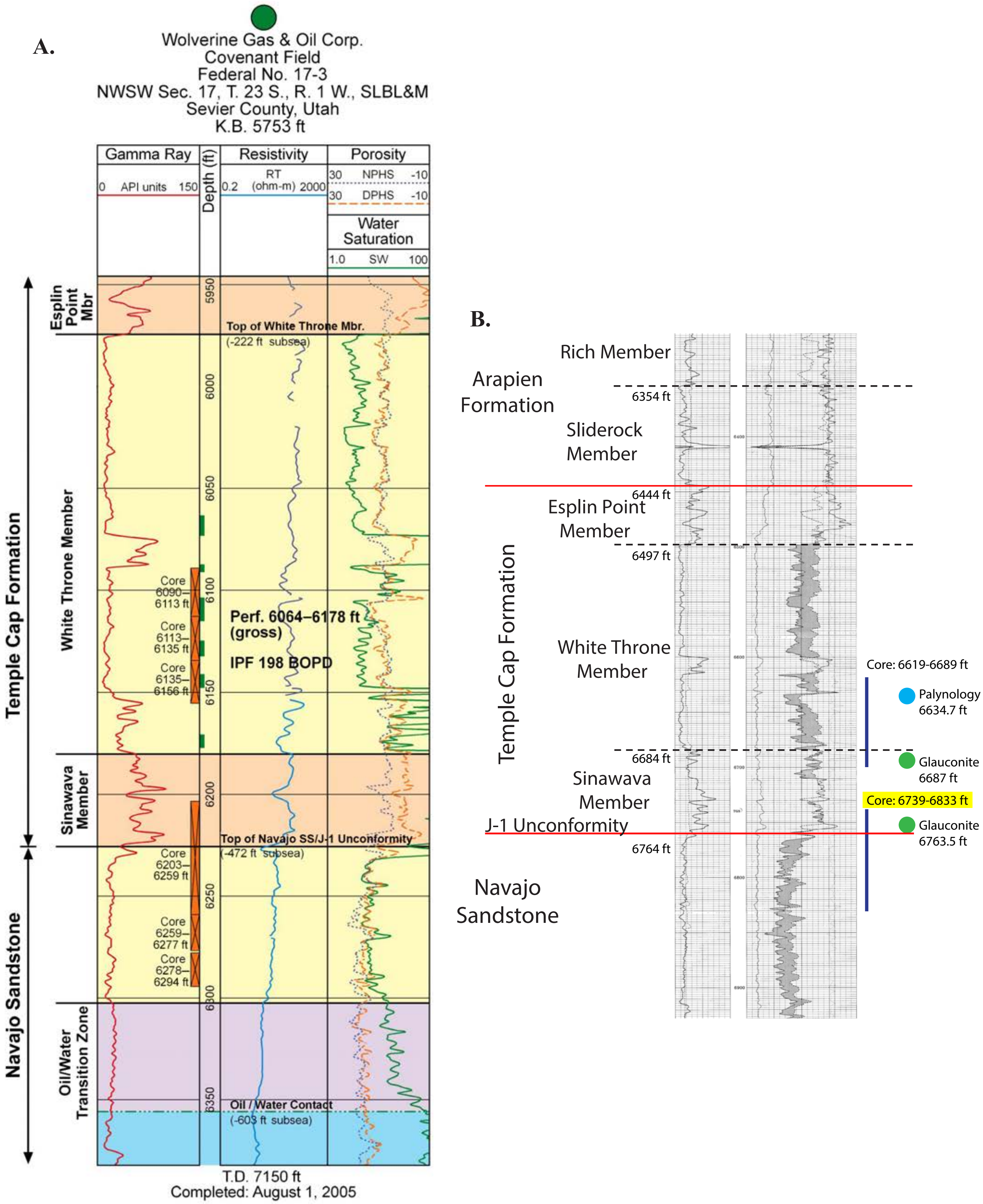

Figure 4.5. *True vertical depth **A** and measured depth **B**. of the combined gamma ray, resistivity, and neutron-density log showing the cored sections (vertical brown bars on A and thin, dark blue bars on B) of the Navajo Sandstone and Temple Cap Formation from the Federal No. 17-3 well, Covenant field. The thin, vertical green bars on A indicate producing (perforated) intervals. See figure 4.3 for well location. The cored interval from 2054 to 2083 meters (6739–6833 ft) is described on figure 4.6 and plate 1.*

CORE DESCRIPTION

The core through the Navajo Sandstone from the Wolverine Gas & Oil Corporation Federal No. 17-3 well (figures 4.3 and 4.5) (SE1/4NW1/4 section 17, T. 23 S., R. 1 W., SLBL&M) was selected for detailed description (figure 4.6, plate 1); appendix B consists of photographs of the core. Although the well is completed in the overlying White Throne Member of the Temple Cap Formation (figure 4.5A), its Navajo core has excellent examples of eolian facies, fracturing, and subtle reservoir heterogeneity, and a wealth of porosity and permeability data from core plug analysis (appendix C). In addition, the core includes both the upper Navajo, the producing interval in all Navajo wells in the field such as the Kings Meadow Ranches No. 17-1 discovery well (figure 4.2), and the lower part of the Sinawava Member of the Temple Cap (figure 4.5).

The core description of the Navajo Sandstone from the Federal No. 17-3 well consists of the lithology and the stratigraphic profile as it would likely be expressed in outcrop, and the facies of the units (figure 4.6 and plate 1). The vertical sequence is tied to its corresponding gamma-ray log profile and includes plotted porosity and permeability analysis from the core plugs (figure 4.6). Several intervals were selected for close-up photographs, thin sections, and scanning electron microscopy for petrographic evaluation—grain mineralogy, size, sorting, and roundness; pore types; cementing; clay presence; and fracturing.

The Federal No. 17-3 core is used for industry and student training core workshops as well as in several previous studies of the Covenant reservoir and regional stratigraphy including those of Chidsey and others (2007), Parry and others (2009), Sprinkel and others (2009, 2011a), Hartwick (2010), Phillips (2012), Phillips and Morris (2013), Phillips and others (2015), and Chidsey and Sprinkel (2016). The Federal No. 17-3 core description provided in our study can be used as a template for other wells in Covenant field and wells in the region that have penetrated the Navajo Sandstone but do not have cores. The lithology, dip-corrected thickness, eolian facies, and other significant characteristics in the Federal No. 17-3 core matched to the outcrops provide a critical datapoint for understanding the Navajo as a hydrocarbon reservoir and aquifer in central Utah.

Lithology and Petrography

The productive part of the Navajo Sandstone in the Federal No. 17-3 core is about 80 meters (240 ft) thick, much of which displays classic eolian cross-stratification in sandstones (figure 4.7). In general, the Navajo consists of moderate to very well sorted, very fine to medium-grained (1/16 mm to 1/2 mm), subangular to rounded (figure 4.8), light-yellow-gray sand or silt grains cemented by silica or carbonate (calcite and dolomite) cement. However, some intervals show a bimodal grain-size distribution representing silty laminae between sand beds (figures 4.8C and 4.8D).

The typical sandstone is 97% white or clear quartz grains (usually frosted) having excellent intergranular porosity. Minor amounts of K-feldspar and a few lithic fragments are present (figure 4.8). Feldspar is more common in the Navajo Sandstone than the White Throne Member of the Temple Cap Formation, which was deposited in a marginal marine to marine and intertonguing eolian (coastal dune) environment as opposed to an erg like the Navajo (Hartwick, 2010).

Diagenetic effects in the Navajo reservoir are relatively minor. Some dissolution has occurred along grain-to-grain contacts of quartz grains (figures 4.8B and 4.8D). Feldspar grains often appear corroded and/or fractured (figures 4.8B, 4.8C, and 4.8D). There are only minor overgrowths of quartz and very little clay; in comparison, the White Throne Member has more quartz overgrowth and kaolinite cement (Parry and others, 2009). Authigenic clay mineralization has occurred in the form of grain-coating, pore-bridging, and fibrous illite (figure 4.8; also see figure 13 in Chidsey and others, 2007). Some late dolomite (high-temperature and high-pressure ferroan[?]) cementation has filled pore spaces.

Facies

The Federal No. 17-3 core shows both dune and interdune facies in the Navajo Sandstone (figure 4.6, plate 1, and table 2.1). All dune facies described in outcrop are present: Large Trough Cross-stratification (LTC), Small Trough Cross-stratification (STC), and Reworked Eolian (RWE). Only two interdune facies are recognized in the core: Wavy Algal Mat (WAM) and Sandy Algal Mat (SAM).

Dune

The LTC and STC dune facies consist of (1) foreset beds composed of grainfall laminae, (2) subgraded avalanche laminae, and (3) thin, tightly packed, reworked ripple strata at the dune toe (figure 4.9). Sand grains are fine to medium in large, well-defined trough cross-stratified beds. Foreset laminations are slightly steeper than avalanche. In addition, foreset and avalanche laminations can display a bimodal distribution of very fine and fine to upper medium sizes of grains (figures 4.8C and 4.8D). Laminations in dune toe deposits are low angle to planar; bedding is thinner than in the foreset and avalanche deposits (figure 4.9). In general, the best reservoir quality is within avalanche and dune toe deposits. All intervals display oil staining.

The dune facies in the Federal No. 17-3 core are dominated by the LTC facies (figures 4.6, 4.7, and 4.9A, and plate 1). Nine units totaling 18 meters (60 ft) of the core consist of the LTC facies. Grain sizes observed in the core range from upper fine to upper medium and are well sorted. Porosity and permeability average 14% and 83 mD, respectively, based on core plug analysis (appendix C). The boundaries between LTC units are defined by dune toe deposits or distinct changes in

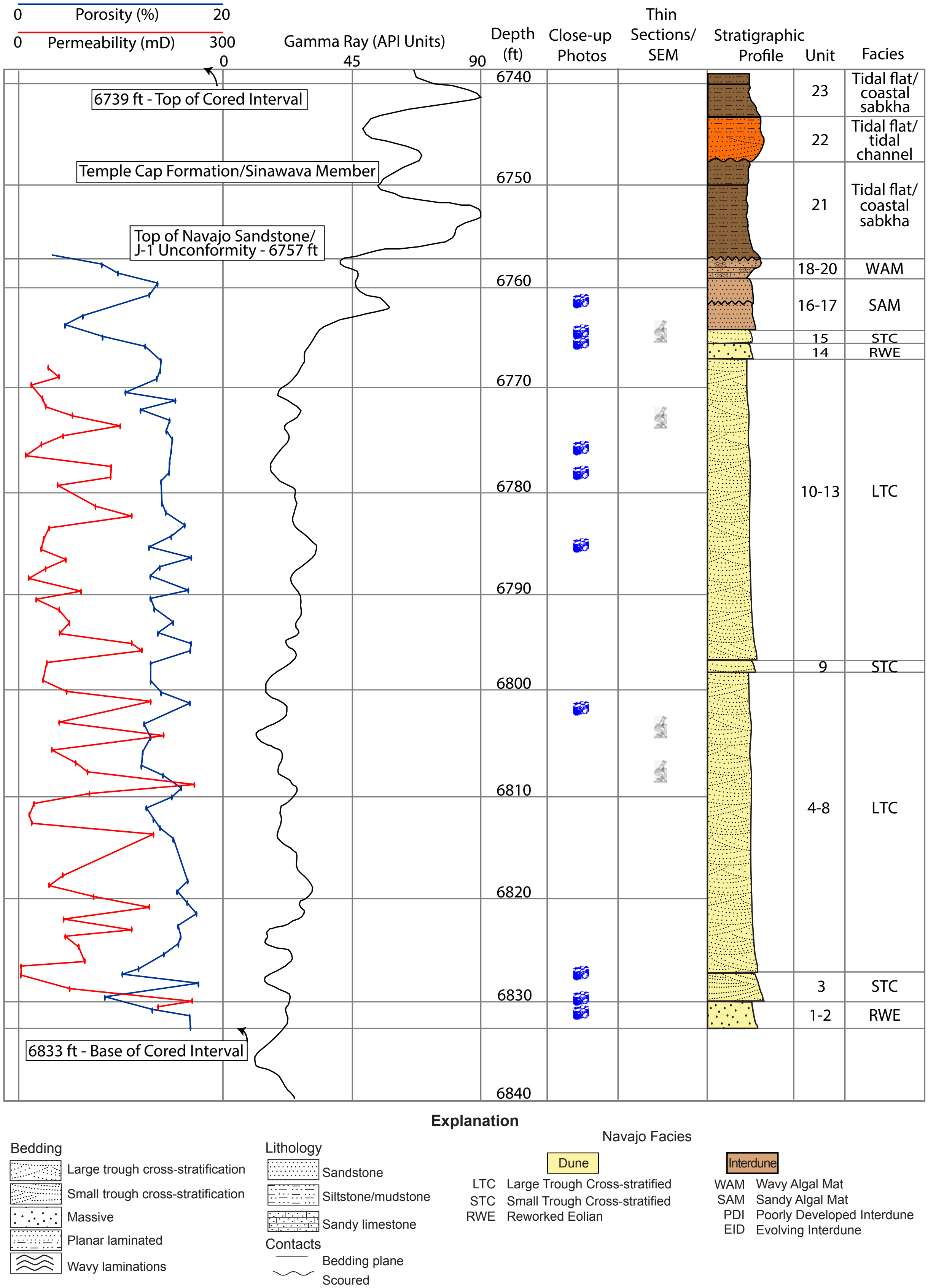

Figure 4.6. *Core description of the Navajo Sandstone from the Federal No. 17-3 well, including porosity/permeability plots, gamma-ray profile, and facies. Intervals are indicated where close-up photographs and thin section/SEM images were taken, shown on figures 4.7 through 4.12. See plate 1 for detailed core description, appendix B for core photographs, table 2.1 for summary of characteristics of Navajo facies, and figure 4.3 for well location.*

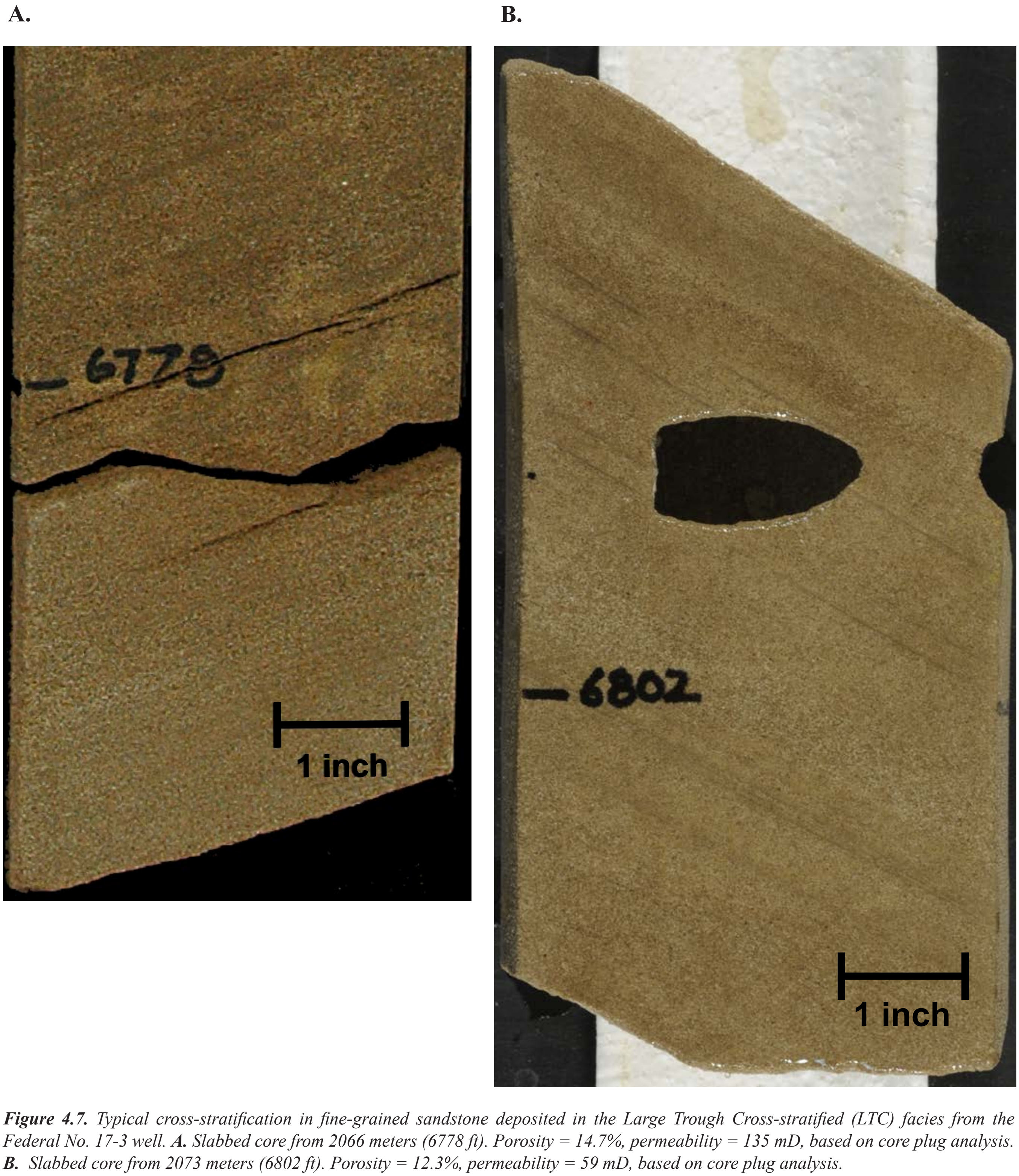

Figure 4.7. *Typical cross-stratification in fine-grained sandstone deposited in the Large Trough Cross-stratified (LTC) facies from the Federal No. 17-3 well.* ***A.*** *Slabbed core from 2066 meters (6778 ft). Porosity = 14.7%, permeability = 135 mD, based on core plug analysis.* ***B.*** *Slabbed core from 2073 meters (6802 ft). Porosity = 12.3%, permeability = 59 mD, based on core plug analysis.*

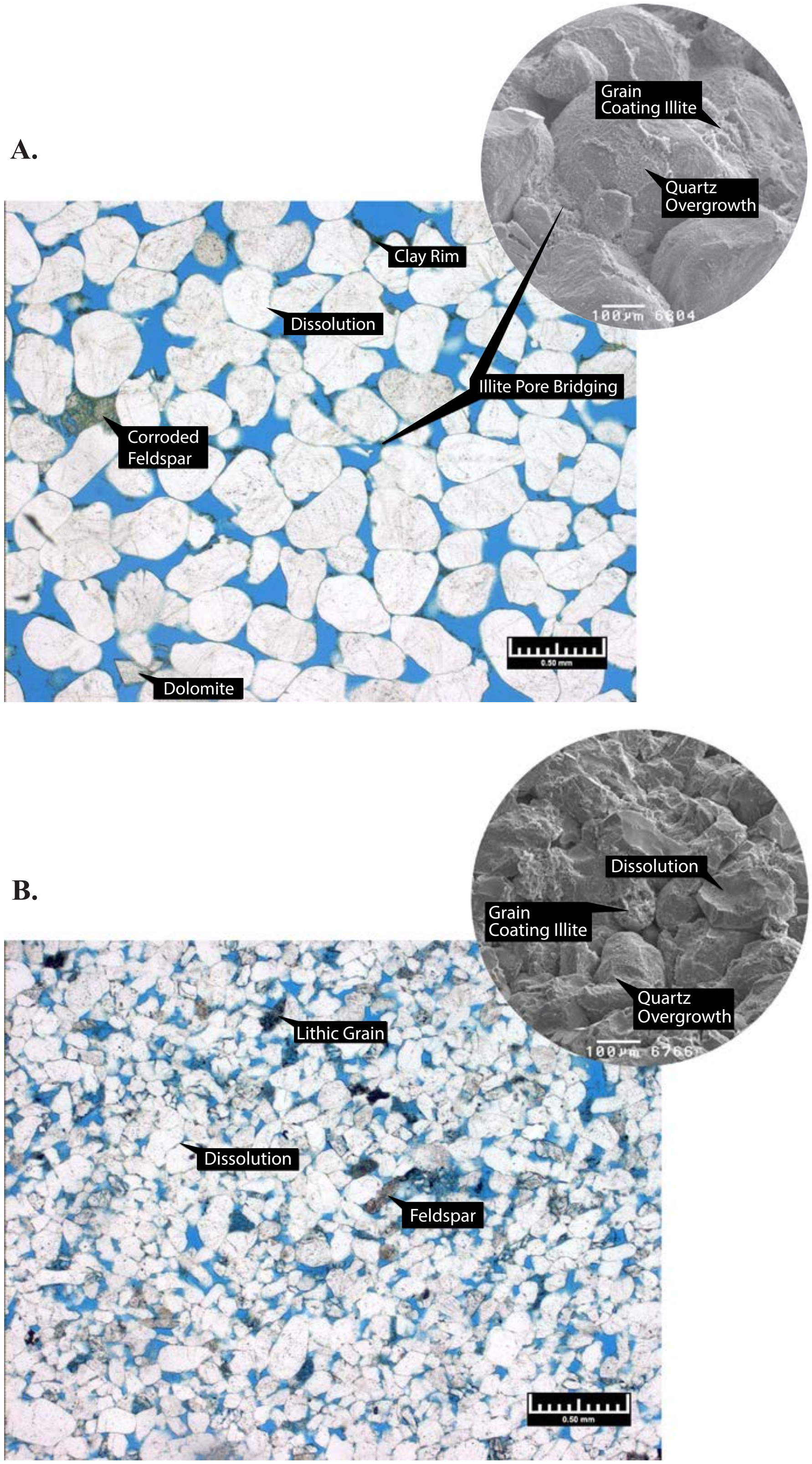

Figure 4.8. *Representative thin section photomicrographs (plane-polarized light, blue space is intergranular porosity) and insets of scanning electron microscope images of eolian facies from the Navajo Sandstone in the Federal No. 17-3 core.* ***A.*** *Subangular to subrounded quartz sand deposited in the Large Trough Cross-stratified (LTC) facies. Note the excellent intergranular porosity (blue space) and very little clay content. Porosity = 12.9%, permeability = 213 mD, based on core plug analysis, 2074 meters (6804 ft).* ***B.*** *Subangular to angular fine quartz sand and silt having some larger subrounded quartz grains. Note the presence of corroded K-feldspar grains and dissolution along grain boundaries of quartz grains. Deposition occurred in the Reworked Eolian (REW) to Small Trough Cross-stratified (STC) facies. Porosity = 12.4%, permeability = 6.3 mD, based on core plug analysis, 2062 meters (6766 ft). See figure 4.10C for core photograph.*

C.

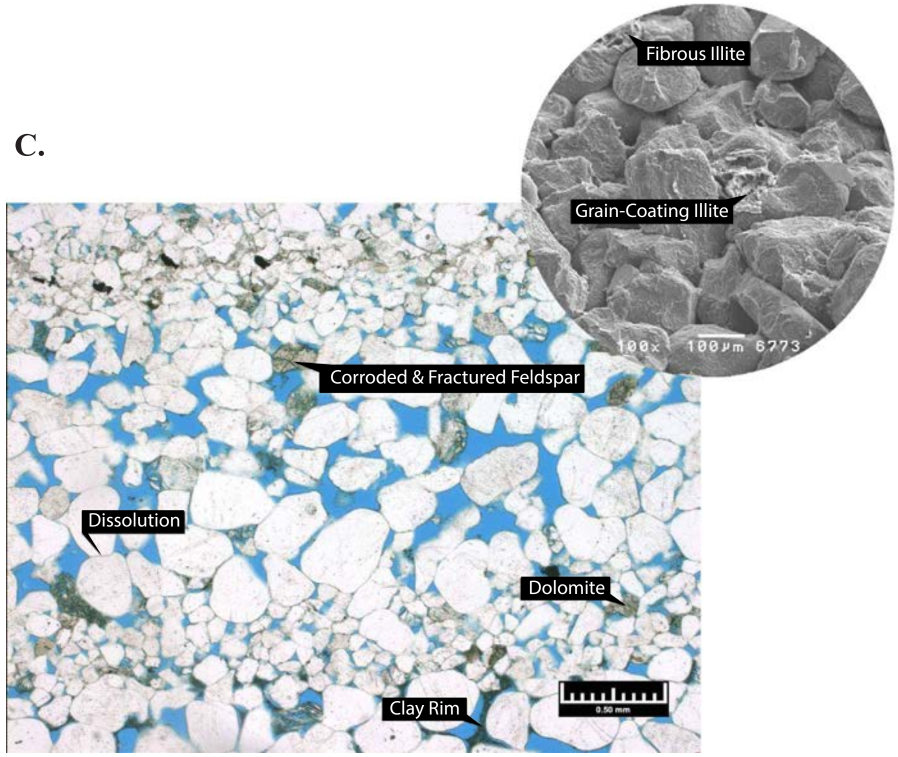

D.

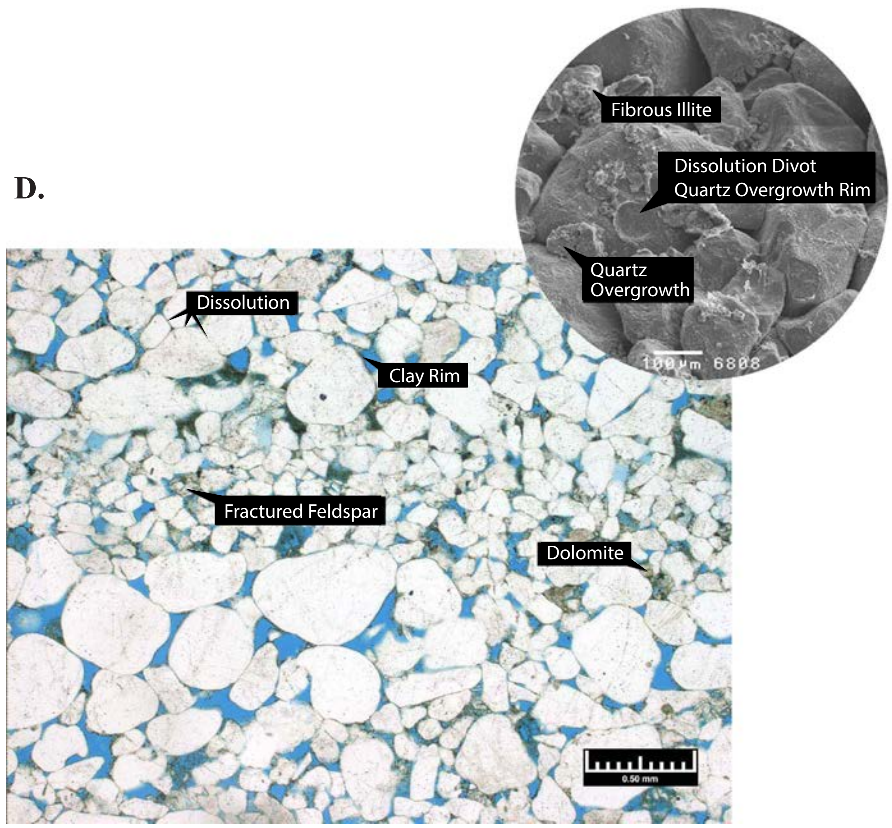

Figure 4.8 continued. *Representative thin section photomicrographs (plane-polarized light, blue space is intergranular porosity) and insets of scanning electron microscope images of eolian facies from the Navajo Sandstone in the Federal No. 17-3 core.* ***C.*** *Bimodal distribution (layered) of subangular to subrounded quartz sand and silt deposited in the LTC facies. Note a few fractured and corroded K-feldspar grains are present. Porosity = 14.8%, permeability = 149 mD, based on core plug analysis, 2064 meters (6773 ft).* ***D.*** *Bimodal distribution of subangular to subrounded layers of quartz silt and large subrounded to rounded quartz sand deposited in the LTC facies. Note the presence of corroded K-feldspar grains primarily in the silty layers and dissolution along grain boundaries of quartz grains of all sizes. Porosity = 15.9%, permeability = 258 mD, based on core plug analysis, 2075 meters (6808 ft). Courtesy of Wolverine Gas & Oil Corporation.*

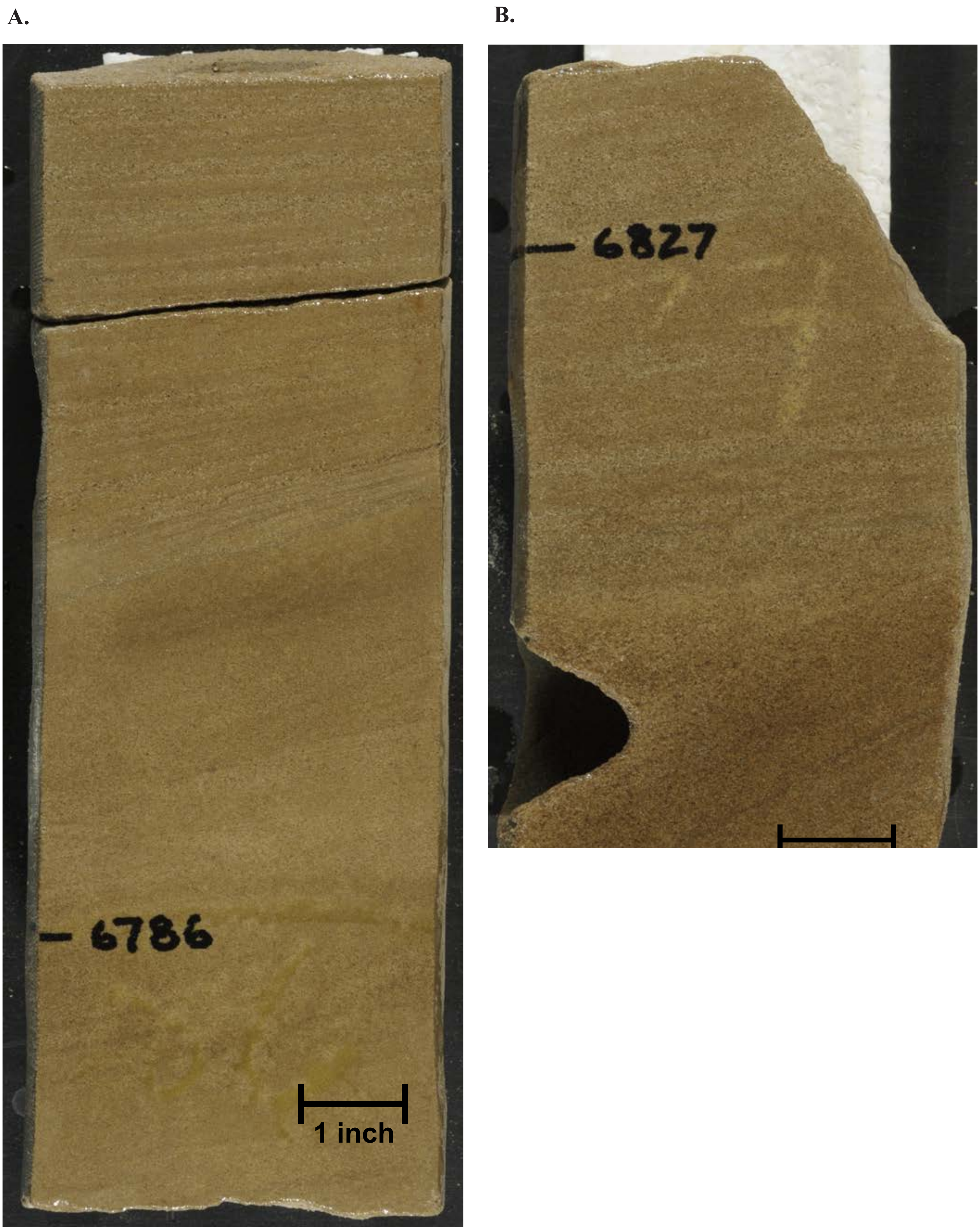

Figure 4.9. *Low-angle cross-stratification representing the dune toe in fine- to medium-grained sandstone in the Federal No. 17-3 core.* ***A.*** *Slabbed core from 2068 meters (6786 ft) in the Large Trough Cross-stratified (LTC) facies. Porosity = 16.9%, permeability = 69 mD, based on core plug analysis.* ***B.*** *Slabbed core from 2081 meters (6827 ft) in the Small Trough Cross-stratified (STC) facies. Porosity = 17.6%, permeability = 1210 mD, the highest values for the Navajo Sandstone in the well based on core plug analysis.*

the orientation of foreset laminations. An exposure surface is postulated at 2066 meters (6780 ft) based on the sharp contact and pink staining; however, an alternative interpretation may be the presence of a small fault. The contacts between the LTC and STC facies are transitional.

The STC facies consists of only three thin units that are less than 1 meter (<3 ft) in thickness in the Federal No. 17-3 core (figures 4.6, 4.9B, and 4.10A, and plate 1). Grain sizes observed in the core range from very fine to upper fine and are well sorted. Porosity averages 12%; however, permeability is highly variable ranging from 2.3 mD to a questionable 1210 mD (fracture) value, based on only four core plugs (appendix C). The top part of the uppermost STC unit is a possible dolomitized calcrete. The contacts between the STC and RWE facies are sharp (figure 4.10A).

There are three units in the Federal No. 17-3 core consisting of the RWE facies (figures 4.6 and 4.10, and plate 1). The lowermost RWE facies are the bottom two units of the core; thus the basal unit's thickness is unknown (figure 4.10A and 4.10B). The other RWE facies is a 0.3-meter-thick (1 ft) unit near the top of the Navajo section of core between underlying LTS and overlying STS facies (figure 4.10C). Bedding is massive although some relict planar lamination and cross-stratification may be present in the lower and upper units, respectively (figure 4.10). Grain sizes observed in the core range from upper fine to medium with one small coarse-grained zone; the sorting appears moderate. Surprisingly, the porosity and permeability averages were relatively high (secondary porosity?), 15% and 156 mD, respectively, based on the analysis of three core plugs (appendix C).

Interdune

Interdune facies in the Federal No. 17-3 core consist of only the WAM and SAM facies, both found at the top of the Navajo section (figure 4.6 and plate 1). The thicknesses of these facies are 0.5 and 1.5 meters (1.8 and 5 ft), respectively.

The WAM facies consists of dark bands of wispy black algal laminae in a light to medium gray silty and muddy matrix. As expected, the WAM facies is a barrier or baffle to fluid flow, having porosity and permeability averaging 5.8% and 0.3 mD, respectively, based on analysis of three core plugs (appendix C). The contact with the underlying SAM facies is sharp but may actually be the J-1 unconformity, as discussed in the following section.

The SAM facies consists of tan colored silt and very fine to upper fine-grained sand that shows medium-angle foreset laminations (figure 4.11). Thin wispy algal laminations indicate an algal influence. Like the WAM facies above, the SAM facies is also a barrier or baffle to fluid flow. However, it is more brittle due to higher silt and sand content, which makes it subject to fracturing and thus a poorer fluid barrier. Porosity and permeability averages 9.4% and 0.23 mD, respectively, based on analysis of five core plugs (appendix C).

The J-1 Unconformity

Background

The Lower Jurassic Navajo Sandstone and the Middle Jurassic Temple Cap Formation are separated by the J-1 unconformity (Pipiringos and O'Sullivan, 1978). Extensive outcrop work, regional well correlations, and isotopic dating of the Middle Jurassic throughout Utah have been conducted by Sprinkel and others (2011a) and Doelling and others (2013) leading to a better definition of the J-1 unconformity. These studies indicated the Temple Cap was deposited during the Bajocian (171 Ma) and that the J-1 is a major regional unconformity representing a time gap of over 10 million years between the Early Jurassic (Pliensbachian for the Navajo [Hintze and Kowallis, 2009]) and Middle Jurassic.

Early study of the core and well logs from the Federal No. 17-3 well interpreted an upper and lower eolian Navajo Sandstone section separated by a red-brown to green-gray interdunal, fluvial-lacustrine (playa and wadi) interval (Chidsey and others, 2007). However, thin, dolomitic and silicified limestone beds, initially interpreted as lacustrine in origin, are interbedded in the upper eolian unit. These carbonate beds yielded Middle Jurassic (Bajocian) marine dinoflagellate cysts in the core (figure 4.5B) (Sprinkel and others, 2011a; Chidsey and others, 2014; Chidsey and Sprinkel, 2016). In addition, the sandstone just above and below the red-brown siltstone unit contained glauconite (figure 4.5B), another marine indicator. Thus, it became apparent that the upper eolian sandstone and the red-brown sandstone and siltstone units are not the Navajo Sandstone because of their Middle Jurassic age and marine origin. This interval was reinterpreted as the Sinawava and White Throne Members of the Temple Cap Formation which is separated from the underlying Navajo by the J-1 unconformity, as shown on figures 4.2 and 4.5.

Interpretations

The contact between the red mudstone of the Sinawava Member of the Temple Cap Formation and the underlying silty sandstone of the "Navajo Sandstone" is the most logical pick for the J-1 unconformity. That contact is also easily identified on gamma-ray logs (figures 4.2 and 4.5). However, the presence of the glauconite in the Federal No. 17-3 core at 2061.4 meters (6763.5 ft) implies that the J-1 unconformity is farther below and not at the base of the red mudstone of the Sinawava.

There are several possible candidates that could be the J-1 unconformity in the Federal No. 17-3 core. There is a small gravel lag at 2061.2 meters (6762.7 feet) marking the top of the SAM facies that is overlain by very fine grained, massive sandstone (figure 4.11A); however, the lag may represent a small channel

Figure 4.10. *Fine- to medium-grained sandstones deposited in Small Trough Cross-stratified (STC) and Reworked Eolian (REW) facies in the Federal No. 17-3 core.* ***A.*** *Contact between cross-stratified, medium-grained sandstone of the STC facies and the underlying massive, fine-grained sandstone of the RWE facies. Slabbed core from 2082 meters (6830 ft). Porosity and permeability in the STC and RWE facies = 13.1% and 16.8%, and 75 mD and 255 mD, respectively, based on core plug analysis.* ***B.*** *Massive, moderately sorted sandstone typically found in REW facies. Slabbed core from 2082 meters (6831 ft). Porosity = 16.8%, permeability = 205 mD, based on core plug analysis.* ***C.*** *Fine-grained sandstone of the RWE facies containing possible relict or poorly developed cross-stratification of the STC facies. Slabbed core from 2062 meters (6766 ft). Porosity = 12.4%, permeability = 6.3 mD, based on core plug analysis. See figure 4.8B for thin section photomicrograph.*

Figure 4.11. Possible candidates for the J-1 unconformity in the Federal No. 17-3 core. ***A.*** Thin, very fine grained sandstone and siltstone displaying wavy laminations, typical of the Sandy Algal Mat (SAM) facies, capped by a small gravel lag (in the middle of the core) that is overlain by very fine grained, massive (homogeneous) sandstone. The gravel lag may represent the J-1 unconformity or a small wadi deposit. Slabbed core from 2061 meters (6763 ft). Porosity in the SAM facies = 6.3%, permeability = 0.02 mD, based on core plug analysis. ***B.*** Wavy laminations in thin, very fine grained sandstone and siltstone of a SAM facies overlies low-angle cross-stratification in fine-grained sandstone of the Small Trough Cross-stratified (STC) facies. The color change between the STC facies (tan with pink zones) and the SAM facies (light to dark gray) near the middle of the core could be an indication of the J-1 unconformity. Note slight offsets of laminae in the upper part of the core. Slabbed core from 2062 meters (6765 ft). Porosity and permeability in the SAM and STC facies = 4.5% and 8.2%, and 0.01 mD and 0.9 mD, respectively, based on core plug analysis.

or wadi deposit. Another possible J-1 candidate is represented by the color change between the tan with pink zones of the STC facies and the light to dark gray SAM facies at 2061.7 meters (6764.5 ft) (figure 4.11B). The contact may represent a calcrete, mentioned earlier, that has been dolomitized. There are indications of faulting (see small offset of laminae on figure 4.11B) that could have provided a pathway for fluids that account for the coloration. In addition, the reported glauconite at 2061.4 meters (6763.5 ft) is in between the two possible J-1 unconformity depths proposed above. It could be a reworked grain within an unconformity transition zone from 2061.2 to 2061.7 meters (6762.7–6764.5 ft) for the J-1. Porosity and permeability averages 6.3% and 0.3 mD, respectively, based on analysis of three core plugs (appendix C), and thus this J-1 transition zone likely represents another barrier or baffle to fluid flow.

Statistical discriminant analysis of X-ray fluorescence (XRF) elemental data, that included both mobile and immobile elements, was used by Phillips (2012), Phillips and Morris (2013), and Phillips and others (2015) to distinguish the Navajo Sandstone from the White Throne Member of the Temple Cap Formation and thus delineate the possible location of the J-1 unconformity in the Kings Meadow Ranches No. 17-3 core. The Navajo and White Throne have similar lithologies, dune facies, and provenance but different diagenetic histories (quantity and type of cements) (Phillips, 2012; Phillips and Morris, 2013; Phillips and others, 2015). In these studies, Ba, Ga, and Fe_2O_3 were used to discriminate between the Navajo and the White Throne. They discovered that the White Throne is more variable in Fe_2O_3 content whereas the Navajo is slightly more enriched in Ba and Ga. Based on the statistical discriminant analysis of XRF elemental data from the Kings Meadow Ranches No. 17-3 core, the J-1 unconformity is placed at 2061.2 meters (6762.7 feet)—the top of the gravel lag described as a possible candidate previously.

Figure 4.12. *Early, bitumen and gouge-filled, silica-cemented, impermeable fractures that have slight offsets in the Federal No. 17-3 core. Cross-stratification in the fine-grained sandstone represents the Large Trough Cross-stratified (LTC) facies. Slabbed core from 2065 meters (6776 ft). Porosity = 15.0%, permeability = 10.2 mD, based on core plug analysis.*

Fractures

Fracturing has both reduced and enhanced the reservoir permeability of the Navajo Sandstone at Covenant field. Fractures in the Federal No. 17-3 core consist of four types: (1) early bitumen-filled fractures, (2) early gouge-filled, silica-cemented, impermeable fractures, and brecciated zones (figure 4.12), (3) early to late intense micro-fractures or deformation bands, and (4) later fractures with open voids (little gouge or cement). Fracture intensity and brecciation increase, as expected, closest to fault zones in the core, and through the field. Some fractures are stylolitic in nature or have a slickenside-like surface. Development of bitumen-filled and silica-cemented fractures and deformation bands locally reduces reservoir permeability. However, these fractures may have been open when oil migration occurred. Fractures with voids and some micro-fractures likely provided additional permeable flow paths for oil migration. Later dissolution of silicate minerals and the development of open fractures increased reservoir permeability. The later fractures are related to fault-propagation folding during the Sevier orogeny after deep burial (Royce and others, 1975).

CHAPTER 5:
A HIGH-RESOLUTION SHALLOW SEISMIC EXPERIMENT—THE NAVAJO SANDSTONE AT JUSTENSEN FLATS

by

John H. McBride

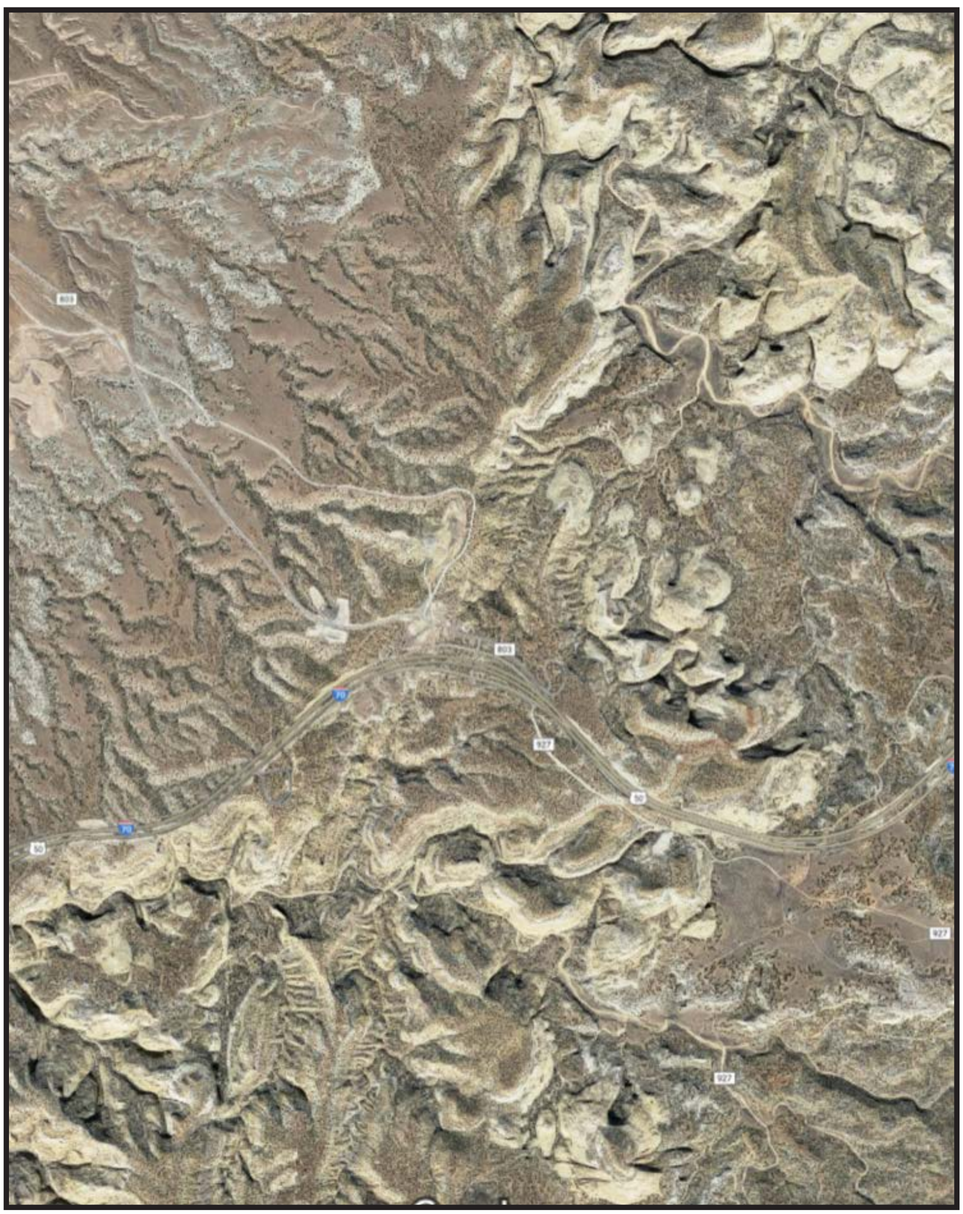

Aerial image (© 2018 Google) of the Navajo Sandstone outcrop belt (light tan areas) in the Devils and Eagle Canyons study area. Shallow, high-resolution seismic reflection profiles were acquired northwest and southeast of I-70.

CHAPTER 5:
A HIGH-RESOLUTION SHALLOW SEISMIC EXPERIMENT—THE NAVAJO SANDSTONE AT JUSTENSEN FLATS

INTRODUCTION

Whereas outcrop data are available in many locations for the Navajo Sandstone, subsurface data are difficult to acquire. Although some core and well log data are available, detailed subsurface data on the sedimentary structures and facies are limited due to the scale at which they change laterally and vertically. These thin facies changes often represent interdune layers within the sandstone that can be barriers and baffles to fluid flow, making them an important target to understand. These layers are thinner than the resolution of industry style seismic-reflection data. High-resolution seismic reflection has the ability to image the subsurface in much more detail due to the higher frequencies used in the surveys.

In a previous study (Morris and others, 2005), two-dimensional (2D) high-resolution seismic was used to image the Middle Jurassic Entrada Sandstone. This survey was successful in creating an image of the top of the Entrada sandstone bodies and was compared to outcrop to verify the results. The high-resolution survey can image shallower and smaller features than the industry standard surveys.

We acquired 2D, shallow P-wave, high-resolution, seismic reflection profiles over an area where the Navajo Sandstone is at or near the surface in an attempt to image interdune deposits interstratified with dune deposits, which would be too thin to distinguish on conventional seismic surveys. Three short seismic reflection profiles were acquired (figure 5.1) for this study. The westernmost and middle profiles (Profiles 3 and 1, respectively) have receiver station coverages of about 735 meters (2412 ft). The easternmost profile (Profile 2) has the longest receiver station coverage of about 1400 m (4600 ft). Due to strong contamination by suspected guided waves on the records from the western two profiles (figure 5.2), only the easternmost profile was processed. On this profile, we hoped to image the lower section of the Navajo Sandstone. This survey could then be compared to the outcrop in the nearby area.

SEISMIC ACQUISITION

The seismic survey resulting from Profile 2 (figure 5.3) was conducted south of Interstate 70 at the Moore Road exit along Justensen Flats. We have interpreted Justensen Flats as the surface expression of a unit in the resistant WAM facies (described in Chapter 2). It separates the upper and lower Navajo Sandstone. Below Justensen Flats we measured approximately 50 meters (150 ft) of section. We measured the lower section of the Navajo Sandstone just east of the seismic survey near the Justensen Flats campground.

DISCUSSION

The seismic data processing consisted of a standard sequence of steps, beginning with first break muting (to suppress headwaves and direct waves) and bottom muting (to suppress surface and air waves). These steps were followed by refraction statics correction and normal move-out velocity analysis. A predictive deconvolution was applied to suppress the effect of reverberation from a strong bedrock impedance contrast and to condense the wavelet. The section shown on figure 5.3 has been time-to-depth converted using a single velocity of 2500 meters/second (m/s), which is similar to the replacement velocity used in the static correction. The datum (equivalent to time or depth equal to zero) is approximately the highest elevation along the profile (i.e., on the southeastern end).

The most noticeable feature of the seismic section is the strong reflection beginning at about 70 m (230 ft) at the northwestern end of the profile, which dips to the northwest (in the plane of the section) and continues up dip across most of the record (figure 5.3). The depth of this reflector is beneath the stratigraphic level observed in nearby outcrop and thus cannot be identified positively. Its depth suggests that it is near the base of the Navajo Sandstone or perhaps deeper. The dip of the event matches the general dip slope of the Navajo in the immediate vicinity of the profile as observed in nearby outcrops. This reflection and associated deeper events are interrupted in two places (CDP 370 and CDP 590), which may be related to small-offset faults or fractures. The westernmost disruption corresponds to a line of Navajo outcrops just to the south of the profile within which significant numbers of deformation bands are present.

Deeper reflections, down to about 100 m (300 ft), are less continuous and are probably within the pre-Navajo section (Jurassic Kayenta Formation or older Jurassic-Triassic Wingate Sandstone), which may include pods of discontinuous sand bodies that could account for the reduced seismic continuity. The Kayenta Formation, a fluvial unit, is lithologically distinct from the Navajo Sandstone above and the Wingate Sand-

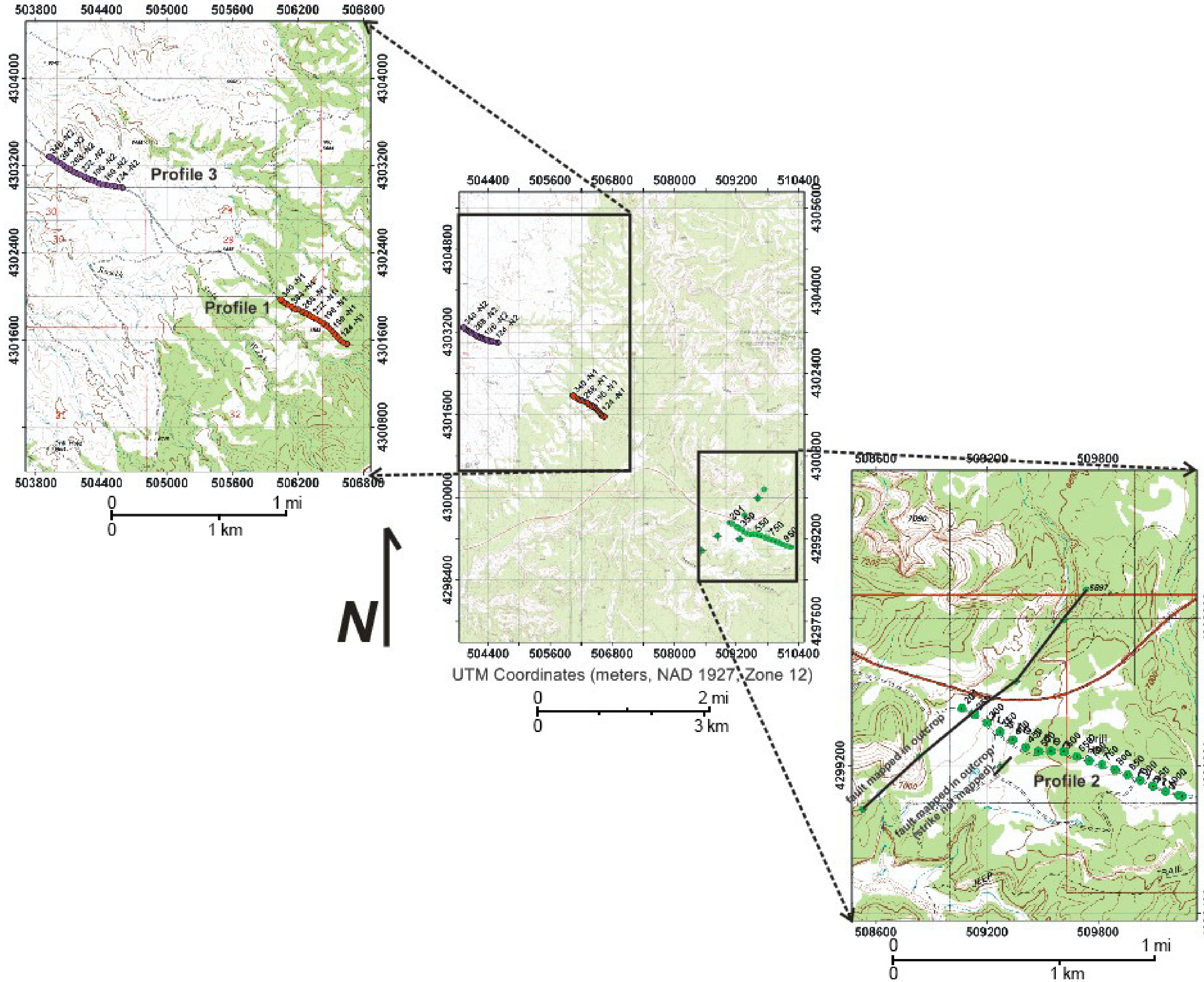

Figure 5.1. Location maps for the seismic reflection surveys. Profiles 1 and 3 are marked by station locations; Profile 2 is marked by common depth points (CDPs). Faults mapped in Justensen Flats in the Devils Canyon area are indicated on map at right. Base taken from U.S. Geological Survey 7.5' topographic maps.

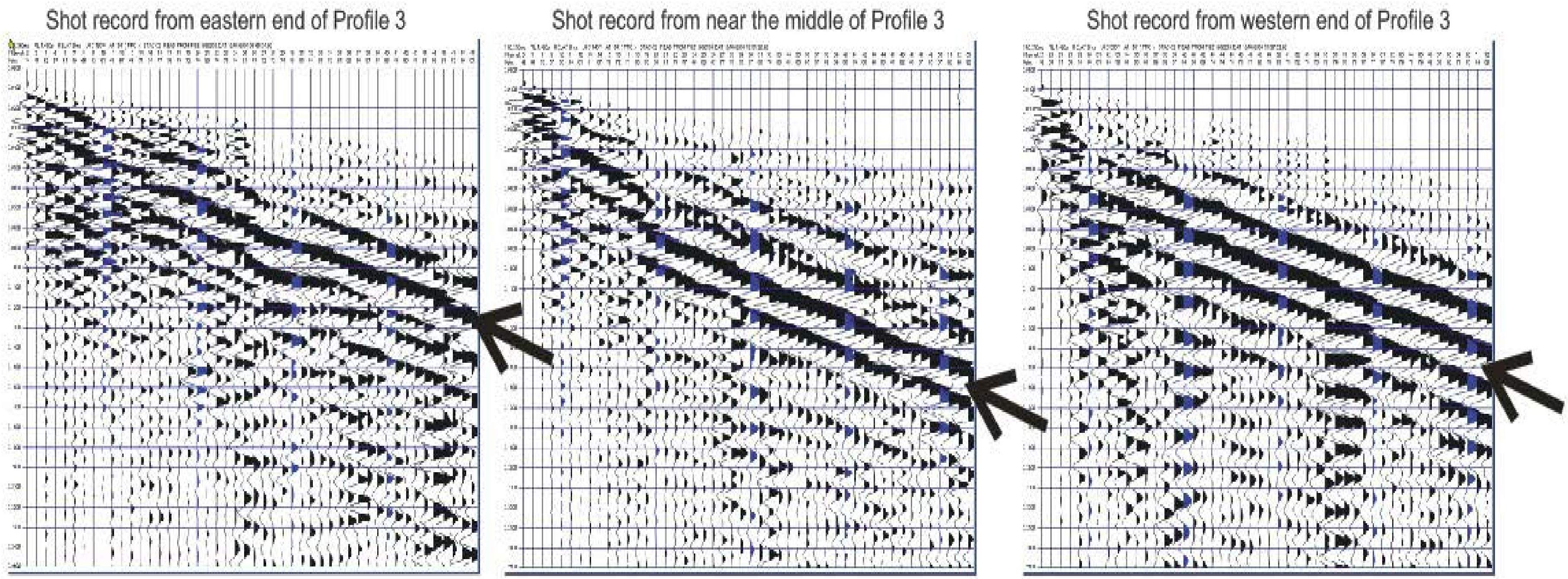

Figure 5.2. *Examples of shot records from Profile 3 showing strong suspected guided wave contamination (bold arrows). A bandpass filter of 200-40 Hz (24 dB roll-off) plus automatic gain control has been applied.*

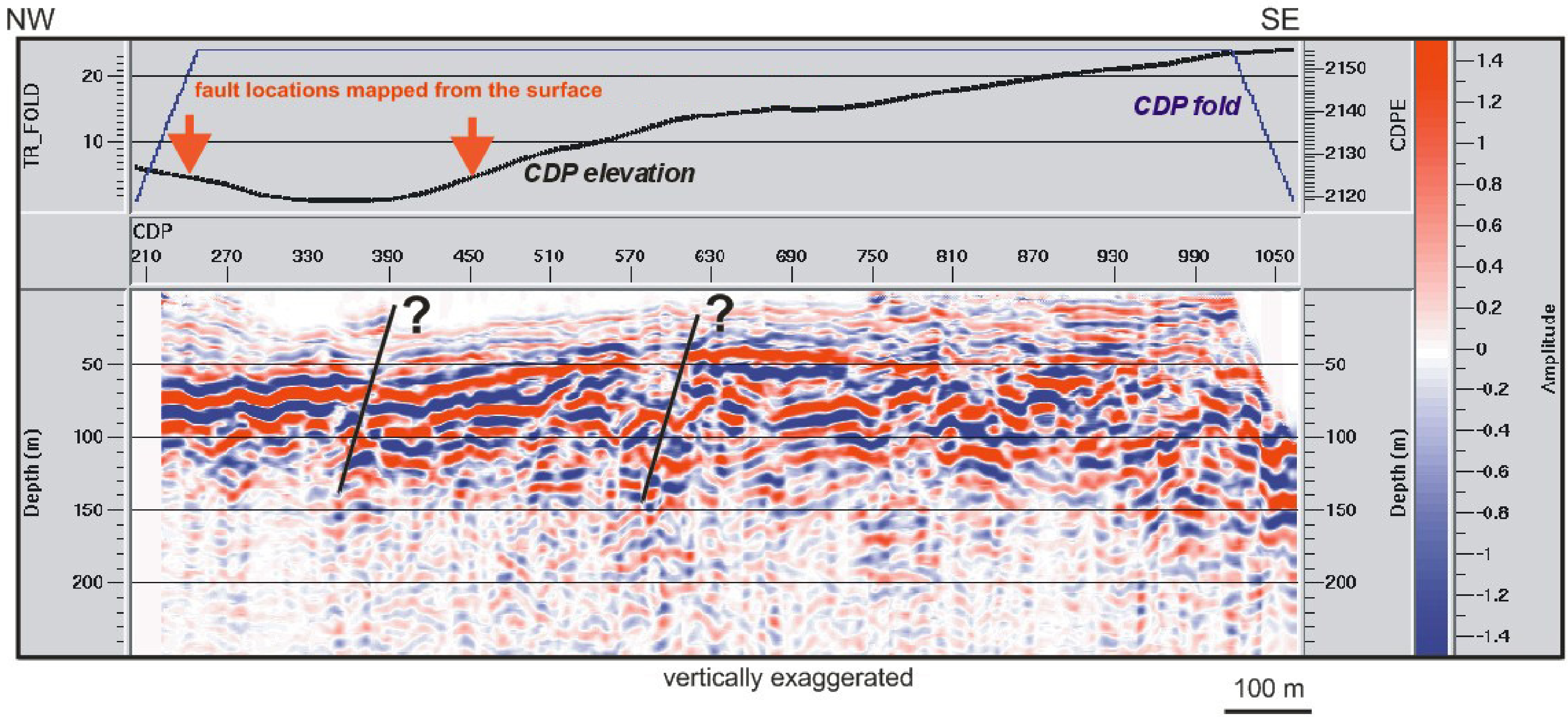

Figure 5.3. Stacked section for Profile 2. Possible (query) faults are shown as dipping lines on the seismic section.

stone below (both of which are dominated by eolian sand deposits). Due to resolution limits of the seismic profile, further interpretation (e.g., cross-stratification lateral facies changes) is not possible.

Other high-resolution geophysical methods are available to more effectively image sedimentary structures and facies variations in the Navajo Sandstone in the subsurface. Jol and others (2003) imaged the Navajo in Zion National Park using ground-penetrating radar (GPR). In their study, they used antenna frequencies from 50 to 900 MHz. At the lowest frequency they were able to image the Navajo to depths greater than 40 meters (120 ft). This thickness is just under the thickness for the lower Navajo Sandstone at Justensen Flats where we did our reflection survey. In the GPR study, Jol and others (2003) were able to image dune foresets and erosional surfaces separating dune sets. We can assume that interdune deposits would likely be imaged with GPR as they are thicker than the foresets. With GPR there is still the future possibility of imaging the interdune deposits in the lower Navajo Sandstone and possibly correlating them to the measured section.

CHAPTER 6:
SUMMARY AND CONCLUSIONS

by

Thomas C. Chidsey, Jr., Thomas H. Morris, Stephanie M. Carney,
Ashley D. Hansen, Craig D. Morgan, and John H. McBride

The Navajo Sandstone exposed in Eagle Canyon, view to the north-northwest, displaying spectacular dune and interdune deposits.

CHAPTER 6:
SUMMARY AND CONCLUSIONS

Spectacular outcrops of the Lower Jurassic Navajo Sandstone in the San Rafael Swell of east-central Utah can be used as a template for evaluation of conventional cores, geophysical and petrophysical logs, and seismic surveys of eolian reservoirs and aquifers throughout Utah and elsewhere. We divide the Navajo into eight facies in the Devils Canyon/Justensen Flats and Eagle Canyon areas: Large Trough Cross-stratified (LTC), Small Trough Cross-stratified (STC), and the Reworked Eolian (RWE) dune facies, and Wavy Algal Mat (WAM), Sandy Algal Mat (SAM), Poorly Developed Interdune (PDI), Evolving Interdune (EID), and Ephemeral Fluvial Channel (EFC) interdune facies. The Navajo Sandstone is dominated by dune facies, principally LTC facies, both vertically and horizontally. These dune facies serve as the primary reservoir for hydrocarbons and naturally occurring CO_2, aquifers for disposal of produced water from coalbed methane fields, and are targets for potential CCS. In addition, the Navajo is the major aquifer for culinary water in much of southern Utah. The barriers and baffles created by interdune facies cause heterogeneity in the reservoir or aquifer that can affect fluid flow rates and, ultimately, drilling strategies including well completion (production, injection, culinary water) plans, placement, and spacing.

The large, high-angle, trough cross-bed sets, which represent the partial preservation of large dunes are separated by more horizontally bedded interdune deposits. We found wide variability in both the lateral extent of different interdune facies as well as a wide variety of petrophysical characteristics between (and sometimes within) each interdune facies. For example, processes involved in the creation of these interdune deposits varied, resulting in different preserved primary and secondary sedimentary structures and different degrees of cementation. Therefore, the seemingly homogenous sandstone contains numerous facies which display a spectrum of reservoir characteristics—desiccated beds, soft-sediment deformation, carbonate lenses, stromatolitic beds and surfaces, ripple laminations, etc. Whereas these interdune facies make up a relatively small amount of the total volume of the Navajo (less than 10%), they have a profound effect on the characteristics of the rock as a reservoir unit. Interdune deposits may serve as baffles and barriers to fluid flow over significant distances (i.e., kilometers) and thereby serve to partition flow units within this tremendous sandstone deposit.

Observable within the Navajo Sandstone in the Devils Canyon area are three eolian-dominated dune facies, four interdune facies, and one interdune fluvial facies. Interpretation of these facies was determined from primary and secondary sedimentary structures, bioturbation, algal mat development, stratigraphic breaks, and the lateral extent of each facies as observed in well-exposed outcrops. Dune and interdune samples from stratigraphic units were classified petrographically. Seventeen of these samples are feldspathic arenites and most of those can be considered quartz-rich (>80% quartz). One dune-dominated unit was a quartz arenite (JFCG-1), two interdune units were classified as feldspathic wackes (JFCG-16, JFCG-10), and a third as originally a mudstone that was later diagenetically altered (DCB-1). Reservoir/aquifer characteristics of the Navajo Sandstone in the Devils Canyon area can be summarized as follows:

1. The Navajo Sandstone can be broadly divided into a lower quality reservoir/aquifer that extends vertically from its basal contact with the Kayenta Formation through the lower one-third of the Navajo and a higher quality reservoir/aquifer that extends vertically through the upper two-thirds of the Navajo.
2. Eolian facies are more porous and permeable than interdune facies by approximately an order of magnitude. This suggests that interdune facies, given the proper orientation over a structural closure, may retard (baffle) or stop (barrier) the flow of liquid hydrocarbons, produced or injected gases, or injected water upward and/or toward the wellbore.
3. Although overlap of porosity and permeability measurements occur between and within dune and interdune facies, the WAM facies consistently has the lowest porosity and permeability. It is likely that this laterally extensive facies would act as a barrier to liquid hydrocarbons, produced or injected gases, or injected water flow within the greater Navajo Sandstone reservoir/aquifer.
4. Production strategies for efficiently draining Navajo Sandstone petroleum reservoirs should consider intraformational barriers and baffles. In the Devils Canyon area, the lower one-third of the reservoir is likely to drain less efficiently than the upper two-thirds of the reservoir. The WAM facies, if identifiable, should be given special consideration as it may partition the reservoir and potentially trap undrained reserves.

Like the Devils Canyon section, the Navajo Sandstone in the Eagle Canyon area can be divided into upper and lower parts. The upper Navajo, which comprises the upper 140 meters (420 ft) of the section, is dominated by the highly porous and permeable LTC dune facies, which is the primary potential reservoir and aquifer facies. The EID facies (unit ECT17) present in the upper section does not have low enough porosity and permeability to act as a barrier to fluid flow but would likely act as a baffle. The lower Navajo is more heterogeneous, dominated by interdune facies with lower porosity and permeability. Most of these interdune facies are not very laterally continuous and therefore would act as baffles to fluid flow in a confined reservoir or aquifer. Unit ECT8, a WAM facies, has the lowest porosity/permeability values and is the most laterally extensive interdune facies. It separates the upper and lower Navajo sections and would likely act as a barrier to fluid flow and compartmentalize a reservoir or aquifer.

Cores through the oil-productive Navajo Sandstone in Covenant field west of the San Rafael Swell in the central Utah thrust belt consists of the LTC, STC, and RWE dune facies and WAM and SAM interdune facies. The recognition of these dune and interdune facies in cores was aided by the outcrop descriptions from the study areas. Combined, both can be used in evaluating areas where well logs are limited and cores unavailable. Interdune facies within the Navajo can be identified on logs as having high gamma-ray readings and are relatively thin layers within larger packages of thick, porous sandstones with low gamma-ray readings as confirmed by both outcrop and core evaluations. Careful interpretation of well logs and evaluation of well core can help to identify these petroleum play components and lead to better informed drilling decisions. These concepts also apply to water disposal or future CO_2 injection wells.

We conclude that the world-class outcrops of the eolian Navajo Sandstone in the San Rafael Swell demonstrate the complex nature of dune and interdune facies, both vertically and horizontally. The heterogeneity in terms of lithology, petrographic properties, etc., created by the facies observed in these outcrops and identified in the core from Covenant field provide the critical information necessary in exploring for and developing new oil fields, disposing of produced water from maturing oil and gas fields, targeting zones to potentially store CO_2 from coal-fired power plants in the region, and managing culinary water aquifers so critical in southern Utah. Finally, the results of this study can be applied to other formations elsewhere in Utah and worldwide that were deposited in eolian environments.

ACKNOWLEDGMENTS

Funding for this research was provided to the BYU Department of Geological Sciences, Provo, Utah, by the UGS (contract no. 066101). BYU students Nicole June, Anne Dangerfield, and Chris Spencer assisted in this study as field and lab assistants. Carol M. Dehler, Department of Geology, Utah State University, Logan, Utah, provided petrography equipment. The reflection surveys were conducted by students and faculty from BYU under the supervision of John H. McBride.

We thank Wolverine Gas & Oil Corporation for donating the Covenant field cores to the Utah Core Research Center (UCRC) and providing core descriptions, photomicrographs, petrophysical data, and other reservoir analyses from Covenant field; the cores were first described by L.F. Krystinik, geologic consultant. Cheryl Gustin, Lori Steadman, and Jay Hill of the UGS drafted and prepared figures. Michael D. Laine (retired) and Thomas Dempster of the UCRC photographed core.

This study was reviewed by Tanner Hicks of Advance Energy Partners, Riley Brinkerhoff of Wasatch Energy Management, and Michael D. Vanden Berg, Kimm M. Harty, Mike Hylland, and Bill Keach of the UGS. Their suggestions and constructive criticisms greatly improved the manuscript. Finally, we thank Jen Miller, John Good, and the UGS editorial production team for their efforts in producing this publication.

REFERENCES

Ahlbrandt, T.S., and Fryberger, S.G., 1982, Introduction to eolian deposits, *in* Scholle, P.A., and Spearing, D., editors, Sandstone depositional environments: American Association of Petroleum Geologists Memoir 31, p. 11–47.

Allen, J., Lee, S., and Potter, S., 2013, Three dimensional geologic model of the eolian Jurassic Navajo Sandstone in central Utah for the evaluation of CO_2 sequestration, *in* Morris, T.H., and Ressetar, R., editors, The San Rafael Swell and Henry Mountains Basin—geologic centerpiece of Utah: Utah Geological Association Publication 42, p. 223–260.

Allen, P.A., Verlander, J.E., Burgess, P.M., and Audet, D.M., 2000, Jurassic giant erg deposits, flexure of the United States continental interior, and timing of the onset of Cordilleran shortening: Geology, v. 28, no. 2, p. 159–162.

Allis, R.G., Chidsey, T.C., Jr., Morgan, C.D., Moore, J., and White, S., 2003, CO_2 injection potential beneath large power plants in the Colorado Plateau, southern Rocky Mountain region, USA: Proceedings Volume, Second Annual Conference on Carbon Sequestration, May 5-8, 2003, Alexandria, VA, 25 p.

Allis, R.G., Bergfield, D., Moore, J.N., McClure, K., Morgan, C., Chidsey, T.C., Jr., Heath, J., and McPherson, B., 2005, Implications of results from CO_2 systems for long-term monitoring: Proceedings Volume, Fourth Annual Conference on Carbon Capture and Sequestration, May 2-5, 2005, Alexandria, VA, p. 1367–1388.

Beitler, B., Parry, W.T., and Chan, M.A., 2005, Fingerprints of fluid flow—chemical diagenetic history of the Jurassic Navajo Sandstone, southern Utah, U.S.A.: Journal of Sedimentary Research, v. 75, no. 4, p. 547–561.

Blakey, R., and Ranney, W., 2008, Ancient landscapes of the Colorado Plateau: Grand Canyon, Arizona, Grand Canyon Association, 156 p.

Boggs, S., Jr., 2006, Principles of sedimentology and stratigraphy (4th edition): Pearson-Prentice Hall, New Jersey, 662 p.

Chan, M.A., Hunter, R.E., Loope, D.B., and Langford, R.P., 1992, Reflections on eolian and erg-margin systems: Journal of Sedimentary Petrology, v. 62, no. 5, p. 917–920.

Chidsey, T.C., Jr., 1993, Jurassic-Triassic Nugget Sandstone, *in* Hjellming, C.A., editor, Atlas of major Rocky Mountain gas reservoirs: New Mexico Bureau of Mines and Mineral Resources, p. 77–79.

Chidsey, T.C., Jr., 2013, Geology of the San Rafael Swell, east-central Utah, *in* Morris, T.H., and Ressetar, R., editors, The San Rafael Swell and Henry Mountains Basin—geologic centerpiece of Utah: Utah Geological Association Publication 42, p. 1–73.

Chidsey, T.C., Jr., 2018, Characteristics and source rocks of Utah crude oils, *in* Emerman, S.H., Bowen, B., Schamel, S., and Simmons, S., editors, Geofluids of Utah: Utah Geological Association Publication 47, p. 149–177, 1 plate, 26 appendices.

Chidsey, T.C., Jr., and Sprinkel, D.A., 2016, Chapter 5—Jurassic Navajo Sandstone/Temple Cap Formation Hingeline play, *in* Chidsey, T.C., Jr., compiler and editor, Major oil plays in Utah and vicinity: Utah Geological Survey Bulletin 137, p. 73–97, https://doi.org/10.34191/B-137.

Chidsey, T.C., Jr., DeHamer, J.S., Hartwick, E.E., Johnson, K.R., Schelling, D.D., Sprinkel, D.A., Strickland, D.K., Vrona, J.P., and Wavrek, D.A., 2007, Petroleum geology of Covenant oil field, central Utah thrust belt, *in* Willis, G.C., Hylland, M.D., Clark, D.L., and Chidsey, T.C., Jr., editors, Central Utah—diverse geology of a dynamic landscape: Utah Geological Association Publication 36, p. 273–296.

Chidsey, T.C., Jr., Hartwick, E.E., Johnson, K.R., Schelling, D.D., Sbarra, Rossella, Sprinkel, D.A., Vrona, J.P., and Wavrek, D.A., 2011, Petroleum geology of Providence oil field, central Utah thrust belt, *in* Sprinkel, D.A., Yonkee, W.A., and Chidsey, T.C., Jr., editors, Sevier thrust belt: northern and central Utah and adjacent areas: Utah Geological Association Publication 40, p. 213–231.

Chidsey, T.C., Jr., Sprinkel, D.A., Kowallis, B.J., Doelling, H.H., and Waanders, G., 2019, Covenant oil field in the central Utah thrust belt—what has been learned in the 15 years since the discovery [abs.]: American Association of Petroleum Geologists Annual Convention Abstracts Volume, non-pagenated.

Chidsey, T.C., Jr, Sprinkel, D.A., Vrona, J.P., Hartwick, E.E., Lester, M., and Sbarra, R., 2014, Covenant oil field, central Utah thrust belt—new interpretation of the reservoir stratigraphy: Rocky Mountain Association of Geologists, The Outcrop, v. 63, no. 12, p. 10–12, 14–17.

Clemmensen, L.B., Olsen, H., and Blakey, R.C., 1989, Erg-margin deposits in the Lower Jurassic Moenave Formation and Wingate Sandstone, southern Utah: Geological Society of America Bulletin, v. 101, p. 759–773.

Colson, C.T., 1993, Farnham Dome, *in* Bereskin, S.R., and Hill, B.G., editors, Oil and gas fields of Utah: Utah Geological Association Publication 22, unpaginated.

Conner, D.C., and Covlin, R.J., 1977, Development geology of Pineview field, Summit County Utah, *in* Heisey, E.L., Lawson, D.E., Norwood, E.R., Wach, P.H., and Hale, L.A., editors, Rocky Mountain thrust belt geology and resources: Wyoming Geological Association 29th Annual Field Conference, p. 639–650.

Constenius, K.M., Esser, R.P., and Layer, P.W., 2003, Extensional collapse of the Charleston-Nebo salient and its relationship to space-time in Cordilleran orogenic belt tectonism and continental stratigraphy, *in* Reynolds, R.G., and Flores, R.M., editors, Cenozoic systems of the Rocky Mountain region: Society for Sedimentary Geology (SEPM), Rocky Mountain Section, p. 303–354.

Dalrymple, A., and Morris, T.H., 2007, Facies analysis and reservoir characterization of outcrop analogs to the Navajo Sandstone in the central Utah thrust belt exploration play, *in* Willis, G.C., Hylland, M.D., Clark, D.L., and Chidsey, T.C., Jr., editors, 2007, Central Utah—diverse geology of a dynamic landscape: Utah Geological Association Publication 36, p. 311–322.

DeCelles, P.G., 2004, Late Jurassic to Eocene evolution of the Cordilleran thrust belt and foreland basin system, western USA: American Journal of Science, v. 304, p. 105–168.

DeCelles, P.G., and Coogan, J.C., 2006, Regional structure and kinematic history of the Sevier fold-and-thrust belt, central Utah: Geological Society of America Bulletin, v. 118, no. 7/8, p. 841–864.

DeCelles, P.G., Lawton, T.F., and Mitra, G., 1995, Thrust timing, growth of structural culminations, and synorogenic sedimentation in the type Sevier orogenic belt, western United States: Geology, v. 23, p. 699–702.

Dickinson, W.R., and Gehrels, G.E., 2003, U-Pb ages of detrital zircons from Permian and Jurassic eolian sandstones of the Colorado Plateau, USA—paleogeographic implications: Sedimentary Geology, v. 163, issues 1-2, p. 29–66.

Dickinson, W.R., and Gehrels, G.E., 2010, Synoptic record in space and time of provenance relations for Mesozoic strata in south-central Utah from U-Pb ages of detrital zircons, *in* Carney, S.M., Tabet, D.E., and Johnson, C.L., editors, Geology of south-central Utah: Utah Geological Association Publication 39, p. 178–193.

Dickinson, W.R., and Suczek, C.A., 1979, Plate tectonics and sandstone compositions: American Association of Petroleum Geologists Bulletin, v. 63, no. 12, p. 2164–2182.

Dickinson, W.R., Beard, I.S., Brakenridge, G.R., Erjavec, J.L., Ferguson, R.C., Inman, K.F., Knepp, R.A., Lindberg, F.A., and Ryberg, P.T., 1983, Provenance of North American Phanerozoic sandstones in relation to tectonic setting: Geological Society of America Bulletin, v. 93, p. 222–235.

Doe, T.W., and Dott, R.H., 1980, Genetic significance of deformed cross bedding—with examples from the Navajo and Weber Sandstones of Utah: Journal of Sedimentary Petrology, v. 50, no. 3, p. 793–812.

Doelling, H.H., and Hylland, M.D., 2002, San Rafael Swell proposed as site of new national monument: Utah Geological Survey, Survey Notes, v. 34, no. 2, p. 9–11, https://doi.org/10.34191/SNT-34-2.

Doelling, H.H., and Kuehne, P.A., 2007, Interim geologic map of the east half of the Loa 30' x 60' quadrangle, Wayne, Garfield, and Emery Counties, Utah: Utah Geological Survey Open-File-Report 489, 29 p., 1 plate, scale 1:62,500, https://doi.org/10.34191/OFR-489.

Doelling, H.H., Sprinkel, D.A., Kowallis, B.J., and Kuehne, P.A., 2013, Temple Cap and Carmel Formations in the Henry Mountains Basin, Wayne and Garfield Counties, Utah, *in* Morris, T.H., and Ressetar, R., editors, The San Rafael Swell and Henry Mountains Basin—geologic centerpiece of Utah: Utah Geological Association Publication 42, p. 279–318.

Dott, R.H., Jr., 1964, Wacke, graywacke, and matrix—what approach to immature sandstone classification?: Journal of Sedimentary Petrology, v. 34, p. 629.

Eichhubl, P., Taylor, W.L., Pollard, D.D., and Aydin, A., 2004, Paleo-fluid flow and deformation in the Aztec Sandstone at the Valley of Fire, Nevada—evidence for the coupling of hydrogeologic, diagenetic, and tectonic processes: Geologic Society of America Bulletin, v. 116, p. 1120–1136.

Eisenberg, L., 2003, Giant stromatolites and a supersurface in the Navajo Sandstone, Capitol Reef National Park, Utah: Geology, v. 31, no. 2, p. 111–114.

Freethey, G.W., and Cordy, G.E., 1991, Geohydrology of Mesozoic rocks in the upper Colorado River basin in Arizona, Colorado, New Mexico, Utah, and Wyoming, excluding the San Juan Basin: U.S. Geological Survey Professional Paper 1411-C, 130 p.

Freethey, G.W., and Stolp, B.J., 2010, Simulation of groundwater flow and solute transport in the Glen Canyon aquifer, east-central Utah: U.S. Geological Survey Scientific Investigations Report 2009-5037, 28 p.

Fryberger, S.G., 1990, Ancient eolian deposits of the Navajo and Weber Sandstones, northeast Utah and Colorado, *in* Fryberger, S.G., Krystinik, L.F., and Schenk, C.J., editors, Modern and ancient eolian deposits—petroleum exploration and production: Society for Sedimentary Geology (SEPM), Rocky Mountain Section Publication, Chapter 19, 12 p.

Fryberger, S.G, Al-Sari, A.M., and Clisham, T.J., 1983, Eolian dune, interdune, sand sheet and siliciclastic sabkha sediments of an offshore prograding sand sea, Dhahran area, Saudi Arabia: American Association of Petroleum Geologists Bulletin, v. 67, no. 2, p. 280–312.

Hamblin, W.K., 2004, Beyond the visible landscape—aerial panoramas of Utah's geology: Provo, Utah, Brigham Young University Department of Geology, p. 232–233.

Hansen, A.D., 2007, Reservoir characterization and outcrop analogs to the Navajo Sandstone in the central Utah thrust belt exploration play: Provo, Utah, Brigham Young University, M.S. thesis, 110 p.

Hartwick, E.E., 2010, Eolian architecture of sandstone reservoirs in the Covenant field, Sevier County, Utah [abs.]: American Association of Petroleum Geologists, Rocky Mountain Section Meeting Program with Abstracts, p. 49.

Hintze, L.F., 1980, Geologic map of Utah: Utah Geological Survey Map M-A-1, 2 sheets, scale 1:500,000, https://doi.org/10.34191/M-A1.

Hintze, L.F., and Kowallis, B.J., 2009, Geologic history of Utah: Provo, Utah, Brigham Young University Geology Studies Special Publication 9, 225 p.

Hintze, L.F., Willis, G.C., Laes, D.Y.M., Sprinkel, D.A., and Brown, K.D., 2000, Digital geologic map of Utah: Utah Geological Survey Map 179DM, scale 1:500,000, https://doi.org/10.34191/M-179dm.

Hunt, C.B., 1956, Cenozoic geology of the Colorado Plateau: U.S. Geological Survey Professional Paper 279, 99 p.

Hunter, R.E., 1977, Basic types of stratification in small eolian dunes: Sedimentology, v. 24, p. 361–387.

Jol, H.M., Bristow, C.S., Smith, D.G., Junck, M.B., and Putnam, P., 2003, Stratigraphic imaging of the Navajo Sandstone using ground-penetrating radar: The Leading Edge, v. 22, p. 882–887.

Keele, D., and Evans, J., 2008, Analysis of reservoir properties of faulted and fractured eolian thrust-belt reservoirs: Utah Geological Survey Open-File Report 529, 50 p., 3 plates, https://doi.org/10.34191/OFR-529.

Kiersch, G.A., 1950, Small-scale structures and other features of Navajo Sandstone, northern part of San Rafael Swell, Utah: American Association of Petroleum Geologists Bulletin, v. 34, no. 5, p. 923–942.

Kocurek, G., 1988, First-order and super bounding surfaces in eolian sequences—bounding surfaces revisited: Sedimentary Geology, v. 56, p. 193–206.

Kocurek, G., and Dott, R.H., 1983, Jurassic paleogeography and paleoclimate of the central and southern Rocky Mountains region, *in* Reynolds, M.W., and Dolly, E.D., editors, Mesozoic paleogeography of the west-central United States: Society for Sedimentary Geology (SEPM), Rocky Mountain Section, p. 101–116.

Kocurek, G., and Hunter, R.E., 1986, Origin of polygonal fractures in sand, uppermost Navajo and Page Sandstones, Page, Arizona: Journal of Sedimentary Petrology, v. 56, p. 895–904.

Lawton, T.F., 1985, Style and timing of frontal structures, thrust belt, central Utah: American Association of Petroleum Geologists Bulletin, v. 69, p. 1145–1159.

Lawton, T.F., Sprinkel, D.A., DeCelles, P.G., Mitra, G., Sussman, A.J., and Weiss, M.P., 1997, Stratigraphy and structure of the Sevier thrust belt and proximal foreland-basin system in central Utah—a transect from the Sevier Desert to the Wasatch Plateau, *in* Link, P.K., and Kowallis, B.J., editors, Mesozoic to Recent geology of Utah: Brigham Young University Geology Studies, v. 42, pt. II, p. 33–67.

Lindquist, S.J., 1983, Nugget formation reservoir characteristics affecting production in the overthrust belt of southwestern Wyoming: Journal of Petroleum Technology, v. 35, p. 1355–1365.

Lindquist, S.J., 1988, Practical characterization of eolian reservoirs for development—Nugget Sandstone, Utah-Wyoming thrust belt: Sedimentary Geology, v. 56, p. 315–339.

Loope, D., Rowe, C., and Joeckel, M., 2001, Annual monsoon rains recorded by Jurassic dunes: Nature, v. 412, p. 64–66.

Lucchitta, I., 1979, Late Cenozoic uplift of the southwestern Colorado Plateau and adjacent Colorado River region: Tectonophysics, v. 61, p. 63–95.

Martin, D.H., Morris, T.H., Sorber, S.C., and Eddleman, J.L., 2007, Geologic map of the Golden Throne quadrangle, Wayne and Garfield Counties, Utah: Utah Geological Survey Miscellaneous Publication 07-1, 2 sheets, scale 1:24,000, https://doi.org/10.34191/MP-07-1.

McLelland, B.E., Morris, T.H., Martin, D.H., and Sorber, S.C., 2007, Geologic map of the Fruita quadrangle, Wayne County, Utah: Utah Geological Survey Miscellaneous Publication 07-2, 2 sheets, scale 1:24,000, https://doi.org/10.34191/MP-07-2.

Milliken, K., Choh, S., and McBride, E., 2002, Sandstone petrology, a tutorial petrographic image atlas: American Association of Petroleum Geologists Datapages, Search and Discovery Series 6 version 1.0.

Moore, B.J., and Sigler, S., 1987, Analyses of natural gases, 1917–1985: U.S. Bureau of Mines, Information Circular 9129, 1197 p.

Montgomery Watson, 1997, Summary of hydrologic modeling of SWD #1 and SWD #2, Emery County, Utah: Salt Lake City, unpublished report submitted to the Utah Division of Oil, Gas and Mining, 33 p.

Morgan, C.D., 2007, Structure, reservoir characterization, and carbon dioxide resources of Farnham Dome field, *in* Willis, G.C., Hylland, M.D., Clark, D.L., and Chidsey, T.C., Jr., editors, Central Utah—diverse geology of a dynamic landscape: Utah Geological Association Publication 36, p. 297–310.

Morgan, C.D., and Chidsey, T.C., Jr., 1991, Gordon Creek, Farnham Dome, and Woodside fields, Carbon and Emery Counties, Utah, *in* Chidsey, T.C., Jr., editor, Geology of east-central Utah: Utah Geological Association Publication 19, p. 301–309.

Morgan, C.D., and Kirby, S.M., 2017, Chapter 4—Uinta Basin reservoirs/aquifers: Triassic-Jurassic Glen Canyon Group through the Cretaceous Cedar Mountain and Dakota Formations, *in* Chidsey, T.C., Jr., compiler and editor, Produced water in the Uinta Basin, Utah—evaluation of reservoirs, water storage aquifers, and management options: Utah Geological Survey Bulletin 138, p. 59–126, 3 plates, 7 appendices, https://doi.org/10.34191/B-138.

Morris, T.H., McBride, J.H., and Monn, W.D., 2005, A multidisciplinary approach to reservoir characterization of the coastal Entrada erg-margin gas play, Utah: Utah Geological Survey Open-File Report 459, 50 p, https://doi.org/10.34191/OFR-459.

Moulton, F.C., 1976, Lower Mesozoic and upper Paleozoic petroleum potential of the Hingeline area, central Utah, *in* Hill, J.G., editor, Symposium on geology of the Cordilleran Hingeline: Rocky Mountain Association of Geologists Guidebook, p. 219–229.

Mountney, N.P., 2006, Periodic accumulation and destruction of Aeolian erg sequences in the Permian Cedar Mesa Sandstone, White Canyon, southern Utah, USA: Sedimentology, v. 53, no. 4, p. 789–823.

Netoff, D., 2002, Seismogenically induced fluidization of Jurassic erg sands, south-central Utah: Sedimentology, v. 49, p. 65–80.

Nuccio, V.F., and Condon, S.M., 1996, Burial and thermal history of the Paradox Basin, Utah and Colorado, and petroleum potential of the Middle Pennsylvanian Paradox Formation, *in* Huffman, A.C., Jr., Lund, W.R., and Godwin, L.H., editors, Geology of the Paradox Basin: Utah Geological Association Publication 25, p. 57–76.

Nuccio, V.F., and Roberts, L.N.R., 2003, Chapter 4 – Thermal maturity and oil and gas generation history of petroleum systems in the Uinta – Piceance province, Utah and Colorado, *in* Petroleum systems and geologic assessment of oil and gas in the Uinta – Piceance province, Utah and Colorado: U.S. Geological Survey Digital Data Series, DDS-69-B, 39 p.

Parrish, J.T., Hasiotis, S.T., and Chan, M.A., 2017, Carbonate deposits in the Lower Jurassic Navajo Sandstone, southern Utah and northern Arizona, U.S.A.: Journal of Sedimentary Research, v. 87, p. 740–762.

Parry, W.T., Forster, C.B., Evans, J.P., Bowen, B.B., and Chan, M.A., 2007, Geochemistry of CO_2 sequestration in the Jurassic Navajo Sandstone, Colorado Plateau, Utah: Environmental Geoscience, v. 14, no. 2, p. 91–109.

Parry, W.T., Chan, M.A., and Nash, B.P., 2009, Diagenetic characteristics of the Jurassic Navajo Sandstone in the Covenant oil field, central Utah thrust belt: American Association of Petroleum Geologists Bulletin, v. 93, no. 8, p. 1039–1061, DOI: 10.1306/04270908170.

Pederson, J.L., Cragun, W.S., Hidy, A.J., Rittenour, T.M., and Grosse, J.C., 2013, Colorado River chronostratigraphy at Lee's Ferry, Arizona, and the Colorado Plateau bull's-eye of incision: Geology, v. 41, no. 4, p. 427–430.

Peterson, F., 1988, Pennsylvanian to Jurassic eolian transportation systems in the western United States: Sedimentary Geology, v. 56, p. 207-260.

Peterson, V.E., 1961, Farnham Dome field, *in* Preston, D., editor, A symposium of the oil and gas fields of Utah: Intermountain Association of Petroleum Geologists Guidebook, unpaginated.

Phillips, S.P., 2012, Discriminant analysis of XRF data from sandstones of like facies and appearance—a method for identifying a regional unconformity, paleotopography, and diagenetic histories: Provo, Utah, Brigham Young University, M.S. thesis, 121 p.

Phillips, S.P., and Morris, T.H., 2013, Identification of an extensive paleotopographic high on the Navajo Sandstone by surface to subsurface correlation of the Temple Cap Formation and time-equivalent portions of the Page Sandstone, *in* Morris, T.H., and Ressetar, R., editors, The San Rafael Swell and Henry Mountains Basin—geologic centerpiece of Utah: Utah Geological Association Publication 42, p. 261–278.

Phillips, S.P., Morris, T.H., Tingey, D.G., Eggett, D.L., and Zhou, W., 2015, Discriminant analysis of elemental data to differentiate formations of like facies vertically across an unconformity and laterally across a paleotopographic divide: Journal of Sedimentary Research, v. 85, no. 11, p. 1293–1309.

Picard, M.D., 1975, Facies, petrography and petroleum potential of Nugget Sandstone (Jurassic), southwestern Wyoming and northeastern Utah, *in* Bolyard, D.W., editor, Symposium on deep drilling frontiers of the central Rocky Mountains: Rocky Mountain Association of Petroleum Geologists Guidebook, p. 109–127.

Picard, M.D., 1977, Stratigraphic analysis of the Navajo Sandstone: a discussion: Journal of Sedimentary Petrology, v. 47, no. 1, p. 475–483.

Pipiringos, G.N., and O'Sullivan, R.B., 1978, Principal unconformities in Triassic and Jurassic rocks, western Interior United States—a preliminary survey: U.S. Geological Survey Professional Paper 1035-A, 29 p.

Poole, F.G., and Claypool, G.E., 1984, Petroleum source-rock potential and crude oil correlation in the Great Basin, *in* Woodward, J., Meissner, F.F., Clayton, J.L., editors, Hydrocarbon source rocks of the greater Rocky Mountain region: Rocky Mountain Association of Geologists Guidebook, p. 179–229.

Rahl, J.M., Reiners, P.W., Campbell, I.H., Nicolescu, S., and Allen, C.M., 2003, Combined single-grain (U-Th)/He and U/Pb dating detrital zircons from the Navajo Sandstone, Utah: Geology, v. 31, no. 9, p. 761–764.

Royse, F., Jr., 1993, Case of the phantom foredeep—Early Cretaceous in west-central Utah: Geology, v. 21, no. 2, p. 133–136.

Royse, F., Jr., Warner, M.A., and Reese, D.L., 1975, Thrust belt structural geometry and related stratigraphic problems, Wyoming-Idaho-northern Utah, *in* Bolyard, D.W., editor, Symposium on deep drilling frontiers of the central Rocky Mountains: Rocky Mountain Association of Geologists Guidebook, p. 41–54.

Sandberg, C.A., and Gutschick, R.C., 1984, Distribution, microfauna, and source-rock potential of the Mississippian Delle Phosphatic Member of Woodman Formation and equivalents, Utah and adjacent states, *in* Woodward, J., Meissner, F.F., and Clayton, J.L., editors, Hydrocarbon source rocks of the greater Rocky Mountain region: Rocky Mountain Association of Geologists Guidebook, p. 135–178.

Sanderson, I.D., 1974, Sedimentary structures and their environmental significance in the Navajo Sandstone, San Rafael Swell, Utah: Brigham Young University Geology Studies, v. 21, pt. 1, p. 215–246.

Schelling, D.D., Strickland, D.K., Johnson, K.R., and Vrona, J.P., 2007, Structural geology of the central Utah thrust belt, *in* Willis, G.C., Hylland, M.D., Clark, D.L., and Chidsey, T.C., Jr., editors, Central Utah—diverse geology of a dynamic landscape: Utah Geological Association Publication 36, p. 1–29.

Schenk, C.J., 1981, Porosity and textural characteristics of eolian stratification [abs.]: American Association of Petroleum Geologists Bulletin, v. 65, no. 5, p. 986.

Sorber, S.C., Morris, T.H., and Gillespie, J.M., 2007, Geologic map of the Twin Rocks quadrangle, Wayne County, Utah: Utah Geological Survey Map 07-3, 2 plates, scale 1:24,000, https://doi.org/10.34191/MP-07-3.

Sprinkel, D.A., 2006, Interim geologic map of the Dutch John 30' x 60' quadrangle, Daggett and Uintah Counties, Utah, Moffat County, Colorado, and Sweetwater County, Wyoming: Utah Geological Survey Open-File Report 491DM, 3 plates, scale 1:100,000, https://doi.org/10.34191/OFR-491dm.

Sprinkel, D.A., 2007, Interim geologic map of the Vernal 30' x 60' quadrangle, Uintah and Duchesne Counties, Utah, and Moffat and Rio Blanco Counties, Colorado: Utah Geological Survey Open-File Report 506DM, compact disc, GIS data, 3 plates, scale 1:100,000, https://doi.org/10.34191/OFR-506dm.

Sprinkel, D.A., Kowallis, B.J., Waanders, G., Doelling, H.H., and Kuehne, P.A., 2009, The Middle Jurassic Temple Cap Formation, southern Utah—radiometric age, palynology, and correlation with the Gypsum Spring Member of the Twin Creek Limestone and Harris Wash Member of the Page Sandstone [abs.]: Geological Society of America Abstracts with Programs, v. 41, no. 7, p. 690.

Sprinkel, D.A., Doelling, H.H., Kowallis, B.J., Waanders, G., and Kuehne, P.A., 2011a, Early results of a study of Middle Jurassic strata in the Sevier fold and thrust belt, Utah, *in* Sprinkel, D.A., Yonkee, W.A., and Chidsey, T.C., Jr., editors, Sevier thrust belt—northern and central Utah and adjacent areas: Utah Geological Association Publication 40, p. 151–172.

Sprinkel, D.A., Kowallis, B.J., and Jensen, P.H., 2011b, Correlation and age of the Nugget Sandstone and Glen Canyon Group, Utah, *in* Sprinkel, D.A., Yonkee, W.A., and Chidsey, T.C., Jr., editors, Sevier thrust belt—northern and central Utah and adjacent areas: Utah Geological Association Publication 40, p. 131–149.

Sprinkel, D.A., and Chidsey, T.C., Jr., 1993, Jurassic Twin Creek Limestone, *in* Hjellming, C.A., editor, Atlas of major Rocky Mountain gas reservoirs: New Mexico Bureau of Mines and Mineral Resources, p. 76.

Steele, P.A., Chan, M.A., and Wheatley, D.F., 2018, Characterization of the Jurassic Navajo Sandstone of central Utah—a potential carbon capture and sequestration reservoir [abs.]: American Association of Petroleum Geologists Annual Convention Abstracts Volume, non-pagenated.

Strickland, D., Johnson, K.R., Vrona, J.P., Schelling, D.D., and Wavrek, D.A., 2005, Structural architecture, petroleum systems, and geological implications for the Covenant field discovery, Sevier County, Utah: Online, American Association of Petroleum Geologists, Search and Discovery Article #110014, http://www.searchanddiscovery.com/pdfz/documents/2005/av/strickland/ndx_strickland.pdf.html.

Swetland, P.J., Clayton, J.L., and Sable, E.G., 1978, Petroleum source-bed potential of Mississippian-Pennsylvanian rocks in parts of Montana, Idaho, Utah, and Colorado: The Mountain Geologist, v. 14, p. 79–87.

Tabet, D.E., 2017, Chapter 9—Handling and management of water produced from oil and gas reservoirs in the Uinta Basin, *in* Chidsey, T.C., Jr., compiler and editor, Produced water in the Uinta Basin, Utah—evaluation of reservoirs, water storage aquifers, and management options: Utah Geological Survey Bulletin 138, p. 231–259, 3 plates, 7 appendices, https://doi.org/10.34191/B-138.

Tabet, D.E., and Burns, T., 1996, Drunkards Wash, *in* Bereskin, S.R., and Hill, B.G., editors, Oil and gas fields of Utah (addendum): Utah Geological Association Publication 22, unpaginated.

Utah Division of Oil, Gas and Mining, 2020, Oil and gas summary production report by field, July 2020: Online, https://oilgas.ogm.utah.gov/oilgasweb/publications/monthly-rpts-by-fld.xhtml?rptType=FLD, accessed October 2020.

Van Der Plas, L., and Tobi, A.C., 1965, A chart for judging the reliability of point counting results: American Journal of Science, v. 263, p. 87–90.

Villien, A., and Kligfield, R.M., 1986, Thrusting and synorogenic sedimentation in central Utah, *in* Peterson, J.A., editor, Paleotectonics and sedimentation in the Rocky Mountain region: American Association of Petroleum Geologists Memoir 41, p. 281–306.

Wavrek, D.A., Strickland, D., Schelling, D.D., Johnson, K.R., and Vrona, J.P., 2005, A major paradigm shift—Carboniferous versus Permian petroleum systems in the central Rocky Mountains, U.S.A. [abs.]: American Association of Petroleum Geologists Annual Convention, Official Program with Abstracts, v. 14, non-paginated.

Wavrek, D.A., Ali-Adeeb, J., Chao, J.C., Santon, L.E., Hardwick, E.A., Strickland, D.K., and Schelling, D.D., 2007, Paleozoic source rocks in the central Utah thrust belt—organic facies response to tectonic and paleoclimatic variables [abs.]: American Association of Petroleum Geologists, Rocky Mountain Section Meeting Official Program, p. 58–59.

Wavrek, D.A., Schelling, D.D., Sbarra, R., Vrona, J.P., and Johnson, K.R., 2010, Central Utah thrust belt discoveries—a tale of two hydrocarbon charges [abs.]: American Association of Petroleum Geologists, Rocky Mountain Section Meeting, Official Program with Abstracts, p. 72–73.

White, R.R., Alcock, T.J., and Nelson, R.A., 1990, Anschutz Ranch East field—U.S.A., Utah-Wyoming thrust belt, *in* Beaumont, E.A., and Foster, N.H., editors, Structural traps III, tectonic fold and fault traps: American Association of Petroleum Geologists Treatise of Petroleum Geology, Atlas of Oil and Gas Fields, v. A-25, p. 31–55.

White, S., Allis, R.G., Moore, J., Chidsey, T.C., Jr., Morgan, C.D., Gwynn, W., and Adams, M., 2003, Injection of CO_2 into an unconfined aquifer located beneath the Colorado Plateau, central Utah, USA: Proceedings Volume, Second Annual Conference on Carbon Sequestration, May 5-8, 2003, Alexandria, VA, 15 p.

White, S.P., Allis, R.G., Bergfield, D., Moore, J.N., Chidsey, T.C., Morgan, C., McClure, K., Adams, M., and Rauzi, S., 2004, Evaluating the seal integrity of natural CO_2 reservoirs of the Colorado Plateau: Proceedings Volume, Third Annual Conference on Carbon Capture and Sequestration, May 3-6, 2004, Alexandria, VA, 31 p.

White, S.P., Allis, R.G., Moore, J., Chidsey, T.C., Jr., Morgan, C., Gwynn, W., and Adams, M., 2005, Simulation of reactive transport of injected CO_2 on the Colorado Plateau, Utah, USA: Chemical Geology, v. 217, issues 3-4, p. 387–405.

Williams, R.M.E., Chidsey, T.C., Jr., and Eby, D.E., 2007, Exhumed paleochannels in central Utah—analogs for raised curvilinear features on Mars, *in* Willis, G.C., Hylland, M.D., Clark, D.L., and Chidsey, T.C., Jr., editors, Central Utah—diverse geology of a dynamic landscape: Utah Geological Association Publication 36, p. 221–235.

Willis, G.C., 1999, The Utah thrust system—an overview, *in* Spangler, L.E., editor, Geology of northern Utah and vicinity: Utah Geological Association Publication 27, p. 1–9.

Winkler, D.A., Jacobs, L.L., Congleton, J.D., and Downs, W.R., 1991, Life in a sand sea—biota from Jurassic interdunes: Geology, v. 19, p. 889.

Witkind, I.J., 1982, Salt diapirism in central Utah, *in* Nielson, D.L., editor, Overthrust belt of central Utah: Utah Geological Association Publication 10, p. 13–30.

APPENDIX A:

GAMMA-RAY SCINTILLOMETER DATA, NAVAJO SANDSTONE, EAGLE CANYON COMPOSITE MEASURED SECTION, EMERY COUNTY, UTAH

APPENDIX A:
GAMMA-RAY SCINTILLOMETER DATA, NAVAJO SANDSTONE, EAGLE CANYON COMPOSITE MEASURED SECTION, EMERY COUNTY, UTAH

UTM Coordinates: 0509581 E., 4300421 N.
ECT = Eagle Canyon Tributary

from base up Meters	Total (ppm)	K (%)	U (ppm)	Th (ppm)	Comments
206.0	11.0	1.4	2.4	3.9	small ledge, ~0.3 meters exposed, thinly bedded, limestone, crystalline on fresh surface, top of mesa, UTM Coordinates: 0509005 E., 4300173 N.
205.0	0.0	0.0	0.0	0.0	covered
204.0	0.0	0.0	0.0	0.0	covered
203.0	12.4	1.8	2.7	4.6	symmetrical ripples, trough cross-stratification (v. small, 2 to 3 meters)
202.0	0.0	0.0	0.0	0.0	covered
201.0	13.7	2.2	2.3	6.9	
200.0	10.7	1.8	2.1	4.6	
199.0	9.3	1.6	1.7	3.1	
198.0	12.2	2.2	1.2	4.4	silty dolomite (?) Jurassic Carmel Formation
197.0	13.7	2.3	2.0	5.7	covered slope
196.0	6.9	1.1	0.6	2.3	near top of Jurassic Navajo Sandstone
195.0	7.2	1.1	0.9	1.8	
194.0	7.6	1.0	1.5	3.5	
193.0	5.2	0.7	0.3	1.9	
192.0	5.6	0.8	0.6	1.8	
191.0	5.6	0.8	1.3	0.8	
190.0	5.7	0.9	0.9	1.2	
189.0	6.3	0.9	0.7	3.2	
188.0	4.8	0.6	1.1	0.5	
187.0	6.4	1.0	1.1	1.6	
186.0	6.4	1.0	1.3	1.9	
185.0	5.5	0.8	0.4	2.0	
184.0	6.6	1.1	1.0	0.6	
183.0	6.0	1.0	0.0	2.9	
182.0	6.3	1.0	0.7	1.9	
181.0	6.0	1.0	1.3	1.3	
180.0	6.6	1.2	0.5	1.8	
179.0	6.3	0.9	0.7	2.0	
178.0	5.9	0.9	0.3	1.5	
177.0	7.2	1.4	1.5	1.4	reading taken by iron-stained band
176.0	6.7	1.0	0.7	2.8	
175.0	5.8	0.9	0.5	1.4	
174.0	7.4	1.3	0.6	2.7	
173.0	6.7	1.1	1.2	0.4	
172.0	7.3	1.2	0.7	1.6	
171.0	6.8	1.2	1.4	0.4	
170.0	7.0	1.3	0.5	2.3	
169.0	6.7	1.2	0.6	1.5	
168.0	6.6	1.2	0.6	0.6	
167.0	6.9	1.3	0.9	1.0	
166.0	7.4	1.3	0.9	1.4	
165.0	7.4	1.4	0.6	2.6	
164.0	6.9	1.2	0.5	2.2	
163.0	7.5	1.3	1.2	1.4	
162.0	8.6	1.5	0.9	3.3	
161.0	9.7	1.8	1.3	1.5	
160.0	9.3	1.7	1.1	2.2	
159.0	8.8	1.6	1.0	1.5	
158.0	7.8	1.5	0.2	2.2	
157.0	6.9	1.1	1.0	1.2	
156.0	7.6	1.3	1.7	2.0	
155.0	7.1	1.3	1.0	1.1	
154.0	9.2	1.7	1.5	1.8	
153.0	9.1	1.7	1.2	3.1	
152.0	8.1	1.5	1.0	0.7	
151.0	8.2	1.5	1.2	1.0	
150.0	9.3	1.6	1.3	2.2	
149.0	10.0	1.7	1.8	2.3	
148.0	9.2	1.7	1.5	1.6	
147.0	8.6	1.8	0.7	1.1	
146.0	8.1	1.5	1.1	1.8	
145.0	7.8	1.4	1.3	2.0	zone of deformation bands located here
144.0	8.4	1.6	0.9	1.4	
143.0	8.3	1.5	0.9	1.4	
142.0	8.4	1.5	1.0	2.4	
141.0	8.1	1.4	1.6	1.6	
140.0	7.6	1.3	1.2	1.2	
139.0	7.6	1.4	1.1	1.4	
138.0	6.9	1.2	0.5	1.9	
137.0	6.7	1.1	0.8	2.2	
136.0	6.1	1.2	0.2	1.7	
135.0	6.2	1.0	1.0	1.5	
134.0	7.6	1.3	0.6	1.9	
133.0	7.1	1.2	1.3	1.9	
132.0	7.9	1.5	0.6	2.2	
131.0	7.6	1.3	1.0	2.2	
130.0	6.9	1.1	1.4	1.6	
129.0	7.2	1.2	0.4	2.5	
128.0	6.5	1.1	0.6	2.2	
127.0	7.3	1.3	0.6	1.8	
126.0	7.0	1.1	1.5	1.2	
125.0	6.8	1.1	1.1	0.4	
124.0	7.1	1.3	1.0	0.6	
123.0	7.1	1.2	0.8	1.8	
122.0	7.5	1.3	0.7	2.2	
121.0	7.2	1.3	0.6	2.0	
120.0	6.9	1.1	0.9	0.8	
119.0	7.0	1.3	0.6	1.9	
118.0	7.1	1.2	0.8	2.3	
117.0	6.4	1.1	0.2	1.9	
116.0	6.1	1.0	0.8	1.0	
115.0	6.8	1.2	0.2	2.3	
114.0	6.3	1.1	0.4	2.0	
113.0	6.7	1.0	1.5	1.6	
112.0	6.8	1.1	0.5	2.2	

from base up Meters	Total (ppm)	K (%)	U (ppm)	Th (ppm)	Comments
111.0	6.7	1.0	0.7	1.8	
110.0	7.3	1.4	1.0	1.1	
109.0	6.1	1.1	0.9	1.6	
108.0	6.7	1.1	0.9	1.2	
107.0	7.1	1.4	0.7	2.5	unit ECT 18
106.0	11.4	1.8	1.5	6.2	
105.0	10.5	1.8	1.9	3.8	UTM Coordinates: 0509270 E., 4300072 N., ± 5 meters
104.0	10.3	1.7	1.6	4.3	unit ECT 17
103.0	11.5	1.8	1.5	5.8	into unit ECT 17
102.0	9.0	1.5	0.6	2.2	very top of unit ECT 16
101.0	7.6	1.3	0.7	2.7	near end of unit ECT 16 ECI
100.0	8.6	1.5	0.5	2.6	
99.0	9.0	1.7	0.9	2.3	
98.0	8.7	1.6	1.1	1.6	
97.0	7.8	1.6	0.1	1.7	
96.0	7.8	1.4	0.6	1.8	
95.0	7.2	1.4	0.1	1.5	
94.0	7.4	1.3	0.9	2.0	
93.0	7.7	1.3	0.7	2.9	
92.0	7.7	1.3	0.8	1.9	
91.0	8.2	1.6	0.6	1.5	
90.0	7.5	1.4	1.3	0.7	
89.0	7.4	1.4	0.8	1.4	
88.0	7.5	1.1	0.9	2.2	
87.0	8.0	1.6	0.7	1.8	
86.0	8.0	1.3	0.7	2.2	
85.0	7.6	1.3	0.9	2.6	
84.0	6.7	1.3	0.1	2.1	
83.0	7.5	1.5	0.4	1.9	
82.0	7.8	1.5	0.7	2.3	
81.0	7.2	1.1	1.0	2.6	
80.0	7.5	1.3	0.7	1.6	
79.0	6.6	1.1	0.9	0.8	
78.0	7.5	1.5	0.6	1.3	
77.0	7.1	1.1	0.9	2.6	in covered area unit ECT 16, last of cross-bedding
76.0	0.0	0.0	0.0	0.0	pickup "contorted bedding"
75.0	0.0	0.0	0.0	0.0	
74.0	0.0	0.0	0.0	0.0	
73.0	0.0	0.0	0.0	0.0	
72.0	8.0	1.4	1.6	0.6	
71.0	7.9	1.4	1.4	1.6	
70.0	7.9	1.3	1.1	1.8	
69.0	8.2	1.6	0.9	1.8	
68.0	6.7	1.1	0.5	1.6	
67.0	6.8	1.2	1.0	1.2	
66.0	5.5	1.0	0.7	1.1	
65.0	7.1	1.2	1.1	2.3	heavily iron-stained cross-beds, deep red/rusty color
64.0	6.8	1.2	0.5	2.3	
63.0	6.0	1.0	0.6	0.8	
62.0	7.1	1.4	0.8	1.1	
61.0	7.4	1.4	0.8	1.4	
60.0	6.6	1.2	0.7	1.0	
59.0	8.2	1.6	1.1	1.0	
58.0	12.4	2.4	1.4	1.5	brown siltstone, unit ECT 16, 0.6 meters thick, variable interfingering with overyling unit
57.5	11.7	2.5	1.0	2.0	0.3 meters below overlying siltstone
57.0	11.0	2.5	0.8	1.2	sandstone
56.5	10.4	2.2	0.8	1.3	sandstone
56.0	11.6	2.4	0.9	2.5	sandstone
55.5	11.5	2.4	0.8	2.9	unit ECT 15, sandstone
55.0	10.6	2.2	0.7	2.5	sandstone
54.5	14.2	2.8	2.5	3.1	green siltstone interbed
54.0	10.8	2.0	1.0	2.5	unit ECT 15, sandstone in thin green siltstone interbeds
53.5	14.9	2.9	1.7	4.2	unit ECT 14
53.0	13.3	2.6	1.4	3.6	top of unit ECT 13, 1.9 meters thick, concretion sandstone at top
52.5	12.4	2.6	1.4	3.0	
52.0	11.5	2.3	1.2	2.5	
51.5	11.3	2.4	1.3	1.8	unit ECT 13, 0.4 meters above base of unit ECT 13
51.0	9.7	1.8	1.1	2.7	unit ECT 12, brown bed, iron stone, 0.3 meters thick
50.5	9.7	1.8	0.8	2.5	0.2 meters below top of unit ECT 11
50.0	10.1	1.9	1.3	2.1	
49.5	9.4	1.8	1.1	1.7	
49.0	8.4	1.7	1.0	1.9	
48.5	10.0	2.0	1.6	1.4	
48.0	9.8	2.0	0.8	1.1	
47.5	9.8	1.9	0.6	1.8	
47.0	9.1	1.9	1.2	1.0	continuing in alcove, unit ECT 11
46.5	9.4	2.0	1.2	2.1	
46.0	9.8	1.9	1.0	1.5	
45.5	9.7	1.8	0.8	2.1	
45.0	8.6	1.8	0.6	1.1	
44.5	8.6	1.7	1.0	0.8	
44.0	8.1	1.7	0.8	1.0	
43.5	8.6	1.8	1.2	1.8	
43.0	8.6	1.7	0.4	2.1	
42.5	8.2	1.6	1.2	1.2	
42.0	8.7	1.7	0.9	1.7	
41.5	8.3	1.8	0.7	1.5	
41.0	8.5	1.7	0.6	1.9	
40.5	8.6	1.7	1.3	1.1	
40.0	8.8	1.4	1.7	1.9	
39.5	8.6	1.6	1.3	1.4	in alcove of unit ECT 11
39.0	7.7	1.4	0.9	1.8	unit ECT 11, bed capping unit ECT 10 locally
38.5	8.8	1.6	0.9	2.1	0.2 meters above base, unit ECT 11
38.0	8.6	1.7	1.3	2.5	0.3 meters below top of unit ECT 10, 4.3 meters thick
37.5	9.4	1.8	1.1	1.1	
37.0	9.2	1.7	1.0	1.4	
36.5	9.2	1.7	1.8	0.8	
36.0	9.5	1.8	1.0	2.1	
35.5	9.5	1.9	1.0	2.2	
35.0	10.8	2.2	1.3	1.1	
34.5	11.4	2.3	0.7	2.4	
34.0	11.2	2.2	1.1	1.4	unit ECT 10, bed capping unit ECT 9 locally

from base up Meters	Total (ppm)	K (%)	U (ppm)	Th (ppm)	Comments
33.5	16.4	3.6	1.3	4.1	very top of bed, unit ECT 10, bounding surface
33.0	13.2	2.6	1.3	3.8	
32.5	12.3	2.3	0.9	3.3	
32.0	13.0	2.5	1.2	2.5	
31.5	11.8	2.3	1.2	3.7	
31.0	12.3	2.4	1.5	3.0	
30.5	11.8	2.2	1.3	3.3	
30.0	10.1	1.9	0.9	2.6	
29.5	12.3	2.3	1.7	3.1	unit ECT 9
29.0	15.2	2.8	1.6	5.6	base of unit ECT 10
28.5	0.0	0.0	0.0	0.0	base of unit ECT 10, covered
28.0	0.0	0.0	0.0	0.0	unit ECT 9, covered
27.5	0.0	0.0	0.0	0.0	unit ECT 9, covered
27.0	0.0	0.0	0.0	0.0	unit ECT 9, covered slope, 1.4 meters thick covered
26.5	8.2	1.2	1.5	1.4	unit ECT 8, top of brown bed
26.0	10.7	2.1	1.7	1.8	unit ECT 8, brown bed
25.5	11.3	1.9	1.7	3.8	top of unit ECT 7
25.0	14.7	2.8	1.9	5.4	
24.5	16.5	3.6	1.4	4.7	
24.0	15.3	3.2	1.4	3.3	
23.5	12.5	2.4	1.9	3.4	
23.0	11.4	2.0	0.8	3.1	
22.5	11.0	2.2	1.0	1.5	
22.0	10.4	2.0	0.9	1.9	
21.5	10.2	1.9	1.4	1.2	
21.0	9.7	1.8	1.5	1.4	
20.5	10.9	2.1	1.2	2.9	
20.0	9.6	1.8	0.7	2.6	ledge
19.5	11.4	2.4	1.3	1.8	
19.0	11.4	2.5	0.9	2.2	
18.5	12.1	2.4	0.5	3.4	
18.0	13.8	2.9	1.4	2.9	
17.5	12.0	2.4	1.4	1.9	
17.0	11.6	2.3	1.2	2.9	
16.5	11.8	2.3	1.0	2.6	
16.0	12.5	2.5	1.7	3.1	
15.5	11.3	2.3	0.7	2.8	
15.0	11.8	2.6	1.1	1.3	
14.5	11.7	2.4	0.7	1.7	
14.0	13.1	2.7	1.3	2.9	
13.5	11.8	2.3	1.5	2.5	
13.0	10.1	1.9	0.9	1.8	
12.5	9.5	1.8	0.7	2.7	
12.0	10.1	1.9	1.3	1.4	
11.5	11.2	2.2	0.8	2.9	
11.0	12.3	2.6	1.1	2.8	
10.5	12.0	2.5	0.2	4.7	
10.0	10.1	2.0	0.6	2.1	unit ECT 7, UTM Cooridinates: 0509568 E., 4300268 N.
9.7	10.8	2.1	0.6	3.8	unit ECT 6, brown bed
9.0	12.2	2.6	1.8	2.7	unit ECT 5, sandstone
8.5	11.7	2.4	1.5	2.1	unit ECT 5, sandstone
8.0	11.3	2.3	1.4	1.9	unit ECT 5
7.5	11.6	2.4	1.0	2.6	
7.0	11.5	2.4	1.2	2.5	
6.5	10.8	2.1	1.1	3.3	unit ECT 5
6.3	11.8	2.1	2.3	2.8	brown stain, unit ECT 4
6.2	10.6	2.0	1.2	1.8	unit ECT 3
6.0	12.6	2.5	1.5	2.1	
5.4	11.4	2.4	0.8	2.9	
4.8	11.6	2.4	1.9	1.7	
4.2	11.8	2.4	1.3	2.9	
3.6	11.3	2.3	1.5	1.8	unit ECT 3
3.0	11.4	2.3	1.1	1.9	unit ECT 3
2.4	11.2	2.0	2.0	2.6	unit ECT 3
1.8	12.5	2.5	1.3	3.4	unit ECT 2, thin, brown
1.2	9.9	2.0	0.9	1.8	unit ECT 1
0.5	12.6	2.6	1.1	2.8	unit ECT 1
0.0	10.9	1.9	1.6	2.2	unit ECT 0, Jurassic Kayenta Formation

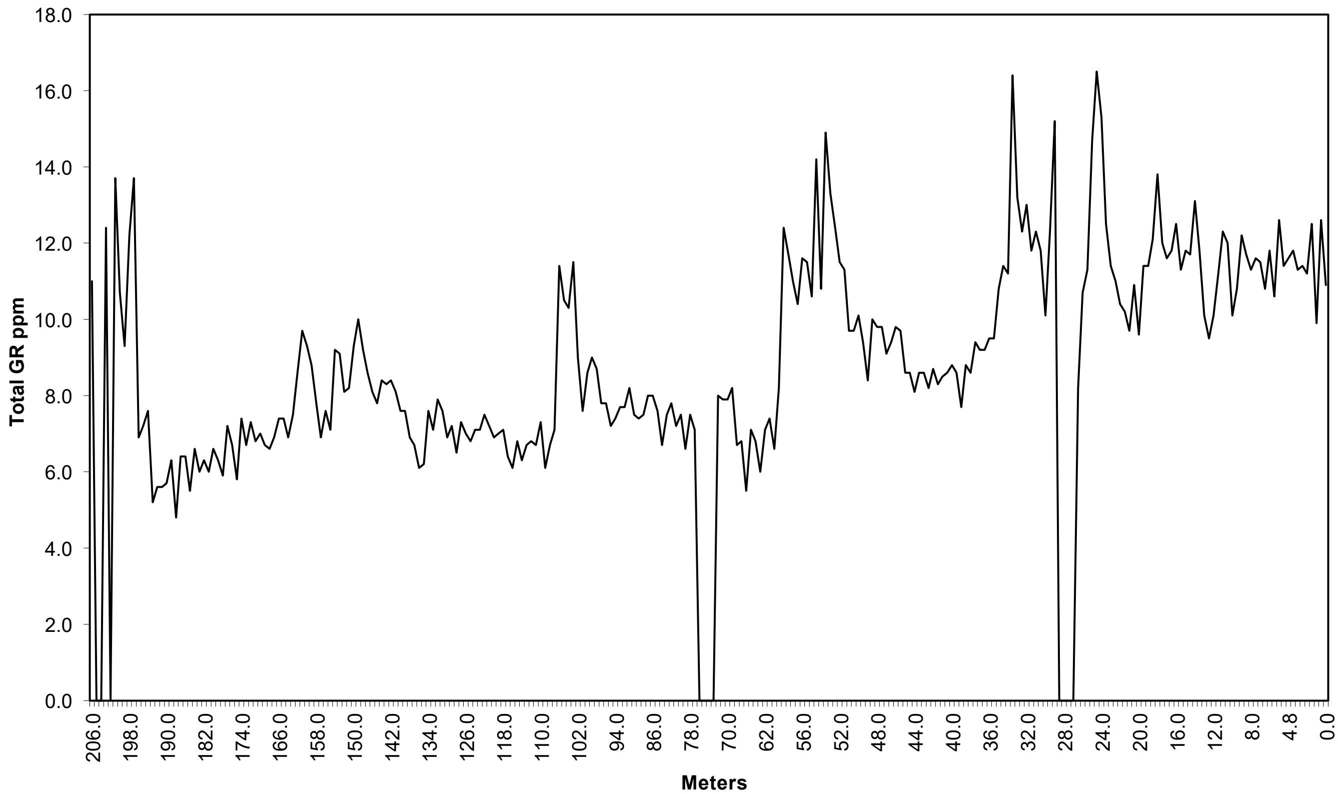

Total GR ppm
18.0
16.0
14.0
12.0
10.0
8.0
6.0
4.0
2.0
0.0
206.0
198.0
190.0
182.0
174.0
166.0
158.0
150.0
142.0
134.0
126.0
118.0
110.0
102.0
94.0
86.0
78.0
70.0
62.0
56.0
52.0
48.0
44.0
40.0
36.0
32.0
28.0
24.0
20.0
16.0
12.0
8.0
4.8
0.0
Meters

APPENDIX B:

CORE PHOTOGRAPHS, NAVAJO SANDSTONE, FEDERAL NO. 17-3 WELL, COVENANT FIELD, SEVIER COUNTY, UTAH

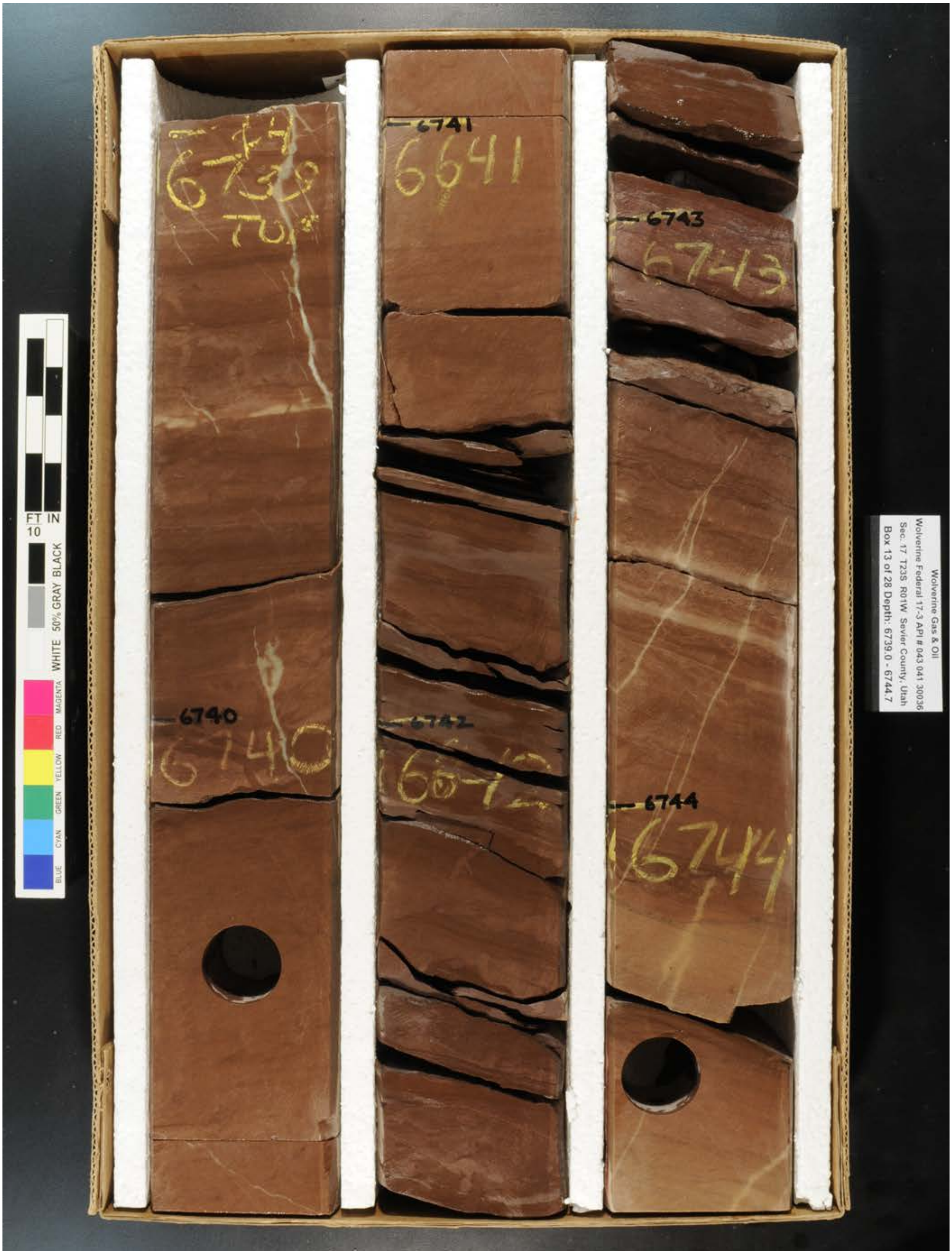
Wolverine Gas & Oil
Wolverine Federal 17-3 API # 043 041 30036
Sec. 17 T23S R01W Sevier County, Utah
Box 13 of 28 Depth: 6739.0 - 6744.7
FT IN
10
BLACK 50% GRAY WHITE
MAGENTA RED YELLOW GREEN CYAN BLUE
6739
6740
6741
6742
6743
6744

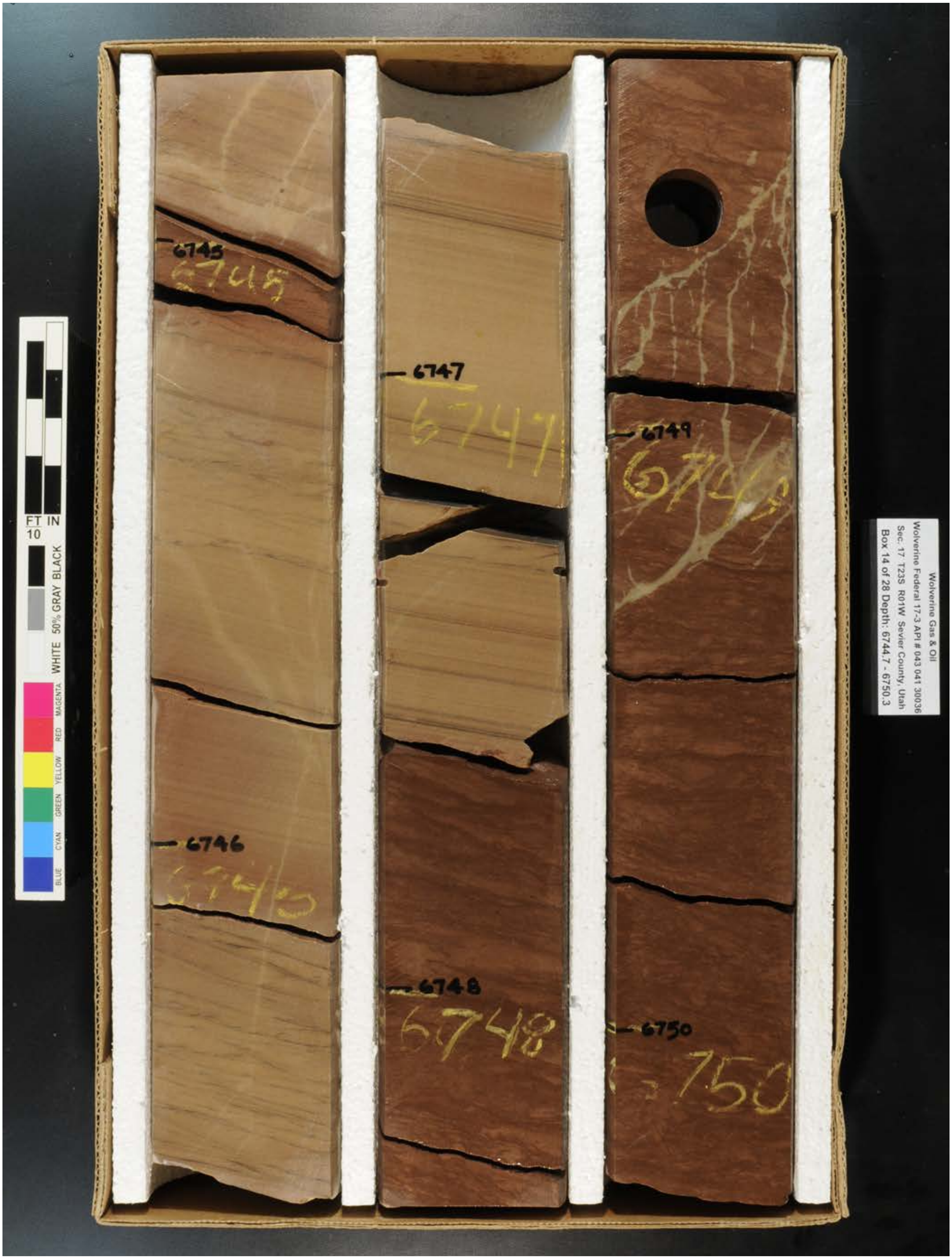
6745
6746
6747
6748
6749
6750
FT IN
10
WHITE 50% GRAY BLACK
BLUE CYAN GREEN YELLOW RED MAGENTA
Wolverine Gas & Oil
Wolverine Federal 17-3 API # 043 041 300036
Sec. 17 T23S R01W Sevier County, Utah
Box 14 of 28 Depth: 6744.7 - 6750.3

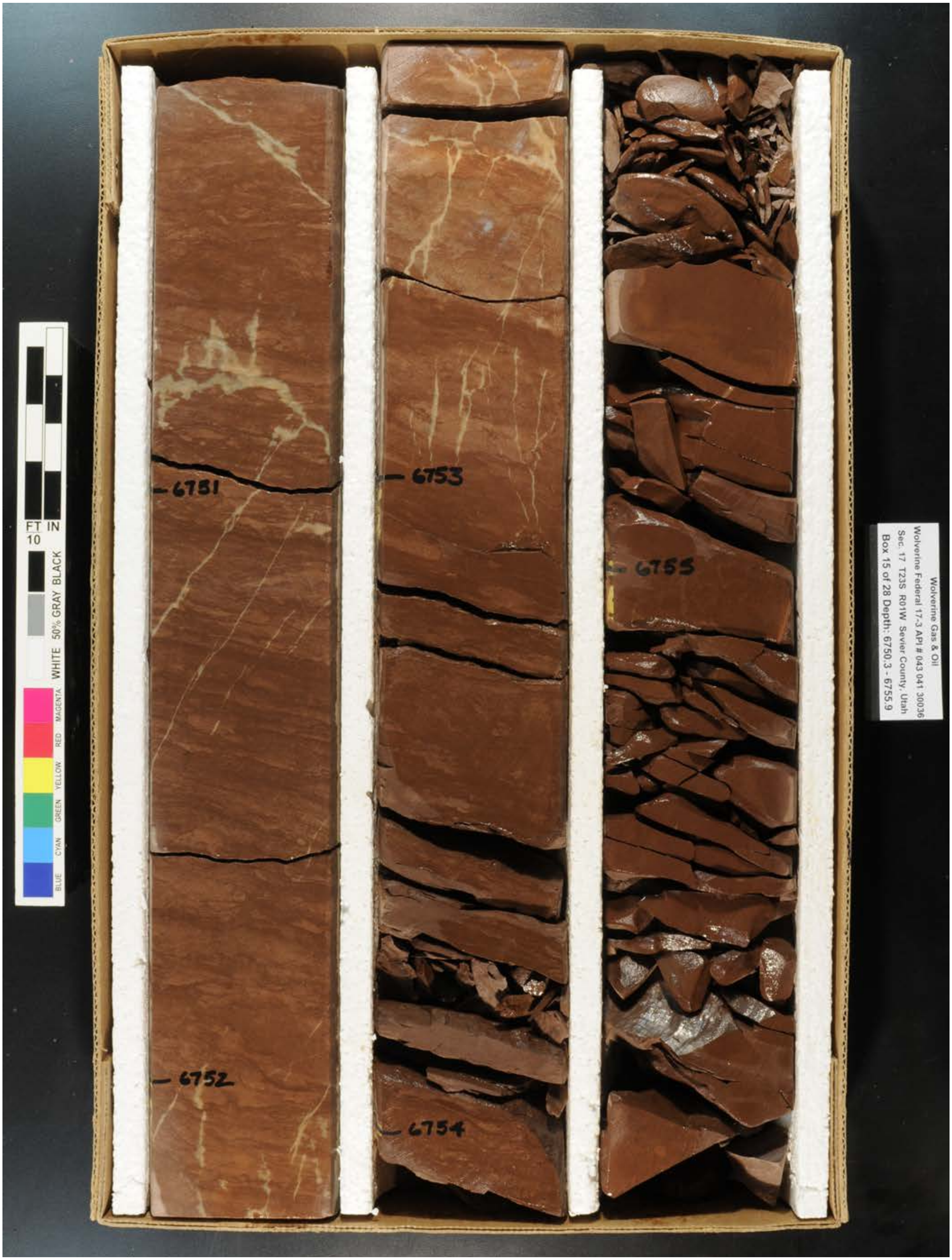
Wolverine Gas & Oil
Wolverine Federal 17-3 API # 043 041 30036
Sec. 17 T23S R01W Sevier County, Utah
Box 15 of 28 Depth: 6750.3 - 6755.9
6751
6752
6753
6754
6755
FT IN
10
WHITE 50% GRAY BLACK
BLUE CYAN GREEN YELLOW RED MAGENTA

6756
6758
6757
FT IN
10
WHITE 50% GRAY BLACK
BLUE CYAN GREEN YELLOW RED MAGENTA
Wolverine Gas & Oil
Wolverine Federal 17-3 API # 043 041 30036
Sec. 17 T23S R01W Sevier County, Utah
Box 16 of 28 Depth: 6755.9 - 6761.7

FT IN
10
WHITE 50% GRAY BLACK
BLUE CYAN GREEN YELLOW RED MAGENTA
6764
6763
6765
6766
6767
Wolverine Gas & Oil
Wolverine Federal 17-3 API # 043 041 30036
Sec. 17 T23S R01W Sevier County, Utah
Box 17 of 28 Depth: 6761.7 - 6767.4

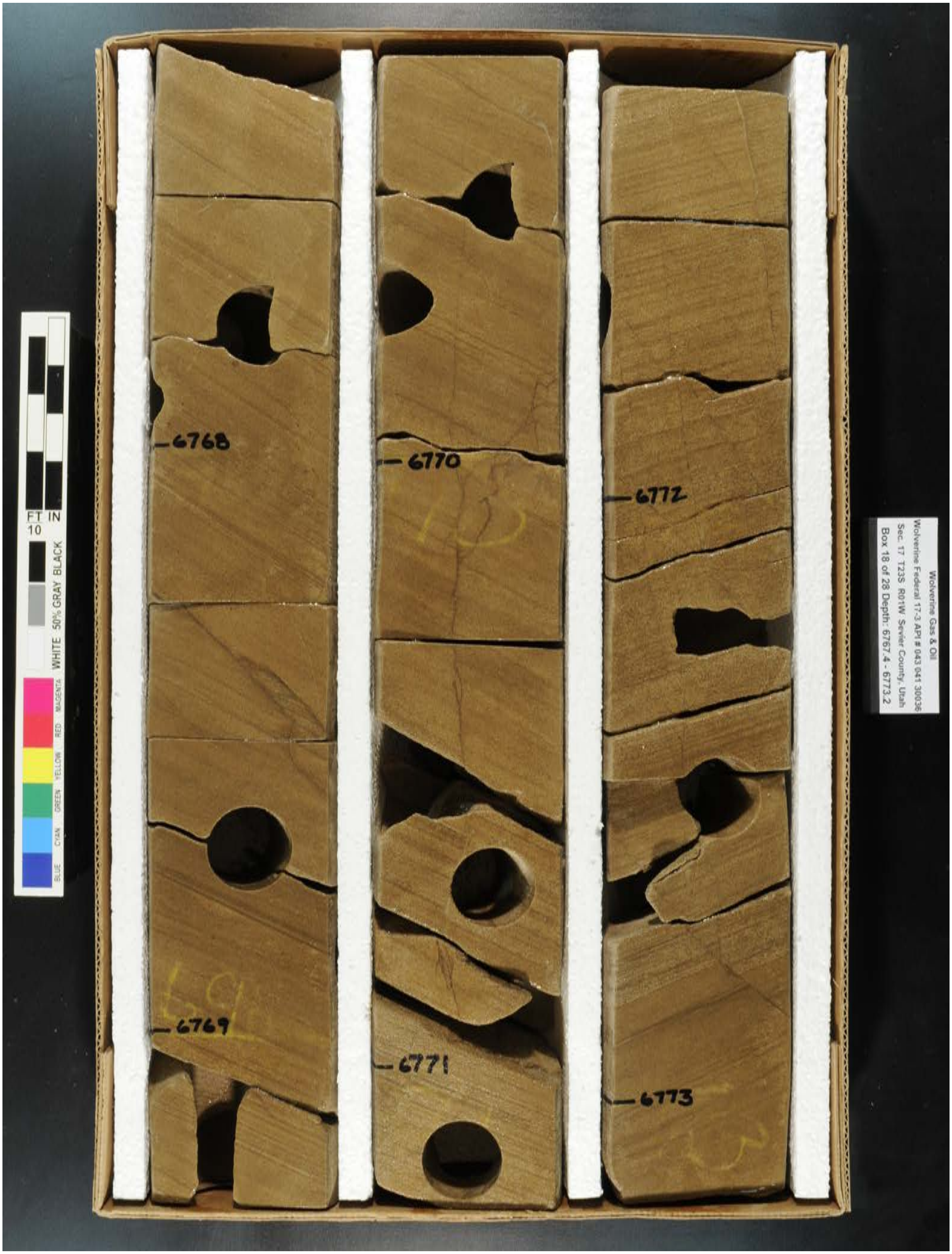
6768
6769
6770
6771
6772
6773
FT IN
10
WHITE 50% GRAY BLACK
BLUE CYAN GREEN YELLOW RED MAGENTA
Wolverine Gas & Oil
Wolverine Federal 17-3 API # 043 041 30036
Sec. 17 T23S R01W Sevier County, Utah
Box 18 of 28 Depth: 6767.4 - 6773.2

6775
6774
6776
6778
FT IN
10
BLACK
50% GRAY
WHITE
MAGENTA
RED
YELLOW
GREEN
CYAN
BLUE
Wolverine Gas & Oil
Wolverine Federal 17-3 API # 043 041 30036
Sec. 17 T23S R01W Sevier County, Utah
Box 19 of 28 Depth: 6773.2 - 6778.9

FT IN
10
WHITE 50% GRAY BLACK
BLUE CYAN GREEN YELLOW RED MAGENTA
6780
6781
6782
6783
6784
Wolverine Gas & Oil
Wolverine Federal 17-3 API # 043 041 30036
Sec. 17 T23S R01W Sevier County, Utah
Box 20 of 28 Depth: 6778.9 - 6784.7

-6785
-6786
-6787
-6788
-6789
-6790
FT IN
10
WHITE 50% GRAY BLACK
BLUE CYAN GREEN YELLOW RED MAGENTA
Wolverine Gas & Oil
Wolverine Federal 17-3 API # 043 041 30036
Sec. 17 T23S R01W Sevier County, Utah
Box 21 of 28 Depth: 6784.7 - 6790.6

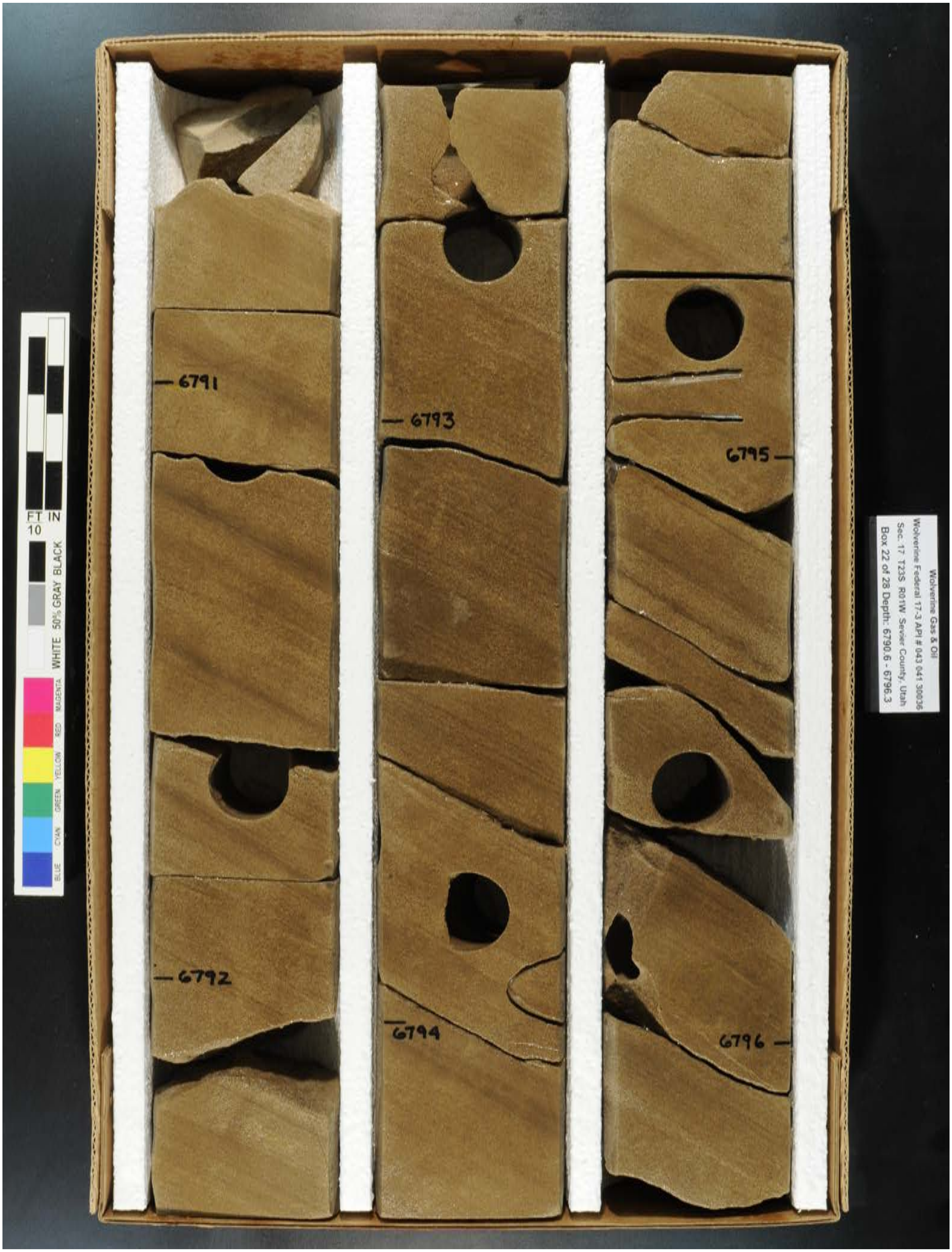

FT IN
10
WHITE 50% GRAY BLACK
BLUE CYAN GREEN YELLOW RED MAGENTA
6791
6792
6793
6794
6795
6796
Wolverine Gas & Oil
Wolverine Federal 17-3 API # 043 041 30036
Sec. 17 T23S R01W Sevier County, Utah
Box 22 of 28 Depth: 6790.6 - 6796.3


Wolverine Gas & Oil
Wolverine Federal 17-3 API # 043 041 30036
Sec. 17 T23S R01W Sevier County, Utah
Box 23 of 28 Depth: 6796.3 - 6802.6
FT IN
10
WHITE 50% GRAY BLACK
BLUE CYAN GREEN YELLOW RED MAGENTA
6797
6798
6799
6800
6801
6802


-6803
6805
-6806
-6807
-6808
FT IN
10
WHITE 50% GRAY BLACK
BLUE CYAN GREEN YELLOW RED MAGENTA
Wolverine Gas & Oil
Wolverine Federal 17-3 API # 043 041 30036
Sec. 17 T23S R01W Sevier County, Utah
Box 24 of 28 Depth: 6802.6 - 6808.5


TOP
6809
6810
6811
6812
FT IN
10
WHITE 50% GRAY BLACK
BLUE CYAN GREEN YELLOW RED MAGENTA
Wolverine Gas & Oil
Wolverine Federal 17-3 API # 043 041 30036
Sec. 17 T23S R01W Sevier County, Utah
Box 25 of 28 Depth: 6808.5 - 6814.0
BOT

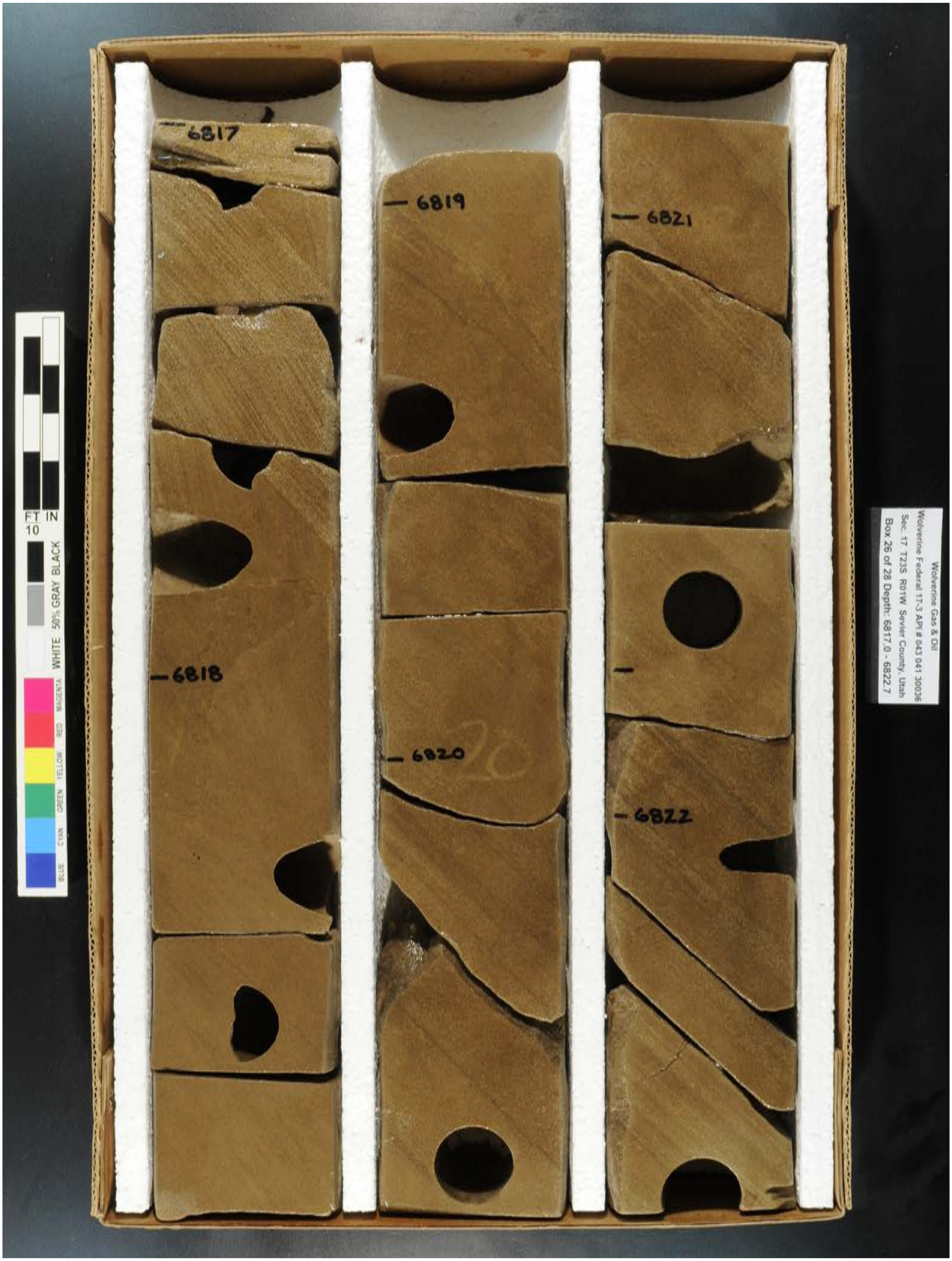
6817
6818
6819
6820
6821
6822
FT IN
10
WHITE 50% GRAY BLACK
BLUE CYAN GREEN YELLOW RED MAGENTA
Wolverine Gas & Oil
Wolverine Federal 17-3 API # 043 041 30036
Sec. 17 T23S R01W Sevier County, Utah
Box 26 of 28 Depth: 6817.0 - 6822.7


6823
6826
6827
FT IN
10
WHITE 50% GRAY BLACK
BLUE CYAN GREEN YELLOW RED MAGENTA
Wolverine Gas & Oil
Wolverine Federal 17-3 API # 043 041 30036
Sec. 17 T23S R01W Sevier County, Utah
Box 27 of 28 Depth: 6822.7 - 6828.7


6829
6830
6831
FT IN
10
WHITE 50% GRAY BLACK
BLUE CYAN GREEN YELLOW RED MAGENTA
Wolverine Gas & Oil
Wolverine Federal 17-3 API # 043 041 30036
Sec. 17 T23S R01W Sevier County, Utah
Box 28 of 28 Depth: 6828.7 - 6833.5

APPENDIX C:

CORE POROSITY AND PERMEABILITY DATA, NAVAJO SANDSTONE, FEDERAL NO. 17-3 WELL, COVENANT FIELD, SEVIER COUNTY, UTAH

APPENDIX C: CORE POROSITY AND PERMEABILITY DATA, NAVAJO SANDSTONE, FEDERAL NO. 17-3 WELL COVENANT FIELD, SEVIER COUNTY, UTAH

Well Location: SENW SEC. 17, T. 23 S., R. 1 W., SLBL&M

Depth (ft)	Orientation	Permeability at 1400 psi NCS* millidarcys to air	Porosity at 1400 psi* NCS, percent	Depth (ft)	Orientation	Permeability at 1400 psi NCS* millidarcys to air	Facies‡
6757.70	Horizontal	0.008	3.3	6757.90	Vertical	0.013	WAM
6758.60	Horizontal	0.041	8.2	6758.90	Vertical	0.041	WAM
6759.40	Horizontal	0.064	9.7	6759.90	Vertical	0.106	SAM
6760.40	Horizontal	0.749	13.6	6760.70	Vertical	0.052	SAM
6761.50	Horizontal	0.323	12.8	6761.90	Vertical	0.257	SAM
6763.50	Horizontal	0.016	6.3	6763.55	Vertical	0.013	SAM
6764.40	Horizontal	0.010	4.5	6764.10	Vertical	0.009	SAM
6765.50	Horizontal	0.897	8.2	6765.40	Vertical	16.300	STC
6766.40	Horizontal	6.340	12.4	6766.30	Vertical	15.800	RWE
6767.80	Horizontal	43.400	13.9	6767.70	Vertical	19.200	LTC
6768.70	Horizontal	59.000	13.9	6768.40	Vertical	61.400	LTC
6769.50	Horizontal	18.200	13.5	6769.20	Vertical	3.230	LTC
6770.80	Horizontal	35.100	10.5	6770.20	Vertical	28.400	LTC
6771.60	Horizontal	39.700	15.4	6771.30	Vertical	46.100	LTC
6772.50	Horizontal	79.100	11.9	6772.40	Vertical	1.080	LTC
6773.50	Horizontal	149.000	14.8	6773.40	Vertical	14.000	LTC
6774.50	Horizontal	65.200	14.5	6774.40	Vertical	37.300	LTC
6775.30	Horizontal	33.400	15.1	6775.20	Vertical	7.570	LTC
6776.40	Horizontal	10.200	15.0	6776.50	Vertical	22.000	LTC
6777.50	Horizontal	136.000	14.8	6777.20	Vertical	49.200	LTC
6778.50	Horizontal	135.000	14.7	6778.10	Vertical	33.700	LTC
6779.30	Horizontal	57.200	14.0	6779.50	Vertical	68.200	LTC
6781.40	Horizontal	113.000	14.0	6781.30	Vertical	14.200	LTC
6782.30	Horizontal	166.000	14.4	6782.40	Vertical	13.800	LTC
6783.50	Horizontal	44.500	16.3	6783.40	Vertical	1.210	LTC
6784.60	Horizontal	36.400	15.0	6784.40	Vertical	2.510	LTC
6785.60	Horizontal	33.000	12.8	6785.50	Vertical	14.300	LTC
6786.60	Horizontal	69.400	16.9	6786.20	Vertical	53.400	LTC
6787.50	Horizontal	39.500	13.8	6787.30	Vertical	29.500	LTC
6788.40	Horizontal	14.800	12.9	6788.80	Vertical	35.700	LTC
6789.70	Horizontal	91.400	16.6	6789.30	Vertical	40.000	LTC
6790.50	Horizontal	25.600	12.9	6790.50	Vertical	20.100	LTC

Depth (ft)	Orientation	Permeability at 1400 psi NCS* millidarcys to air	Porosity at 1400 psi* NCS, percent	Depth (ft)	Orientation	Permeability at 1400 psi NCS* millidarcys to air	Facies‡
6791.50	Horizontal	59.400	13.3	6790.80	Vertical	36.000	LTC
6792.80	Horizontal	74.600	15.1	6792.50	Vertical	63.900	LTC
6793.80	Horizontal	59.800	13.6	6793.60	Vertical	52.200	LTC
6794.80	Horizontal	166.000	16.9	6794.60	Vertical	34.100	LTC
6795.50	Horizontal	181.000	16.8	6795.10	Vertical	34.600	LTC
6796.70	Horizontal	41.300	12.9	6796.90	Vertical	64.100	LTC
6798.40	Horizontal	35.600	12.9	6798.50	Vertical	32.900	LTC
6799.50	Horizontal	70.300	14.0	6799.40	Vertical	3.500	LTC
6800.50	Horizontal	194.000	16.8	6800.90	Vertical	49.800	LTC
6802.50	Horizontal	59.400	12.3	6802.10	Vertical	19.600	LTC
6803.80	Horizontal	213.000	12.9	6803.50	Vertical	38.200	LTC
6805.20	Horizontal	48.800	12.1	6805.70	Vertical	20.900	LTC
6806.50	Horizontal	83.800	12.0	6806.40	Vertical	15.700	LTC
6807.40	Horizontal	101.000	14.2	6807.70	Vertical	58.000	LTC
6808.60	Horizontal	258.000	15.9	6808.20	Vertical	114.000	LTC
6809.50	Horizontal	104.000	15.0	6809.20	Vertical	70.200	LTC
6810.50	Horizontal	22.600	12.5	6810.40	Vertical	55.000	LTC
6811.60	Horizontal	15.400	13.2	6811.90	Vertical	37.700	LTC
6812.40	Horizontal	19.300	13.8	6812.30	Vertical	23.500	LTC
6813.50	Horizontal	198.000	15.2	6813.70	Vertical	28.800	LTC
6817.50	Horizontal	64.800	16.6	6817.40	Vertical	91.400	LTC
6818.50	Horizontal	44.800	15.5	6818.70	Vertical	36.700	LTC
6819.60	Horizontal	110.000	16.5	6819.90	Vertical	42.900	LTC
6820.60	Horizontal	192.000	17.4	6820.90	Vertical	144.000	LTC
6821.80	Horizontal	66.200	15.6	6821.70	Vertical	103.000	LTC
6822.80	Horizontal	166.000	15.9	6822.70	Vertical	34.000	LTC
6823.50	Horizontal	68.400	15.6	6823.40	Vertical	71.300	LTC
6824.50	Horizontal	88.100	14.2	6824.60	Vertical	75.200	LTC
6825.90	Horizontal	97.000	11.8	6825.20	Vertical	15.000	LTC
6826.40	Horizontal	3.480	10.2	6826.80	Vertical	3.240	LTC
6827.30	Horizontal	1210.000	17.6	6827.50	Vertical	30.000	STC
6828.60	Horizontal	3.230	8.4	6828.50	Vertical	0.143	STC
6829.80	Horizontal	75.000	13.1	6829.10	Vertical	59.300	STC
6830.40	Horizontal	255.000	16.8	6830.60	Vertical	256.000	RWE
6831.50	Horizontal	205.000	16.8	6831.80	Vertical	174.000	RWE

* psi NCS = pounds per square inch, Net Confining Stress

‡ Facies: WAM = Wavy Algal Mat, SAM = Sandy Algal Mat, STC = Small Trough Cross-Stratification, LTC = Large Trough Cross-Stratified, RWE = Reworked Eolian

Plate 1
Utah Geological Survey Special Study 167
Surface to Subsurface Reservoir/Aquifer Characterization
and Facies Analysis of the Jurassic Navajo Sandstone, Central Utah

CORE DESCRIPTION, FEDERAL NO. 17-3 WELL, COVENANT FIELD, SEVIER COUNTY, UTAH

Unit #	Nature of Basal Contact	Measured Depth (m)	Lithology	Sedimentary Structures	Facies	Notes
21	Sharp	6756, 6757		Core Continues Sinawava Member, Temple Cap Formation		red-brown color
20					WAM	
19				dark band of wispy/ wavy black laminae	WAM	incipient WAM facies(?)
18		6758			WAM	continued light color deformation bands(?) fractures
17		6759, 6760, 6761, 6762		medium angle foreset lamination lamination (foreset) break in last wispy laminae (fluidized?)	SAM	fractures, deformation bands stylolitic in nature – tectonic movement along surface makes slickenside-like soapy texture cross-cut by deformation band(?) or duel fracture zone lighter in color fracture swarm
16		6763, 6764		last wispy laminae, candidate hiatus (J-1 unconformity?) upper fine wispy laminae (thin - wrinkle) = algal influence candidate for J-1 unconformity	SAM	dark banded zone – wet time of erg, possible marine encroachment (glauconite [green] grain found at 6763.5 ft)
15		6765			STC	calcrete(?) that has been dolomitized(?)
14		6766		upper fine sandstone, massive (non-descript)	RWE	
13	Sharp Sharp	6767, 6768, 6769, 6770, 6771, 6772, 6773, 6774		two avalanche sets upper fine to upper medium sandstone upper fine to upper medium sandstone only 3 ft but begins and ends with high angle trough cross-stratification high angle trough cross-stratification dune to dune contact	LTC trans-itioning to STC LTC trans-itioning to STC	slightly steeper laminae relative to deformation band
12		6775, 6776		depositional lamination is near horizonal–dune toe dune toe(?)	LTC	deformation band(?), vertical fracture swarm inclined fracture swarm
11	Sharp Slightly sharp (not knife edge – a bit fuzzy)	6777, 6778, 6779, 6780, 6781, 6782, 6783, 6784, 6785, 6786		candidate for exposure surface bimodal grain size is obvious bimodal grain size is obvious bimodal grain size is obvious slight change in foreset lamination good toe of dune	LTC	inclined fracture swarm, bitumen stained open fault conjugate fractures
10		6787, 6788, 6789, 6790, 6791, 6793, 6794, 6795, 6796, 6797		alternating finer and coarser bands no dune toes observable here	LTC	open fracture
9					STC(?)	fragments with different orientation, suspect something structural here
8		6798, 6799, 6800, 6801, 6802, 6803, 6804, 6805, 6806		fine grained avalanche(?) band deposits avalanche band toe of dune	LTC	deformation band(?), fractures
7		6807, 6808, 6809, 6810, 6811, 6812, 6813, 6814		bimodal lamination is obvious	LTC	deformation bands fracture mosaic (chicken wire)
		6815, 6816		planar lamination (toe of dune)	(?)	no core fault(?)
6		6817		bimodal grain size from upper fine to upper medium massive		
5		6818, 6819			LTC	conjugate fracture set – one en echelon; one inclined (closed fractures)
4		6820, 6823, 6824, 6825, 6826, 6827		bimodal lamination from upper fine and upper medium good toe of dune	LTC	
3		6828, 6829, 6830		high angle trough cross-stratification	STC	
2	Sharp	6831		massive bedded upper fine sandstone with two laminee of upper medium sandstone	RWE	
1		6832, 6833		indication of planar lamination chunks of sandstone; one chunk has coarse grains	RWE	
				Base of Core		

Explanation

Lithology
- Granular Sandstone
- Sandstone
- Sandy Limestone
- Mudstone

Bedding and Sedimentary Structures
- Trough Cross-Stratification
- Foreset Lamination
- Avalanche Deposit
- Planar Lamination
- Massive
- Wispy/Wavy Laminae
- Sandstone Fragments

Contacts
- Bedding Plane
- Scoured/Unconformity
- Fault

Navajo Facies

Dune
- LTC - Large Trough Cross-Stratification
- STC - Small Trough Cross-Stratification
- RWE - Reworked Eolian

Interdune
- WAM - Wavy Algal Mat
- SAM - Sandy Algal Mat

Diagenesis
- Fractures
- Deformation Bands
- Alteration (Dolomitization)